IDAHO TRANSPORTATION DEPARTMENT

RESEARCH REPORT

Your Safety • Your Mobility
Your Economic Opportunity

RP 246

Seismic Performance of Columns with Grouted Couplers in Idaho Accelerated Bridge Construction Applications

By
Arya Ebrahimpour, Barbara E. Earles,
Supreme Maskey, Maria Tangarife,
and Andrew D. Sorensen

Prepared for
Idaho Transportation Department
Research Program, Contracting Services
Division of Engineering Services
http://itd.idaho.gov/alt-programs/?target=research-program

October 2016

Standard Disclaimer

This document is disseminated under the sponsorship of the Idaho Transportation Department and the United States Department of Transportation in the interest of information exchange. The State of Idaho and the United States Government assume no liability of its contents or use thereof.

The contents of this report reflect the view of the authors, who are responsible for the facts and accuracy of the data presented herein. The contents do not necessarily reflect the official policies of the Idaho Transportation Department or the United States Department of Transportation.

The State of Idaho and the United States Government do not endorse products or manufacturers. Trademarks or manufacturers' names appear herein only because they are considered essential to the object of this document.

This report does not constitute a standard, specification or regulation.

1. Report No. FHWA-ID-16-246	2. Government Accession No.	3. Recipient's Catalog No.
4. Title and Subtitle Seismic Performance of Columns with Grouted Couplers in Idaho Accelerated Bridge Construction Applications		5. Report Date October 2016 6. Performing Organization Code
7. Author(s) (LIST ALL AUTHORS- erase this phrase before final) Arya Ebrahimpour, Barbara E. Earles, Supreme Maskey, Maria Tangarife, and Andrew D. Sorensen		8. Performing Organization Report No.
9. Performing Organization Name and Address Department of Civil and Environmental Engineering Idaho State University Pocatello, Idaho 83209		10. Work Unit No. (TRAIS) 11. Contract or Grant No. ISU-15-01
12. Sponsoring Agency Name and Address Idaho Transportation Department Division of Engineering Services, Contracting Services, Research Program PO Box 7129 Boise, ID 83707-7129		13. Type of Report and Period Covered Final Report 01/09/15 – 10/01/2016 14. Sponsoring Agency Code RP 246
15. Supplementary Notes Project performed in cooperation with the Idaho Transportation Department and the Federal Highway Administration.		

16. Abstract

In Accelerated Bridge Construction (ABC) methods, one way to connect prefabricated columns is by using grouted steel bar couplers. As of October 2016, in the U.S., only Utah DOT allows the use of grouted couplers in plastic hinge locations in seismic zones. The main focus of this research project is on seismic performance of grouted coupler column-to-footing and column-to-bent cap connections under Idaho seismic conditions. The performance of grouted coupler connections is compared to the conventional cast-in-place connections. Three Idaho bridges were selected for computer analysis. They were placed in the most seismically active location in Idaho. All three bridge columns performed well. The stresses in both the longitudinal reinforcing bars and the grouted coupler regions are well within acceptable range. The largest column drift, using combination of orthogonal displacements, is 1.6 percent. The single column analysis under large drift shows that grouted couplers may be used to connect precast columns to footings or cap beams for columns with less than 4 percent drift. The low-cycle fatigue analysis indicates that at higher strains the use of ASTM A706 steel will significantly improve the fatigue life of the reinforcing bars.

17. Key Words Bridge, column, seismic, design, prefabricated structures, accelerated bridge construction	18. Distribution Statement Copies available online at http://itd.idaho.gov/alt-programs/?target=research-program

19. Security Classification (of this report) Unclassified	20. Security Classification (of this page) Unclassified	21. No. of Pages 213	22. Price None

FHWA Form F 1700.7

METRIC (SI*) CONVERSION FACTORS

APPROXIMATE CONVERSIONS TO SI UNITS

Symbol	When You Know	Multiply By	To Find	Symbol
		LENGTH		
in	inches	25.4		mm
ft	feet	0.3048		m
yd	yards	0.914		m
mi	Miles (statute)	1.61		km
		AREA		
in^2	square inches	645.2	millimeters squared	cm^2
ft^2	square feet	0.0929	meters squared	m^2
yd^2	square yards	0.836	meters squared	m^2
mi^2	square miles	2.59	kilometers squared	km^2
ac	acres	0.4046	hectares	ha
		MASS (weight)		
oz	Ounces (avdp)	28.35	grams	g
lb	Pounds (avdp)	0.454	kilograms	kg
T	Short tons (2000 lb)	0.907	megagrams	mg
		VOLUME		
fl oz	fluid ounces (US)	29.57	milliliters	mL
gal	Gallons (liq)	3.785	liters	liters
ft^3	cubic feet	0.0283	meters cubed	m^3
yd^3	cubic yards	0.765	meters cubed	m^3

Note: Volumes greater than 1000 L shall be shown in m^3

		TEMPERATURE (exact)		
^oF	Fahrenheit temperature	5/9 (^oF-32)	Celsius temperature	^oC
		ILLUMINATION		
fc	Foot-candles	10.76	lux	lx
fl	foot-lamberts	3.426	candela/m^2	cd/cm^2
		FORCE and PRESSURE or STRESS		
lbf	pound-force	4.45	newtons	N
psi	pound-force per square inch	6.89	kilopascals	kPa

APPROXIMATE CONVERSIONS FROM SI UNITS

Symbol	When You Know	Multiply By	To Find	Symbol
		LENGTH		
mm	millimeters	0.039	inches	In
m	meters	3.28	feet	Ft
m	meters	1.09	yards	yd
km	kilometers	0.621	Miles (statute)	mi
		AREA		
mm^2	millimeters squared	0.0016	square inches	in^2
m^2	meters squared	10.764	square feet	ft^2
km^2	kilometers squared	0.39	square miles	mi^2
ha	hectares (10,000 m^2)	2.471	acres	ac
		MASS (weight)		
g	grams	0.0353	Ounces (avdp)	oz
kg	kilograms	2.205	Pounds (avdp)	Lb
mg	megagrams (1000 kg)	1.103	short tons	T
		VOLUME		
mL	milliliters	0.034	fluid ounces (US)	fl oz
liters	liters	0.264	Gallons (liq)	gal
m^3	meters cubed	35.315	cubic feet	ft^3
m^3	meters cubed	1.308	cubic yards	yd^3

		TEMPERATURE (exact)		
^oC	Celsius temperature	9/5 ^oC+32	Fahrenheit temperature	^oF
		ILLUMINATION		
lx	lux	0.0929	foot-candles	fc
cd/cm^2	candela/m^2	0.2919	foot-lamberts	Fl
		FORCE and PRESSURE or STRESS		
N	newtons	0.225	pound-force	lbf
kPa	kilopascals	0.145	pound-force per square inch	psi

Acknowledgements

The authors would like to thank the Idaho Transportation Department for supporting this research project. We would like to thank the members of the Technical Advisory Committee, Matt Farrar, Dan Gorley, Leonard Ruminski and Ned Parish for their support and valuable input. Leonard Ruminski provided extensive input in several key parts of this project, including the procedure for estimating abutment stiffness. Dr. Saiidi of the University of Nevada, Reno, served as the peer reviewer for this project. We appreciate his input. This project provided experience in seismic research, structural computer modeling, and data analysis for two graduate students and two undergraduate students at the Idaho State University. Kyle Gagnon, currently a graduate student at the University of Texas at Austin, assisted the project team in the initial computer modeling using OpenSees. We thank him for his assistance.

Technical Advisory Committee

Each research project is overseen by a technical advisory committee (TAC), which is led by an ITD project sponsor and project manager. The Technical Advisory Committee (TAC) is responsible for monitoring project progress, reviewing deliverables, ensuring that study objective are met, and facilitating implementation of research recommendations, as appropriate. ITD's Research Program Manager appreciates the work of the following TAC members in guiding this research study.

Project Sponsor – Matt Farrar, P.E.

Project Manager – Dan Gorley, P.E.

TAC Members
Leonard Ruminski, P.E.
Ned Parrish

FHWA-Idaho Advisor – Ed Miltner

Table of Contents

List of Tables

List of Figures

List of Acronyms

ABC	Accelerated Bridge Construction
AKDOT	Alaska Department of Transportation
Caltrans	California Department of Transportation
CIP	Cast-in-place
CWC	Column(s) with couplers
DOT	Department of Transportation
FGSS	Fastened-Grouted Splice Sleeve, a designation used in the University of Utah project
FHWA	Federal Highway Administration
GCNP	Grouted Coupler with No Pedestal, a designation used in UNR project
GCPP	Grouted Coupler and Precast Pedestal, a designation used in UNR project
GGSS	Grouted-Grouted Splice Sleeve, a designation used in the University of Utah project
HCNP	Headed Coupler with No Pedestal, a designation used in UNR project
HCPP	Headed Coupler and Precast Pedestal, a designation used in UNR project
ISU	Idaho State University
ITD	Idaho Transportation Department
NTS	Not to Scale
ODOT	Oregon Department of Transportation
SDC	Seismic Design Category
UDOT	Utah Department of Transportation
UNR	University of Nevada, Reno
USGS	United States Geological Survey
WSDOT	Washington State Department of Transportation
TAC	Technical Advisory Committee for the project

Executive Summary

Introduction

Accelerated Bridge Construction (ABC) methods have been limited in moderate-to-high seismic regions because of concerns about the performance of the connections. Bridge engineers are concerned about the substructure joints between the precast components. The main focus of this research project is on the seismic performance of grouted coupler column-to-footing and column-to-bent cap connections under Idaho seismic conditions. The performance of grouted coupler connections is compared to the conventional cast-in-place connections.

Objectives and Tasks

The objectives of this research project are to (a) assess the performance of grouted coupler column connections under Idaho seismic conditions; and (b) to develop recommendations on the use of columns with grouted couplers.

To carry out the objectives, the following tasks were assigned:

- Task 1: Perform a comprehensive literature review on seismic requirements of the column-to-footing and column-to-bent cap connections in ABC applications.
- Task 2: Develop computer models for the cast-in-place (CIP) column and the column with grouted couplers with no pedestal (GCNP) connection that were used in the experimental project at the University of Nevada, Reno (UNR). Good correlation between our computer model results with those of UNR experiments serves as a validation of the computer model to be used in Task 3. OpenSees finite element analysis program is used in this task.
- Task 3: Using the models developed in Task 2 perform seismic analyses of three Idaho bridges. For each bridge consider (a) a bridge with CIP columns, and (b) a bridge with grouted couplers at the bottom and top of the columns. Later another subtask was added that included analyses of single columns from two of the three bridges to examine (a) coupler and steel reinforcing bar stress-strain under large drifts, and (b) the low cycle fatigue behavior of the connecting steel bar.
- Task 4: In collaboration with the ITD Bridge Section staff, develop a section for inclusion in the Idaho Bridge Design Manual showing acceptable applications of grouted coupler connections.

Literature Review

The relevant work involving grouted couplers are those by Jansson (2008); Haber, Saiidi, and Sanders (2013); Pantelides, Ameli, Parks, and Brown (2014); Haber, Saiidi, and Sanders (2015); and Tazarv and Saiidi (2015). These research projects are summarized in Chapter 2 of this report. Two significant projects involving experimental columns with grouted couplers were performed by Haber, et al. (2013) and Pantelides, et al. (2014). Both research projects tested half-scale columns with grouted couplers

under quasi-static seismic loading. Haber, et al., concluded that (a) mechanical bar splices are a viable option in ABC applications in seismic zones; and (b) with demands of less than six percent drift, the use of grouted couplers is acceptable. The report by Pantelides, et al., concluded that the fastened-grouted couplers and grouted-grouted couplers may be used in ABC applications if the reduced ductility is accounted for.

The Departments of Transportation in several western states in the U.S. were contacted in May 2015 and again in June 2016 regarding the use of grouted couplers in bridge plastic hinge zones. Only Utah allows the use of grouted couplers in these zones. Utah's Structures Design and Detailing Manual has a section entitled Commercial Grouted Splice Couplers. This section has been added to the manual as a result of the work by Pantelides, et al. (2014).

Single Column Models

Using OpenSees, we developed computer models of the cast-in-place (CIP) and grouted couplers with no pedestal (GCNP) columns of the University of Nevada, Reno (UNR) laboratory models. The details of the experiments and computer molding were documented in the report by Haber, et al. (2013). The laboratory columns had a diameter of 2 ft and a height of 9 ft, resulting in an aspect ratio (height over diameter) of 4.5. Eleven No. 8 bars gave a steel to concrete ratio of 1.92 percent. For the GCNP columns, the grouted coupler stress-strain data for No. 8 bar were obtained from the manufacturer. The manufacturer's data provided us with the force versus elongation of the coupler region. The average strain of the coupler region is obtained by dividing elongation of the coupler region by the length of the coupler region. The results of our computer models compared well with both the experimental and analytical results of the UNR project.

Computer Modeling of Idaho Bridges

This section provide the background information for modeling a typical highway bridge. The two-span continuous cast-in-place concrete box girder bridge modeled in FHWA "Seismic Design of Bridges Design Example No. 1" document is used to compare results with those obtained using STAAD and OpenSees programs.

Next, we present the models of the three bridges suggested by the ITD Bridge Section using OpenSees computer program. These bridges are referred to as Parma, Dubois, and Salmon River. The bridges are placed in the most seismically active location in Idaho (i.e., Montpelier) with soil Site Class D. Using the USGS seismic design map, this combination of conditions results in a design short duration acceleration of S_{DS} = 0.907 and a design one-second acceleration of S_{D1} = 0.486. The S_{D1} of 0.486 (i.e., in the range of $0.30 \leq S_{D1} \leq 0.50$) places the structure in Seismic Design Category (SDC) C.

The bridge at Parma is a two-span bridge with a three-column bent. The superstructure is made up of an 8 in. thick concrete deck that rests on 5 prestressed WF66G girders. The columns are 3.5 ft in diameter with a height of 25.6 ft.

The Dubois bridge is also a two-span bridge with a four-column bent. The superstructure is made up of an 8-in. thick concrete deck that rests on eight steel girders. The columns are 3.5 ft in diameter with a height of 14.05 ft.

The Salmon River bridge is a three-span bridge with two single-column piers. The superstructure is made up of 8-½ in. precast deck panels and five 72 in. prestressed bulb-tee girders. The substructure has a pier cap and a single oval column on a cast-in-place footing in each pier. The columns' major and minor dimensions are 9.5 ft and 3.5 ft, respectively. The length of the southwest and northeast columns are 15.47 ft and 15.97 ft, respectively. The pier caps and columns are made of precast concrete. Grouted couplers were used to connect the columns to the footing.

Three computer models are used for each bridge considered: (a) model with cracked linear-elastic columns, (b) nonlinear model with cast-in-place (CIP) columns, and (c) nonlinear model with precast columns (having the same material properties as CIP columns) with grouted couplers at the top and bottom of the columns.

The bridge seismic analyses include both the transverse and longitudinal directions. To keep the analysis simple, the single-mode spectral method was used. In all cases the transverse loading controlled. Table 1 summarizes the transverse displacements, drifts, and column base reactions.

Table 1. Top of Column Displacements, Drifts, and Column Base Reactions under Transverse Load

Bridge	Results	Column Model		
		Cracked Linear-elastic	Nonlinear CIP	Nonlinear w/ coupler
Parma	Top of Column Displ., ft	0.315	0.376	0.375
	Column Drift, %	1.23	1.46	1.46
	Col. Base Shear, k	385	271.6	272.4
	Col. Base Moment, k-ft	5,440	3,624	3,634
Dubois	Top of Column Displ., ft	0.080	0.117	0.123
	Column Drift, %	0.57	0.830	0.877
	Col. Base Shear, k	347	245.3	245.1
	Col. Base Moment, k-ft	2,802	1,749	1,747
Salmon River	Top of Column Displ., ft	0.063	0.072	0.071
	Column Drift, %	0.41	0.47	0.46
	Col. Base Shear, k	679	553	551
	Col. Base Moment, k-ft	20,560	15,312	15,241

Results of Table 1 indicate that the displacement/drift behavior of all three bridges are almost identical when comparing the nonlinear results of bridge models with CIP columns with the results of bridge models having precast columns and grouted couplers (i.e., the last two columns in Table 1). The stresses in both the longitudinal reinforcing bars and grouted coupler regions (not shown in Table 1) are well within acceptable range. Only the steel bar in the Parma bridge goes slightly into the strain hardening region.

Next, we obtained the displacement/drift capacity and demand as per equations presented in the AASHTO Guide Specifications for LRFD Seismic Bridge Design Articles 4.8.1 and 4.3.3, respectively. On

the demand side, we used both the results of the cracked linear-elastic and nonlinear models. This is done to examine if the results of the magnified linear-elastic analysis compare well with the nonlinear analysis results. Furthermore, the combination of orthogonal seismic displacements are used as per Seismic Guide's Article 4.4 to obtain the linear-elastic and nonlinear displacement/drift demand values.

Partial results are given in Table 2. As it can be seen from Table 2, the drift demand for Parma, Dubois, and Salmon River bridge columns estimated using the magnified linear-elastic approach are 1.57 percent, 1.13 percent, and 0.72 percent, respectively. The corresponding values obtained through nonlinear approach (either for CIP column or column with grouted couplers) are 1.56 percent, 0.91 percent, and 0.53 percent, respectively. Therefore, for the three bridges considered, the AASHTO Seismic Guide's approximate relations for the magnified linear-elastic displacement/drift demand result in either the same or larger values (i.e., more conservative) than the corresponding displacements/drift demand values obtained through nonlinear analysis.

Table 2. Displacement and Drift Capacity and Demand for Bridge Columns (Partial Result)

	Parma	Dubois	Salmon River
Capacity			
Displacement, Δ_C, ft	0.458	- [a]	0.155
Drift, %	1.79	- [a]	1.00
Demand, Magnified Linear-elastic Analysis			
Displacement, Δ_D, ft	0.402	0.159	0.112
Drift, %	1.57	1.13	0.72
Demand, Nonlinear Analysis			
Displacement, Δ_D, ft	0.400	0.128	0.082
Drift, %	1.56	0.91	0.53

[a] Column Height <15 ft. LRFD Bridge Seismic Guide Article 4.8.1 equations may only be used for clear heights greater than or equal to 15 ft.

In accordance with the request of the ITD Technical Advisory Committee, next we considered two columns with grouted couplers at top and bottom; one from Parma bridge and one from Dubois bridge to examine coupler and steel reinforcing bar behavior under large drifts. Each column was analyzed under fixed-fixed (fixed at the bottom; top free to translate, but rotation prevented) boundary conditions. In addition, the number of "half cycles" to fatigue failure of Grade 60 steel were determined for both ASTM A706 and ASTM A615 rebars. This is because experimental results of University of Nevada, Reno clearly indicate that low-cycle fatigue failure (i.e., under large strain) of steel rebar is a possible mode of column failure. Partial results of the single column analyses under large drifts are given in Table 3. As shown in Table 3, the most stressed couplers in Parma and Dubois bridge columns reach their ultimate stress and strain values at nonlinear drift values of 4.4 percent and 4.9 percent, respectively. The last two columns of Table 3 provide the number of half cycles until low-cycle fatigue failure of ASTM A706 and ASTM A615 reinforcing bars. Since the low-cycle fatigue relations apply only to larger strains in steel, the number of half cycles are only evaluated for strains larger than 0.01 in./in. From Table 3, it is clear that the use of ASTM A706 steel bar will significantly improve (by a factor of at least two at larger strains) the low-cycle fatigue life of rebars.

Table 3. Stress and Strain in Coupler Region and Steel Bar and Number of Half Cycles for Steel Bar Fatigue Failure for Fixed-fixed Column with Grouted Couplers (Partial Results)

Bridge Column From	Column Nonlinear Drift, %	Coupler Region		Steel Bar		No. of Half Cycles to Fatigue Failure of Grade 60 Steel Rebar	
		Stress, ksi	Strain, in./in.	Stress, ksi	Strain, in./in.	ASTM A706	ASTM A615
Parma	3	20.50	0.0126	83.14	0.0236	81	36
	3.5	21.08	0.0144	86.12	0.0285	55	22
	4	21.56	0.0165	88.64	0.0338	39	14
	4.4	**21.80**[a]	**0.0185**[a]	90.43	0.0386	29	10
Dubois	3	15.60	0.0058	68.00	0.0056	-	-
	3.5	16.12	0.0070	68.00	0.0088	-	-
	4	17.37	0.0100	73.59	0.0165	172	93
	4.5	18.77	0.0137	84.44	0.0294	52	20
	4.9	**19.54**[b]	**0.0164**[b]	87.92	0.0360	34	12

[a] Ultimate stress and strain values for coupler region with SSNA No. 14 U-X grouted coupler
[b] Ultimate stress and strain values for coupler region with SSNA No. SNX11 grouted coupler

Recommendations

Based on the findings in the literature review and the results of computer modeling, the recommended guidelines when using precast columns with grouted couplers are given below. A table of approved grouted couplers and typical detailed drawings are shown in Chapter 5 of this report.

1. Grouted splice couplers may be used to connect precast columns to footings or cap beams for columns with less than 4 percent drift. Drift is determined by dividing the maximum displacement at the top of the column by its height. Displacements may be obtained through nonlinear analysis or by linear-elastic analysis (i.e., using cracked column section), which for short period structures may have to be multiplied by magnification factors as per AASHTO Guide Specifications for LRFD Seismic Bridge Design Article 4.3.3. In both cases, combination of orthogonal seismic displacements are to be used as per Seismic Guide's Article 4.4.
2. The total length of grouted splice couplers shall not exceed 15 times the diameter of the longitudinal reinforcing bar.
3. Grouted couplers in plastic hinge zones must develop 150% of the specified yield strength of the connected reinforcing bar.
4. Minimum clear distance between grouted splice couplers is recommended to be the same as those specified for the longitudinal reinforcing bars. The clear cover for the shear reinforcement over grouted couplers in the precast column shall be 2".
5. Grout for grouted couplers shall be provided by the manufacturer.

Chapter 1
Introduction

Description of the Problem

Accelerated Bridge Construction (ABC) methods are relatively new in the U.S. The ABC techniques have been limited in moderate-to-high seismic regions because of concerns about the performance of the connections. One important consideration is the substructure joints between the precast components. A ductile performance of the connection is essential to satisfy seismic requirements. The main focus of this research project is on the seismic performance of grouted coupler column-to-footing and column-to-bent cap connections under Idaho seismic conditions. The performance of grouted coupler connections is compared to the conventional cast-in-place connections.

Project Objectives

The project objectives are:

- To assess the performance of grouted coupler column connections under Idaho seismic conditions.
- To develop recommendations regarding the use of columns with grouted couplers for Idaho Transportation Department (ITD).

Project Tasks

The project tasks are:

- Task 1: Perform a comprehensive literature review on seismic requirements of the column-to-footing and column-to-bent cap connections in ABC applications.
- Task 2: Develop computer models for the cast-in-place (CIP) column and the column with grouted couplers with no pedestal (GCNP) connection that were used in the experimental project at the University of Nevada, Reno (UNR).[1] The results of the experimental cyclic push-pull loading conducted at the University of Nevada, Reno (UNR) is used for this comparison. Good correlation between the ISU computer model results with those of UNR experiments serves as a validation of the computer model to be used in Task 3. OpenSees finite element analysis program is used in this task.[2]
- Task 3: Using the models developed in Task 2 perform seismic analyses of three Idaho bridges. For each bridge consider (a) a bridge with CIP columns, and (b) a bridge with grouted couplers at the bottom and top of the columns.
- Task 4: In collaboration with the ITD Bridge Section staff, develop a section for inclusion in the Idaho Bridge Design Manual showing acceptable applications of grouted coupler connections.

- Task 5: The project principal investigators (PI and Co-PI) are to make a presentation to the ITD Bridge Section Designers regarding the outcomes of this project and recommendations in the design of precast columns with the grouted couplers.

This report addresses Tasks 1 to 4.

Report Overview

The report is divided into six chapters and several appendices:

- Chapter 1 presented an introduction to the research problem, the objectives, and project tasks.
- Chapter 2 presents a literature review with focus on the grouted column connections in seismic regions.
- Chapter 3 presents modeling of the single columns that were used in the UNR experimental project.
- Chapter 4 presents the results of computer modeling of three Idaho bridges. Results of models with (a) linear-elastic columns, (b) nonlinear cast-in-place columns, and (c) nonlinear columns with grouted couplers are presented.
- Chapter 5 presents the proposed guidelines on the use of grouted couplers in Idaho bridge columns. A list of acceptable couplers and a typical detail drawing are presented.
- Chapter 6 presents conclusions and recommendations.
- Several appendices present bridge modeling verifications, procedure for estimating the integral abutment stiffness values, grouted coupler experimental data and other dimensional data from the manufacturers, bridge data, computer models, and detailed results.

Chapter 2
Literature Review

Review of Relevant Research Projects

The American Concrete Institute ACI 439.3R-07 report describes grouted couplers as grout-filled ductile iron sleeves having deformations similar to reinforcing bar patterns on the inner wall.[3] A non-shrink, high strength, proprietary grout is pumped or poured in the chambers. Two types of grouted couplers are shown in Figure 1.

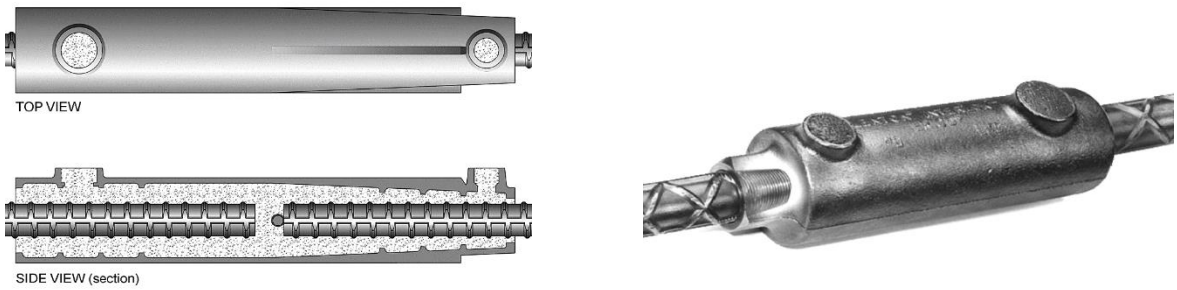

Figure 1. Grouted Couplers: (a) Both Ends Grouted and (b) One End Grouted and the Other End Threaded[3]

The sections that follow describe recent research on behavior of couplers, with focus on the grouted couplers. For convenience, each section's figures (if any) are grouped together at the end of the corresponding section.

Jansson (2008)

In this research project, conducted by the Michigan Department of Transportation (MDOT), two types of grout-filled mechanical connections underwent a combination of slip, fatigue, and ultimate load tests in accordance with ASTM A1034, *Standard Test Method for Testing Mechanical Splices for Steel Reinforcing Bars*.[4] The focus of the study was not on seismic applications. The connections tested were produced by NMB Splice Sleeve (see Figure 1a) and Lenton Interlok (see Figure 1b). Three specimens with No. 6 bars and three with No. 11 bars were prepared for each type of connection for the slip, fatigue, and ultimate load tests. An additional six specimens for No. 6 bars only, three for each type of splice, were tested for creep. The report concluded that (a) both products met the slip tests of the AASHTO LRFD requirements; (b) slip tests improved after 1,000,000 cycles of fatigue; (c) all specimens met the AASHTO LRFD fatigue requirements; (d) both splices are capable of exceeding 125 percent of the reinforcing bar's yield strength, and in most cases 150 percent of the reinforcing bar's yield strength; and (e) creep testing showed that neither product experiences significant displacements under sustained load.

Furthermore, it was shown that both products have relatively simple installation procedures. The report recommended approving the products for use on the departmental projects.

Haber, Saiidi, and Sanders (2013)

Haber, et al. studied two types of couplers in precast column-to-footing connections in seismic zones. The project focused on three areas: (a) uniaxial testing of up-set headed couplers (HC) and grout-filled sleeve couplers (GC); (b) testing of five half-scale precast reinforced concrete columns; and (c) analytical studies.[1] The columns had a diameter of 2 ft and a height of 9 ft, resulting in an aspect ratio (height over diameter) of 4.5. Eleven No. 8 bars gave a steel to concrete ratio of 1.92 percent. Five specimens were tested: (a) a cast-in-place (CIP) column, (b) a column with up-set headed couplers and no pedestal (HCNP), (c) a column with grouted couplers and no pedestal (GCNP), (c) a column with up-set headed couplers and precast pedestal (HCPP), and (e) a column with grouted couplers and precast pedestal (GCPP).

Figure 2 shows a detail view of an upset headed coupler, a photo of the coupler, and its placement in the HCNP column. Figure 3 shows a detail view of the grout-filled sleeve coupler (also see Figure 1a), and two photos of placement in the GCNP column. Figure 4(a) shows a photo of the test set-up. The half-scale columns were tested under a combined constant axial compression and a slow cyclic horizontal load with increasing amplitudes. The cyclic loading was drift-based as shown in Figure 4(b). Drift is defined as the horizontal displacement of the top of the column to the height of the column. Figure 4 shows the cyclic force-drift behavior of HCNP vs. CIP and GCNP vs. CIP columns in the UNR study. As shown in Figure 5(a) by the added blue circle, abrupt drop in load occurred in the second cycle of -10 percent drift in the CIP and HCNP columns. While, Figure 5(b) shows (also by a blue circle) an abrupt drop in load occurred during the second cycle of -6 percent drift for the GCNP column.

The average force-displacement envelopes for CIP and GCNP columns are shown in Figure 6, with damage states noted on the envelopes. The damage states, as defined by Vosooghi and Saiidi are defined in Figure 7.[5] The damage progression of the HCNP column (not shown here) was similar to the CIP column and achieved Damage State 5 (DS-5). The damage progression of GCNP model was also similar to that of CIP column, see Figure 5(b), but the column with grouted coupler did not achieve DS-5 prior to failure due to localized damage and subsequent failure of the connection.

The analytical models were developed using the OpenSees finite element software. Half-scale columns were modeled with nonlinear materials for unconfined concrete, confined concrete, steel and couplers. Uniaxial fiber-sections were used in the models. Bond-slip spring elements were used to represent the bar slip relative to the concrete in the footing. This slip causes rotation at the column-footing interface, resulting in additional displacement (or drift) in the column. More details on the computer modeling for CIP and GCNP columns will be presented in Chapter 3 of this report.

The report noted that in tension tests of individual couplers, all samples had bar fracture failure away from the coupler itself. Primary mode of failure in all columns was fracture of longitudinal bars. Grouted coupler connections required less installation time compared to up-set headed couplers.

Analytical models gave similar force-displacements compared to laboratory test results. Among the report's conclusions were: (a) mechanical bar splices are a viable option in ABC applications in seismic zones; and (b) with demands of less than 6 percent drift, the use of grouted couplers is acceptable.

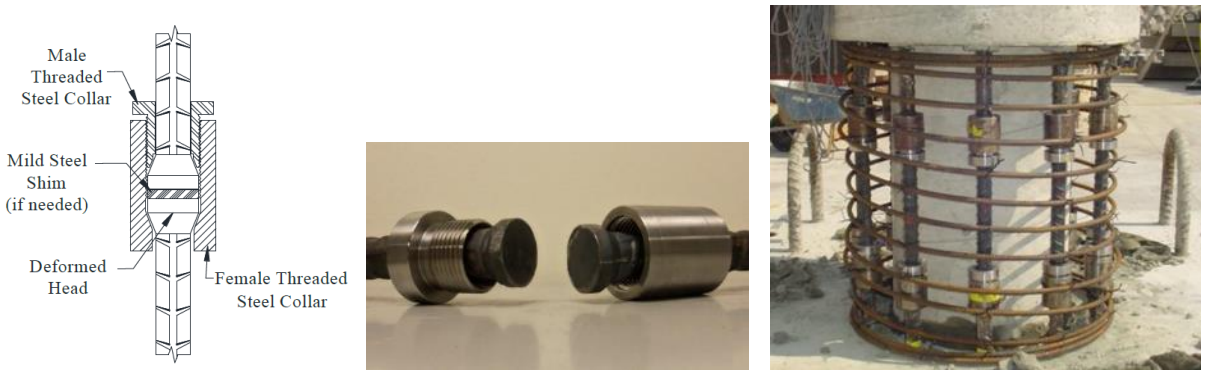

Figure 2. Upset Headed Coupler and Placement in the HCNP Column[1]

Figure 3. Grout-filled Sleeve Coupler and Placement in the GCNP Column[1]

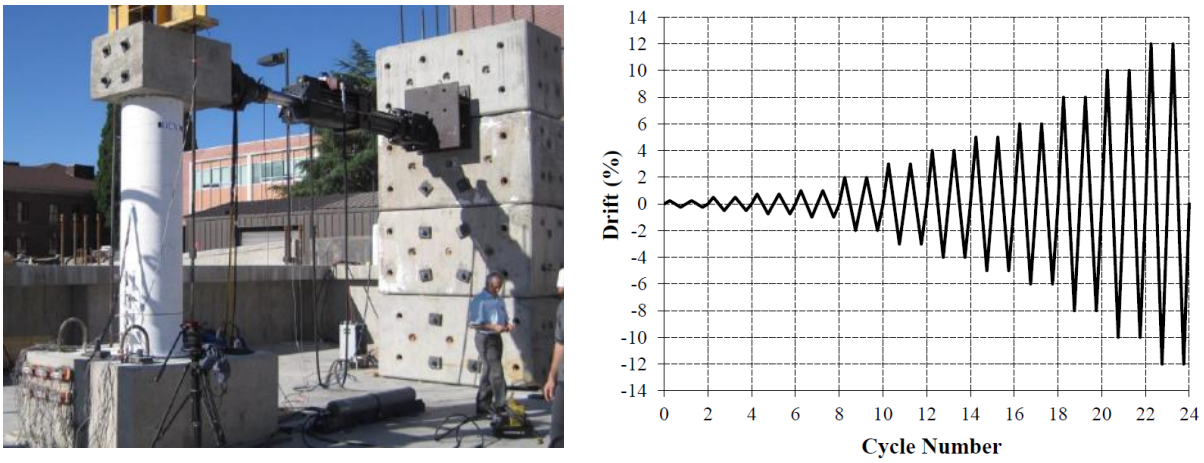

Figure 4. (a) Photo of the Test Set-up and (b) Loading Protocol[1]

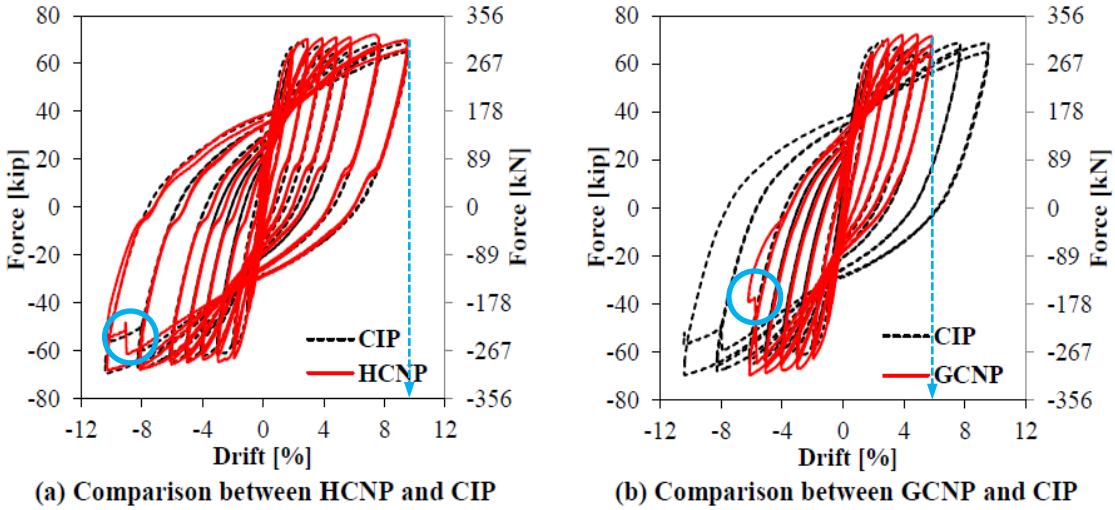

(a) Comparison between HCNP and CIP (b) Comparison between GCNP and CIP

Figure 5. Hysteretic Force-displacement of (a) HCNP vs. CIP and (b) GCNP vs. CIP Columns[1]
Note: The blue lines and circles are added.

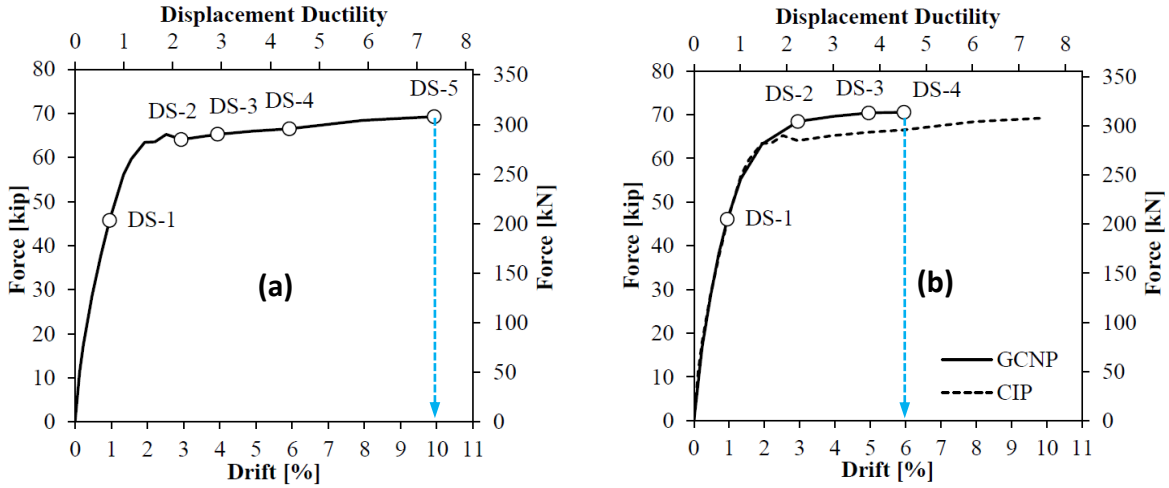

Figure 6. (a) CIP and (b) GCNP vs. CIP Force-displacement Envelopes with Damage States [1]

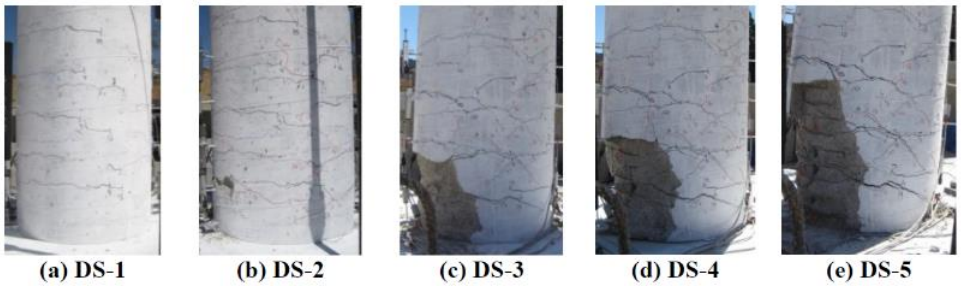

Figure 7. Damage States as Defined by Vosooghi and Saiidi (2010)[1, 5]

Pantelides, Ameli, Parks, and Brown (2014)

Pantelides, et al., tested eight half-scale column connections under cyclic quasi-static loading at the University of Utah.[6] The loading protocol was similar to the one used at the University of Nevada, Reno. Tests were performed on (a) three column-to-cap beams with Fastened-Grouted Splice Sleeve (FGSS) connections and one cast-in-place (CIP) control specimen; and (b) three Grouted-Grouted Splice Sleeve (GGSS) connections and one cast-in-place (CIP) control specimen. Figure 8(a) shows the column-to-cap beam connection and Figure 8(b) shows the column-to-footing connection tested in this project. As shown in Figure 9, three coupler placements were selected. These are: (a) couplers placed in the column (GGSS-1 and FGSS-1); couplers placed in footing (GGSS-2) or in the column cap (FGSS-2); and couplers placed in the column with 8 in. debonded regions in the footing (GGSS-3) or in the column cap (FGSS-2). All columns had an octagonal cross-sectional shape with a minimum dimension (i.e., the distance between two parallel sides) of 21 in. A height of 8 ft-6 in. gave an aspect ratio of 4.86. Six No. 8 steel bars in a circular arrangement resulted in a steel reinforcement to concrete ratio of 1.3 percent.

Figure 10 shows the hysteresis curve for the cyclic test of GGSS-1 specimen. The backbone versus the idealized elasto-plastic curve for GGSS-1 is shown in Figure 11. The idealized curve intersects the backbone at 70 percent of yield as per ACI 374.[7] The displacement ductility capacity, μ_Δ, was defined as the ratio of ultimate displacement, Δ_u, to the yield displacement, Δ_y. The ultimate displacement was defined as the displacement corresponding to a 20 percent drop in the lateral load capacity. For example, for the GGSS-1 (see Figure 11) displacement ductility is: $\mu_\Delta = \Delta_u/\Delta_y = 7.79/1.45 = 5.4$. The backbone curves, in terms of force versus drift, for all the tests in the project are shown in Figure 12. The displacement ductility, μ_Δ, values are also noted in Figure 12. The low value of displacement ductility for FGSS-3 (i.e., $\mu_\Delta = 3.1$ circled in blue in Figure 12) was attributed to a pre-test unintentional damage experienced by the specimen.

The research report noted that (a) CIP specimens had the best ductile performance; (b) specimens with grouted connectors in the column had more localized damage compared to CIP; (c) for specimens with grouted couplers in the column, more lateral force capacity was observed due to the presence of cast iron sleeves; (d) rebar fracture occurred in all column-to-footing specimens with grouted couplers (i.e., the specimens with GGSS connectors) indicating that the tensile strength of the bars was developed; (e) for column-to-cap beam connections (i.e., those specimens that used GFSS connectors), a premature rebar fracture occurred in one bar of the FGSS-2 at a 7 percent drift ratio followed by the pull out failure of the opposite extreme bar, and specimens FGSS-1 and FGSS-3 failed because of rebar pull out due to an excessive bond-slip; (f) specimens that had grouted connectors in the footing (GGSS2) and column cap (FGSS2) had damage similar to the CIP specimens; and (g) the displacement ductility values of all columns with grouted connections were more than 3.0 which is the minimum required in the Caltrans Seismic Design Criteria (SDC). The report concluded that FGSS and GGSS connectors are found to be promising for use in ABC applications if the reduced ductility is accounted for.

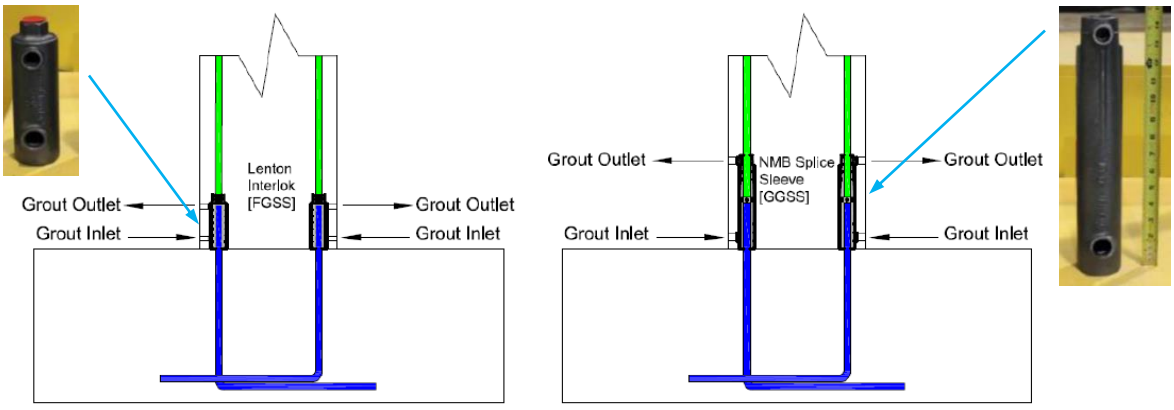

Figure 8. (a) FGSS Column-to-cap Beam and (b) GGSS Column-to-footing Connections[6]

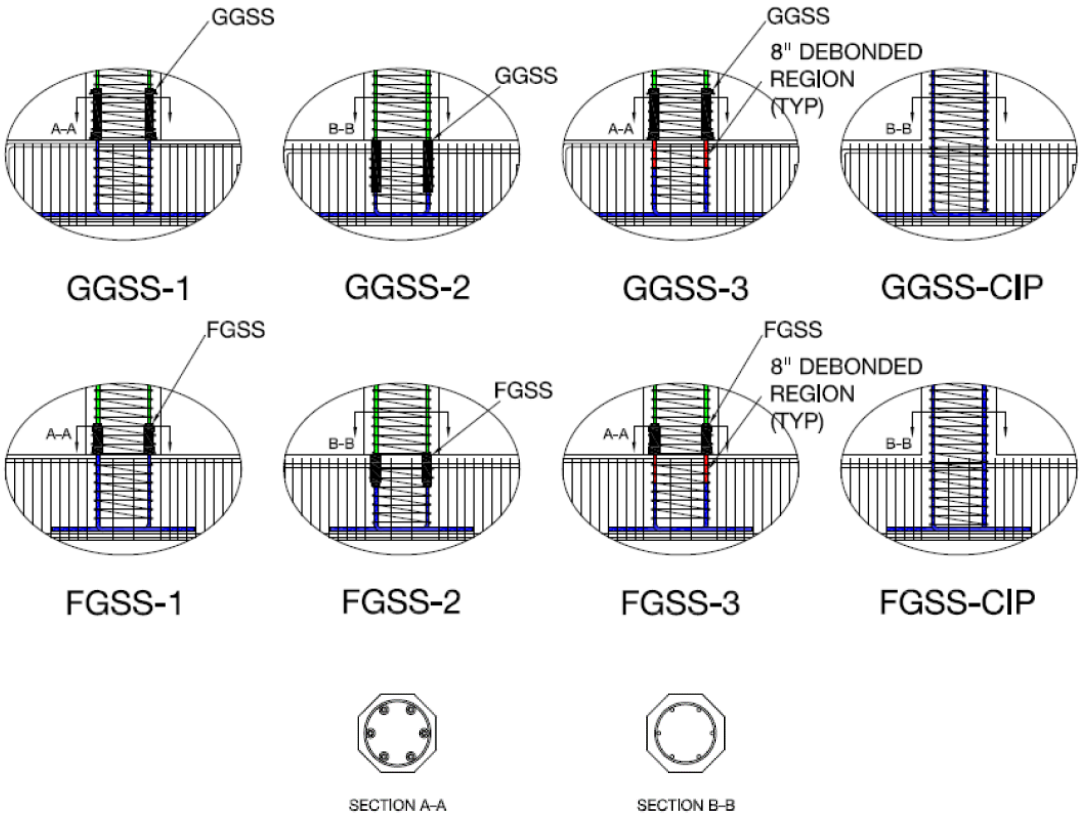

Figure 9. Test Specimen Alternatives[6]

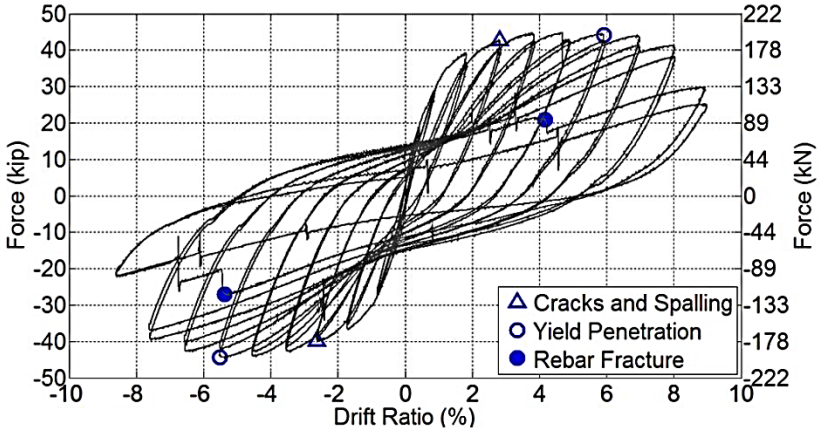

Figure 10. Hysteresis Curve for GGSS-1[6]

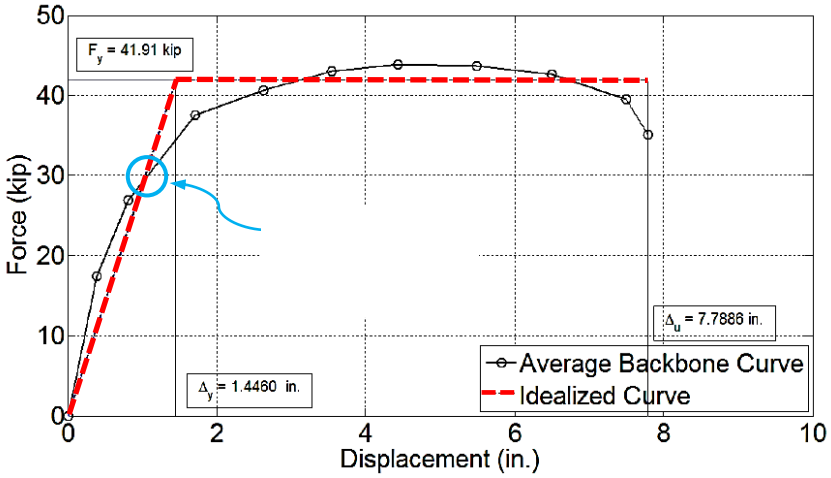

Figure 11. Backbone vs. Idealized Elasto-plastic Curve for GGSS-1[6]
Note: The blue circle and text are added.

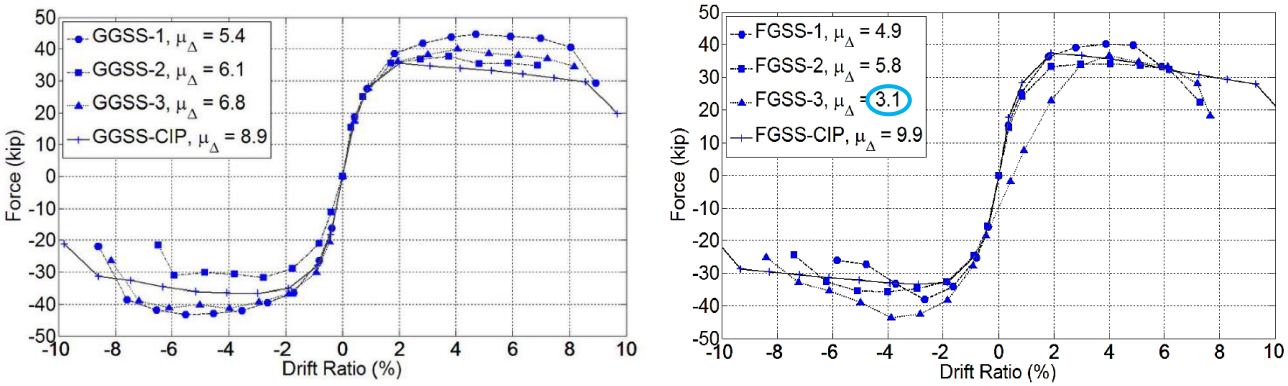

Figure 12. Backbone Curves for all Tests[6]

Haber, Saiidi, and Sanders (2015)

In a paper published after their 2013 research report, Haber, et al. presented a simplified method for modeling precast columns with mechanical reinforcing bar splices.[8] An effective uniaxial stress-strain relationship is used for the coupler. See the dashed curve in Figure 13(a). In the case of a grouted coupler, this relationship is obtained by the set-up as shown in Figure 14. The stress in the steel bar is plotted versus the effective (average) strain in the coupler region. The coupler effective strain is measured by an extensometer (see Figure 14) monitoring the deformation of the length of coupler region (L_{CR}). The solid line in Figure 13(a) is the bar stress versus the corresponding strain, with the strain measured by a strain gage attached to the steel outside the coupler region. Figure 13(b) shows the OpenSees model of the column with grouted couplers. Unlike the previous (2013) version of the computer model, this model only uses one bond-slip element and the stress-strain relations described

above in the fiber sections. This method is used later in Chapter 3 for creating an analytical model of the column with grouted couplers in order to compare results with those of the UNR project.[8]

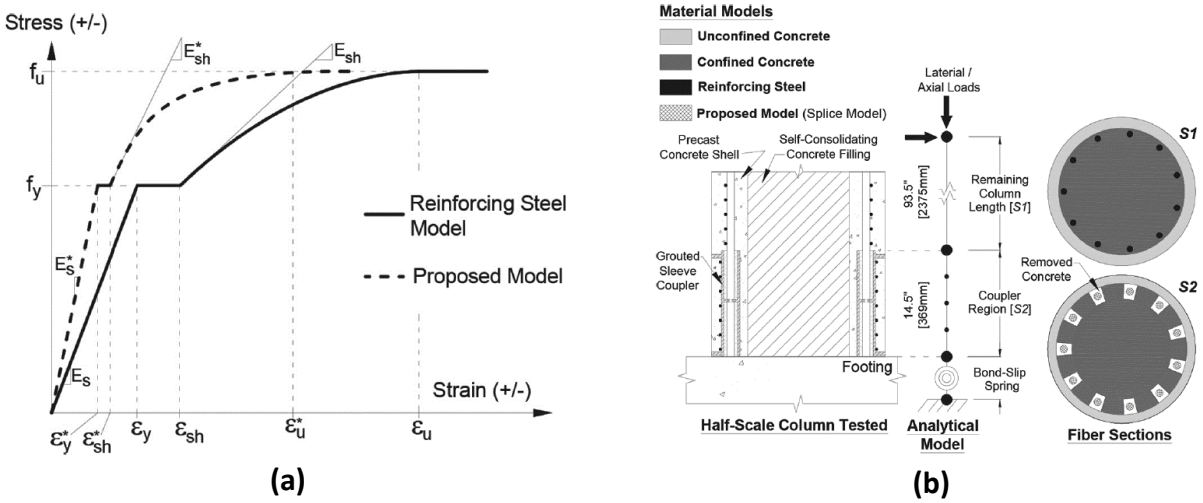

Figure 13. (a) Stress-strain Models and (b) Simplified GCNP OpenSees Column Model[8]

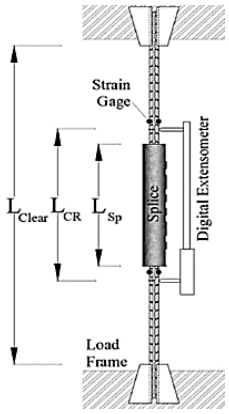

Figure 14. Coupler Uniaxial Test Set-up[8]

Tazarv and Saiidi (2015)

Tazarv and Saiidi studied the behavior of five types of mechanical bar splices individually and also when installed in bridge concrete columns.[9] Five tasks were conducted: (a) literature search, (b) seismic performance of different types of couplers and columns with couplers (CWC), (c) constructability of couplers and columns with these couplers, (d) methods to estimate column ductility demand capacity, and (e) developing design guidelines for columns with coupler connections.

Concerning seismic response of ductile columns with couplers (CWC) in plastic hinge region (i.e., part of the second task), the authors proposed the following acceptance criteria: *"(1) When the displacement ductility capacity of CIP is five or less, the displacement ductility capacity of CWC should be at least equal to the ductility capacity of CIP. For other cases, the displacement ductility capacity of CWC should be the*

greatest of (a) 90% of CIP ductility capacity, and (b) five. Either displacement or drift capacity may be used in evaluation of columns with advanced materials. (2) The lateral load strength of CWC should not be less than 95% of the CIP strength when the displacement ductility capacity of CIP is five or less. For other cases, the lateral strength of CWC should not be less than 90% of CIP strength." Based on these acceptability criteria, six laboratory columns incorporating grouted couplers were evaluated. Only one of the six passed the proposed acceptability criteria.

Regarding the last task (design guidelines), the authors provided seven recommendations (indicated as R1 to R7) with the corresponding commentaries (indicated as C1 to C7). Among the recommendations that apply to this study are: (a) R2: the length of the coupler (L_{sp} in Figure 15) shall not exceed 15 times the reinforcing bar diameter; (b) R3: only couplers in which failure occurs due to bar fracture outside of coupler region shall be used in the plastic hinge zones (see Figure 15); and (c) R6: the displacement ductility capacity of the mechanically spliced column shall be calculated based on the conventional cast-in-place column displacement ductility capacity using an equation provided in the report.

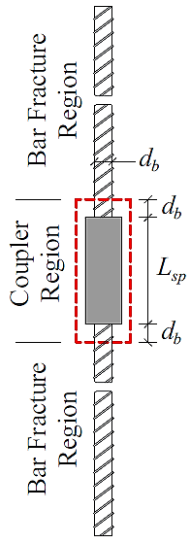

Figure 15. Coupler and Fracture Regions[9]

Use of Grouted Couplers in Bridge Columns by Western State DOTs

Several western states were contacted in May 2015 and again in June 2016 regarding the use of grouted couplers in the bridge column plastic hinge zones. Table 4 shows these state DOTs and their responses.

Table 4. Use of Grouted Couplers by Western DOTS in Bridge Column Plastic Hinge Zones

State	Grouted Couplers in Column Plastic Hinge Zones	Comments

Alaska	No	AKDOT prefers the use of grouted pockets or ducts when connecting precast caps to columns/piles.
California	No	The findings from UNR were presented, but it was voted not to allow grouted couplers in the plastic hinge zones columns. [(1)]
Hawaii	No	State of Hawaii is not currently using any ABC methodologies.
Nevada	No	Although research on ABC column connections at the University of Nevada Reno (UNR) had been considered, no ABC column connections is currently used in the State of Nevada.
Oregon	No	ODOT does not have any special specs for splices for ABC.
Utah	Yes	UDOT Structures Design and Detailing Manual has a section on grouted couplers in ABC applications. This section is based on the report by the University of Utah research reported by reported on by Pantelides, et al.[(6)]
Washington	No	WSDOT does not approve the use of mechanical couplers for connections of precast bridge members. The WSDOT prefers the use of grouted ducts similar to the ones used by AKDOT.

Utah's Structures Design and Detailing Manual dated Feb. 2015, Section 20.4.6.3, Commercial Grouted Splice Couplers states:[(10)]

"*… The use of grouted splice couplers is permissible in plastic hinging zones. The standard requirements for column confinement apply around the couplers. Adjust the cover to the reinforcing and spiral or ties to accommodate the larger grouted splice coupler section. Refer to the SD drawings for examples of how grouted splice couplers are used. The preferred configuration for constructability is to locate the grouted splice coupler above the joint, which reduces the chance of contamination with debris. Grouted splice couplers located below the joint must be sealed during fabrication and shipping. Also, placing the grouted splice coupler above the joint allows the reinforcing extensions at the top of the element, making shipping and handling easier. Placement of grouted couplers in the footing or in the cap improves the connection ductility capacity. Locate the coupler in the footing or in the cap when the ductility demand exceeds 4. Design the reinforcing size and grouted splice couplers to allow for crossing reinforcing patterns. Detail the spacing at approximately the maximum reinforcing spacing requirements in the LRFD Specifications. Base the spacing on the connected reinforcing. Do not use the diameter of the grouted splice couplers in the calculations. Check the clear spacing between the grouted splice couplers using the following approach.*

Use a grouted splice coupler sleeve size one reinforcing size larger than the reinforcing size used. Detail the minimum gap between the grouted splice couplers to be the greatest of the following:

- *1 in.*
- *1.33 × (maximum aggregate size of the coarse aggregate)*
- *Nominal diameter of the connected reinforcing*

Provide cover for the element based on the diameter of the grouted splice coupler. The practice requires increased cover to the reinforcing to obtain the cover over the grouted splice couplers ..."

Discussion

Since 2013 there have been two major experimental results published concerning performance of columns with grouted couplers under quasi-static seismic loading. The results have been promising, but only the state of Utah has allowed the use of grouted couplers plastic hinging zones in moderate to high seismic regions.

Regarding the work by Tazarv and Saiidi, we believe the acceptability criteria for columns with couplers (CWC) must be interpreted carefully. In that study, the performance of a CWC was compared to the performance of a CIP columns having high values of displacement ductility capacity. However, if for example the abutments of a bridge restrict the column displacement ductility demand to a small value (say 2), then the performance of a column with grouted couplers having a low displacement ductility capacity may be adequate for that particular application.

The fatigue of grouted couplers has been studied in low amplitude fatigue tests by Jansson (2008) as well as Haber, et al.[11, 1] In both cases, the grouted couplers performed well in the standard fatigue tests. However, no information was found on grouted couplers tested individually in low-cycle large-amplitude fatigue tests. In experimental work on columns with grouted couplers with both ends grouted, no fracture of the grouted couplers were reported by Haber et al. and Pantelides, et al.[1, 6] However, failures due to bond slip in grouted-fastened couplers were observed at higher column drifts according to the University of Utah's report.[6] Therefore, one can observe that grouted-grouted couplers perform better in the columns than the grouted-fastened couplers. Furthermore, couplers with both ends grouted force the rebar to fracture away from the couplers which is the desired mode of failure.

Regarding the low-cycle high-amplitude fatigue behavior of steel bars, there are some published data in the literature. These data were used by Haber, et al. in order to predict the fracture of steel bars during the large amplitude cyclic tests of the UNR laboratory columns.[1] In the work presented here, we will use the large amplitude fatigue data to approximately determine the possibility of fracture of the steel bars in columns of the three Idaho bridges during a seismic event.

Chapter 3
Single Column Models

Background

In this chapter OpenSees computer models of the half-scale cast-in-place (CIP) column and the half-scale column with grouted couplers with no pedestal (GCNP) used in the experimental project of University of Nevada, Reno (UNR) are presented.[1] Good correlation between our computer model results and the experimental and analytical results of the UNR project ensures that the bridge columns in Chapter 4 are properly modeled. Since we did not have access to the UNR's OpenSees input files, we have independently developed the computer input files for the CIP and GCNP columns.

Cast-in-place Column

Figure 16 shows the cast-in-place (CIP) column used in the UNR study. Figure 17 shows the OpenSees model of the CIP column. In order to duplicate the same results as the UNR study, we also used OpenSees' *Concrete01*, *Concreter04*, and *ReinforcingSteel* nonlinear material models for unconfined concrete, confined concrete, and longitudinal steel bars, respectively.[2] The properties for the CIP column materials are given in the report by Haber, et al.[1] The computer model uses distributed plasticity frame elements with uniaxial fiber sections. The model shown in Figure 17 has six nodes and five elements. Two elements are nonlinear and three elements are linear-elastic. The nonlinear element E1 is a *zeroLength* element that represents the bond-slip at the base of the column. The other nonlinear element (element E2) is a *nonlinearBeamColumn* element that uses fiber sections with the three materials noted above. E3, E4, and E5 are *elasticBeamColumn* elements with high stiffness values.

Bond-slip Rotation at the Base of Column

The rotation caused by the bond-slip at the base of the column is modeled using a rotational spring with a *Hysteretic* material behavior. The rotational spring uses a bi-linear curve to describe the moment-rotation relationship. For more details, see the report by Haber, et al.[1] The idealized (fitted) bi-linear curve is shown in Figure 18. The model developed in Haber's study (which is used here) employs the method developed by Wehbe, et al.[1, 12] The tensile stress and strain in the extreme longitudinal bar and the location of the neutral axis are determined using a moment-curvature analysis. The calculation process for obtaining the moment-rotation (M-θ) curve and the moment-curvature input file are presented in Appendix A. Using the approach outlined in Appendix A, Table 5 shows the moment and rotation values corresponding to the points labeled $\left(M_1^+,\ \theta_1^+\right)$ and $\left(M_2^+,\ \theta_2^+\right)$ on Figure 18 for the UNR's study and those that we estimated (called ISU values). These points are for the direction that UNR's report calls "push" direction (see Appendix A). Since the "push" and "pull" values are within 5 percent, we used the ISU "push" values in our computer models of the column.

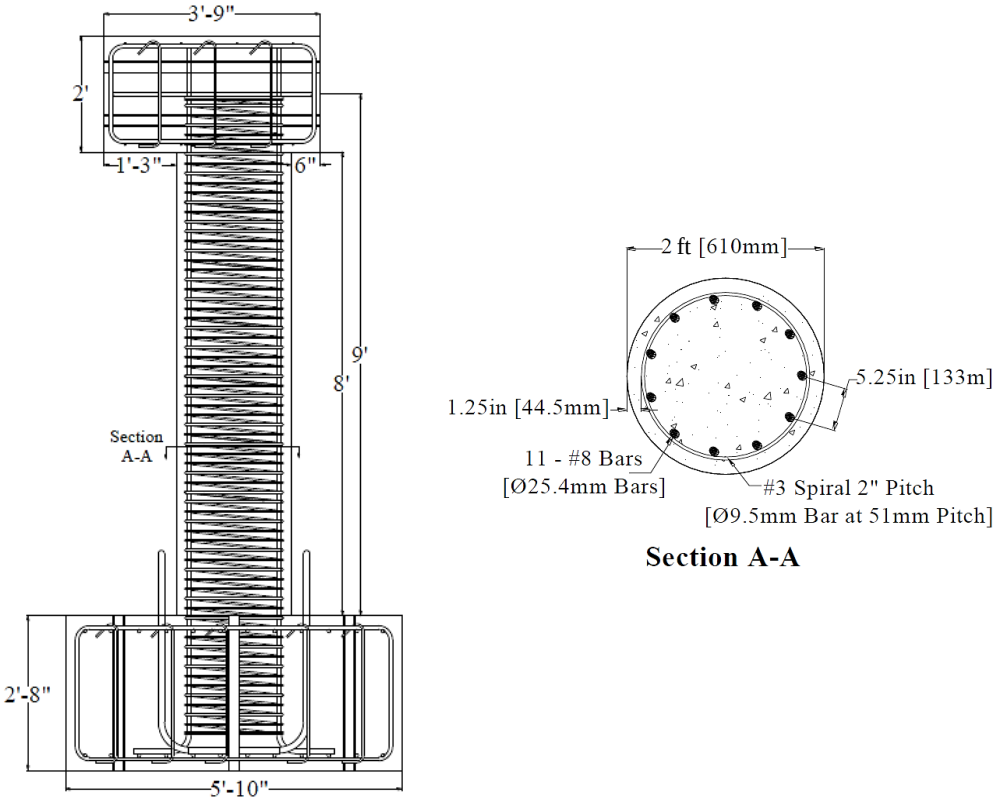

Figure 16. Cast-in-place Column used in the UNR Study[1]

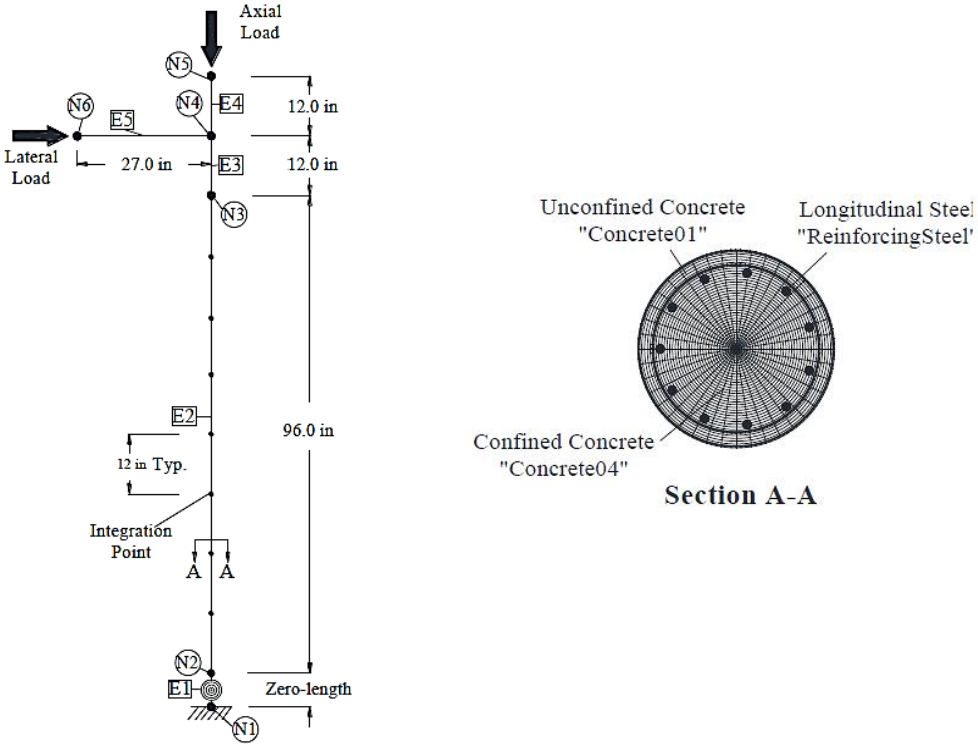

Figure 17. The OpenSees Model of the UNR Cast-in-place Column[1]

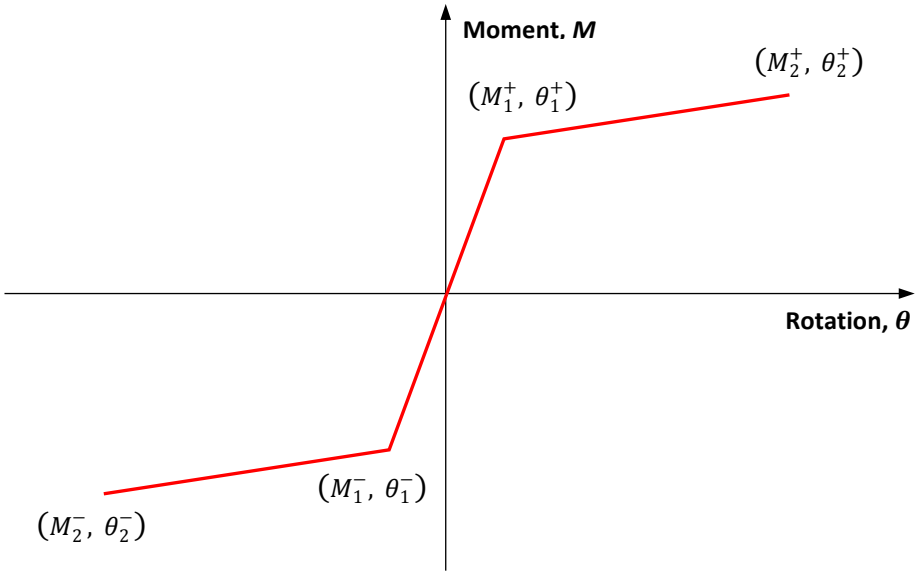

Figure 18. Schematic of the Fitted Bi-linear Curve for the Footing Bond-slip Moment-rotation

Table 5. Footing Bond-slip Moment-rotation Values of UNR versus ISU for the "Push" Direction

	UNR		ISU	
	Moment (kip-in.)	**Rotation (rad)**	**Moment (kip-in.)**	**Rotation (rad)**
Point 1	6,746	0.0028	6,580	0.0021
Point 2	7,859	0.0452	7,883	0.0422

CIP Column Force-displacements

As shown in Figure 17, an axial compressive force of 208 kip is applied at node 5 of the CIP column model. Node 6 is subjected to a horizontally-applied displacement-controlled increasing cyclic load that was used in the UNR experimental work (see Figure 4(b)). The vertical axis in Figure 4(b) is converted to displacement by multiplying percent drift by the height of the column which was 9 ft.

Figure 19 shows the UNR's experimentally measured and calculated as well as the ISU's calculated hysteretic force-displacement curves for the CIP column. Figure 20 shows the UNR's measured and calculated average envelope curves (i.e., curves representing the maximum force values for Figure 19(a)) and the ISU calculated pushover curve. Our pushover curve was generated by pushing the column in one direction and recording the force and top of the column displacement values. Displacements are converted to drift by dividing them by the height of the column (i.e., 9 ft = 108 in.). The OpenSees input files for (a) the cyclic push-pull and (b) pushover of the CIP column are given in Appendix A.

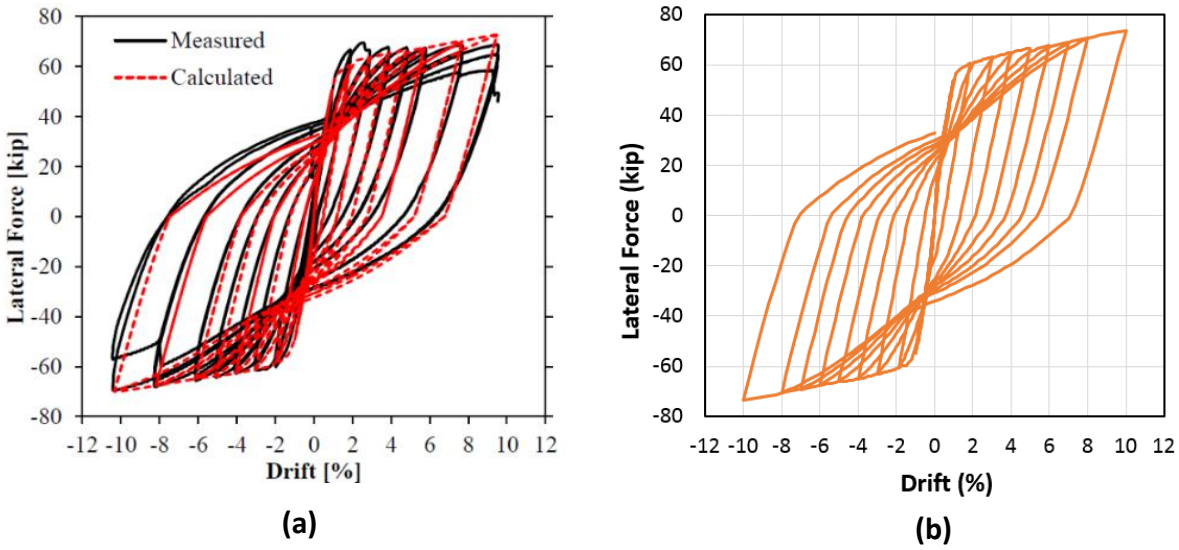

Figure 19. (a) UNR Measured and Calculated and (b) ISU Calculated Hysteretic Force-displacement Curves of the CIP Column

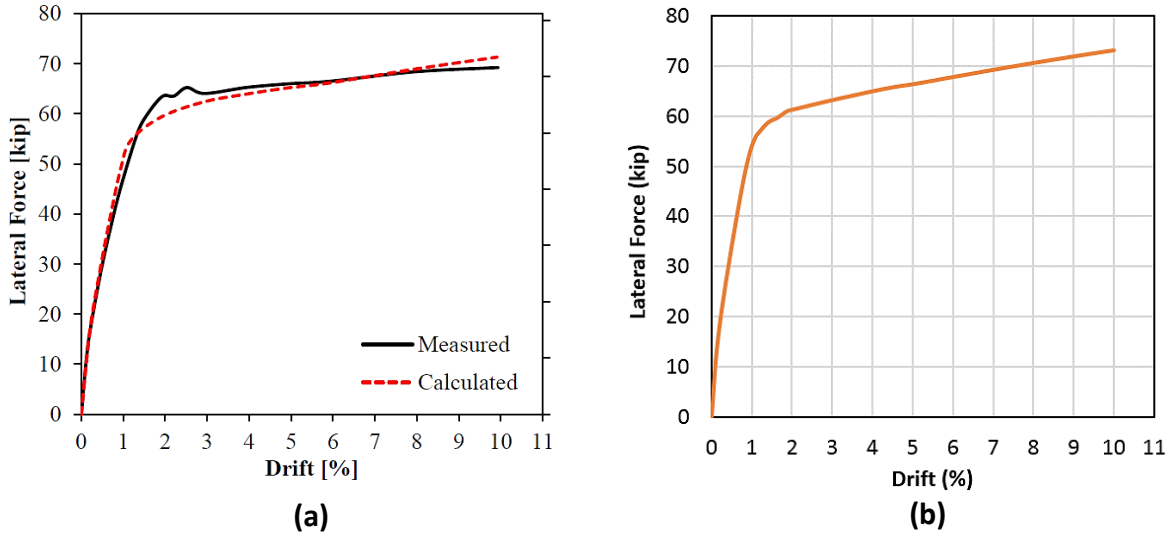

Figure 20. (a) UNR Measured and Calculated Average Envelope Curves and (b) ISU Calculated Pushover Curve for the CIP Column

GCNP Column

Figure 21 shows the column with grouted couplers and no pedestal (GCNP) used in the UNR study. For modeling the GCNP column, we used the revised OpenSees modeling procedure of Haber, et al. as illustrated in Figure 13(b) of Chapter 2.[8] The column is composed of two fiber sections: one for the grouted coupler segment (the bottom 14.5 in.), and the other one for the segment having steel reinforcing bars (the upper portion of the column).

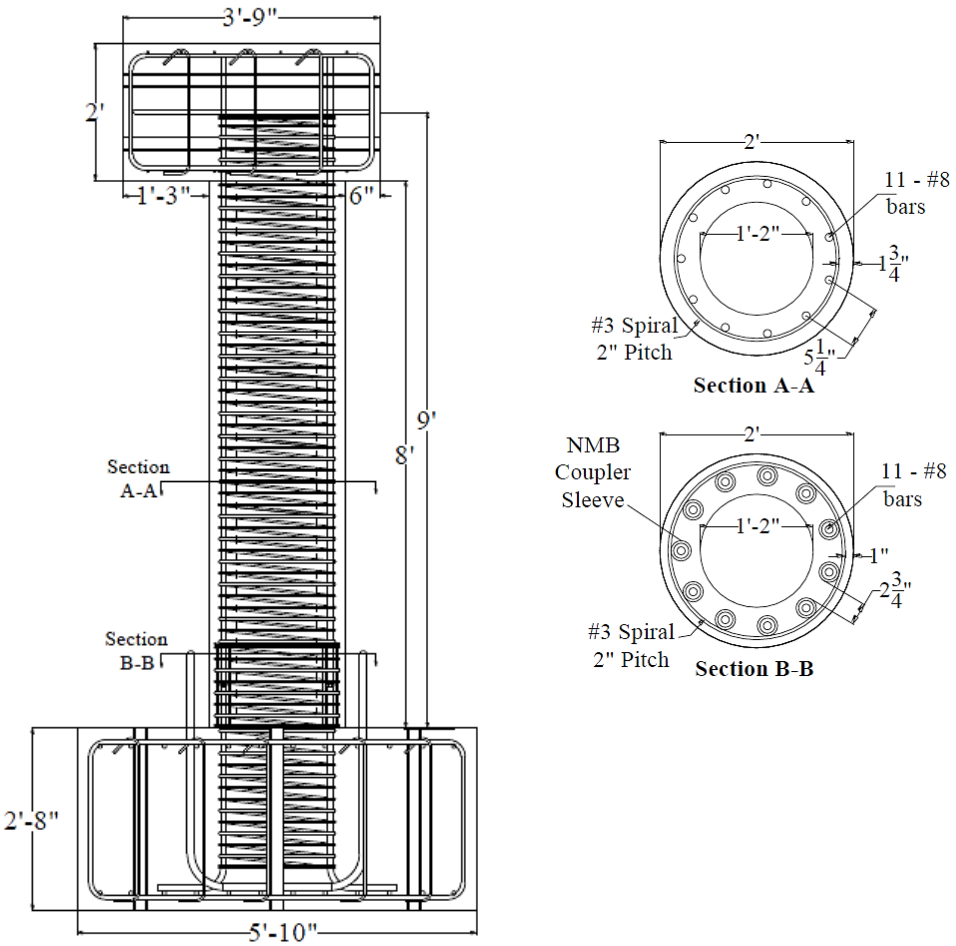

Figure 21. The GCNP Column used in the UNR Study[1]

For the grouted couplers (NMB coupler sleeves for No. 8 bar), we also used the OpenSees *ReinforcingSteel* nonlinear material. The stress in the No. 8 bar versus the coupler region strain data is used for this purpose. This relationship is shown with the dashed line curve in Figure 13(a). The grouted coupler data for No. 8 bar (as well as No. 11 and No. 14) were obtained from the manufacturer.[13] The idealized stress versus strain curves for No. 8 grouted coupler are shown in Figure 22. The idealized curve of the grouted coupler stress versus coupler strain shown in Figure 22 is the best fit of five experimental curves. The manufacturer data provided the force versus elongation of the coupler region (called "slip" by the manufacturer). See Figure 22 parts (b) and (c). The effective stress in the coupler is found by dividing the force by the area of the grouted coupler (4.94 in.^{2} for No. 8 coupler). The average strain of the coupler is obtained by dividing elongation of the coupler region by the length of the coupler region.

The stress in the No. 8 bar versus the coupler strain shown in Figure 22 (i.e., the upper curve) is obtained by multiplying the stress values of the coupler by the ratio of the area of coupler over the area of the No. 8 bar (i.e., a factor equal to (4.94 in.^{2})/(0.79 in.^{2}) = 6.253). It should be noted that the yielding in the lower curve of Figure 22 is caused by the steel bar within the coupler region, not the coupler sleeve.

The same is true in the upper curve which is used in the OpenSees model. The detailed raw experimental data and the processed data for coupler stress-strain are presented in Appendix B.

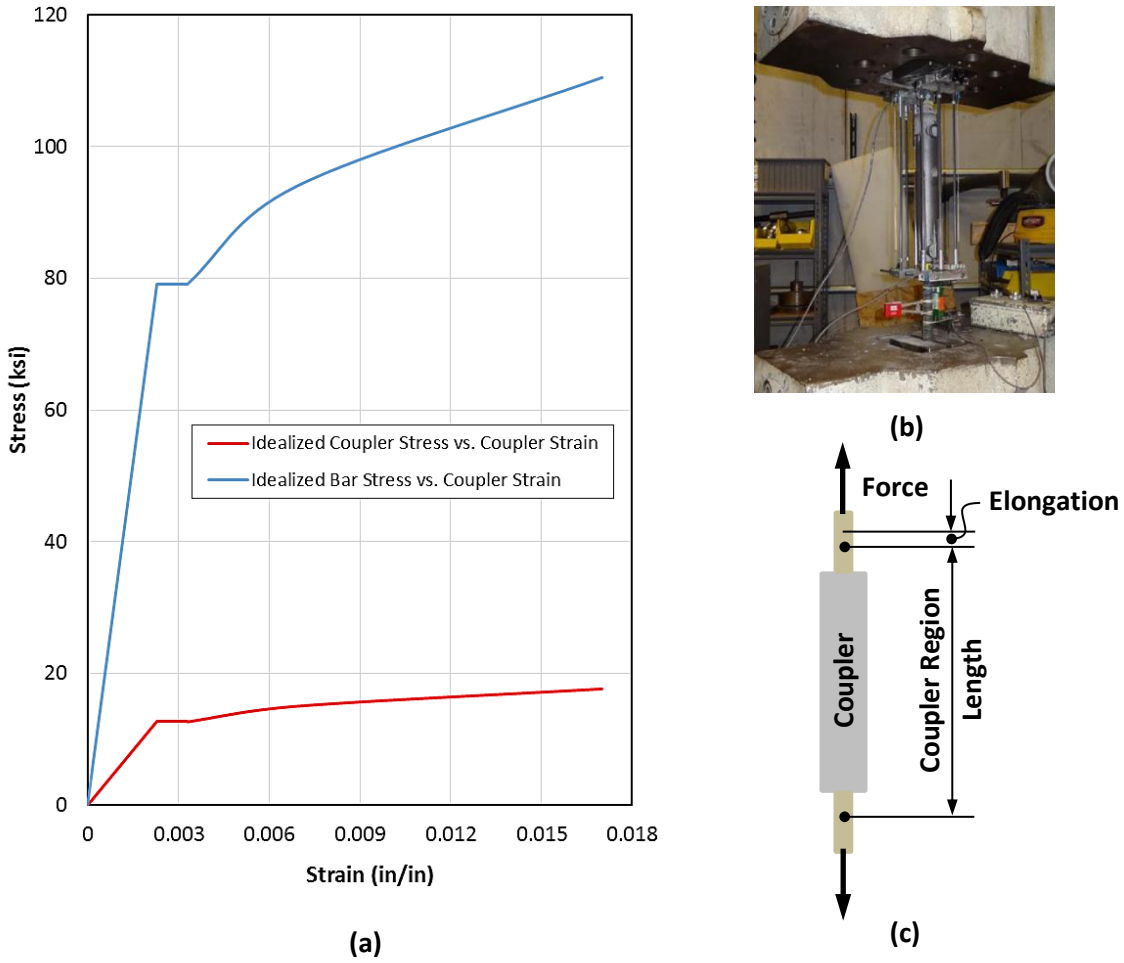

Figure 22. (a) No. 8 Coupler Stress vs. Strain, (b) Experimental Set-up for Testing Grouted Coupler, and (c) Schematic Describing Coupler Region and the Elongation (Slip)[13]

In the OpenSees input file, in the grouted section of the GCNP column model, the same area of fiber is used as the No. 8 steel bar, but the properties of the curve corresponding to bar stress versus coupler strain (i.e., the upper curve in Figure 22(a)) are used. Table 6 shows the coupler properties used in the OpenSees GCNP model. For comparison, the steel bar properties are also listed. In the fiber section of the grouted coupler segment (see Section S2 in Figure 13(b)), areas of confined concrete that are displaced by the couplers (i.e., each equal to 4.94 in^2) are removed.

Table 6. Properties of Coupler and Steel Bar used in *ReinforcingSteel* nonlinear material

	Yield Stress (ksi)	Ultimate Stress (ksi)	Modulus of Elasticity (ksi)	Strain Hardening Modulus (ksi)	Initial Strain Hardening Strain (in./in.)	Ultimate Strain (in./in.)
Coupler	79.4	110.5	35,179	4,136	0.0033	0.017
Steel Bar	66.8	111.3	29,000	1,247	0.0050	0.090

Similar to the CIP model, we produced the force-displacement curves for the GCNP column. The OpenSees input files for (a) the cyclic push-pull and (b) pushover of the GCNP column are also given in Appendix A. Figure 23 shows the UNR project's experimentally measured and calculated as well as the ISU's calculated hysteretic force-displacement curves for the GCNP column. Figure 24 shows the UNR's measured and calculated average envelope curves and the ISU's calculated curve for the GCNP column.

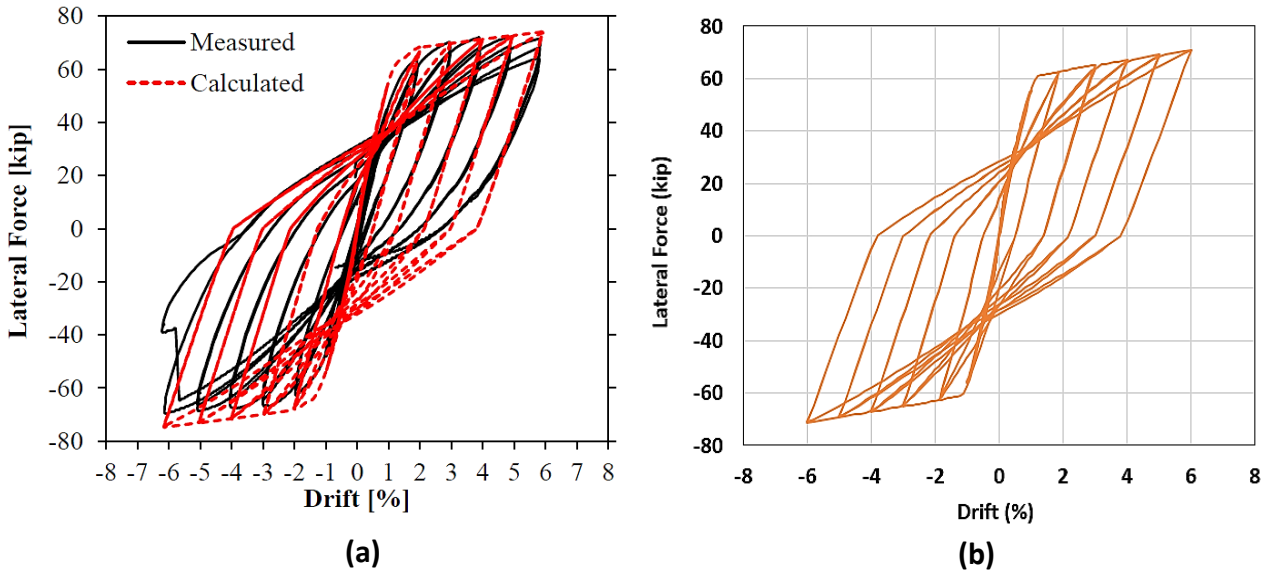

Figure 23. (a) UNR Measured and Calculated and (b) ISU Calculated Hysteretic Force-displacement Curves for the GCNP Column

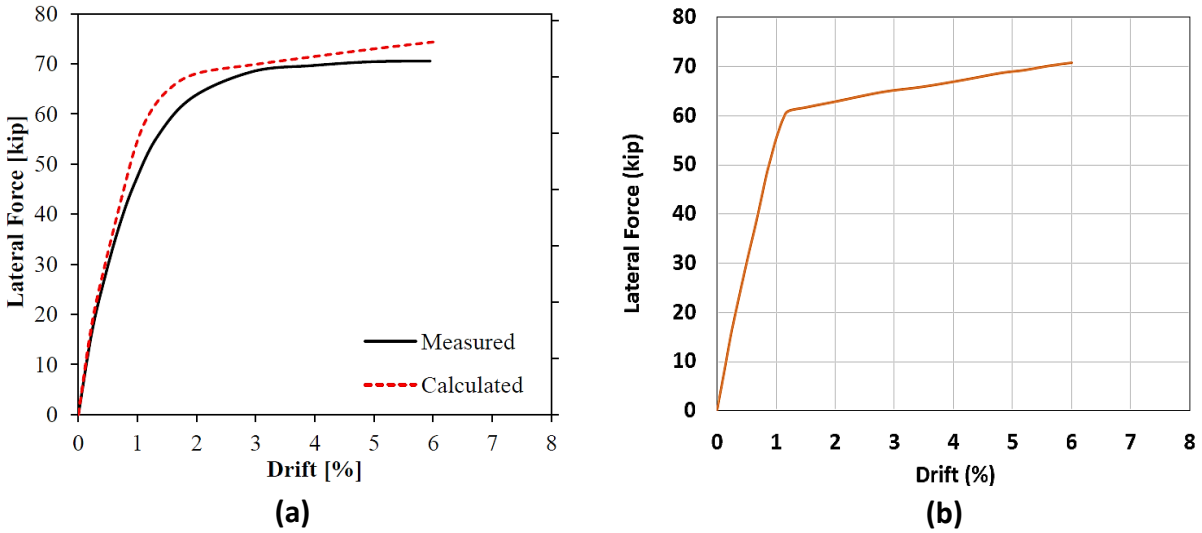

Figure 24. (a) UNR Measured and Calculated Average Envelope Curves and (b) ISU Calculated Curve for the GCNP Column

Discussion

Computer models of both CIP and GCNP columns of the UNR laboratory models were presented in this chapter. The detailed bond-slip procedure and the OpenSees input files are all given in Appendix A. The results of our computer models compare well with both the experimental and analytical results of the UNR project.[1] In addition, it can be observed that for the same drift value, the GCNP column provides more force capacity. For example, at the drift of 6 percent, the force experienced by the CIP column is about 67 kip, while the corresponding force for the GCNP column is over 70 kip. This difference can be explained by examining the data in Table 6. This table compares the properties of bar stress versus coupler strain to that of steel bar stress versus steel strain. When converted to having the same cross-sectional area to that of steel bar (i.e., considering bar stress versus coupler strain), the grouted coupler for No. 8 bar has larger yield strength, larger modulus of elasticity and larger strain hardening modulus compared to those of steel bar. As it will be seen later in Chapter 4, not all grouted coupler sizes have higher initial stiffness compared to their corresponding steel bar. Although strain parameters of all coupler sizes (i.e., strain values at strain hardening and ultimate) have smaller values compared to the corresponding steel bar values.

Chapter 4
Models of Typical Bridges in Idaho

Introduction

This chapter provides the background information for modeling typical highway bridges, followed by details of modeling three bridges suggested by the Idaho Transportation Department (ITD) Bridge Section using OpenSees computer program. Models use cracked linear-elastic columns, cast-in-place (CIP) columns, and precast columns (having the same material properties as CIP columns) with grouted couplers. The final section examines the behavior of single columns with grouted couplers under large drifts.

Background

The sections below present (a) the background information to verify bridge computer modeling using two software and comparing results with those of a Federal Highway Administration (FHWA) design example, (b) the process used by ITD in modeling spring stiffness values of integral abutments, and (c) methods and assumptions in modeling the three Idaho bridges.

Linear-elastic Modeling Verification Using FHWA Bridge Design Example 1

In order to gain confidence in typical highway bridge modeling and to compare results with an existing example, the bridge modeled in the FHWA "*Seismic Design of Bridges Design Example No. 1*" document is used to compare results with those obtained using STAAD and OpenSees programs.[14, 15] As shown in Figure 25, the example bridge is a two-span continuous cast-in-place concrete box girder. Two linear-elastic models of the bridge were analyzed under a 100 kip/ft uniform transverse load. One model uses the "Basic Support Condition" in which the column supports are fixed and the column gross moment of inertia, I_{gross}, is used. The abutments are unrestrained longitudinally and restrained (pinned) in the transverse direction. The second model uses the "Spring Support Condition" in which springs are used at the bases of the columns as well as in the longitudinal and transverse directions at the abutments. The columns are modeled using effective (cracked) moment of inertia, I_{eff}. Both support conditions add a distance equal to half of the footing depth to the length of the columns. Detailed information about the bridge, the computer input files, and results are given in Appendix C. As shown in Tables C2 and C4 of Appendix C, the displacement results obtained from STAAD, OpenSees, and SAP (used by the FHWA Design Example 1 document) matched very well.

Three models were employed for each of the three ITD bridges selected for this study. These are: (a) bridge with linear-elastic cast-in-place columns, (b) bridge with nonlinear cast-in-place columns, and (c) bridge with nonlinear precast columns and grouted couplers. The assumptions for these models will be explained in the Section "Methods and Assumptions in Modeling the Three Idaho Bridges."

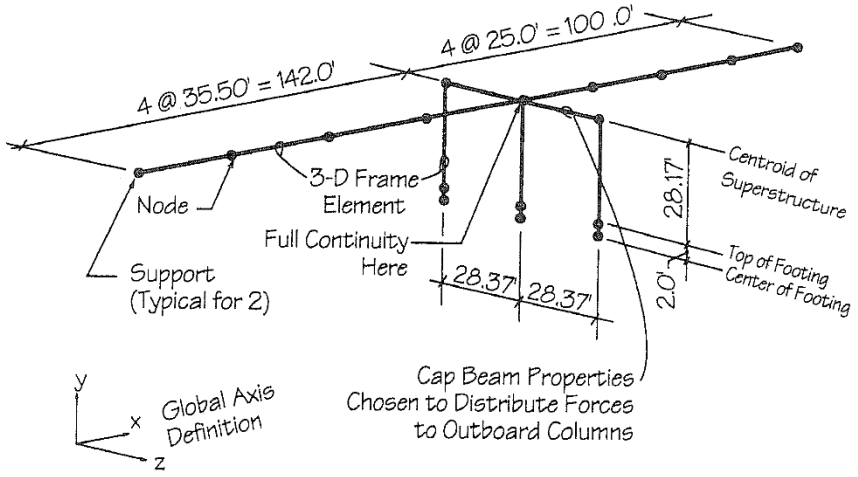

Figure 25. The Two-span Concrete Box Girder Bridge used in the FHWA Design Example 1[14]

Estimating Integral Abutment Stiffness Values

The three bridges considered in this study have integral abutments. The procedures for estimating the bridge transverse and longitudinal abutment stiffness values for bridges with integral abutments are presented in Appendix D. The procedures were developed with input from the ITD Bridge Section. The procedures assume that abutment pile lateral displacement at ground level (depth = 0) versus force is available from the foundation investigation reports. Furthermore, it is assumed that the use of a linear-elastic bridge model with column effective (cracked) moment of inertia, I_{eff}, is acceptable for estimating the abutment stiffness values.

Methods and Assumptions in Modeling the Three Idaho Bridges

Basic Assumptions

In accordance with the request by the project Technical Advisory Committee (TAC), the selected bridges were placed in the most seismically active location in Idaho. We found that Montpelier, located in southeast Idaho, is the most seismically active city in Idaho. In accordance with the TAC request, site soil classification D (stiff soil) was assumed for all three bridges. Using the USGS seismic design map, this combination of conditions gives a design short duration acceleration of S_{DS} = 0.907 and a one-second design acceleration of S_{D1} = 0.486.[16]

For simplicity, the bridges were assumed to have zero skew. Column bases were assumed to be fixed. For the model with cracked linear-elastic columns, the columns were assumed to extend half the footing depth below the top of the footing (as per FHWA Bridge Design Example 1).[14] For the models with nonlinear materials for columns, the actual length of the columns were used, but bond-slip elements were added at the bottom and top of the columns. In addition, in the nonlinear models only the columns were assumed to behave in a nonlinear manner; the superstructure was assumed to be linear-elastic.

Column Sections

For the linear-elastic bridge models (i.e., models with cracked linear-elastic columns), the effective column section properties were obtained using a procedure outlined in Section 5.6 of the AASHTO Guide Specifications for LRFD Seismic Bridge Design.[17] For torsional behavior of columns, 20 percent of torsional stiffness of the columns were used (see AASHTO Guide Specifications for LRFD Seismic Bridge Design Sec. 5.6.5).[17]

For the nonlinear column's bending and axial behavior, there was no need to use the procedure outlined in Section 5.6 of AASHTO Seismic Design Guide. Nonlinear materials were used for the unconfined concrete, confined concrete, and longitudinal steel bars, and in the case of columns with grouted couplers, nonlinear coupler behavior. In the nonlinear models, the torsional behavior was assumed to be linear-elastic. Similar to the linear model, 20 percent of torsional stiffness of the columns was "aggregated" with (i.e., added to) the nonlinear bending and axial effects.

Material Properties in Nonlinear Columns

For longitudinal steel reinforcing bars the appropriate material properties for ASTM A706 steel were used as per Table 8.4.2-1 of the LRFD Seismic Bridge Design Guide.[17] OpenSees *ReinforcingSteel* model was used to model steel stress-strain behavior. It should be noted that ITD is currently using ASTM A615 for longitudinal steel reinforcing. The only difference between ASTM A706 steel and ASTM A615 steel is the ultimate strain value. For the bar sizes that we considered for the Idaho bridges, the ultimate strains are 0.09 for A706 and 0.06 for A615. As it will be seen in the later sections, the most stressed bar is in the Parma bridge with a steel strain of approximately 0.01. Using the ASTM A706 steel in our models will allow us to compare the low-cycle fatigue of steel reinforcing bars. We will predict the number of cycles to fracture of the steel bars for both types of steel.

For unconfined concrete in both cast-in-place column and precast columns (to be used in columns with grouted couplers), the strength of cast-in-place concrete as specified in the bridge plans were used. OpenSees *Concrete01* stress-strain model was used for unconfined concrete. As per Sec. 8.4.4 of the LRFD Seismic Bridge Design Guide, a compressive strain of 0.002 at maximum compressive strength was used. The ultimate unconfined concrete compression strain of 0.005 was used.[17]

For the confined concrete (again, for cast-in-place columns as well as the precast columns to be used with grouted couplers), OpenSees *Concrete04* stress-strain model was used with concrete confined strength and strain values determined by Mander's model (as per Sec. 8.4.4 of the LRFD Seismic Bridge Design Guide).[17, 18]

The experimental data from laboratory tests performed for Splice Sleeve North America, Inc. (2013) were used for grouted coupler stress-strain models. OpenSees *ReinforcingSteel* model was also used here but with grouted coupler material properties. Only the data for No. 11 bar and No. 14 bar couplers were processed since these two bar sizes were used in the bridge models with column grouted coupler connections. The grouted coupler experimental data and the parameters for the stress-strain model are presented in Appendix B.

Method of Seismic Analysis

To keep the analysis simple, the single-mode spectral method was used for all three bridge analyses. Since we are comparing the behavior of two different types of nonlinear columns (cast-in-place columns versus columns with grouted couplers), a more complex analysis is not necessary. In addition, the abutment stiffness values were obtained using the bridge model with cracked linear-elastic columns and the procedure used by ITD (explained above). The same abutment stiffness values were assumed in the bridge models with nonlinear columns.

To obtain the longitudinal and transverse seismic loads, the bridge model with cracked linear-elastic columns was analyzed. This was done by following the single-mode spectral procedure outlined in the FHWA Seismic Design Example 1.[14] The only difference was that, as per ITD Technical Advisory Committee recommendation, column bases were assumed to be fixed.

The same longitudinal and transverse seismic loads obtained from the bridge with cracked linear-elastic columns were also used for the bridge models with nonlinear columns (i.e., one with cast-in-place columns, and the other with precast columns and grouted couplers). In accordance with the LRFD Bridge Seismic Reference Manual (2014), the use of the uniform load method or single-mode method is one of the two options in "nonlinear static analysis."[19] Obviously, the procedure in the "nonlinear static analysis" is much less tedious than the "nonlinear dynamic analysis."

Analysis of Idaho Bridges

Bridge on US-95 over US-20/26 and UPRR at Parma

Bridge Description

The bridge at Parma is a two-span bridge with a three column bent. The skew in the bridge was removed for ease of modeling. The overall dimensions of the bridge were maintained and the bent and abutment lengths were shortened to match the deck width. The superstructure is made up of an 8 in. thick concrete deck that rests on 5 prestressed WF66G girders. The substructure is made up of a pier cap, three columns, and footings all of which are cast-in-place. Figures 26 and 27 show the plan and elevation views of the bridge, respectively. The bridge has a non-integral superstructure-pier connection. Columns are 3.5 ft in diameter with a height of 25.6 ft.

The column reinforcing is shown in Figure 28. The original section with 32 No. 10 steel reinforcing bars were replaced with 16 No. 14 steel bars. This scheme better allows the use of grouted couplers for the bridge with precast columns and grouted couplers. For the model with grouted couplers, 16 SSNA No. 14 U-X couplers were placed at the bottom and the top portions of the columns.

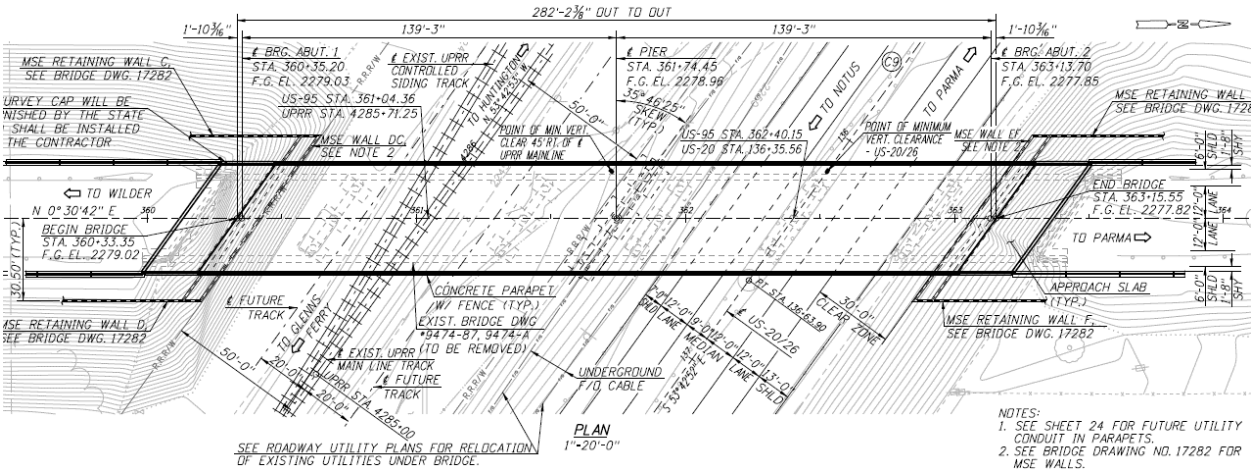

Figure 26. Plan View of US-95 over US-20/26 and UPRR at Parma (NTS)

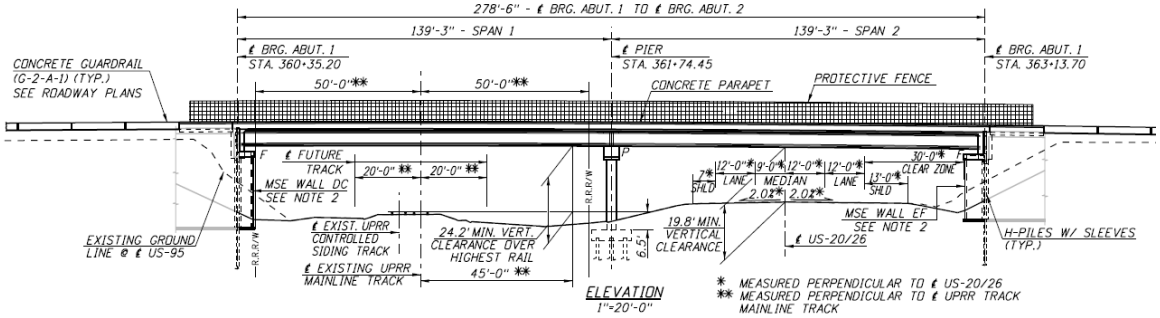

Figure 27. Elevation View of US-95 over US-20/26 and UPRR at Parma (NTS)

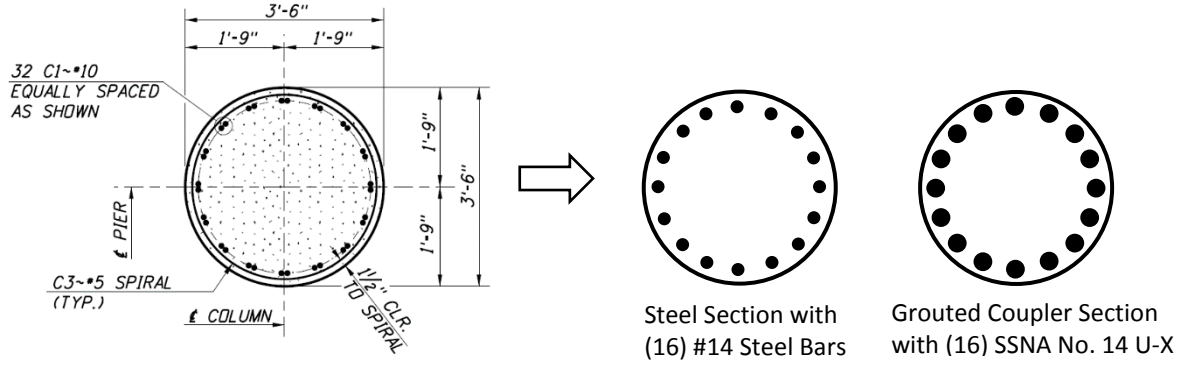

Figure 28. Parma Bridge Column Steel and Grouted Coupler Sections (NTS)

Results of Computer Analyses

Using the iterative method outlined in Appendix D and the model with cracked linear-elastic columns, the bridge integral abutment stiffness values were estimated in the longitudinal and transverse directions. These stiffness values were used in all three models of the bridge. Appendix E presents the

details of bridge seismic load calculations using the single-mode spectral method and the model with cracked linear-elastic columns. As noted above in the section "Method of Seismic Analysis," the same seismic transverse and longitudinal forces were used with the two bridge models with nonlinear columns. The bond-slip moment-rotation values were obtained similar to the approach used to duplicate UNR's bond-slip parameters. The approach is outlined in Appendix A in section "Procedure for Determining Bond-Slip Model Parameters." The bond-slip values for Parma bridge are given in Appendix E, Table E7. Appendix E also presents the schematics of the three computer models, OpenSees input files, and the resulting displacements, column base reactions, and the top of the column drift values. Table 7 shows a summary of the column displacements, drifts, and base reactions at the maximum design load for both transverse and longitudinal loading directions. As it can be seen in Table 7, in all three cases, the displacements, drifts, and reactions for the transverse loading controlled. In the longitudinal direction, because of small displacement, cracked linear-elastic model gives smaller reactions and slightly larger displacement. The column drift was obtained by dividing the displacement by the column height. From Table 7, it can be seen that for the range of loading considered, the nonlinear analysis results of the CIP column and the column with grouted couplers are almost identical.

Table 7. Parma Bridge Displacements, Drifts, and Column Base Reactions

	Column Model		
	Cracked Linear-elastic	**Nonlinear CIP**	**Nonlinear w/ coupler**
Transverse			
Top of Column Displ., ft	0.315	0.376	0.375
Column Drift, %	1.23	1.46	1.46
Col. Base Shear, k	385	271.6	272.4
Col. Base Moment, k-ft	5,440	3,624	3,634
Longitudinal			
Top of Column Displ., ft	0.082	0.081	0.080
Column Drift, %	0.32	0.31	0.31
Col. Base Shear, k	87	97	98
Col. Base Moment, k-ft	1,298	1,347	1,366

Figures 29-33 graphically present some of the key results as related to the Parma bridge. Figures 29 and 30 show the percent of transverse and longitudinal seismic loads versus the top of the column displacement for the three models considered. Figure 31 shows the locations where stress-strain values were measured. Figure 32 shows the stress-strain values for the most stressed steel bars (one under the transverse load and the other under the longitudinal load) in the bridge model with the cast-in-place columns.

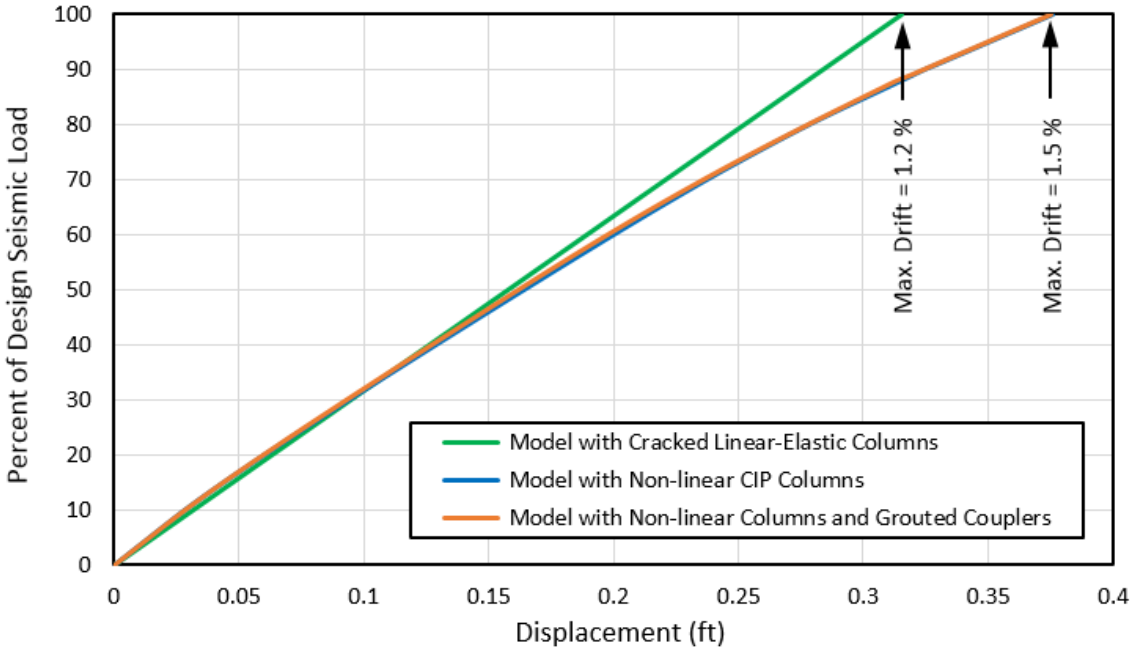

Figure 29. Parma Bridge Column Displacements/Drifts under Transverse Load

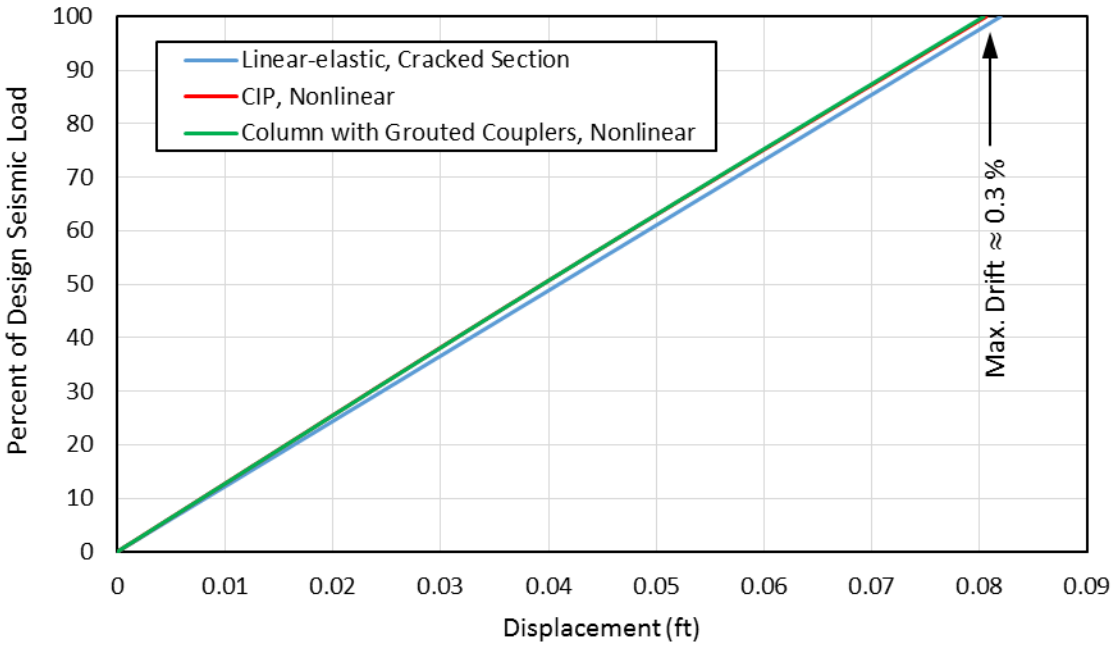

Figure 30. Parma Bridge Column Displacements/Drifts under Longitudinal Load

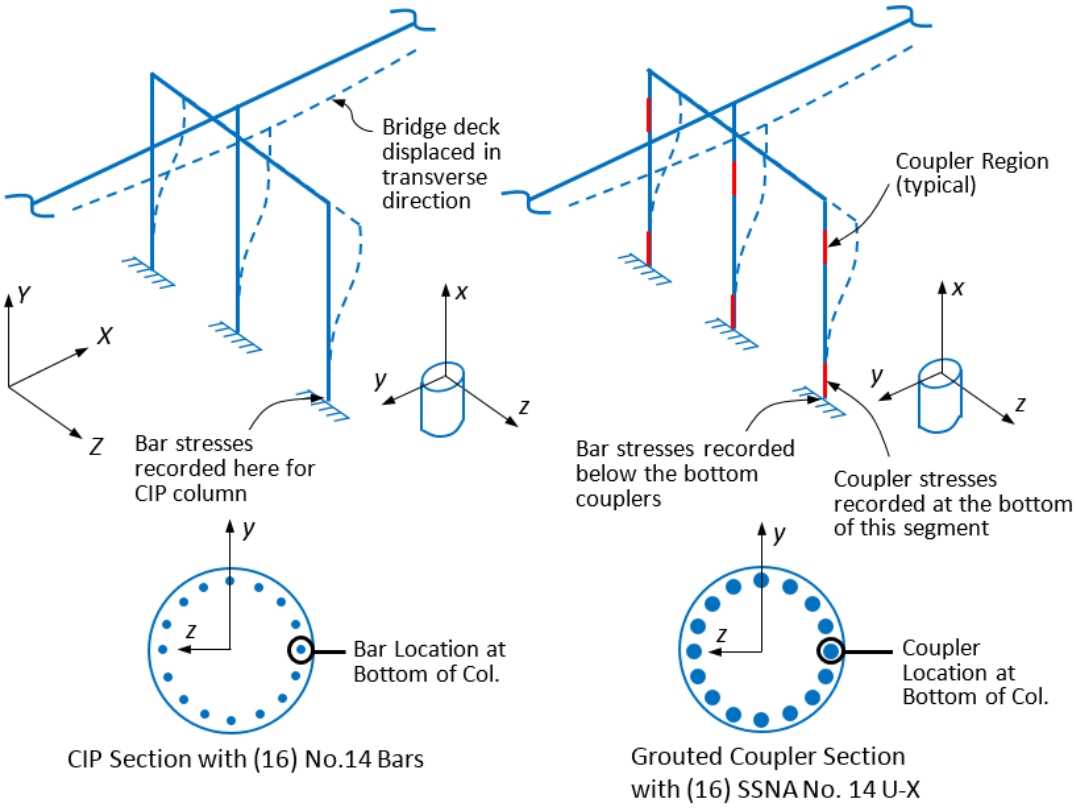

Figure 31. Stress-strain Locations: Left CIP Column, Right Column with Couplers

Figure 33 shows the stress-strain values in the most stressed steel bar and grouted coupler in the bridge model with precast columns and grouted couplers. The lower curve of Figure 33 gives the impression that the coupler itself yields. This is not the case. The coupler region includes small portions of steel bar at the top and bottom (see Figures 15, 22 (b) and 22(c) in Chapter 2). The yielding of the steel in the coupler region causes this apparent "yielding". The maximum stresses at the top and bottom of the columns are the same. This is because in our model we used a very stiff column cap beam (i.e., having large moment of inertia for bending under the transverse and longitudinal loads). Stresses in Figures 32 and 33 correspond to the bottom of the column. As shown in Figure 31, the coupler stress is measured at the bottom of the bottom coupler, while the steel stress is measured right below the bottom coupler (i.e., at the interface of the column and the footing). It should also be noted that the strains and stresses in the steel bar of the CIP column were almost the same as the corresponding values of the steel in the column with grouted couplers. In Figures 32 and 33, the strain and stress values in the steel bars under transverse loading are (0.0117, 72.9 ksi) and (0.0121, 73.2 ksi), respectively.

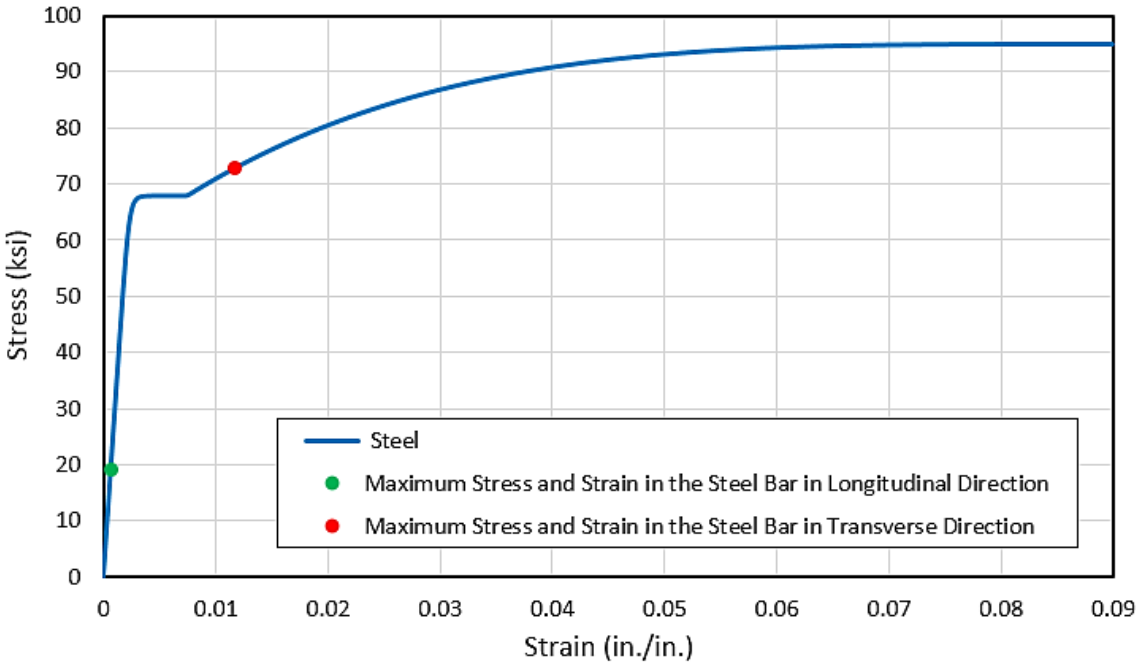

Figure 32. Parma Bridge Stress-strain Values in the Most Stressed Steel Bar in the CIP Column

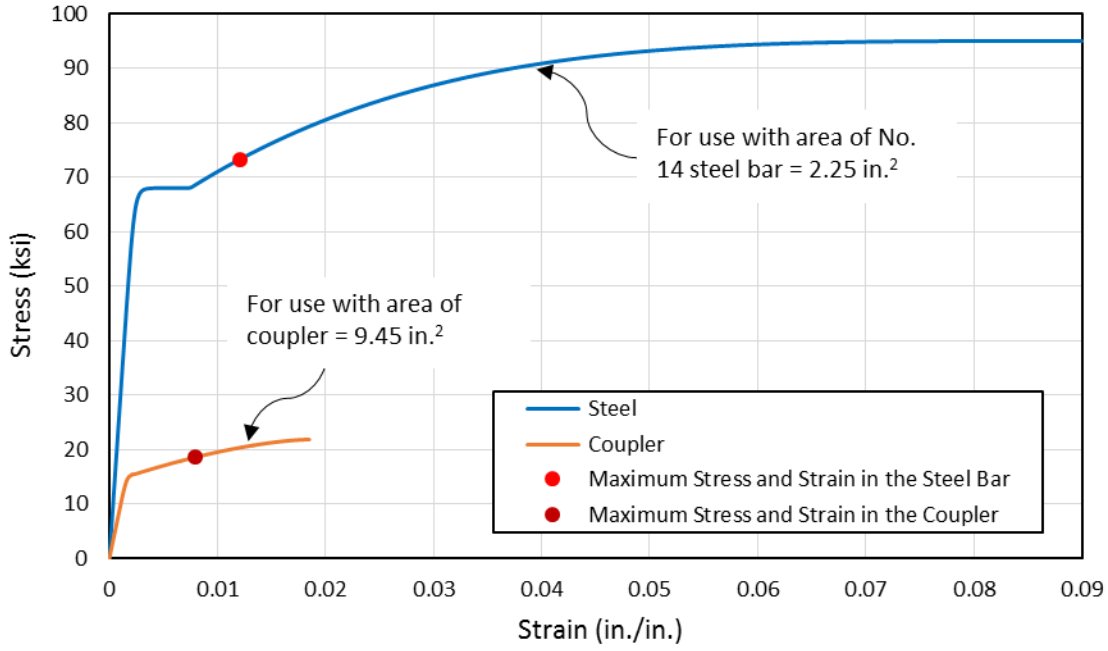

Figure 33. Parma Bridge Stress-strain Values in the Most Stressed Steel Bar and Grouted Coupler in the Column with Grouted Couplers under Transverse Loading

Bridge on SH-22 over I-15 at Dubois

Bridge Description

The bridge on SH-22 over I-15 at Dubois is a two-span bridge with a four-column bent. The superstructure is made up of an 8-in. thick concrete deck that rests on eight steel girders. The substructure is composed of the pier cap, four columns, and footings all cast-in-place (CIP). Figures 34 and 35 show the plan and elevation views of the bridge, respectively. This bridge also has a non-integral superstructure-pier connection. The Columns are 3.5 ft in diameter with a height of 14.05 ft.

The column reinforcing is shown in Figure 36. The column section has 13 No. 11 steel reinforcing bars. For the model with grouted couplers, 13 SSNA No. SNX 11 couplers were placed at the bottom and top portions of the columns.

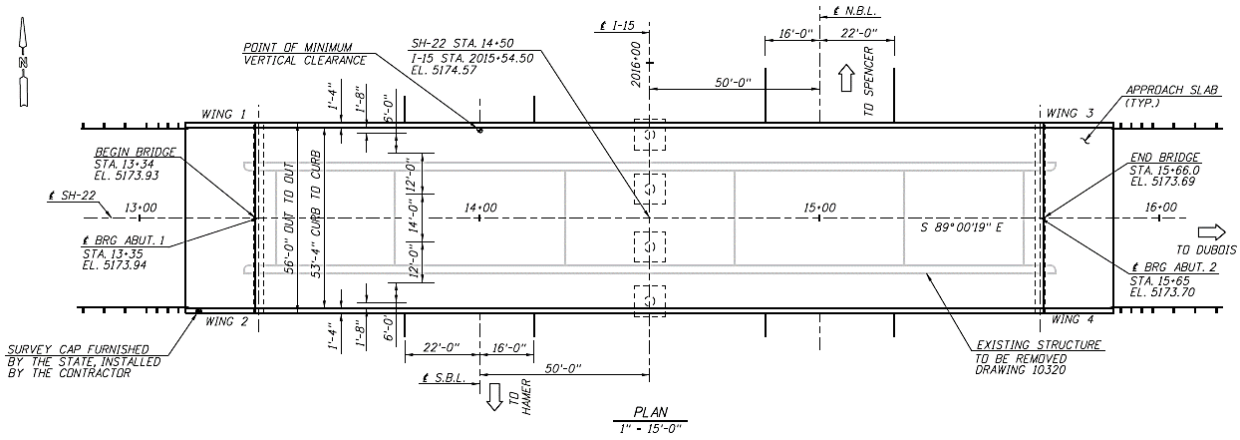

Figure 34. Plan View of the SH-22 over I-15 Bridge at Dubois (NTS)

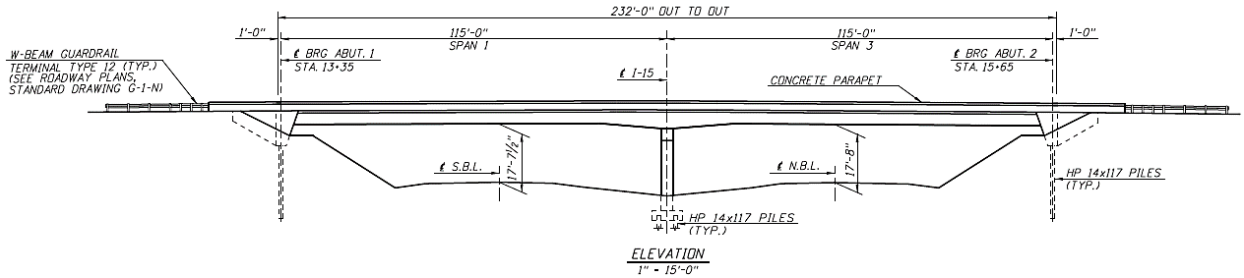

Figure 35. Elevation View of the SH-22 over I-15 Bridge at Dubois (NTS)

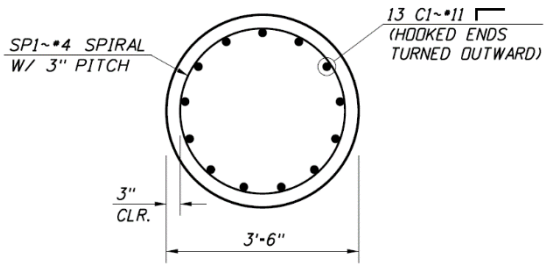

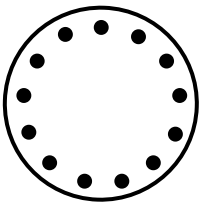

Grouted Coupler Section
with (13) SSNA No. SNX 11

Figure 36. Dubois Bridge Column Steel and Grouted Coupler Sections (NTS)

Results of Computer Analyses

The same process of data analysis used for the bridge at Parma was also used for the Dubois bridge. Appendix E presents the schematics of the three computer models and the output displacements, column base reactions, and the top of the column drift values. For brevity, the OpenSees input files are not given in Appendix E for the Dubois bridge. The ends of the column bond-slip values are given in Appendix E, Table E22. Table 8 shows a summary of the column displacements, drifts, and base reactions at the maximum design load for both transverse and longitudinal directions. In all three cases, the displacements, drifts, and reactions for the transverse loading controlled. The nonlinear analysis results of the CIP column and the column with grouted couplers are very similar.

Table 8. Dubois Bridge Displacements, Drifts, and Column Base Reactions

	Column Model		
	Cracked Linear-elastic	**Nonlinear CIP**	**Nonlinear w/ coupler**
Transverse			
Top of Column Displ., ft	0.080	0.117	0.123
Column Drift, %	0.57	0.830	0.877
Col. Base Shear, k	347	245.3	245.1
Col. Base Moment, k-ft	2,802	1,749	1,747
Longitudinal			
Top of Column Displ., ft	0.036	0.035	0.035
Column Drift, %	0.26	0.25	0.25
Col. Base Shear, k	109	118	117
Col. Base Moment, k-ft	1,011	991	981

Figures 37 and 38 graphically present the key stress-strain results as related to the Dubois bridge. Figure 37 shows the stress-strain values for the most stressed steel bars (one under the transverse load and the other under the longitudinal load) in the bridge with the cast-in-place columns. Figure 38 shows the stress-strain values in the most stressed steel bar and grouted coupler in the bridge model with precast columns and grouted couplers. Similar to Parma's bridge, the maximum stresses at the top and bottom of the columns were the same. Again, the strains and stresses in the steel bar of the CIP column were almost the same as the strain and stress values of the steel in the column with grouted couplers.

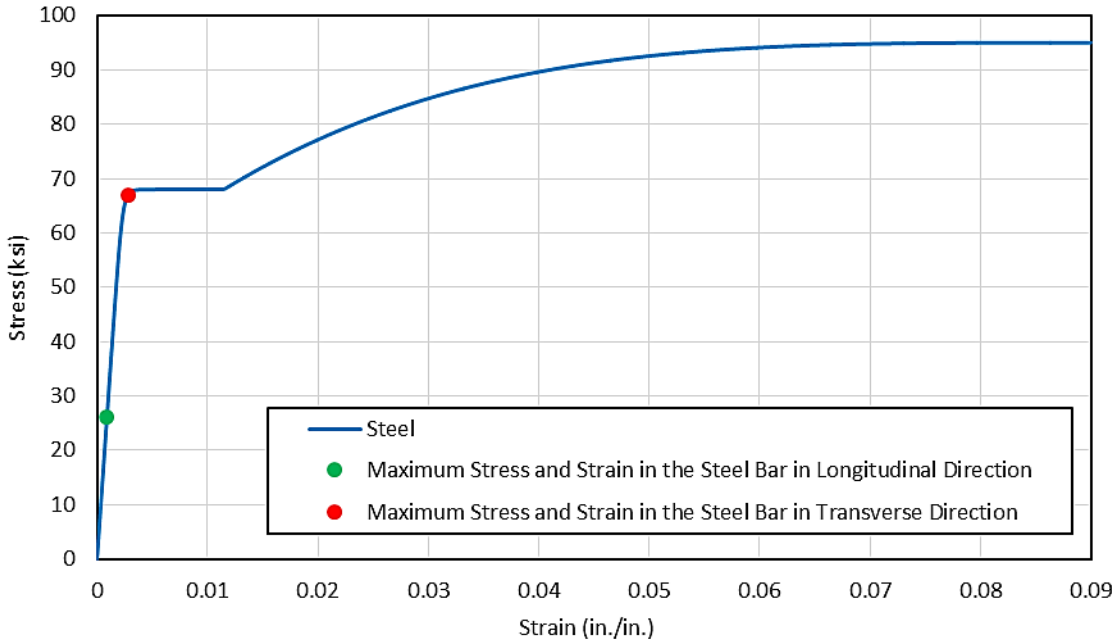

Figure 37. Dubois Bridge Stress-strain Values in the Most Stressed Steel Bar in the CIP Column

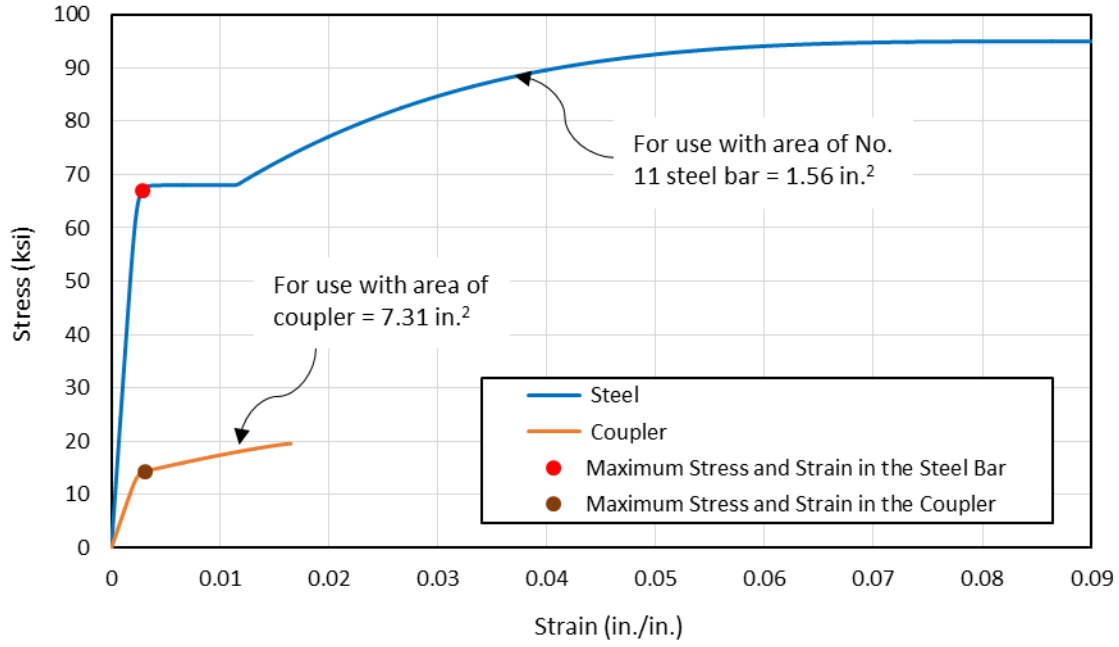

Figure 38. Dubois Bridge Stress-strain Values in the Most Stressed Steel Bar and Grouted Coupler in the Column with Grouted Couplers under Transverse Loading

Bridge on SH-75 over Salmon River East of Clayton

Bridge Description

The bridge over the Salmon River east of Clayton is a 260 foot three-span bridge with two piers located 90 ft and 210 ft from the southwest end of the bridge. The skew in the bridge was removed to make it easier to model. The overall dimensions of the bridge were maintained and the pier cap and abutment lengths were shortened to match the deck width of 43.5 ft. The superstructure is made up of 8-½ in. precast deck panels and five 72 in. prestressed bulb-tee girders. The substructure has a pier cap and a single oval column on a cast-in-place footing in each pier. The pier caps and columns are made of precast concrete. Grouted couplers were used to connect the columns to the footing.

Figures 39 and 40 show the plan and elevation views of the bridge, respectively. The column reinforcing is shown in Figure 41. The column cross-sections have the same oval shape with major and minor dimensions of 9.5 ft by 3.5 ft. The length of the southwest and northeast columns are 15.47 ft and 15.97 ft, respectively. When the skew was removed, the columns were rotated such that under the bridge transverse loading the columns bend about the strong axis (i.e., about the minor axis). And, when loaded in the longitudinal direction, the columns bend about the weak axis (i.e., about the major axis).

As shown in Figure 42, the columns are reinforced with 34 No. 11 bars within four overlapping No. 5 spirals in the main part of the column. The spiral reinforcing has a 4 in. pitch. Figure 43 shows the close-up view of a column showing grouted coupler locations. There are 34 splice sleeves within five sets of four No. 5 hoops as shown in Figures 41-43. Because of the use of grouted couplers, the columns have more cover over the steel reinforcing bars. When modeling the equivalent cast-in-place model of the columns, we used the same cover thickness as when modeling the column with grouted couplers. Since we had data available for grouted couplers for No. 11 bar (i.e., for SSNA No. SNX 11), we used this coupler in the column model with couplers.

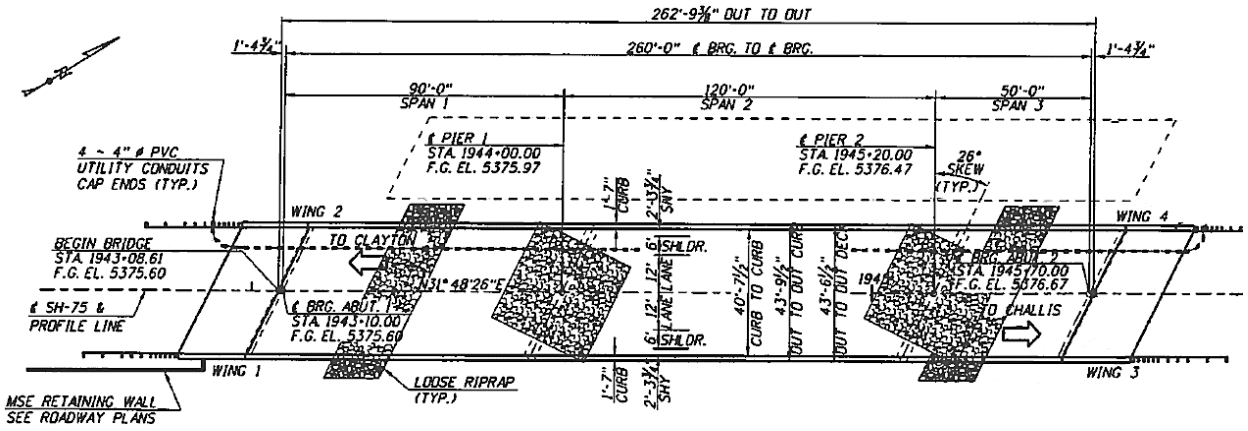

Figure 39. Plan View of the Bridge on SH-75 over Salmon River (NTS)

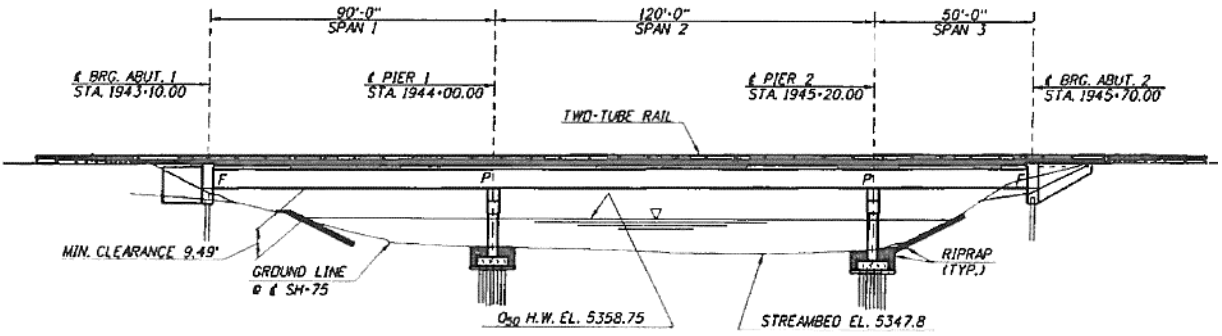

Figure 40. Elevation View of the Bridge on SH-75 over Salmon River (NTS)

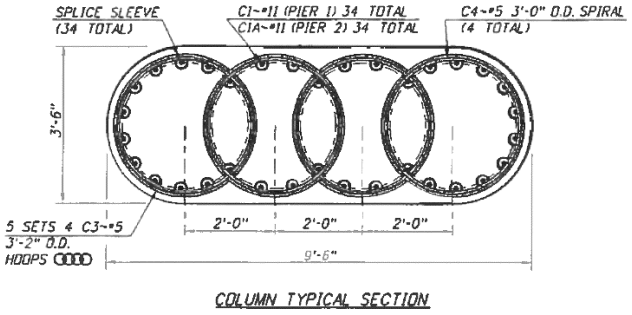

Figure 41. Salmon River Bridge Column Section with Steel and Grouted Coupler Locations (NTS)

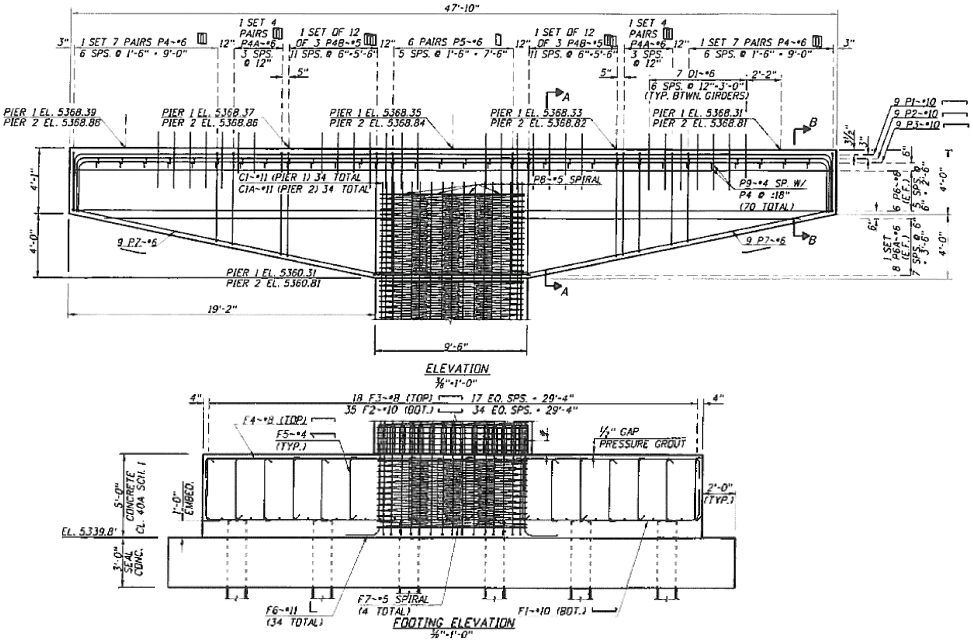

Figure 42. Salmon River Bridge Column Cap, Column, and Footing Elevation Views (NTS)

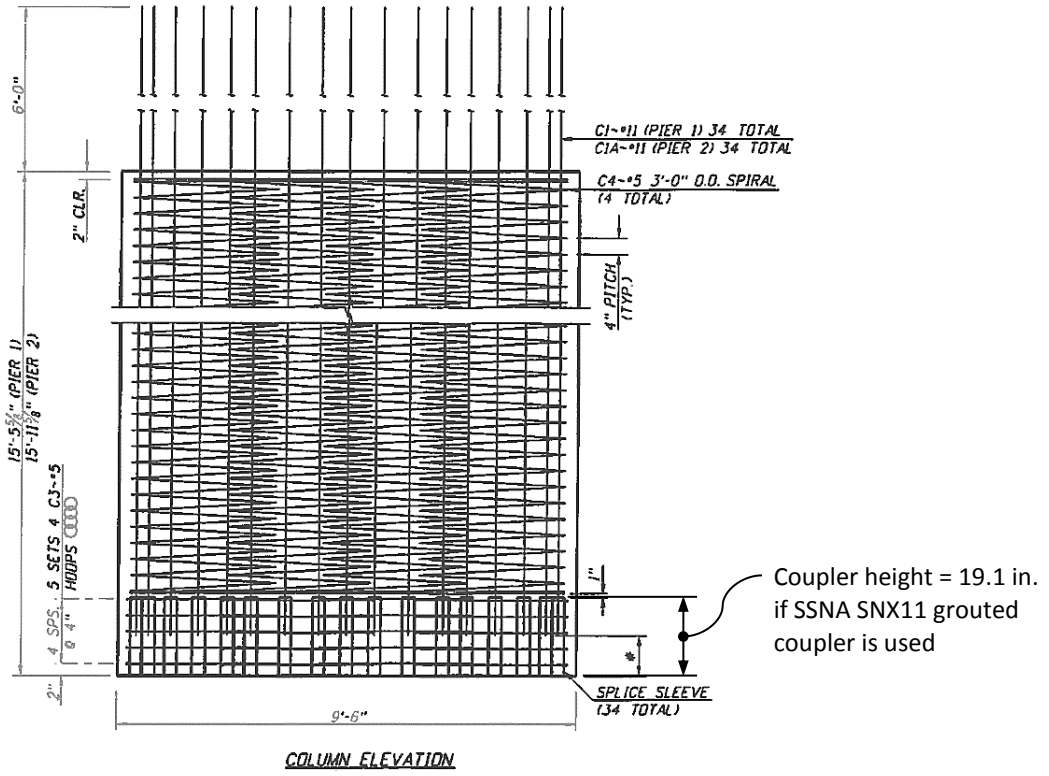

Figure 43. Salmon River Bridge Close-up View of a Column Showing Grouted Coupler Locations (NTS)

Verification of Column Modeling and Deck Torsional Rigidity

Because of the complexity of the column's oval cross-section, for the nonlinear models we made simplifying assumptions. As shown in Figure 44, the confined concrete was assumed to be composed of two half circular areas and a rectangle. The unconfined concrete was assumed to have the same thickness all around the confined concrete. As shown in Appendix E, several verifications were made to ensure proper modeling of the composite cross-section. The verification results are summarized in Table E37.

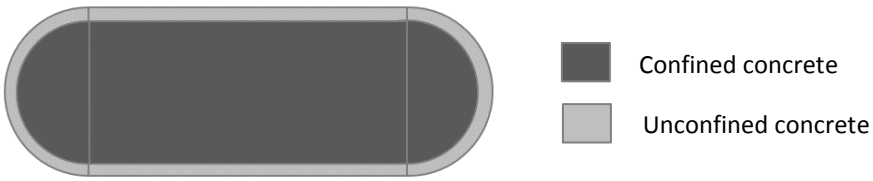

Figure 44. Simplifying Assumption for Column Confined and Unconfined Concrete

In addition, unlike the two previous bridge models (i.e., multi-column bents with rigid column caps), we observed that the torsional rigidity of the deck significantly affects the Salmon River bridge column

displacements. For this reason we followed AASHTO LRFD Specifications' recommended approach for estimating the deck torsional moment of inertia by using the Specifications' Eq. C 4.6.2.2.1-2.[20]

Results of Computer Analyses

The same process of data analysis used for the previous two bridges was also used for the Salmon River Bridge. Appendix E presents the schematics of the three computer models and the output displacements, column base reactions, and the top of the column drift values. For brevity, the OpenSees input files are not given in Appendix E for the Salmon River bridge. The ends of the column bond-slip values are given in Appendix E, Table E38. Table 9 summarizes the results of column displacement, drifts, and the base reactions at the maximum design load for both transverse and longitudinal directions for the southwest column. Although the southwest column is slightly shorter than the northeast column, it carries more of the deck tributary load. For this reason, in the transverse direction, the top of the southwest column experiences slightly more displacement. In the longitudinal direction, because of small displacements, the cracked linear-elastic model overestimates the drifts and underestimates the column reactions. The nonlinear analysis results of the CIP column and the column with grouted couplers are almost identical.

Table 9. Salmon River Bridge Displacements, Drifts, and Base Reactions for the Southwest Column

	Column Model		
	Cracked Linear-elastic	**Nonlinear CIP**	**Nonlinear w/ coupler**
Transverse			
Top of Column Displ., ft	0.063	0.072	0.071
Column Drift, %	0.41	0.47	0.46
Col. Base Shear, k	679	553	551
Col. Base Moment, k-ft	20,560	15,312	15,241
Longitudinal			
Top of Column Displ., ft	0.036	0.034	0.034
Column Drift, %	0.23	0.22	0.22
Col. Base Shear, k	363	433	423
Col. Base Moment, k-ft	3,556	3,691	3,617

Figures 46 and 46 show the stress-strain values in the most stressed steel bar and grouted coupler at the bottom portion of the column in the bridge model with precast columns and grouted couplers in the southwest and northeast columns under transverse and longitudinal loading, respectively. As expected, in this bridge maximum stresses occurred at the bottom of the columns. Again, the strains and stresses in the steel bar of the CIP column were almost the same as the strain and stress values of the steel in the columns with grouted couplers. Stresses and strains under the transverse loading controlled.

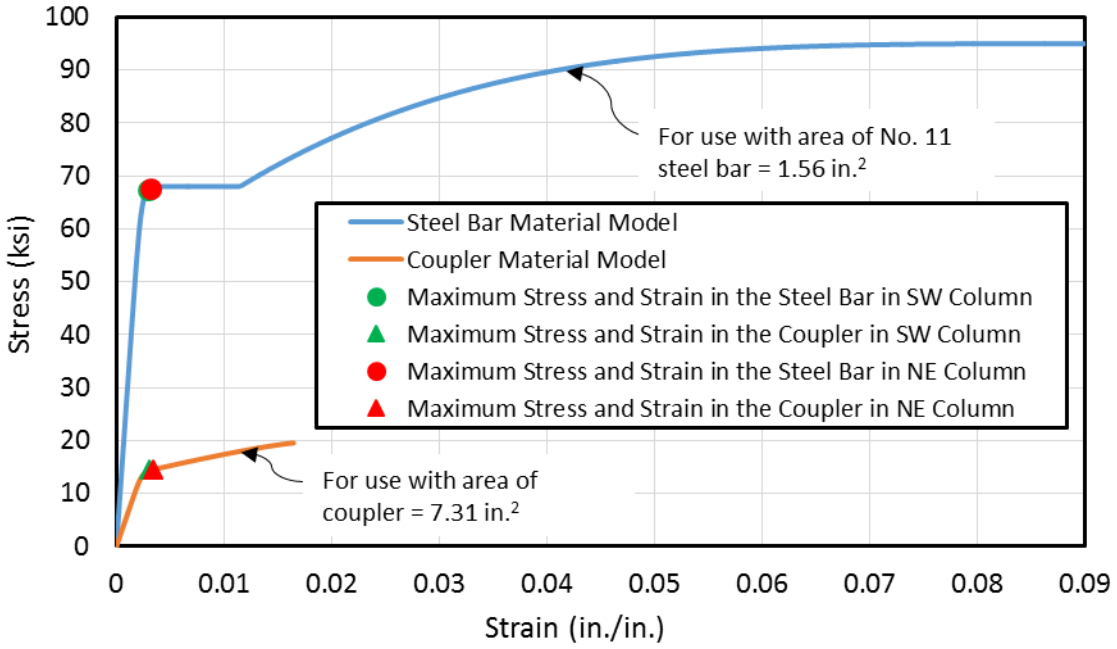

Figure 45. Salmon River Bridge Stress-Strain Values in the Most Stressed Steel Bar and Grouted Coupler in the Column with Grouted Couplers under Transverse Loading

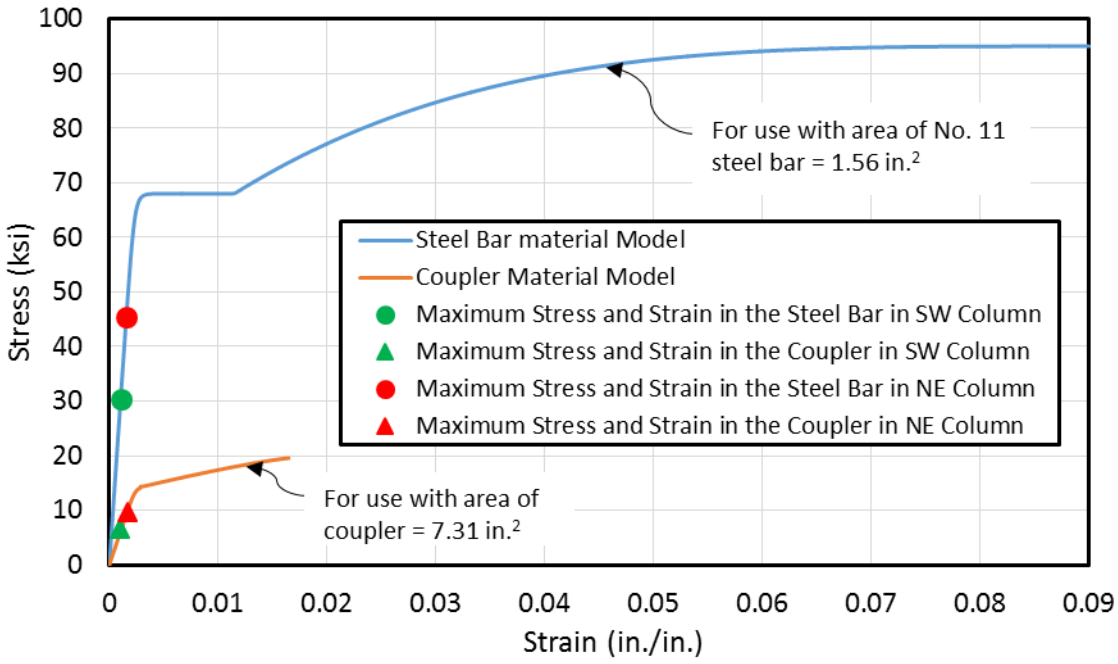

Figure 46. Salmon River Bridge Stress-Strain Values in the Most Stressed Steel Bar and Grouted Coupler in the Column with Grouted Couplers under Longitudinal Loading

Comparison of Results with AASHTO Guide Specifications for LRFD Seismic Bridge Design

In this section, we will compare the displacement/drift results with the displacement/drift capacity and demand as per AASHTO Seismic Guide Specifications.[17] The three bridges considered for this study were placed in the most seismically active location in Idaho with soil Site Class D. Using the USGS seismic design map (see Appendix E, Figure E7), this combination of conditions results in a design short duration acceleration of S_{DS} = 0.907 and a design one-second acceleration of S_{D1} = 0.486. According to the Seismic Guide Table 3.5-1, S_{D1} of 0.486 (i.e., in the range of $0.30 \leq S_{D1} \leq 0.50$) places the structure in Seismic Design Category (SDC) C.[17]

Using the approximate equation given in Seismic Guide Articles 4.8.1 for Type 1 structure (ductile substructure with essentially elastic superstructure) in SDC C, the displacement capacity, Δ_C, in inches is:

$$\Delta_C = 0.12\, H_o\{-2.32 \ln(x) - 1.22\} \geq 0.12\, H_o$$

Figure 47. AASHTO Seismic Guide Displacement Capacity Equation for Type 1 Structure in SDC C

Where, $x = {\Lambda B_o}/{H_o}$, $H_o =$ clear column height in ft, $B_o =$ column diameter in ft, and $\Lambda =$ end restraint factor ($\Lambda = 2.0$ for fixed top and bottom and $\Lambda = 1.0$ for fixed-free).

The displacement demand may be obtained through elastic analysis and multiplied by displacement magnification factor, R_d, as per Seismic Guide's Article 4.3.3 and used with combination of orthogonal seismic displacements as per Seismic Guide's Article 4.4. Since the transverse displacement is larger in all of our bridge models, we need to use 100% of transverse displacement with 30% of longitudinal displacement. The demand becomes:

$$\Delta_{D,\ Linear\ Magnified} = \left(R_d\, \Delta_{D,\, Linear}\right)_T + 0.3\left(R_d\, \Delta_{D,\, Linear}\right)_L$$

Figure 48. Displacement Demand Using Elastic Analysis and Orthogonal Combination

Where, $\Delta_{D,\ Linear\ Magnified}$ = magnified displacement demand through linear-elastic analysis, $\left(R_d\, \Delta_{D,\, Linear}\right)_T$ = magnified transverse displacement demand, and $\left(R_d\, \Delta_{D,\, Linear}\right)_L$ = magnified longitudinal displacement demand. R_d is obtained as follows:

$$R_d = \left(1 - \frac{1}{\mu_D}\right)\frac{T^*}{T} + \frac{1}{\mu_D} \geq 1.0 \text{ for } \frac{T^*}{T} > 1.0$$

Figure 49. Equation for Magnification Factor for *T*/T* > 1

$$R_d = 1.0 \text{ for } \frac{T^*}{T} \leq 1.0$$

Figure 50. Equation for Magnification Factor for *T*/T ≤ 1*

Where, $T^* = 1.25T_s$, μ_D= maximum local member displacement demand = 3.0 for SDC C, and $T_s = \frac{S_{D1}}{S_{DS}}$.

Alternatively, one may use the transverse and longitudinal displacements obtained through nonlinear analysis. With the combination of orthogonal displacements, the nonlinear demand becomes:

$$\Delta_{D,\ Nonlinear} = \left(\Delta_{D,\,Nonlinear}\right)_T + 0.3\left(\Delta_{D,\,Nonlinear}\right)_L$$

Figure 51. Displacement Demand Using Nonlinear Analysis and Orthogonal Combination

Where, $\Delta_{D,\ Nonlinear}$ = displacement demand through nonlinear analysis, $\left(\Delta_{D,\,Nonlinear}\right)_T$ = transverse nonlinear displacement demand, and $\left(\Delta_{D,\,Nonlinear}\right)_L$ = longitudinal nonlinear displacement demand.

Following the above steps, Table 10 summarizes the displacement demand and capacity of the three bridge columns considered.

Table 10. Displacement and Drift Capacity versus Demand for Bridge Columns

	Parma	Dubois	Salmon River
Capacity			
H_o, ft	25.60	14.05	15.47
B_o, ft	3.5	3.5	9.5[b]
Δ_C, ft	0.458	-[a]	0.155
Drift = Δ_C/H_o, %	1.79	-[a]	1.00
Demand, Magnified Linear-elastic Analysis			
Transverse R_d	1.149	1.711	1.420
Longitudinal R_d	1.632	2.077	2.051
$\Delta_{D,\ Linear\ Magnified}$, ft	0.402	0.159	0.112
Drift = $\left(\Delta_{D,\ Linear\ Magnified}\right)/H_o$, %	1.57	1.13	0.72
Demand, Nonlinear Analysis			
$\Delta_{D,\ Nonlinear}$, ft	0.400	0.128	0.082
Drift = $\left(\Delta_{D,\ Nonlinear}\right)/H_o$, %	1.56	0.91	0.53

[a] LRFD Bridge Seismic Guide Article 4.8.1 equations may only be used for clear heights greater than or equal to 15 ft.
[b] Using the transverse direction, thus the major dimension of the oblong cross-section is used.

As it can be seen from Table 10, the drift demand for Parma, Dubois, and Salmon River bridge columns estimated using the magnified linear-elastic approach are 1.57 percent, 1.13 percent, and 0.72 percent, respectively. The corresponding values obtained through nonlinear approach (either for CIP column or column with grouted couplers) are 1.56 percent, 0.91 percent, and 0.53 percent, respectively.

Discussion on the Results of Idaho Bridge Modeling

The Seismic Design Category C is perhaps the highest category that any location in Idaho will experience. Although none of the bridges were designed for this seismic condition, all three bridge columns performed well. The stresses in both the longitudinal reinforcing bars and grouted couplers were well within acceptable range. Only the steel bar in the Parma bridge went slightly into the strain hardening region (see Figures 32 and 33). In addition, the displacement/drift behavior of all three bridges were almost identical when comparing the results of bridge models with cast-in-place columns with the results of bridge models having precast columns and grouted couplers. Furthermore, using nonlinear analysis, all three bridges had low drift values. The highest drift is in the transverse direction of the Parma bridge at about 1.5 percent (and about 1.6 percent when combination of orthogonal displacements is used). Recall that the University of Nevada, Reno's laboratory experiments showed that up to about 2 percent drift there is no significant difference between the cast-in-place column and the GCNP (Grouted Coupler with No Pedestal) column force-displacement envelopes (see Figure 6 in Chapter 2). In addition, as shown in Table 10, AASHTO Seismic Guide's approximate relations for estimating the magnified linear-elastic displacement/drift demand result in either the same or larger values (i.e., more conservative) than the corresponding displacements/drift demand values obtained through nonlinear analysis.

Analysis of Single Columns with Grouted Couplers under Large Drifts

Introduction

In accordance with the request of the ITD Technical Advisory Committee, next we considered two columns with grouted couplers at top and bottom; one from Parma bridge and one from Dubois bridge to examine coupler and steel reinforcing bar behavior under large drifts. Each column was analyzed under fixed-fixed (fixed at the bottom; top free to translate, but rotation prevented) boundary conditions. Using fixed-fixed boundary conditions seems more appropriate (and a conservative assumption) for columns in a multi-column bent with a rigid cap beam. The loading is as shown in Figure 52. The columns were pushed horizontally until the grouted coupler failure was observed.

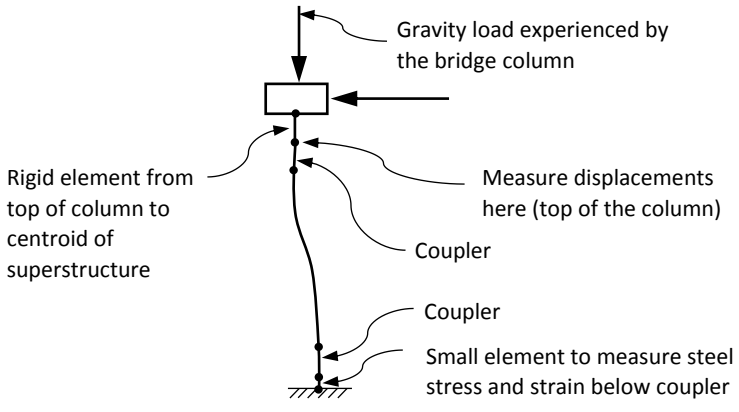

Figure 52. Single Column with Fixed-fixed Boundary Conditions

In addition, the number of "half cycles" to fatigue failure of the Grade 60 steel were determined for both ASTM A706 and ASTM A615 rebars. This is because experimental results of University of Nevada, Reno clearly indicate that low-cycle fatigue failure (i.e., under large strain) of steel rebar is a possible mode of column failure. Before the results of the single columns of Parma and Dubois are presented, a brief background is provided on the low-cycle fatigue of steel reinforcing bars.

Low Cycle Fatigue in Steel Reinforcing Bars

The failure of longitudinal bars in concrete columns during a seismic event is influenced by the low cycle fatigue behavior of steel. The fatigue model proposed by Koh and Stephens (1991) developed relationships between the total strain amplitude and the number of "half cycles" to failure ($2N_f$).[21] Figure 53 illustrates the idea of a simple constant amplitude strain history. Note that $2N_f$ is referred to as the number of half cycles, thus N_f is the number of full cycles.

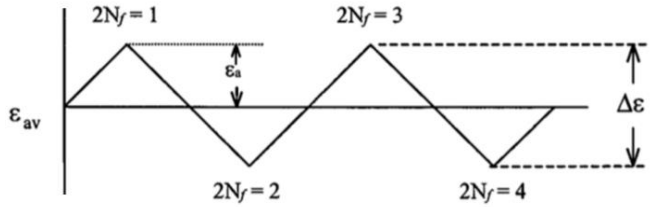

Figure 53. Simple Constant Amplitude Strain History[22]

Brown and Kunnath (2000) and Zhou, et al. (2008) followed the same approach of fatigue strain-life relationship and developed fatigue curves for No. 6, No. 7, No. 8 rebars.[22, 23] For No. 8 steel bar, Haber, et al. (2013) summarized the fatigue data for ASTM A615 and ASTM A706 Grade 60 bars as shown in Figures 54 and 55.[1] Brown and Kunnath and Zhou, et al. did not have data for No. 11 bars (used in the Dubois bridge) and No. 14 bars (used in the Parma bridge). Here, it is assumed that the low-cycle fatigue curves obtained for No. 8 bars shown in Figures 54 and 55 are appropriate for No. 11 and No. 14 bars.

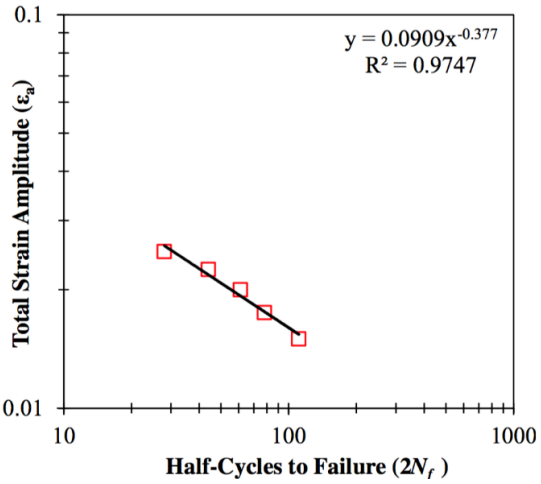

Figure 54. Data Reported by Brown and Kunnath for No. 8 A615 Gr. 60 Bars[1]

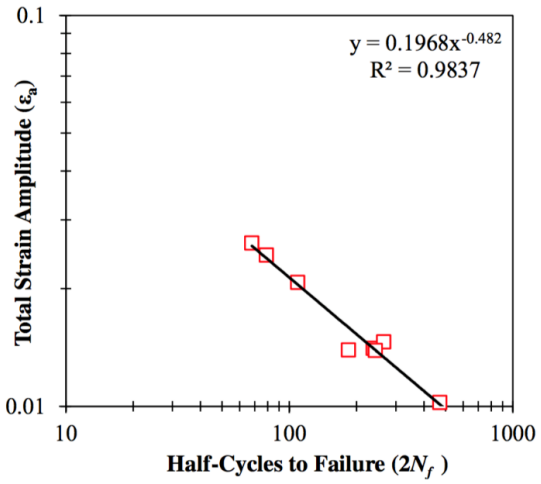

Figure 55. Data Reported by Zhou et al. for No. 8 A706 Gr. 60 bars[1]

Single Column from Parma Bridge

Figure 56 shows the moment reaction at the base of column versus displacement for a single column from the Parma bridge. In addition to the curve for the nonlinear column with grouted couplers at top and bottom of the column (see Figure 52), the curves for cracked linear-elastic column and nonlinear cast-in-place (CIP) column are also shown in Figure 56. For the nonlinear columns, the points where the steel or the coupler at the extreme location failed (i.e., reached their ultimate values) are noted. Note that in OpenSees once the fiber material (steel or coupler) reaches its ultimate values, the stress remains constant while the strain increases. The displacement in column with grouted coupler corresponding to failure of the SSNA No. 14 U-X grouted coupler (used in the Parma bridge model) and ASTM A615 steel are 1.126 ft and 1.237 ft, respectively. With the column being 25.6 ft in length, these displacements correspond to drift values of 4.4 percent and 4.8 percent, respectively. Table 11 shows the stress and strain values in the most stressed coupler and steel bar and the number of half cycles for steel bar fatigue failure for the column in the Parma bridge.

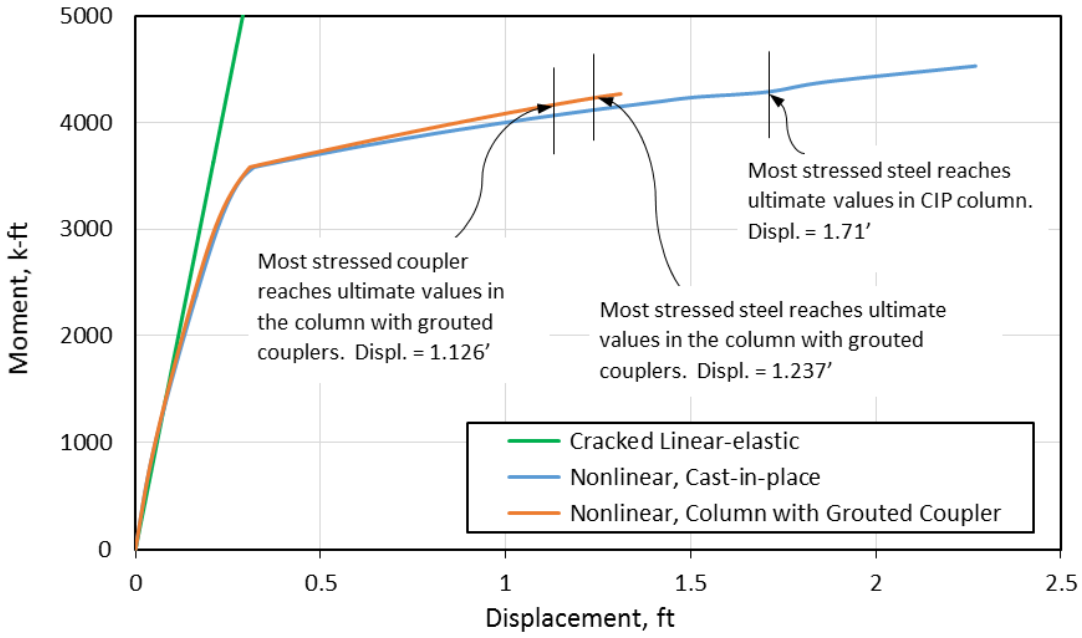

Figure 56. Parma Fixed-fixed Column Base Moment versus Top of Column Displacement

Table 11. Stress and Strain in Coupler Region and Steel Bar and Number of Half Cycles for Steel Bar Fatigue Failure for Parma Fixed-fixed Column with Grouted Couplers

Column Nonlinear Drift, %	Coupler Region		Steel Bar		No. of Half Cycles to Fatigue Failure of Grade 60 Steel Rebar	
	Stress, ksi	Strain, in./in.	Stress, ksi	Strain, in./in.	ASTM A706	ASTM A615
0.25	4.50	0.0005	16.32	0.0006	-	-
0.5	11.25	0.0012	43.40	0.0015	-	-
0.75	15.40	0.0021	65.16	0.0025	-	-
1	16.65	0.0044	67.99	0.0045	-	-
1.5	18.59	0.0080	73.51	0.0123	315	201
2	19.21	0.0094	76.78	0.0156	192	107
2.5	19.88	0.0110	80.14	0.0195	121	59
3	20.50	0.0126	83.14	0.0236	81	36
3.5	21.08	0.0144	86.12	0.0285	55	22
4	21.56	0.0165	88.64	0.0338	39	14
4.4	21.80[a]	0.0185[a]	90.43	0.0386	29	10
4.5	-	-	90.95	0.0402	-	-
4.8	-	-	95.00[b]	0.06[b]	-	-
4.9	-	-	95.00[c]	0.09[c]	-	-

[a] Ultimate stress and strain values for SSNA No. 14 U-X grouted coupler
[b] Ultimate stress and strain values for ASTM A615 Grade 60 steel bar
[c] Ultimate stress and strain values for ASTM A706 Grade 60 steel bar

As shown in Table 11, the most stressed coupler reaches its ultimate stress and strain values (i.e., 21.80 ksi and 0.0185 in./in.) at a nonlinear drift value of 4.4 percent. The last two columns of Table 11 provide the number of half cycles until low-cycle fatigue failure of ASTM A706 and ASTM A615 reinforcing bars. Since the low-cycle fatigue relations apply only to large strains in steel, the number of half cycles were only evaluated for strains larger than 0.01 in./in.

Single Column from Dubois Bridge

Table 12 shows the stress and strain values in coupler region and steel bar and the number of half cycles for steel bar fatigue failure for a Dubois column with grouted couplers and fixed-fixed boundary conditions.

Table 12. Stress and Strain in Coupler Region and Steel Bar and Number of Half Cycles for Steel Bar Fatigue Failure for Dubois Fixed-fixed Column with Grouted Couplers

Column Nonlinear Drift, %	Coupler Region		Steel Bar		No. of Half Cycles to Fatigue Failure of Grade 60 Steel Rebar	
	Stress, ksi	Strain, in./in.	Stress, ksi	Strain, in./in.	ASTM A706	ASTM A615
0.25	7.34	0.0012	33.79	0.0012	-	-
0.5	14.12	0.0029	66.25	0.0026	-	-
0.75	14.36	0.0030	66.80	0.0028	-	-
1	14.40	0.0031	67.24	0.0029	-	-
1.5	14.55	0.0035	67.73	0.0032	-	-
2	14.78	0.0040	67.92	0.0037	-	-
2.5	15.11	0.0047	67.99	0.0044	-	-
3	15.60	0.0058	68.00	0.0056	-	-
3.5	16.12	0.0070	68.00	0.0088	-	-
4	17.37	0.0100	73.59	0.0165	172	93
4.5	18.77	0.0137	84.44	0.0294	52	20
4.94	19.54[a]	0.0164[a]	87.92	0.0360	34	12

[a] Ultimate stress and strain values for SSNA No. SNX11 grouted coupler

As shown in Table 12, the most stressed coupler reaches its ultimate stress and strain values (i.e., 19.54 ksi and 0.0164 in./in.) at a nonlinear drift value of 4.9 percent. The last two columns of Table 9 provide the number of half cycles until low-cycle fatigue failure of ASTM A706 and ASTM A615 reinforcing bars. Again, only steel strain values larger than 0.01 were used to estimate the number of half cycles.

Discussion

The results from the single column analysis indicate that both Parma and Dubois columns are able to withstand at least 4 percent of nonlinear drift before the failure of grouted coupler. It should be noted

that both columns have the same diameter of 3.5 ft, but Parma's column is 25.6 ft in height, while Dubois' column is 14.05 ft in height.

There are several factors that may influence the behavior of the two columns considered. These are: (a) Parma's bridge column aspect ratio (the ratio of column height to diameter) is larger than the Dubois bridge column aspect ratio; (b) Parma's column has a steel to concrete ratio of 2.90 percent, while Dubois's column has a steel to concrete ratio 1.46 percent; (c) Parma's column resulted in a larger confined concrete compressive strength (about 11 percent higher) than Dubois; and (d) in analysis of Parma's column, we used SSNA No. 14 U-X grouted coupler, while for Dubois, we used for SSNA No. SNX 11 grouted coupler.

The low cycle fatigue life analysis indicates that at higher strains, only a few half cycles are allowed before fatigue failure. However, it is probably very unlikely that in a given earthquake several strain cycles will be endured at the highest amplitude. Also, it should be noted that even if one or two rebars fracture, there are still others that can function. In addition, from Tables 11 and 12, it is obvious that the use of ASTM A706 steel will significantly improve (by a factor of at least two at larger strains) the low-cycle fatigue life of rebars.

Chapter 5
Guidelines for use of Grouted Couplers in Idaho Bridge Columns

Introduction

Based on the findings in the literature review (Chapter 2), the results of computer modeling of Idaho bridges (Chapter 4), and the detailed information presented in Appendix F, this chapter provides guidelines for ITD bridge designers when using precast columns with grouted couplers.

NMB Splice Sleeve and Erico Lenton Interlok couplers meet the ACI Type 2 and AASHTO's Full Mechanical Connection (FMC) coupler strength requirements. ACI Type 1 couplers are capable of developing the ultimate strength of the bar in tension (i.e., $1.0\ f_u$). The AASHTO's FMC couplers must be able to achieve 1.25 times the specified yield stress (i.e., $1.25\ f_y$) of the coupled bar. The grouted couplers in Table 13 meet the ACI and AASHTO strength requirements.[24, 20] In addition, using a specified 90 ksi ultimate strength for Grade 60 bars, these couplers are also capable of reaching $1.5\ f_y$ as required by Utah's Structures Design and Detailing Manual (see Appendix F, Section "Key Items Found in the Literature or by Contacting the Manufacturers").[10]

Table 13. List of Approved Grouted Couplers

ASTM A706 or ASTM A615 Grade 60 Bar Size	NMB Splice Sleeve[25]	Erico Lenton Interlok[26]
#5	-	LK5
#6	6U-X	LK6
#7	7U-X	LK7
#8	8U-X	LK8
#9	9U-X	LK9
#10	10U-X	LK10
#11	11U-X, SNX11	LK11
#14	14U-X	LK14
#18	-	LK18

Recommendations for Idaho Bridge Manual

1. Grouted splice couplers may be used to connect precast columns to footings or cap beams for columns with less than 4 percent drift. Drift is determined by dividing the maximum displacement at the top of the column by its height. Displacements may be obtained through nonlinear analysis (i.e., bridge columns having nonlinear materials for unconfined concrete, confined concrete, and reinforcing steel). Alternatively, the displacements may be obtained by linear-elastic analysis (i.e., using cracked column section) and magnification factors as per

AASHTO Guide Specifications for LRFD Seismic Bridge Design Article 4.3.3. In both cases, combination of orthogonal seismic displacements are to be used as per Seismic Guide's Article 4.4.[17]

2. The total length of grouted splice couplers shall not exceed $15d_b$, where d_b is the longitudinal reinforcing bar diameter. See Table 13 for a list of approved grouted couplers
3. Grouted couplers in plastic hinge zones must develop 150% of the specified yield strength of the connected reinforcing bar. See Table 13 for a list of approved grouted couplers.
4. Minimum clear distance between grouted splice couplers is recommended to be the same as those specified for reinforcing bars. See the typical detail drawings in Figure 57. Note that Figure 57 is not to scale (NTS). The clear cover for the shear reinforcement over grouted couplers in the precast column shall be 2". See the typical detail drawings in Figure 57.
5. Grout for grouted couplers shall be provided by the manufacturer.

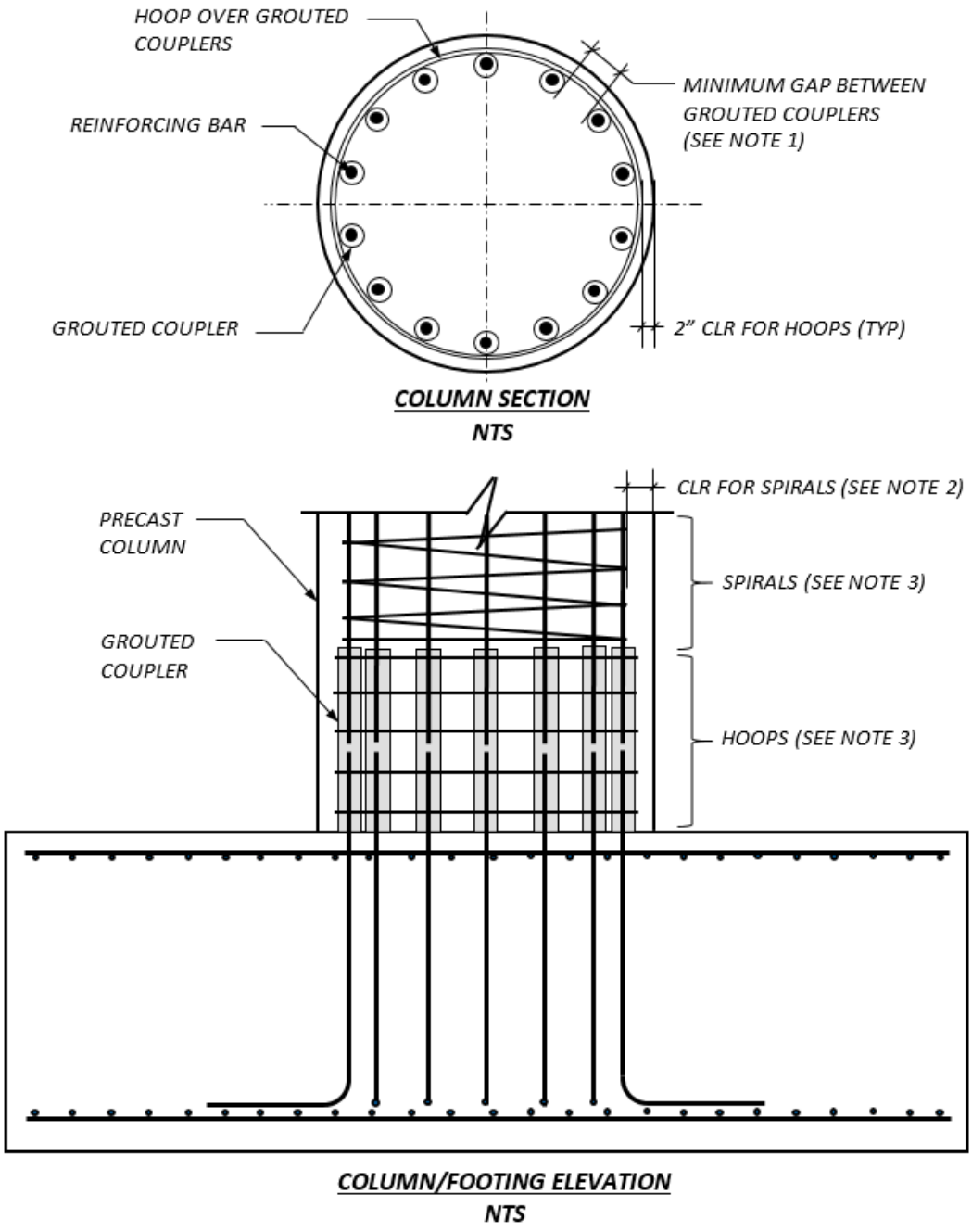

NOTES:

1. LARGER OF (1) 1 IN., (2) 1.33 TIMES MAX. COARSE AGGREGATE SIZE, AND (3) NOMINAL DIAMETER OF CONNECTED REINFORCING.
2. CLEAR COVER FOR SPIRALS = 2" + (DIAM. OF COUPLER – DIAMETER OF BAR)/2
3. FOLLOW THE REQUIREMENTS OF AASHTO LRFD BRIDGE DESIGN SPECIFICATIONS SECTION 5.10.6.

Figure 57. Typical Precast Column with Grouted Couplers to Footing Connection Details

Chapter 6
Conclusions and Recommendations

The objectives of this research project were to (a) assess the performance of grouted coupler column connections under Idaho seismic conditions; and (b) to develop recommendations on the use of columns with grouted couplers. To accomplish these objectives, four tasks were performed. The conclusions that were arrived by completing Tasks 1-3 and the recommendations of Task 4 are summarized below:

Task 1 was to perform a literature review. In this task we concluded that there were two major experimental projects on the behavior of columns with grouted couplers in seismic zones. Both projects concluded that the use of grouted couplers is acceptable. University of Nevada Reno's report noted that grouted couplers may be used in cases where the drift is less than 6 percent. However, at the present time, only the state of Utah allows the use of grouted couplers in plastic hinging zones of reinforced concrete columns in seismic zones.

As a part of Task 2, using OpenSees we developed computer models of the cast-in-place (CIP) column and the column with grouted couplers and no pedestal (GCNP) used in an experimental project at the University of Nevada, Reno (UNR). The force-displacement results of our computer models matched the results of UNR's experimental tests and computer models.

In the first part of Task 3, using computer simulations, we performed seismic analyses of three highway bridges in Idaho by placing them in the most seismically active location in Idaho. In each case, three models were considered; these are: (a) a bridge with cracked linear-elastic columns, (b) a bridge with cast-in-place columns having nonlinear material behavior, and (c) a bridge with prefabricated columns having nonlinear material behavior that are connected at the top and bottom with grouted couplers. The grouted couplers were placed in the column, not in the footing nor in the column cap. Although none of the bridges were designed for the seismic condition considered in this study, using computer simulations, columns from all three bridges performed well. The stresses in the longitudinal reinforcing steel bars and grouted couplers were well within the acceptable range. The highest drift experienced was in the transverse direction of the Parma bridge at about 1.6 percent when considering combination of orthogonal displacements. The AASHTO Guide Specifications for LRFD Seismic Bridge Design equations for estimating the magnified linear-elastic drift demand resulted in either the same or larger values compared to the corresponding drift demand values obtained using nonlinear analysis.

In the second part of Task 3, we performed analyses of single columns from two of the bridges under large drifts. This was done in order to obtain relations between column drift and grouted coupler behavior and the low cycle fatigue of the steel reinforcing. The columns considered are able to withstand at least 4 percent of drift before failure of the most stressed grouted coupler. The low cycle fatigue life analysis indicates that at higher strains, only a few half cycles is endured by the steel reinforcing before fatigue failure. In addition, the use of ASTM A706 steel will significantly improve the low cycle fatigue life of the steel reinforcing bars.

Task 4 was on developing a section to be included in the Idaho Bridge Manual. The detailed recommendations are presented in Chapter 5 of this report. The main recommendation is that grouted couplers may be used in bridge columns experiencing up to 4 percent drift. The column drift may be obtained by (a) analysis of the bridge having nonlinear column materials (i.e., for unconfined concrete, confined concrete, and reinforcing steel) or (b) using displacements of cracked linear-elastic columns in a bridge coupled with magnification factors. The procedures for estimating the magnified linear-elastic drift are outlined in Chapters 4 and 5 of this report using AASHTO Guide Specifications for LRFD Seismic Bridge Design. Chapter 5 also presents a table of approved grouted couplers and a typical grouted coupler connection drawing to aid the bridge designer.

References

1. **Haber, Z. B., M. S. Saiidi, and D. H. Sanders**. *Precast Column-Footing Connections for Accelerated Bridge Construction in Seismic Zones,* Department of Civil Engineering, University of Nevada, Reno, NV, Report No. CCEER 13-08, 2013.

2. **University of California, Berkeley.** *OpenSees.* University of California, Berkeley. 2016. http://opensees.berkeley.edu/OpenSees/user/index.php Accessed July 20, 2016.

3. **ACI Committee 439**. *Types of Mechanical Splices for Reinforcing Bars,* Farmington Hills, MI: American Concrete Institute, Report No. ACI 439.3R-07, 2007.

4. **ASTM International.** *Standard Test Methods for Testing Mechanical Splices for Steel Reinforcing Bars,* West Conshohocken, PA: ASTM International, Report no. A 1034/A 1034M-05, 2005.

5. **Vosooghi, A. and M. S. Saiidi.** "Seismic Damage States and Performance Parameters for Bridge Columns," ACI Special Publication Series SP-271, Structural Concrete in Performance-based Seismic Design of Bridges, May 2010, pp. 29-46.

6. **Pantelides, C. P., M. J. Ameli, J. E. Parks, and D. N. Brown**. *Seismic Evaluation of Grouted Splice Sleeve Connections for Precast RC Bridge Piers in ABC,* Salt Lake City, UT: University of Utah Department of Civil and Environmental Engineering, Report No. UT-14.09, 2014.

7. **ACI Committee 374.** *Guide for Testing Reinforced Concrete Structural Elements under Slowly Applied Simulated Seismic Loads,* Farmington Hills, MI: American Concrete Institute, ACI 374.2R-13, 2013.

8. **Haber, Z. B., M. S. Saiidi, and D. H. Sanders**. "Behavior and Simplified Modeling of Mechanical Reinforcing Bar Splices." *ACI Structural Journal,* Title No. 112-S16, (March-April 2015).

9. **Tazarv, M. and M. S. Saiidi**. *Design and Construction of Bridge Columns Incorporating Mechanical Bar Splices in Plastic Hinge Zones,* Reno, NV: Department of Civil and Environmental Engineering, University of Nevada, Reno, Report No. CCEER 15-07, 2015.

10. **Utah Department of Transportation**. *Structures Design and Detailing Manual*, Salt Lake City, UT: Utah Department of Transportation, 2015.

11. **Jansson, P. O**. *Evaluation of Grout-filled Mechanical Splices for Precast Concrete Construction*, Lansing, MI: Michigan Department of Transportation, Report No. R-1512, 2008.

12. **Wehbe, N. I., M. S. Saiidi, and D. H. Sanders**. "Seismic Performance of Rectangular Bridge Columns with Moderate Confinement," ACI Structural Journal. Vol. 96, No. 2, pp. 248-258, 1999.

13. **Wiss, Janney, Elstner Associates, Inc.** *Splice Sleeve North America Laboratory Tests for Conversion of Legacy Report,* Chicago, IL: WJE, Inc., Report No. ER-5645, 2013.

14. **Mast, R., L. Marsh, C. Spry, S. Johnson, R. Griebenow, J. Guarre, and W. Wilson.** *Seismic Design of Bridges – Design Example No. 1: Two-Span Continuous CIP Concrete Box Bridge.* U. S. Department of Transportation Federal Highway Administration Central Federal Lands Highway Division, FHWA-SA-97-006, 1996.

15. **Bentley Systems, Inc.** *STAAD.Pro V8i Technical Reference Manual.* Exton, PA, 2013.

16. **U. S. Geological Survey.** *U.S. Seismic Design Maps.* U. S. Geological Survey, http://www.earthquake.usgs.gov/designmaps/us/application.php . Accessed October 1, 2015.

17. **American Association of State Highway and Transportation Officials.** *AASHTO Guide Specifications for LRFD Seismic Bridge Design*, Washington, D. C.: American Association of State Highway and Transportation Officials, 2015.

18. **Mander, J. B., M. J. N. Priestley, and R. Park.** "Theoretical Stress-Strain Model for Confined Concrete"*, Journal of Structural Engineering,* Vol. 114, No. 8 (August 1988): pp. 1804 – 1826.

19. **Marsh, M. L., Buckle, I. G., Kavazanjian, E.** *LRFD Seismic Analysis and Design of Bridges Reference Manual*, Washington, D. C.: Federal Highway Administration, Report No. FHWA-NHI-15-004, 2014.

20. **American Association of State Highway and Transportation Officials**. *AASHTO LRFD Bridge Design Specifications*, Washington, D. C.: American Association of State Highway and Transportation Officials, 2014.

21. **Koh, S. K. and R. I. Stephens.** "Mean Stress Effects of Low Cycle Fatigue for a High Strength Steel", *Fatigue Fracture of Engr. Materials and Structures,* Vol. 14, No. 4 (1991): pp. 413 – 428.

22. **Brown, J. and S. K. Kunnath**. *Low-cycle Fatigue Behavior of Longitudinal Reinforcement of Reinforced Concrete Bridge Columns*, University at Buffalo, The State University of New York, Report No. MCEER 00-0007, 2000.

23. **Zhou, Y., Y-C Ou, G. C. Lee, and J. S. O'Connor.** *Pilot Experimental Study on the Low Cycle Fatigue Behavior of Stainless Steel Rebars for Earthquake Engineering Applications,* University at Buffalo, The State University of New York, 2008.

24. **ACI Committee 318.** *Building Code Requirements for Reinforced Concrete,* Detroit, MI: American Concrete Institute, 2014.

25. **Splice Sleeve North America, Inc.** (2016). *NMB Splice Sleeve Type U-X, SNX11, and A11W Systems for Connecting Reinforcing Bars,* Splice Sleeve North America, Inc., ICC-ES Report ESR-3433, 2016.

26. **Erico.** *Instruction Manual Lenton Interlok Rebar Splicing System,* Erico, 2013.

27. **Caltrans.** *Memo to Designers 20-9*, Sacramento, CA: California Department of Transportation, 2015.

Appendix A
Single Column Computer Models

Cast-in-place Column

This section of the Appendix A presents the procedure and OpenSees input files for modeling the cast-in-place (CIP) column used in the University of Nevada, Reno (UNR) study. Specifically the sections that follow present: (a) the procedure for determining the bond slip parameters, (b) the moment-curvature input file, (c) the cyclic push-pull input file, and (d) the pushover input file.

Procedure for Determining Bond-Slip Model Parameters

The steps below are for estimating the bond-slip moment-rotation values that are used in the Opensees input file developed by Idaho State University (ISU) for the UNR's CIP column.

1. Run the moment-curvature input file given in the next section. This input file is for the UNR's CIP column. Figure A1 shows the column rebar stressed in the direction UNR report calls the "push" direction.[(1)] The program is set up with a tributary weight of 208 kip in compression and a displacement-controlled moment is applied such that the bar at (9.375", 0") is in compression and the two bars at (-8.955", 2.641") and at (-8.995", -2.641") are in tension.

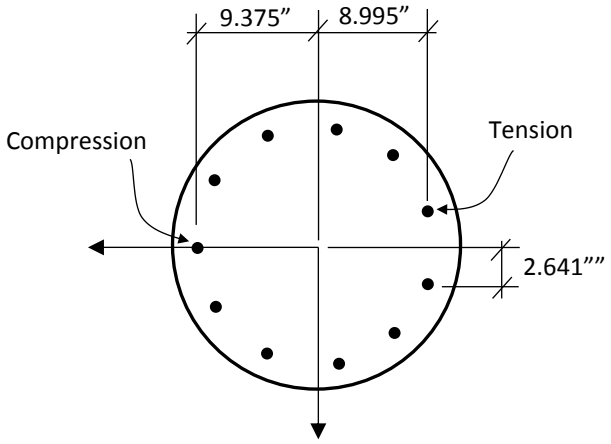

Figure A1. UNR's CIP Column Cross-section (Column Diameter = 2.0 ft)

2. Using the relationships below in create Table A1 in a spreadsheet.

$$\delta_{slip} = \begin{cases} \frac{\varepsilon_s L_1}{2} & if \ \ \varepsilon_s \le \varepsilon_y \\ \frac{\varepsilon_y L_{1y}}{2} + \frac{(\varepsilon_s + \varepsilon_y) L_2}{2} & if \ \ \varepsilon_s > \varepsilon_y \end{cases}$$

Where, δ_{slip} is the slip in the extreme tension bar as shown in Figure A2. ε_s is the steel tensile strain in the extreme location (see Figure A1) and ε_y is the steel yield strain. Lengths L_1 and L_2 are determined using the following relationships.

$$L_1 = \frac{f_s d_b}{4u}$$

$$L_2 = \frac{(f_s - f_y)\, d_b}{4u}$$

$$u = \frac{9.5\sqrt{f_c'}}{d_b} \leq 800 \ psi$$

Where, f_s = stress in the extreme tension steel, d_b= diameter of the bar = 1 in., f_y =steel yield strength = 66.8 ksi, and f_c' = core concrete compressive strength = 4,446 psi. The yellow cells in Table A1 in the δ_{slip} column indicate that the second part of the equation for δ_{slip} controlled. As shown in Figure A2, once the slip is known, the bond-slip rotation at the base of the column corresponding to each value of moment is determined by:

$$\theta_{slip} = tan^{-1}\left(\frac{\delta_{slip}}{c - d}\right)$$

Where, c = distance to the neutral axis from the compression edge obtained from the moment-curvature analysis (see Figure A2) and d = column diameter. With steel tensile strain (ε_t) and compressive strain (ε_c) known, and the dimensions given in Figure A1, the formula for c is:

$$c = 2.65 + \frac{|\varepsilon_c|}{(\varepsilon_t - \varepsilon_c)}(18.37) \ \ in.$$

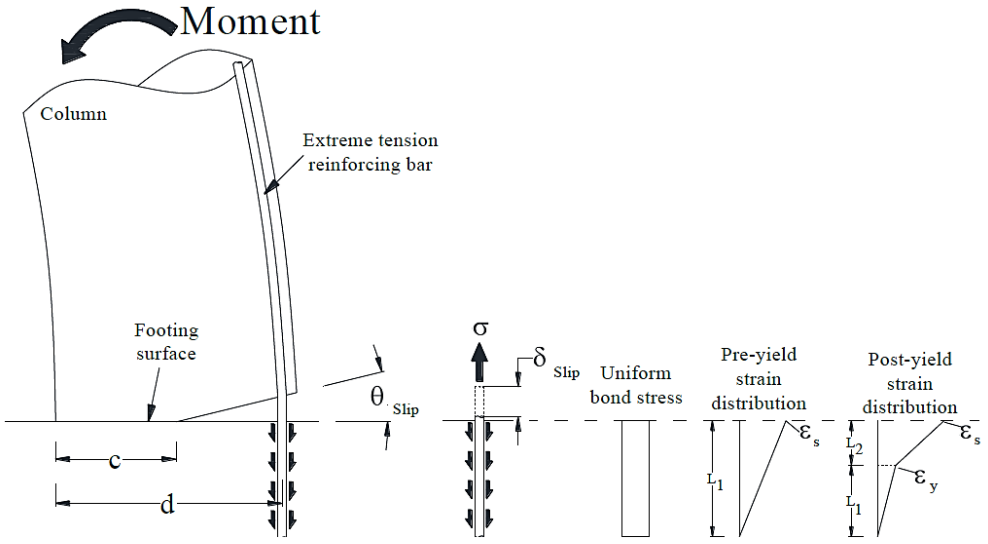

Figure A2. Schematic for Determining the Bond-Slip Rotation[12]

Table A1. Spreadsheet File for Determining Bond-slip Moment-rotation

Comp. Strain	Tensile Stress f_s (ksi)	Tensile Strain, ε_s	Neutral Axis, c (in.)	u (ksi)	L_1 (in)	L_2 (in)	δ_{slip} (in)	θ (Rad)	Moment (Kip-in)
-0.0002126	0.0168168	5.779E-07	20.945	0.633	0.007	-26.357	0.000000	0.000	-847.203
-0.0003017	3.62425	1.246E-04	15.627	0.633	1.430	-24.933	0.000089	0.000	-1332.41
-0.0003767	7.64222	2.627E-04	13.448	0.633	3.016	-23.348	0.000396	0.000	-1665.86
-0.0004455	11.8409	4.071E-04	12.223	0.633	4.673	-21.691	0.000951	0.000	-1954.24
-0.0005115	16.1171	5.543E-04	11.441	0.633	6.361	-20.003	0.001763	0.000	-2224.53
-0.0005750	20.4638	7.040E-04	10.884	0.633	8.076	-18.287	0.002843	0.000	-2481.7
-0.0006379	24.8259	8.542E-04	10.478	0.633	9.798	-16.566	0.004185	0.000	-2732.83
-0.0007003	29.1975	1.005E-03	10.170	0.633	11.523	-14.840	0.005790	0.000	-2978.92
-0.0007628	33.5669	1.156E-03	9.929	0.633	13.248	-13.116	0.007655	-0.001	-3220.96
-0.0008251	37.9312	1.306E-03	9.736	0.633	14.970	-11.394	0.009779	-0.001	-3458.91
-0.0008874	42.2724	1.457E-03	9.577	0.633	16.684	-9.680	0.012157	-0.001	-3692.85
-0.0009499	46.5528	1.608E-03	9.447	0.633	18.373	-7.991	0.014771	-0.001	-3922.47
-0.0010125	50.7061	1.758E-03	9.337	0.633	20.012	-6.352	0.017595	-0.001	-4146.4
-0.0010751	54.6136	1.909E-03	9.243	0.633	21.554	-4.810	0.020574	-0.001	-4362.01
-0.0011372	58.0976	2.060E-03	9.159	0.633	22.929	-3.435	0.023618	-0.002	-4565.4
-0.0011984	60.9676	2.212E-03	9.080	0.633	24.062	-2.302	0.026613	-0.002	-4752.02
-0.0012581	63.1125	2.365E-03	9.003	0.633	24.908	-1.455	0.026063	-0.002	-4918.49
-0.0013162	64.5645	2.521E-03	8.927	0.633	25.482	-0.882	0.027332	-0.002	-5064.34
-0.0013725	65.4747	2.677E-03	8.851	0.633	25.841	-0.523	0.028158	-0.002	-5190.85
-0.0014272	66.0182	2.836E-03	8.775	0.633	26.055	-0.309	0.028667	-0.002	-5299.95
-0.0014803	66.336	2.996E-03	8.700	0.633	26.181	-0.183	0.028975	-0.002	-5393.32
-0.0015318	66.5211	3.158E-03	8.626	0.633	26.254	-0.110	0.029160	-0.002	-5471.33
-0.0015830	66.6293	3.320E-03	8.557	0.633	26.296	-0.067	0.029271	-0.002	-5535.95
-0.0016334	66.6936	3.482E-03	8.490	0.633	26.322	-0.042	0.029339	-0.002	-5591.77
-0.0016840	66.7324	3.645E-03	8.430	0.633	26.337	-0.027	0.029381	-0.002	-5639.82
-0.0017344	66.7562	3.808E-03	8.374	0.633	26.347	-0.017	0.029407	-0.002	-5682.04
-0.0017847	66.7711	3.970E-03	8.322	0.633	26.352	-0.011	0.029424	-0.002	-5720.06
-0.0018355	66.7807	4.133E-03	8.275	0.633	26.356	-0.008	0.029436	-0.002	-5755.1
-0.0018870	66.7868	4.294E-03	8.233	0.633	26.359	-0.005	0.029443	-0.002	-5786.96
-0.0019386	66.7909	4.456E-03	8.194	0.633	26.360	-0.004	0.029448	-0.002	-5817.16
-0.0019902	66.7936	4.618E-03	8.158	0.633	26.361	-0.003	0.029452	-0.002	-5845.76
-0.0020418	66.8006	4.779E-03	8.124	0.633	26.364	0.000	0.029461	-0.002	-5872.75
-0.0020936	66.8423	4.940E-03	8.093	0.633	26.381	0.017	0.029521	-0.002	-5897.78
-0.0021456	66.9498	5.102E-03	8.064	0.633	26.423	0.059	0.029679	-0.002	-5921.16
Missing lines in the Excel file ⋮									

3. Plot moment versus rotation curve as shown in Figure A3. This graph is drawn using the last two columns of Table A1, but the signs have been changed.

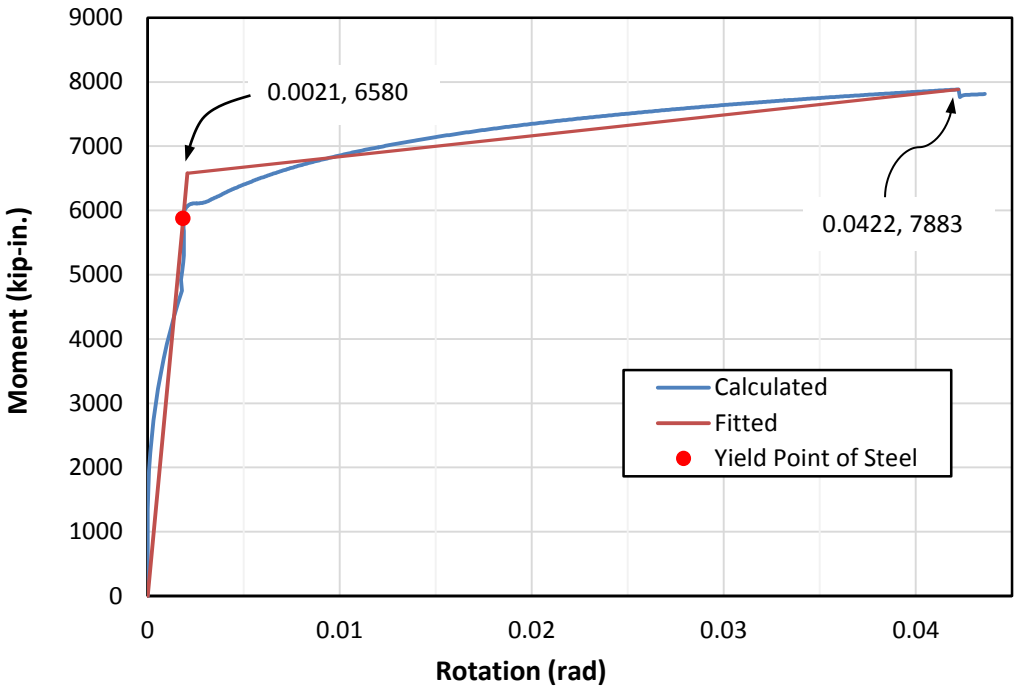

Figure A3. Bond-Slip Moment versus Rotation

4. Fit two straight lines. The first line starts at (0, 0) and crosses the moment corresponding to the yield tensile stress in the tension bar (see the orange cells in Table A1 corresponding to steel tensile stress of 66.8 ksi). Extend the first line beyond this point. Then, draw the second line by balancing the area between the calculated and the second line after the first yield point.

Using the above approach, the ISU's fitted lines correspond to the points shown in Figure A3. These points are 6,580 kip-in. and 0.0021 radian and 7,883 kip-in. and 0.0422 radian. The corresponding values for the UNR project were 6,746 kip-in. and 0.0028 radian and 7,859 kip-in. and 0.0452 radian. Since the longitudinal steel reinforcement in the UNR columns were not symmetrically placed (see Figure A1), the values obtained in Figure A3 are for direction that UNR report calls "push" direction. Since the "push" and "pull" values are within 5 percent, we used the ISU "push" values in our computer models of the UNR column.

Moment-Curvature Input File for UNR's CIP Column

```
#Create uniaxial materials for Concrete and Steel
uniaxialMaterial Concrete01  1  -4.446   -0.002  0  -0.005
uniaxialMaterial Concrete04  2  -6.944     -0.0076  -0.0318  3801
uniaxialMaterial ReinforcingSteel  3  66.8   111.3   29000   1247   0.005   0.09

#Create fiber section with Defined Concrete and Rebar
```

```
section Fiber  1  {
patch circ 1 44  2  0  0  10.25  12.0  0  360
patch circ 2 44  10  0  0  0  10.25  0  360
layer circ 3  11  0.79  0  0  9.375
}

#Create nodes
#       tag   x     y
node     1    0.0   0.0
node     2    0.0   0.0

#Fix node 1
fix  1  1  1  1
fix  2  0  1  0

element zeroLengthSection 1 1 2 1
recorder Node -file MomentSection1Corrected.out -node 1 -dof 3 reaction
recorder Element -file TensStrain.out -ele 1 section fiber -8.955 2.641 stressStrain
recorder Element -file CompStrain-steel.out -ele 1 section fiber  9.375 0 3 stressStrain
recorder Element -file CompStrain-concrete.out -ele 1 section fiber  9.375 0 2 stressStrain

pattern Plain 1 "Constant" {
load 2  -208 0  0
}

integrator LoadControl 0.0
system SparseGeneral -piv
test NormUnbalance 1.0e-9 10
numberer Plain
constraints Plain
algorithm Newton
analysis Static
analyze 1

pattern Plain 2 "Linear" {
load 2  0.0  0.0  -1.0
}
integrator DisplacementControl 2  3  .000011515
analyze 500
```

OpenSees Input File for CIP Column Cyclic Push-Pull

```
#Clear cached data existing in the program
wipe

#Create Model with 3 dimensions and 6 degrees of freedom
model BasicBuilder -ndm 3 -ndf 6
#Create 6 DOF nodes

#       tag   x     y     z
node     1    0.0   0.0   0.0
node     2    0.0   0.0   0.0
node     3    0.0   96.0  0.0
node     4    0.0   108.0 0.0
node     5    0.0   120.0 0.0
node     6    -27.0 108.0 0.0

#Specifify geometric transoformation
geomTransf Linear 1  0  0  1
```

```
#Fix node 1
fix  1  1  1  1  1  1  1
fix  2  1  1  1  0  0  0

#Create uniaxial materials for Concrete and Steel
uniaxialMaterial Concrete01  1  -4.446   -0.002  0  -0.005
uniaxialMaterial Concrete04  2  -6.944     -0.0076  -0.0318  3801
uniaxialMaterial ReinforcingSteel  3  66.8   111.3   29000   1247   0.005   0.09

#Create hysteretic material to model Bond-Slip
uniaxialMaterial Hysteretic 4  6580  0.002079  7883  0.04223  -6580  -0.002079   -7883
-0.04223    1  1  0  0  0.35

#Create fiber section with Defined Concrete and Rebar
section Fiber  1  {
patch circ 1 44  2  0  0  10.25  12.0  0  360
patch circ 2 44  10  0  0  0  10.25  0  360
layer circ 3  11  0.79  0  0  9.375
}

#Create zero length element between nodes 1 and 2
element zeroLength 1  1  2  -mat 4 4 4 -dir 4  5  6

#Create nonlinear beam column between nodes 2 and 3
element nonlinearBeamColumn  2  2  3  9  1  1

#Create elastic beam column elements for the loading head
element elasticBeamColumn 3  3  4  1080  3656  1523.3  365880  122880  243000  1
element elasticBeamColumn 4  4  6  768  3656  1523.3  88704  51840  36864  1
element elasticBeamColumn 5  4  5  1080  3656  1523.3  365880  122880  243000  1

#Set up time series

timeSeries Linear 1

#Create two recorder files: displacements and reactions
recorder Node  -file ColumnDispCIPISU08272015.out -time -node 4 -dof 1 6 disp
recorder Node  -file ColumnreactionCIPISU08272015.out -time -node 2 -dof 1 reaction
recorder Node  -file ColumnmomentCIPISU08272015.out -time -node 1  -dof  6 reaction

#Set loading pattern for vertical loading
pattern Plain 1 1 {
load 5  0  -208  0  0  0  0
}

#Perform Following Analysis Commands for Vertical Loading
constraints Plain
numberer Plain
system BandGeneral
test NormDispIncr  1.0e-8  6
algorithm Newton
integrator LoadControl 1
analysis Static
analyze 1

#Reset time to perform pushover analysis
loadConst -time 0.0
pattern Plain  2  1  {
load 6 -200  0  0  0  0  0
}
```

```
constraints Plain
numberer Plain
system BandGeneral
test EnergyIncr  1.0e-8  8  0
algorithm Newton
analysis Static

integrator DisplacementControl  6  1  .009
analyze 30
integrator DisplacementControl  6  1  -.009
analyze 60
integrator DisplacementControl  6  1  .009
analyze 30
integrator DisplacementControl  6  1  .018
analyze 30
integrator DisplacementControl  6  1  -.018
analyze 60
integrator DisplacementControl  6  1  .018
analyze 30
integrator DisplacementControl  6  1  .027
analyze 30
integrator DisplacementControl  6  1  -.027
analyze 60
integrator DisplacementControl  6  1  .027
analyze 30
integrator DisplacementControl  6  1  .036
analyze 30
integrator DisplacementControl  6  1  -.036
analyze 60
integrator DisplacementControl  6  1  .036
analyze 30
integrator DisplacementControl  6  1  .1008
analyze 20
integrator DisplacementControl  6  1  -.1008
analyze 40
integrator DisplacementControl  6  1  .1008
analyze 20
integrator DisplacementControl  6  1  .108
analyze 30
integrator DisplacementControl  6  1  -.108
analyze 60
integrator DisplacementControl  6  1  .108
analyze 30
integrator DisplacementControl  6  1  .144
analyze 30
integrator DisplacementControl  6  1  -.144
analyze 60
integrator DisplacementControl  6  1  .144
analyze 30
integrator DisplacementControl  6  1  .18
analyze 30
integrator DisplacementControl  6  1  -.18
analyze 60
integrator DisplacementControl  6  1  .18
analyze 30
integrator DisplacementControl  6  1  .216
analyze 30
integrator DisplacementControl  6  1  -.216
analyze 60
integrator DisplacementControl  6  1  .216
```

```
analyze 30
integrator DisplacementControl  6  1  .252
analyze 30
integrator DisplacementControl  6  1  -.252
analyze 60
integrator DisplacementControl  6  1  .252
analyze 30
integrator DisplacementControl  6  1  .288
analyze 30
integrator DisplacementControl  6  1  -.288
analyze 60
integrator DisplacementControl  6  1  .288
analyze 30
integrator DisplacementControl  6  1  .36
analyze 30
integrator DisplacementControl  6  1  -.36
analyze 60
integrator DisplacementControl  6  1  .36
analyze 30
```

OpenSees Input File for the CIP Column Pushover

```
#Clear cached data existing in the program
wipe

#Create Model with 3 dimensions and 6 degrees of freedom
model BasicBuilder -ndm 3 -ndf 6

#Create 6 DOF nodes
#       tag   x     y     z
node     1    0.0   0.0   0.0
node     2    0.0   0.0   0.0
node     3    0.0   96.0  0.0
node     4    0.0   108.0 0.0
node     5    0.0   120.0 0.0
node     6    -27.0 108.0 0.0

#Specifify geometric transoformation
geomTransf Linear 1  0  0  1

#Fix node 1
fix  1  1  1  1  1  1  1
fix  2  1  1  1  0  0  0

#Create uniaxial materials for Concrete and Steel
uniaxialMaterial Concrete01  1  -4.446   -0.002  0  -0.005
uniaxialMaterial Concrete04  2  -6.944     -0.0076  -0.0318  3801
uniaxialMaterial ReinforcingSteel  3  66.8   111.3   29000   1247   0.005   0.09

#Create hysteretic material to model Bond-Slip
uniaxialMaterial Hysteretic 4  6580  0.002079  7883  0.04223  -6580  -0.002079   -7883
-0.04223    1  1  0  0  0.35

#Create fiber section with Defined Concrete and Rebar

section Fiber  1  {
patch circ 1 44  2  0  0  10.25  12.0  0  360
patch circ 2 44  10  0  0  0  10.25  0  360
layer circ 3  11  0.79  0  0  9.375
```

```
}

#Create zero length element between nodes 1 and 2
element zeroLength 1  1  2  -mat 4 4 4 -dir 4  5  6

#Create nonlinear beam column between nodes 2 and 3
element nonlinearBeamColumn  2  2  3  9  1  1

#Create elastic beam column elements for the loading head
element elasticBeamColumn 3  3  4  1080  3656  1523.3  365880  122880  243000  1
element elasticBeamColumn 4  4  6  768  3656  1523.3  88704  51840  36864  1
element elasticBeamColumn 5  4  5  1080  3656  1523.3  365880  122880  243000  1

#Set up time series
timeSeries Linear 1

#Create two recorder files: displacements and reactions
recorder Node  -file ColumnDispCIPPushoverISU08272015.out -time -node 4 -dof 1 6 disp
recorder Node  -file ColumnreactionCIPPushoverISU08272015.out -time -node 2 -dof 1 reaction
recorder Node  -file ColumnmomentCIPPushoverISU08272015.out -time -node 1  -dof  6 reaction

#Set loading pattern for vertical loading
pattern Plain 1 1 {
load 5  0  -208  0  0  0  0
}

#Perform Following Analysis Commands for Vertical Loading
constraints Plain
numberer Plain
system BandGeneral
test NormDispIncr  1.0e-8  6
algorithm Newton
integrator LoadControl 1
analysis Static
analyze 1

#Reset time to perform pushover analysis
loadConst -time 0.0

pattern Plain  2  1  {
load 6 -200  0  0  0  0  0
}

constraints Plain
numberer Plain
system BandGeneral
test EnergyIncr  1.0e-8  8  0
algorithm Newton
analysis Static
integrator DisplacementControl  6  1  .108
analyze 100
```

GCNP Column

This section of the Appendix A presents (a) the cyclic push-pull input file and (b) the pushover input file for the UNR's GCNP column.

OpenSees Input File for GCNP Column Cyclic Push-Pull

```
#Clear cached data existing in the program
wipe

#Create Model with 3 dimensions and 6 degrees of freedom
model BasicBuilder -ndm 3 -ndf 6

#Create 6 DOF nodes
#       tag   x     y     z
node     1    0.0   0.0   0.0
node     2    0.0   0.0   0.0
node     3    0.0   14.5  0.0
node     4    0.0   108.0 0.0

#Specifify geometric transoformation
geomTransf Linear 1  0  0  1

#Fix node 1
fix  1  1  1  1  1  1  1
#Fix node 2 except for rotation
fix  2  1  1  1  0  0  0

#Create unconfined concrete
uniaxialMaterial Concrete01  1  -4.228   -0.002  0  -0.005

#Create confined concrete in precast shell
uniaxialMaterial Concrete04  2  -6.704     -0.0079  -0.0328  3706

#Create confined SCC in core of precast shell
uniaxialMaterial Concrete04  3  -7.543    -0.0071   -0.0296  4029

#Create reinforcing steel
uniaxialMaterial ReinforcingSteel  4  66.8   111.3   29000   1247   0.005   0.09

#Create Sleeve Section modeled as reinforcing steel
uniaxialMaterial ReinforcingSteel  7  79.4   110.5   35179   4116   0.0033   0.0170

#Create hysteretic material to model Bond-Slip at footing interface
uniaxialMaterial Hysteretic 5  6580  .002079  7883  .04223  -6580  -0.002079  -7883  -0.04223
1  1  0  0  0.35

#Create fiber section for Column Shaft
section Fiber  1  {
patch circ 1 44  2  0  0  10.25  12.0   0  360
patch circ 2 44  3  0  0  7      10.25  0  360
patch circ 3 44  7  0  0  0      7      0  360
layer circ 4  11  0.79  0  0  9.375
}

section Fiber 2 {
patch circ  1  44  2  0  0  10.25  12.0   0  360
patch circ  2  4  3  0  0  7      10.25  5.02  27.71
patch circ  2  4  3  0  0  7      10.25  37.75  60.44
```

```
patch circ  2  4  3  0  0  7      10.25  70.48  93.17
patch circ  2  4  3  0  0  7      10.25  103.21  125.9
patch circ  2  4  3  0  0  7      10.25  135.94  158.63
patch circ  2  4  3  0  0  7      10.25  168.67  191.36
patch circ  2  4  3  0  0  7      10.25  201.4  224.09
patch circ  2  4  3  0  0  7      10.25  234.13  256.82
patch circ  2  4  3  0  0  7      10.25  266.86  289.55
patch circ  2  4  3  0  0  7      10.25  299.59  322.28
patch circ  2  4  3  0  0  7      10.25  332.32  355.01
patch circ  3  44  7  0  0  0      7      0  360
layer circ  7  11  0.79  0  0  9.375
}

#Create zero length element between nodes 1 and 2
element zeroLength 1  1  2  -mat 5 5 5 -dir 4  5  6

#Create element between nodes 2 and 3
element nonlinearBeamColumn 2  2  3  5  2  1

#Create nonlinear beam column between nodes 3 and 4
element nonlinearBeamColumn 3  3  4  5  1  1

#Set up time series
timeSeries Linear 1

#Create two recorder files: displacements and reactions
recorder Node  -file ColumnDisp09222015.out -node 4 -dof 1 disp
recorder Node  -file ColumnReaction09222015.out -node 2 -dof 1 reaction

#Set loading pattern for vertical loading
pattern Plain 1 1 {
load 4  0  -208  0  0  0  0
}

#Perform Following Analysis Commands for Vertical Loading
constraints Plain
numberer Plain
system BandGeneral
test NormDispIncr  1.0e-8  6
algorithm Newton
integrator LoadControl 1
analysis Static
analyze 1

#Reset time to perform pushover analysis
loadConst -time 0.0
pattern Plain  2  1  {
load 4  200  0  0  0  0  0
}

constraints Plain
numberer Plain
system BandGeneral
test EnergyIncr  1.0e-8  8  0
algorithm Newton
analysis Static
integrator DisplacementControl  4  1  .009
analyze 30
integrator DisplacementControl  4  1  -.009
analyze 60
integrator DisplacementControl  4  1  .009
```

```
analyze 30
integrator DisplacementControl  4  1  .009
analyze 30
integrator DisplacementControl  4  1  -.009
analyze 60
integrator DisplacementControl  4  1  .009
analyze 30
integrator DisplacementControl  4  1  .018
analyze 30
integrator DisplacementControl  4  1  -.018
analyze 60
integrator DisplacementControl  4  1  .018
analyze 30
integrator DisplacementControl  4  1  .018
analyze 30
integrator DisplacementControl  4  1  -.018
analyze 60
integrator DisplacementControl  4  1  .018
analyze 30
integrator DisplacementControl  4  1  .027
analyze 30
integrator DisplacementControl  4  1  -.027
analyze 60
integrator DisplacementControl  4  1  .027
analyze 30
integrator DisplacementControl  4  1  .027
analyze 30
integrator DisplacementControl  4  1  -.027
analyze 60
integrator DisplacementControl  4  1  .027
analyze 30
integrator DisplacementControl  4  1  .036
analyze 30
integrator DisplacementControl  4  1  -.036
analyze 60
integrator DisplacementControl  4  1  .036
analyze 30
integrator DisplacementControl  4  1  .036
analyze 30
integrator DisplacementControl  4  1  -.036
analyze 60
integrator DisplacementControl  4  1  .036
analyze 30
integrator DisplacementControl  4  1  .1008
analyze 20
integrator DisplacementControl  4  1  -.1008
analyze 40
integrator DisplacementControl  4  1  .1008
analyze 20
integrator DisplacementControl  4  1  .1008
analyze 20
integrator DisplacementControl  4  1  -.1008
analyze 40
integrator DisplacementControl  4  1  .1008
analyze 20
integrator DisplacementControl  4  1  .108
analyze 30
integrator DisplacementControl  4  1  -.108
analyze 60
integrator DisplacementControl  4  1  .108
analyze 30
```

```
integrator DisplacementControl  4  1  .108
analyze 30
integrator DisplacementControl  4  1  -.108
analyze 60
integrator DisplacementControl  4  1  .108
analyze 30
integrator DisplacementControl  4  1  .144
analyze 30
integrator DisplacementControl  4  1  -.144
analyze 60
integrator DisplacementControl  4  1  .144
analyze 30
integrator DisplacementControl  4  1  .144
analyze 30
integrator DisplacementControl  4  1  -.144
analyze 60
integrator DisplacementControl  4  1  .144
analyze 30
integrator DisplacementControl  4  1  .18
analyze 30
integrator DisplacementControl  4  1  -.18
analyze 60
integrator DisplacementControl  4  1  .18
analyze 30
integrator DisplacementControl  4  1  .18
analyze 30
integrator DisplacementControl  4  1  -.18
analyze 60
integrator DisplacementControl  4  1  .18
analyze 30
integrator DisplacementControl  4  1  .216
analyze 30
integrator DisplacementControl  4  1  -.216
analyze 60
integrator DisplacementControl  4  1  .216
analyze 30
integrator DisplacementControl  4  1  .216
analyze 30
integrator DisplacementControl  4  1  -.216
analyze 60
integrator DisplacementControl  4  1  .216
analyze 30
```

OpenSees Input File for the GCNP Column Pushover

```
#Clear cached data existing in the program
wipe

#Create Model with 3 dimensions and 6 degrees of freedom
model BasicBuilder -ndm 3 -ndf 6

#Create 6 DOF nodes
#       tag   x     y     z
node     1    0.0   0.0   0.0
node     2    0.0   0.0   0.0
node     3    0.0   14.5  0.0
node     4    0.0   108.0 0.0

#Specifify geometric transoformation
```

```
geomTransf Linear 1  0  0  1

#Fix node 1
fix  1  1  1  1  1  1  1

#Fix node 2 except for rotation
fix  2  1  1  1  0  0  0
#Create unconfined concrete
uniaxialMaterial Concrete01  1  -4.228   -0.002  0  -0.005

#Create confined concrete in precast shell
uniaxialMaterial Concrete04  2  -6.704     -0.0079  -0.0328  3706

#Create confined SCC in core of precast shell
uniaxialMaterial Concrete04  3  -7.543    -0.0071   -0.0296  4029

#Create reinforcing steel
uniaxialMaterial ReinforcingSteel  4  66.8   111.3   29000   1247   0.005   0.09

#Create Sleeve Section modeled as reinforcing steel
uniaxialMaterial ReinforcingSteel  7  79.4   110.5   35179   4116   0.0033   0.0170

#Create hysteretic material to model Bond-Slip at footing interface
uniaxialMaterial Hysteretic 5  6580  .002079  7883  .04223  -6580  -0.002079  -7883  -0.04223
1  1  0  0  0.35

#Create fiber section for Column Shaft
section Fiber  1  {
patch circ 1 44  2  0  0  10.25  12.0   0  360
patch circ 2 44  3  0  0  7      10.25  0  360
patch circ 3 44  7  0  0  0      7      0  360
layer circ 4  11  0.79  0  0  9.375
}

section Fiber 2 {
patch circ  1  44  2  0  0  10.25  12.0   0  360
patch circ  2  4  3  0  0  7      10.25  5.02  27.71
patch circ  2  4  3  0  0  7      10.25  37.75  60.44
patch circ  2  4  3  0  0  7      10.25  70.48  93.17
patch circ  2  4  3  0  0  7      10.25  103.21  125.9
patch circ  2  4  3  0  0  7      10.25  135.94  158.63
patch circ  2  4  3  0  0  7      10.25  168.67  191.36
patch circ  2  4  3  0  0  7      10.25  201.4  224.09
patch circ  2  4  3  0  0  7      10.25  234.13  256.82
patch circ  2  4  3  0  0  7      10.25  266.86  289.55
patch circ  2  4  3  0  0  7      10.25  299.59  322.28
patch circ  2  4  3  0  0  7      10.25  332.32  355.01
patch circ  3  44  7  0  0  0      7      0  360
layer circ  7  11  0.79  0  0  9.375
}

#Create zero length element between nodes 1 and 2
element zeroLength 1  1  2  -mat 5 5 5 -dir 4  5  6

#Create element between nodes 2 and 3
element nonlinearBeamColumn 2  2  3  5  2  1

#Create nonlinear beam column between nodes 3 and 4
element nonlinearBeamColumn 3  3  4  5  1  1

#Set up time series
```

```
timeSeries Linear 1

#Create two recorder files: displacements and reactions
recorder Node  -file ColumnDispSmallArea09302015.out -node 4 -dof 1 disp
recorder Node  -file ColumnReactionSmallArea09302015.out -node 2 -dof 1 reaction

#Set loading pattern for vertical loading
pattern Plain 1 1 {
load 4  0  -208  0  0  0  0
}

#Perform Following Analysis Commands for Vertical Loading
constraints Plain
numberer Plain
system BandGeneral
test NormDispIncr  1.0e-8  6
algorithm Newton
integrator LoadControl 1
analysis Static
analyze 1

#Reset time to perform pushover analysis
loadConst -time 0.0
pattern Plain  2  1  {
load 4  200  0  0  0  0  0
}

constraints Plain
numberer Plain
system BandGeneral
test EnergyIncr  1.0e-8  8  0
algorithm Newton
analysis Static
integrator DisplacementControl  4  1  .0648
analyze 100
```

Appendix B
Grouted Coupler Experimental Data

This appendix presents the grouted coupler stress-strain data obtained by processing the laboratory test data provided in a report that was prepared for Splice Sleeve North America (SSNA), Inc.[13] The report was obtained from SSNA, Inc. The experimental set up is shown in Figure B1. For our project, we needed the stress-strain data for grouted couplers for No. 8, No. 11, and No. 14 reinforcing bars. Table B1 shows the dimensions for these couplers (i.e., 8U-X, SNX11, and 14U-X).

A typical cyclic test experimental data in Appendix E of the test report for SSNA grouted couplers is shown in Figure B2. For each of the three couplers used in this project, we had data for five specimens that were used with ASTM A615 Grade 60 steel bars. The data provided the force versus elongation of the coupler region (called "slip" in the test report) as shown in Figure B1(b). The effective stress in the coupler is found by dividing the force by the area of the grouted coupler. The average strain of the coupler is obtained by dividing elongation of the coupler region by the length of the coupler region. Tables B2 to B4 show the stress-strain data needed for OpenSees' *ReinforcingSteel* uniaxial material used to model the grouted couplers. The graphs of the data are shown in Figures B3 to B5 along with the best fit curves.

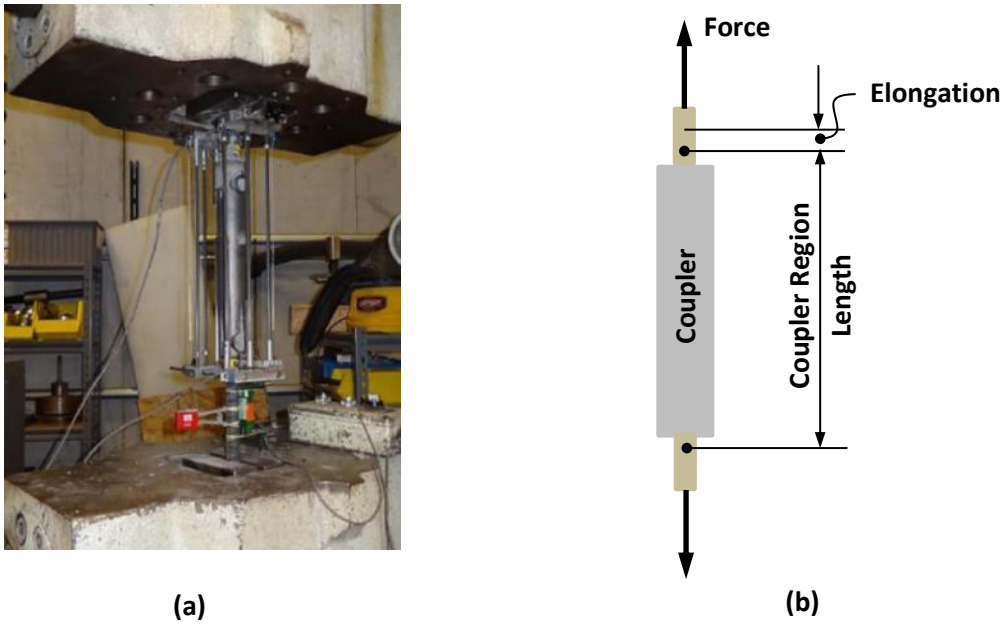

Figure B1. (a) Experimental Set-up for Testing Grouted Coupler, and (b) Schematic Describing Coupler Region and the Elongation (Slip) [13]

Table B1. Measured Grouted Coupler Sleeve Dimensions[13]

Bar Size	Coupler Type	Diameter (mm)	Overall Length (mm)	Wall Thickness (mm)
6	U-X	51.8	285.1	4.73
8	U-X	63.7	369.6	4.71
10	U-X	72.6	455.3	5.45
14	U-X	88.1	620.4	8.08
11	SNX	77.5	485.9	6.53

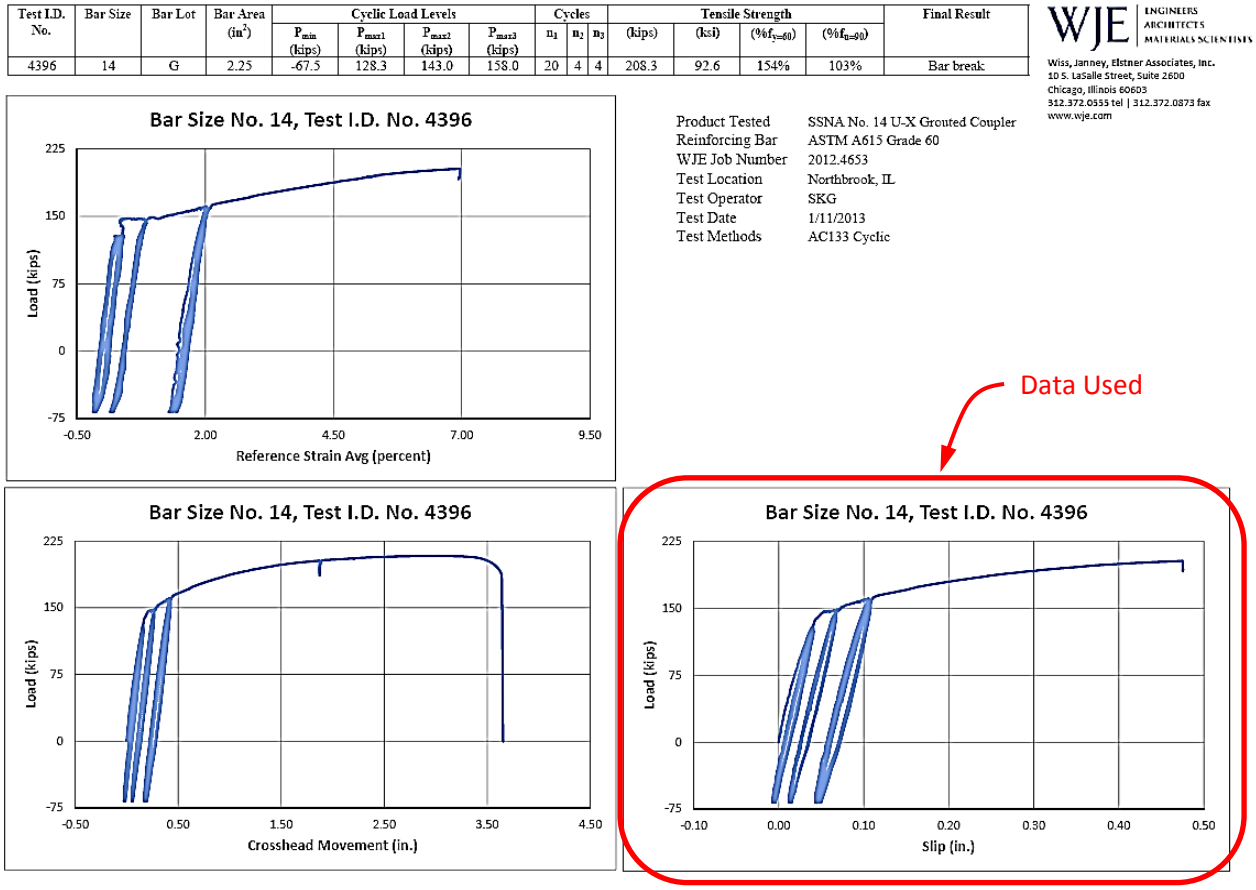

Figure B2. Typical Cyclic Test Experimental Data

Table B2. Stress-Strain Data for SSNA 8U-X

Test I.D.	Yield Stress (ksi)	Ultimate Stress (ksi)	Modulus of Elasticity (ksi)	Strain Hardening Modulus (ksi)	Initial Strain Hardening Strain (in./in.)	Ultimate Strain (in./in.)
4382	12.6	17.714	5,814	720.7	0.003361	0.0169
4383	12.7	17.714	5,548	705.5	0.003285	0.0170
4384	12.6	17.471	5,078	651.6	0.003361	0.0175
4385	12.6	17.713	5,708	664.7	0.003065	0.0166
4386	12.8	17.714	5,981	564.4	0.003285	0.0170
Average	**12.7**	**17.665**	**5,626**	**661.4**	**0.003271**	**0.0170**

Note: Sleeve area = 4.94 in^2.

Table B3. Stress-Strain Data for SSNA SNX11

Test I.D.	Yield Stress (ksi)	Ultimate Stress (ksi)	Modulus of Elasticity (ksi)	Strain Hardening Modulus (ksi)	Initial Strain Hardening Strain (in./in.)	Ultimate Strain (in./in.)
4402	14.5	19.67	5,259	722.5	0.0044	0.0161
4403	14.0	19.37	5,978	713.7	0.0046	0.0169
4404	13.8	19.37	5,838	669.4	0.0043	0.0167
4405	14.6	19.38	6,106	707.0	0.0041	0.0151
4406	14.2	19.94	6,398	682.0	0.0037	0.0176
Average	**14.2**	**19.54**	**5,916**	**698.9**	**0.0042**	**0.0165**

Note: Sleeve area = 7.31 in^2.

Table B4. Stress-Strain Data for SSNA SNX14

Test I.D.	Yield Stress (ksi)	Ultimate Stress (ksi)	Modulus of Elasticity (ksi)	Strain Hardening Modulus (ksi)	Initial Strain Hardening Strain (in./in.)	Ultimate Strain (in./in.)
4396	15.2	21.70	8,324	704.1	0.0020	0.0196
4397	15.7	21.70	8,472	714.7	0.0020	0.0186
4398	15.4	22.23	8,472	721.8	0.0018	0.0179
4399	15.3	21.70	8,206	776.8	0.0020	0.0183
4400	15.3	21.70	9,591	761.2	0.0017	0.0180
Average	**15.4**	**21.80**	**8,613**	**735.7**	**0.0019**	**0.0185**

Note: Sleeve area = 9.45 in^2.

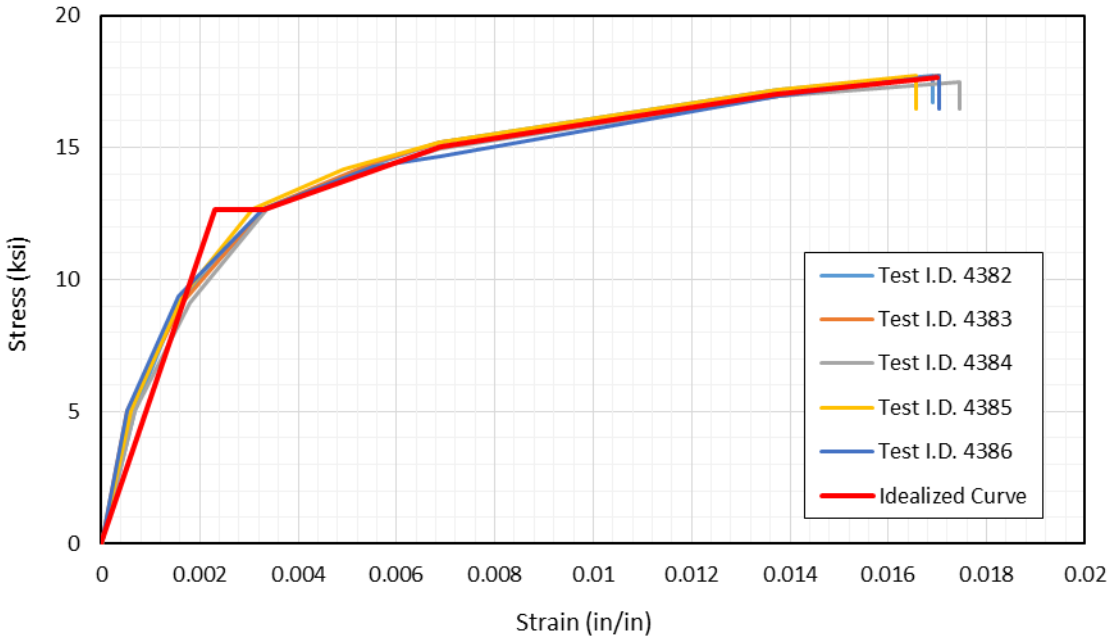

Figure B3. Stress-Strain Relationship for SSNA 8U-X

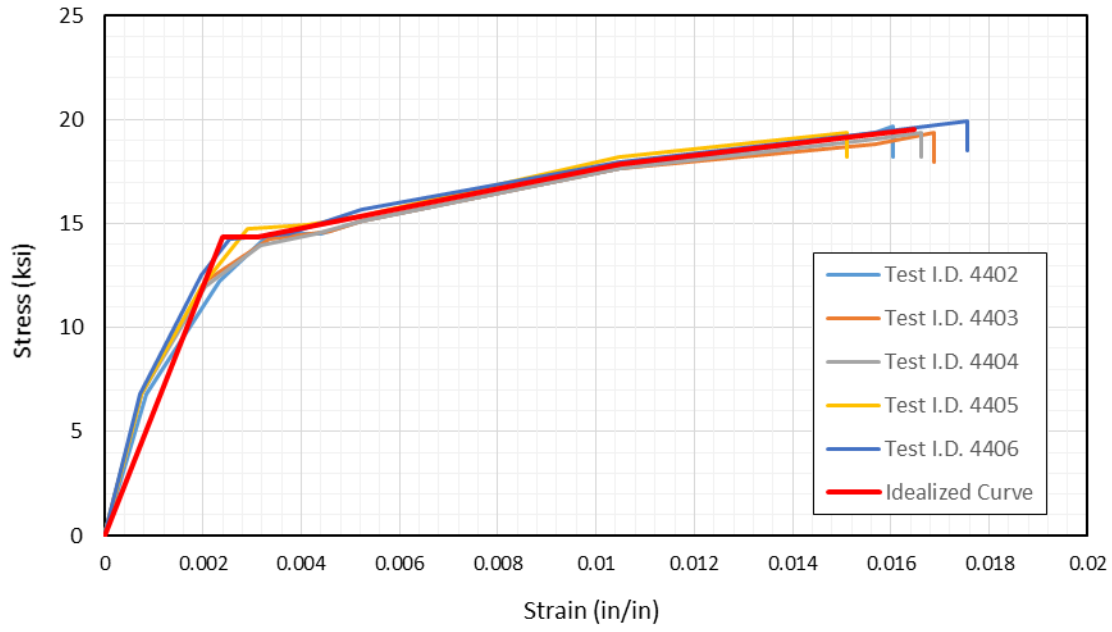

Figure B4. Stress-Strain Relationship for SSNA SNX11

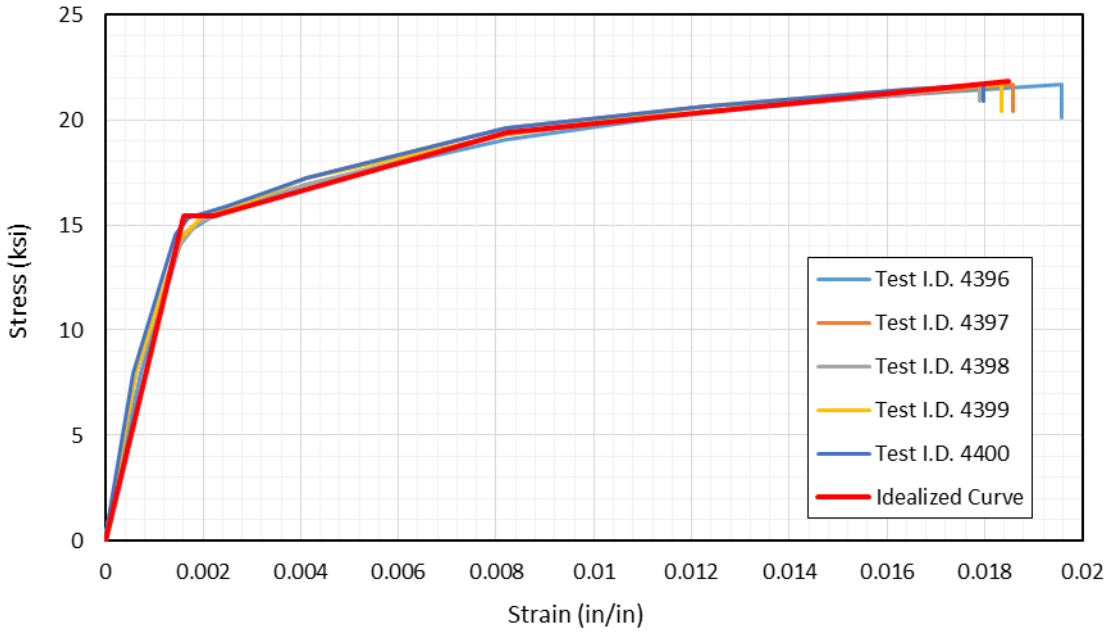

Figure B5. Stress-Strain Relationship for SSNA 14U-X

Appendix C
Verifications Using FHWA Bridge Design Example 1

Basic Support Condition

Support stiffness: Rigid
Column stiffness: I_{gross}
Abutment type: Seat type
Restraint of superstructure: Unrestrained longitudinally, restrained (pinned) in the transverse direction.

Superstructure

L = 242 ft	Overall bridge length
A_d = 120 ft^2	Cross-sectional area of superstructure
A_{cb} = 25 ft^2	Cross-sectional area of cap beam
I_{yd} = 51,000 ft^4	Moment of inertia of superstructure cross-sec. about local y-axis
I_{zd} = 575 ft^4	Moment of inertia of superstructure cross-sec. about local z-axis
f_c = 4,000 lb/in^2	Compressive strength of concrete
E_c = 3,600 kip/in^2	Young' modulus of elasticity of concrete
= 5.184 x 10^5 kip/ft^2	

Substructure

$I_c = \pi d^4/64 = \pi(4)^4/64 = 12.57$ ft^4 Moment of inertia of one column (about local y- or z-axes)
$A_c = \pi d^2/4 = \pi(4)^2/4 = 12.57$ ft^2 Cross-sectional area of one column
Rigid end zone of the upper part of columns = 2.83 ft. Assign a large stiffness to this zone.

Model of Structure

Let's use the same number of nodes and elements as the SAP computer analysis files in the Example 1. Except in the upper 2.83 ft of the columns, include a rigid element. In SAP this end condition can be specified. In STAAD and OpenSees, let's add a stiff element at these locations (three locations).

STAAD Model and Results

The lines below show the STAAD input file. Figures C1 and C2 show the nodes and elements. Figures C3 and C4 show the model under transverse and longitudinal 100 kip/ft loads, respectively. Figures C5 and C6 show the displaced shapes of the structure under the transverse and longitudinal loads, respectively.

```
STAAD SPACE
START JOB INFORMATION
ENGINEER DATE 02-Jun-15
END JOB INFORMATION
INPUT WIDTH 79
UNIT FEET KIP
JOINT COORDINATES
```

```
1 0 30.17 0; 2 35.5 30.17 0; 3 71 30.17 0; 4 106.5 30.17 0; 5 142 30.17 0;
6 167 30.17 0; 7 192 30.17 0; 8 217 30.17 0; 9 242 30.17 0; 10 142 0 28.375;
11 142 2 28.375; 12 142 27.34 28.375; 13 142 30.17 28.375; 14 142 0 0;
15 142 2 0; 16 142 27.34 0; 17 142 0 -28.375; 18 142 2 -28.375;
19 142 27.34 -28.375; 20 142 30.17 -28.375;
MEMBER INCIDENCES
1 1 2; 2 2 3; 3 3 4; 4 4 5; 5 5 6; 6 6 7; 7 7 8; 8 8 9;
9 10 11; 10 11 12; 11 12 13; 12 14 15; 13 15 16; 14 16 5; 15 17 18; 16 18 19;
17 19 20; 18 20 5; 19 5 13;
DEFINE MATERIAL START
ISOTROPIC CONCRETE
E 518400
POISSON 0.17
DENSITY 0.150336
ALPHA 5e-006
DAMP 0.05
TYPE CONCRETE
STRENGTH FCU 576
END DEFINE MATERIAL
MEMBER PROPERTY AMERICAN
1 TO 8 PRIS AX 120 IX 6000 IY 51000 IZ 575
9 10 12 13 15 16 PRIS AX 12.6 IX 25 IY 12.6 IZ 12.6
11 14 17 PRIS AX 1e+008 IX 1e+008 IY 1e+008 IZ 1e+008
18 19 PRIS AX 25 IX 10000 IY 1e+008 IZ 1e+008
CONSTANTS
MATERIAL CONCRETE ALL
SUPPORTS
10 14 17 FIXED
1 9 FIXED BUT FX MY MZ
LOAD 1 LOADTYPE None TITLE 100 KIP/FT TRANSVERSE
MEMBER LOAD
1 TO 8 UNI GZ -100
LOAD 2 LOADTYPE None TITLE 100 KIP/FT LONGITUDINAL
MEMBER LOAD
1 TO 8 UNI GX 100
PERFORM ANALYSIS
PRINT JOINT DISPLACEMENTS ALL
FINISH
```

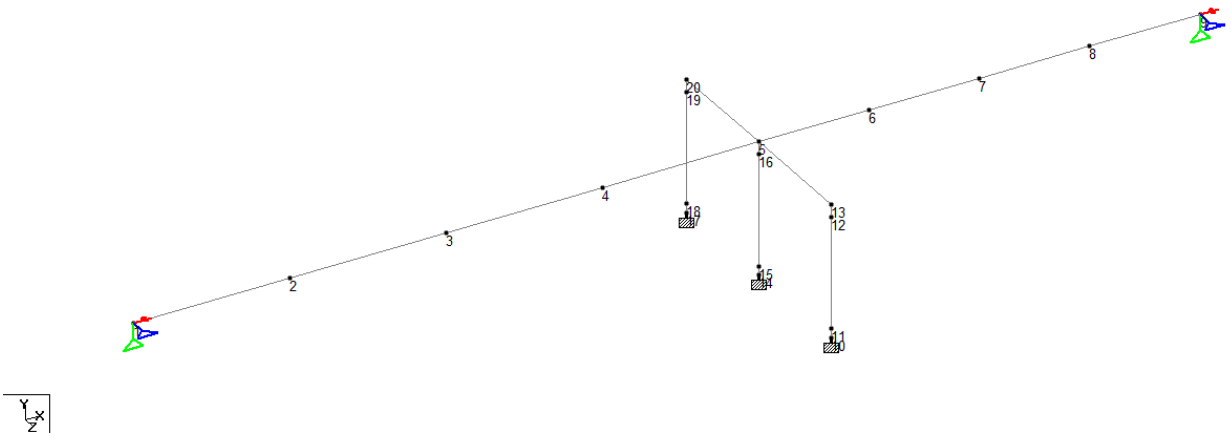

Figure C1. Bridge Model Nodes and Boundary Conditions

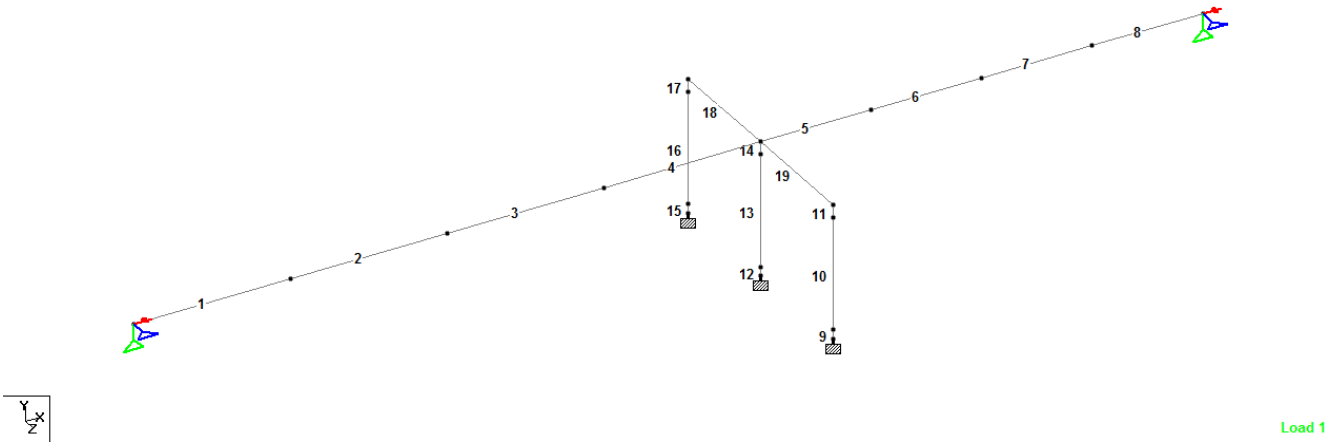

Figure C2. Bridge Model Elements

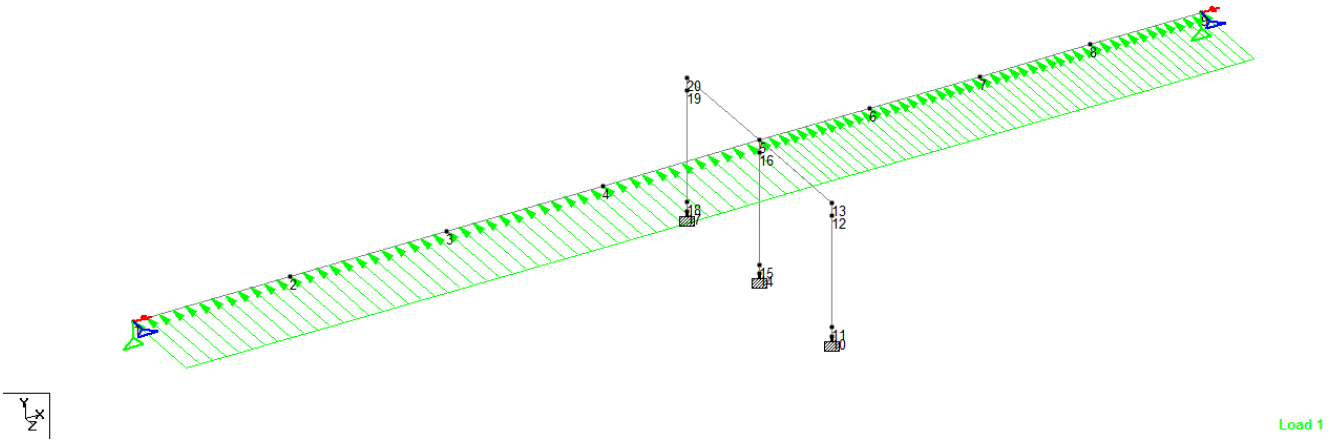

Figure C3. Bridge Model under Transverse Load of 100 kip/ft

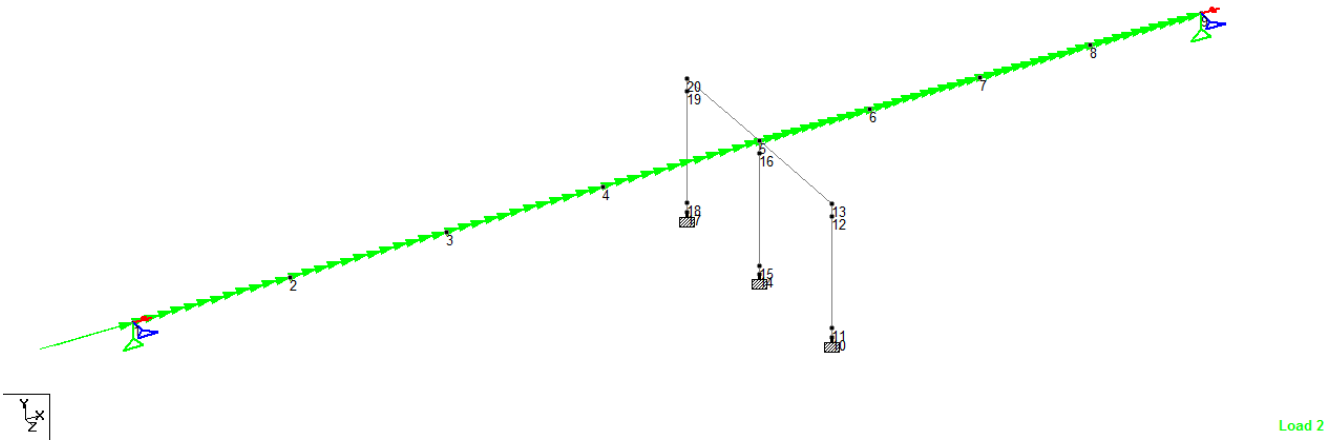

Figure C4. Bridge Model under Longitudinal Load of 100 kip/ft

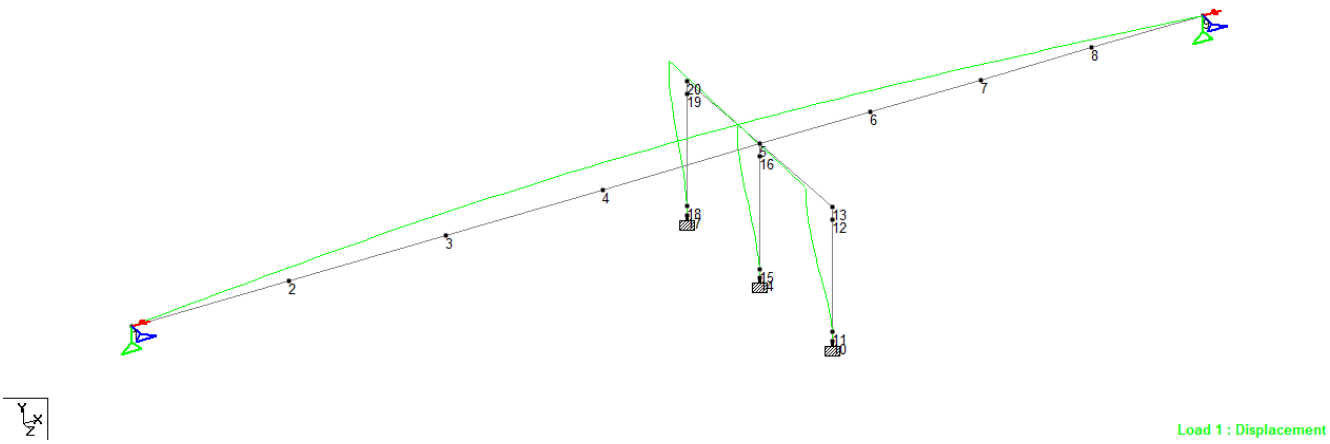

Figure C5. Displaced shape under transverse load

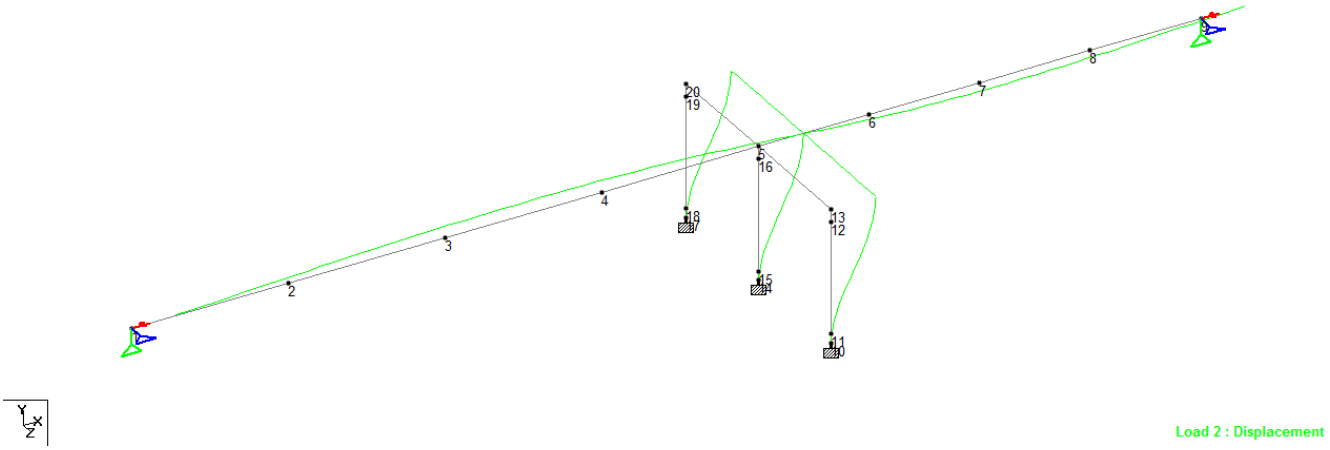

Figure C6. Displaced Shape under Longitudinal Load

Portion of the STAAD output file is shown in Table C1. Only the superstructure nodal displacements are shown. Dimensions are in inch and Radian. Load 1 is transverse load and Load 2 is longitudinal load.

Table C1. Portion of the STAAD Output File

JOINT DISPLACEMENT (INCH RADIANS) STRUCTURE TYPE = SPACE

JOINT	LOAD	X-TRANS	Y-TRANS	Z-TRANS	X-ROTAN	Y-ROTAN	Z-ROTAN
1	1	0.00000	0.00000	0.00000	0.00000	0.00202	0.00000
	2	30.59186	0.00000	0.00000	0.00000	0.00000	0.01251
2	1	0.00000	0.00000	-0.82583	-0.00002	0.00178	0.00000
	2	30.57970	4.99514	0.00000	0.00000	0.00000	0.01016
3	1	0.00000	0.00000	-1.46215	-0.00003	0.00116	0.00000
	2	30.54324	7.99410	0.00000	0.00000	0.00000	0.00313
4	1	0.00000	0.00000	-1.78553	-0.00005	0.00034	0.00000
	2	30.48246	7.00072	0.00000	0.00000	0.00000	-0.00858
5	1	0.00000	0.00000	-1.74464	-0.00007	-0.00052	0.00000
	2	30.39737	0.01882	0.00000	0.00000	0.00000	-0.02498
6	1	0.00000	0.00000	-1.50313	-0.00005	-0.00108	0.00000
	2	30.43957	-4.90077	0.00000	0.00000	0.00000	-0.00860
7	1	0.00000	0.00000	-1.10576	-0.00003	-0.00155	0.00000
	2	30.46971	-5.60760	0.00000	0.00000	0.00000	0.00310
8	1	0.00000	0.00000	-0.58723	-0.00002	-0.00188	0.00000
	2	30.48779	-3.50593	0.00000	0.00000	0.00000	0.01013
9	1	0.00000	0.00000	0.00000	0.00000	-0.00200	0.00000
	2	30.49382	0.00000	0.00000	0.00000	0.00000	0.01247

OpenSees Model and Results

The OpenSees elements require geometric transformation. From OpenSees Command Manual: "*The x-axis is a vector given by the two element nodes; The vector vecxz is a vector the user specifies that must not be parallel to the x-axis. The x-axis along with the vecxz Vector define the xz plane. The local y-axis is defined by taking the cross product of the x-axis vector and the vecxz vector (Vy = Vxz X Vx). The local z-axis is then found simply by taking the cross product of the y-axis and x-axis vectors (Vz = Vx X Vy). The section is attached to the element such that the y-z coordinate system used to specify the section corresponds to the y-z axes of the element.*"

The three types of geometric transformation used for OpenSees elements are shown in Figure C7.

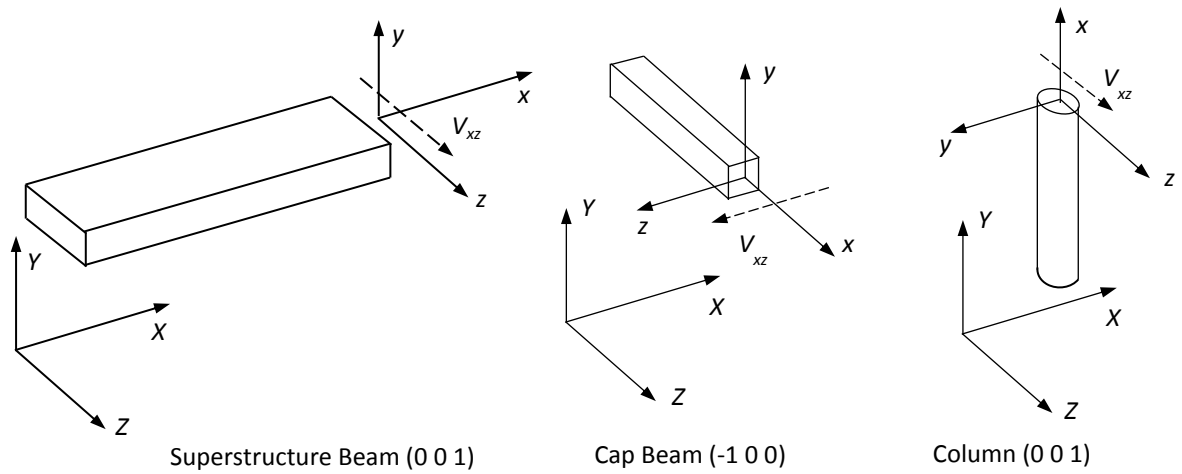

Figure C7. OpenSees Geometric Transformation (*XYZ* is global CS and *xyz* is local CS)

The OpenSees input file for the linear-elastic Basic Support Condition model is shown below. The same node and element numbers are used as those used in the STAAD model. The model uses the *elasticBeamColumn* elements.

```
#Clear cached data existing in the program
wipe
#Create Model with 3 dimensions and 6 degrees of freedom
model BasicBuilder -ndm 3 -ndf 6

#Create 6 DOF nodes
#      tag    X       Y        Z
node   1    0.00   30.17     0.000
node   2   35.50   30.17     0.000
node   3   71.00   30.17     0.000
node   4  106.50   30.17     0.000
node   5  142.00   30.17     0.000
node   6  167.00   30.17     0.000
node   7  192.00   30.17     0.000
node   8  217.00   30.17     0.000
node   9  242.00   30.17     0.000
node  10  142.00    0.00    28.375
node  11  142.00    2.00    28.375
node  12  142.00   27.34    28.375
node  13  142.00   30.17    28.375
node  14  142.00    0.00     0.000
node  15  142.00    2.00     0.000
node  16  142.00   27.34     0.000
node  17  142.00    0.00   -28.375
node  18  142.00    2.00   -28.375
node  19  142.00   27.34   -28.375
node  20  142.00   30.17   -28.375

# Constraints
fix 10  1  1  1  1  1  1
fix 14  1  1  1  1  1  1
fix 17  1  1  1  1  1  1
fix  1  0  1  1  1  0  0
```

```
fix  9  0  1  1  1  0  0

# Superstructure main beam elements
geomTransf Linear 1  0 0 1
# element elasticBeamColumn $eleTag $iNode $jNode $A $E $G $J $Iy $Iz $transfTag <-mass
$massDens> <-cMass>
element elasticBeamColumn 1  1  2  120  518400  222000  1e10  51000  575  1
element elasticBeamColumn 2  2  3  120  518400  222000  1e10  51000  575  1
element elasticBeamColumn 3  3  4  120  518400  222000  1e10  51000  575  1
element elasticBeamColumn 4  4  5  120  518400  222000  1e10  51000  575  1
element elasticBeamColumn 5  5  6  120  518400  222000  1e10  51000  575  1
element elasticBeamColumn 6  6  7  120  518400  222000  1e10  51000  575  1
element elasticBeamColumn 7  7  8  120  518400  222000  1e10  51000  575  1
element elasticBeamColumn 8  8  9  120  518400  222000  1e10  51000  575  1

# Substructure column elements
# geomTransf Linear 2  0 0 1
geomTransf PDelta 2  0 0 1; # PDelta may be needed when nonlinear material under gravity load
is used.

element elasticBeamColumn  9  10  11  12.6  518400  222000  25  12.6  12.6  2
element elasticBeamColumn 10  11  12  12.6  518400  222000  25  12.6  12.6  2
element elasticBeamColumn 11  12  13  1e10  518400  222000  1e10  1e10  1e10  2
element elasticBeamColumn 12  14  15  12.6  518400  222000  25  12.6  12.6  2
element elasticBeamColumn 13  15  16  12.6  518400  222000  25  12.6  12.6  2
element elasticBeamColumn 14  16   5   1e10 518400  222000  1e10  1e10  1e10  2
element elasticBeamColumn 15  17  18  12.6  518400  222000  25  12.6  12.6  2
element elasticBeamColumn 16  18  19  12.6  518400  222000  25  12.6  12.6  2
element elasticBeamColumn 17  19  20  1e10  518400  222000  1e10  1e10  1e10  2

# Superstructure cap beam elements
geomTransf Linear 3  -1 0 0
element elasticBeamColumn 18  20  5  25  518400  222000  1e10  1e10  1e10  3
element elasticBeamColumn 19   5  13  25  518400  222000  1e10  1e10  1e10  3

#Create recorder files for displacements
recorder Node -file Nodes1-9DisplTrans.out -time -nodeRange 1 9 -dof 3 disp
recorder Node -file Nodes1-9DisplLong.out -time -nodeRange 1 9 -dof 1 disp

# 100 kip/ft transverse load
# Create a Plain load pattern with a linear TimeSeries:
# command pattern Plain $tag $timeSeriesTag { $loads }
pattern Plain 1 Linear {
# eleLoad -ele $eleTag1 <$eleTag2 ....> -type -beamUniform $Wy $Wz <$Wx>
  eleLoad -ele 1 2 3 4 5 6 7 8 -type beamUniform 0 100 0
}

# 100 kip/ft longitudinal load
pattern Plain 2 Linear {
# eleLoad -ele $eleTag1 <$eleTag2 ....> -type -beamUniform $Wy $Wz <$Wx>
  eleLoad -ele 1 2 3 4 5 6 7 8 -type beamUniform 0 0 100
}

# Create the system of equations
system BandSPD
# Create the DOF numberer, the reverse Cuthill-McKee algorithm
numberer RCM
# Create the constraint handler, a Plain handler is used as homo constraints
constraints Plain
# Create the integration scheme, the LoadControl scheme using steps of 1.0
integrator LoadControl 1.0
```

```
# Create the solution algorithm, a Linear algorithm is created
algorithm Linear
# create the analysis object
analysis Static
analyze 1
```

Comparison of Results

The displacements obtained from STAAD, OpenSees and those given in the FHWA Design Example 1 for the superstructure node 5 (directly above the cap beam) are given in Table C2.

Table C2. Node 5 Displacements under 100 kip/ft for Basic Support Condition

Displacement	FHWA Example 1	STAAD	OpenSees
Transverse, ft	0.145	0.145	0.145
Longitudinal, ft	2.53	2.53	2.52

Spring Support Condition

Spring Support Condition

Support stiffness: Springs
Column stiffness: $0.5I_{gross}$
Abutment type: Stub wall
Restraint of superstructure: Restrained longitudinally

Superstructure

L = 242 ft	Overall bridge length
A_d = 120 ft^2	Cross-sectional area of superstructure
A_{cb} = 25 ft^2	Cross-sectional area of cap beam
I_{yd} = 51,000 ft^4	Moment of inertia of superstructure cross-sec. about local y-axis
I_{zd} = 575 ft^4	Moment of inertia of superstructure cross-sec. about local z-axis
f_c = 4,000 lb/in^2	Compressive strength of concrete
E_c = 3,600 kip/in^2	Young' modulus of elasticity of concrete
= 5.184 x 10^5 kip/ft^2	

Substructure

$0.5I_c = 0.5\pi d^4/64 = 0.5\pi(4)^4/64 = 6.3$ ft^4 Reduced col. mom. of inertia (local y- & z-axes)
$A_c = \pi d^2/4 = \pi(4)^2/4 = 12.57$ ft^2 Cross-sectional area of one column
Rigid end zone of the upper part of columns = 2.83 ft. Assign a large stiffness to this zone.

Model of Structure

Let's use the same number of nodes and elements as the SAP computer analysis files in the Example 1 Appendix. Except in the upper 2.83 ft of the columns, include a rigid element. In SAP this end condition can be specified. In STAAD and OpenSees, let's add a stiff element at these locations (three locations).

Abutment Soil Spring

Translational: Ktx = 83,250 k/ft (83,000 used as per SAP input in Appendix),
Kty = large, Ktz = 53,200 k/ft (52,000 used as per SAP input)
Rotational: Krx = large, Kry = Krz = 0

Column Base Soil Springs

Translational: Ktx = Kty = Ktz = large
Rotational: Kry = large,
Krx = Krz = 4,800,000 k.ft/rad *1 rad/(57.2957795 degree) = 83,776 k.ft/degree

STAAD Model and Results

The lines below show are the STAAD input file. Figures C8 and C29 show the nodes and elements. Figures C10 and C11 show the model under transverse and longitudinal 100 kip/ft loads, respectively. Figures C12 and C13 show the displaced shapes of the structure under the transverse and longitudinal loads, respectively.

```
STAAD SPACE
START JOB INFORMATION
ENGINEER DATE 02-Jun-15
END JOB INFORMATION
INPUT WIDTH 79
UNIT FEET KIP
JOINT COORDINATES
1 0 30.17 0; 2 35.5 30.17 0; 3 71 30.17 0; 4 106.5 30.17 0; 5 142 30.17 0;
6 167 30.17 0; 7 192 30.17 0; 8 217 30.17 0; 9 242 30.17 0; 10 142 0 28.375;
11 142 2 28.375; 12 142 27.34 28.375; 13 142 30.17 28.375; 14 142 0 0;
15 142 2 0; 16 142 27.34 0; 17 142 0 -28.375; 18 142 2 -28.375;
19 142 27.34 -28.375; 20 142 30.17 -28.375;
MEMBER INCIDENCES
1 1 2; 2 2 3; 3 3 4; 4 4 5; 5 5 6; 6 6 7; 7 7 8; 8 8 9; 9 10 11; 10 11 12;
11 12 13; 12 14 15; 13 15 16; 14 16 5; 15 17 18; 16 18 19; 17 19 20; 18 20 5;
19 5 13;
DEFINE MATERIAL START
ISOTROPIC CONCRETE
E 518400
POISSON 0.17
DENSITY 0.150336
ALPHA 5e-006
DAMP 0.05
TYPE CONCRETE
STRENGTH FCU 576
END DEFINE MATERIAL
MEMBER PROPERTY AMERICAN
1 TO 8 PRIS AX 120 IX 6000 IY 51000 IZ 575
```

```
9 10 12 13 15 16 PRIS AX 12.6 IX 25 IY 6.3 IZ 6.3
11 14 17 PRIS AX 1e+008 IX 1e+008 IY 1e+008 IZ 1e+008
18 19 PRIS AX 25 IX 10000 IY 1e+008 IZ 1e+008
CONSTANTS
MATERIAL CONCRETE ALL
SUPPORTS
1 9 FIXED BUT MY MZ KFX 83000 KFY 1e+012 KFZ 52000 KMX 1e+012
10 14 17 FIXED BUT KFX 1e+12 KFY 1e+12 KFZ 1e+12 KMX 83776 KMY 1e+012 KMZ 83776
LOAD 1 LOADTYPE None TITLE 100 KIP/FT TRANSVERSE
MEMBER LOAD
1 TO 8 UNI GZ -100
LOAD 2 LOADTYPE None TITLE 100 KIP/FT LONGITUDINAL
MEMBER LOAD
1 TO 8 UNI GX 100
PERFORM ANALYSIS
PRINT JOINT DISPLACEMENTS ALL
FINISH
```

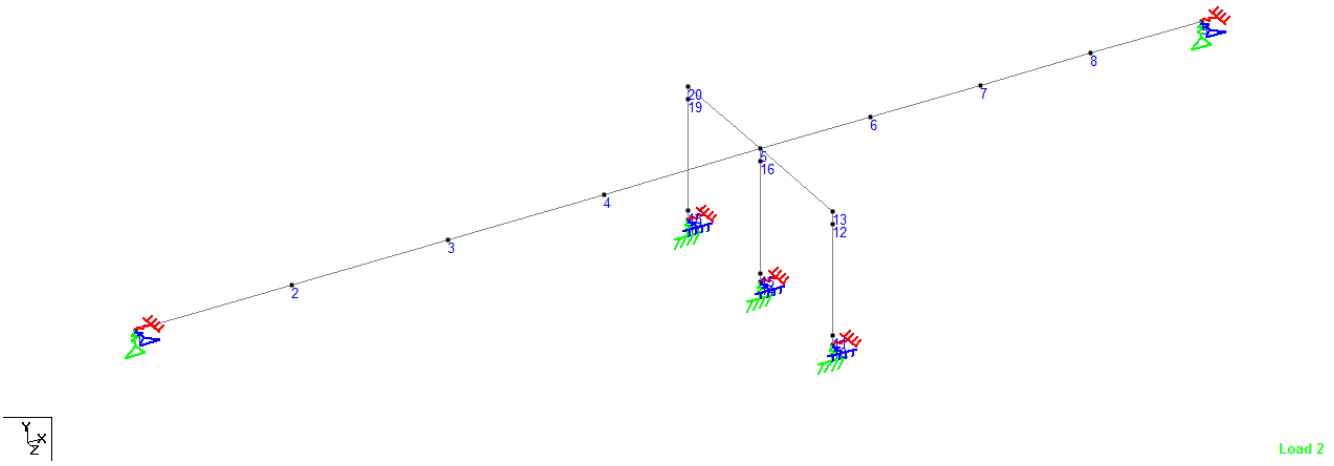

Figure C8. Bridge Model Nodes and Boundary Conditions

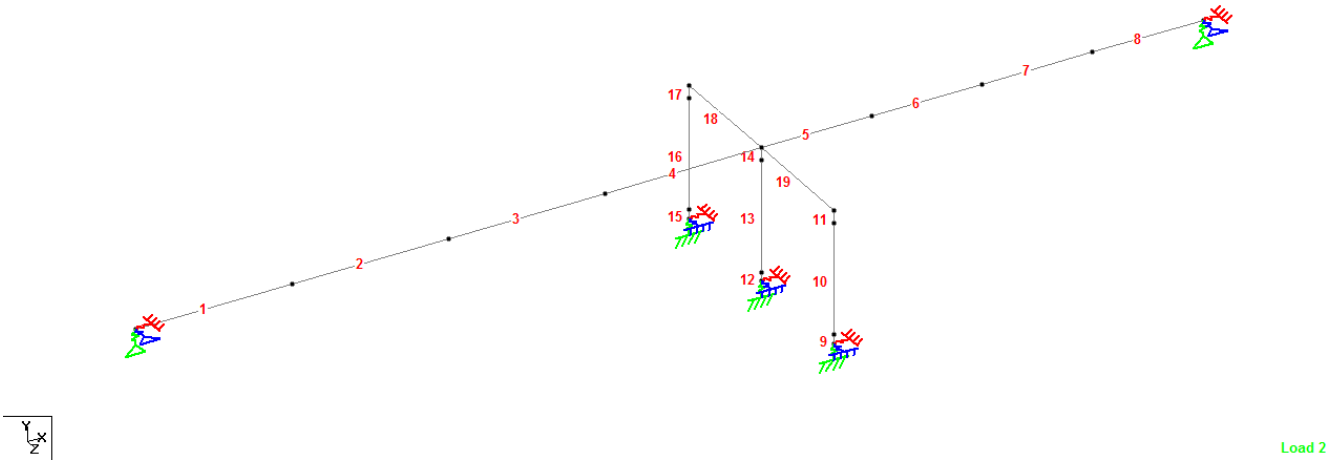

Figure C9. Bridge Model Elements

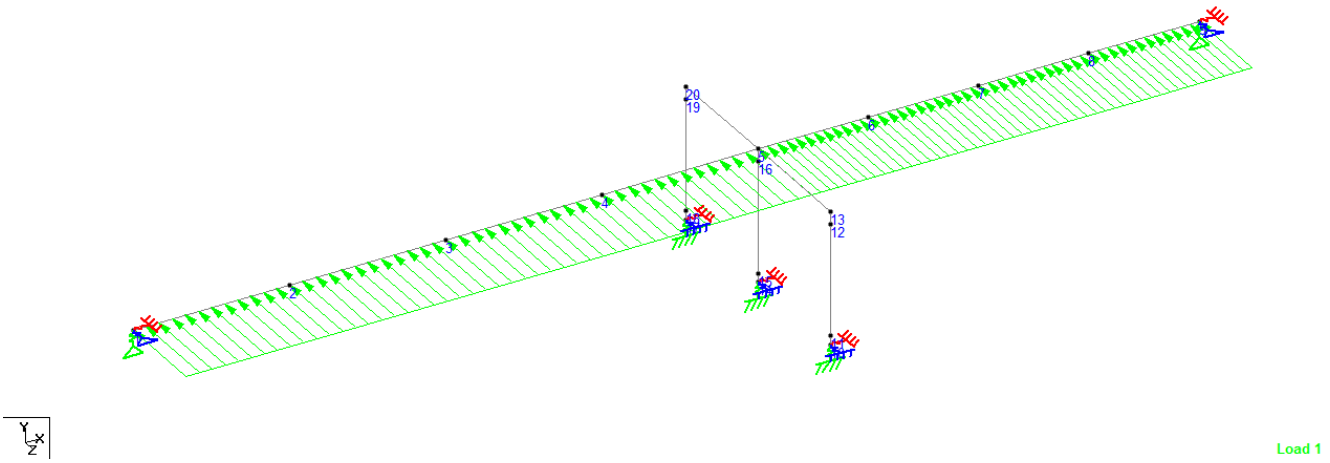

Figure C10. Bridge Model under Transverse Load of 100 kip/ft

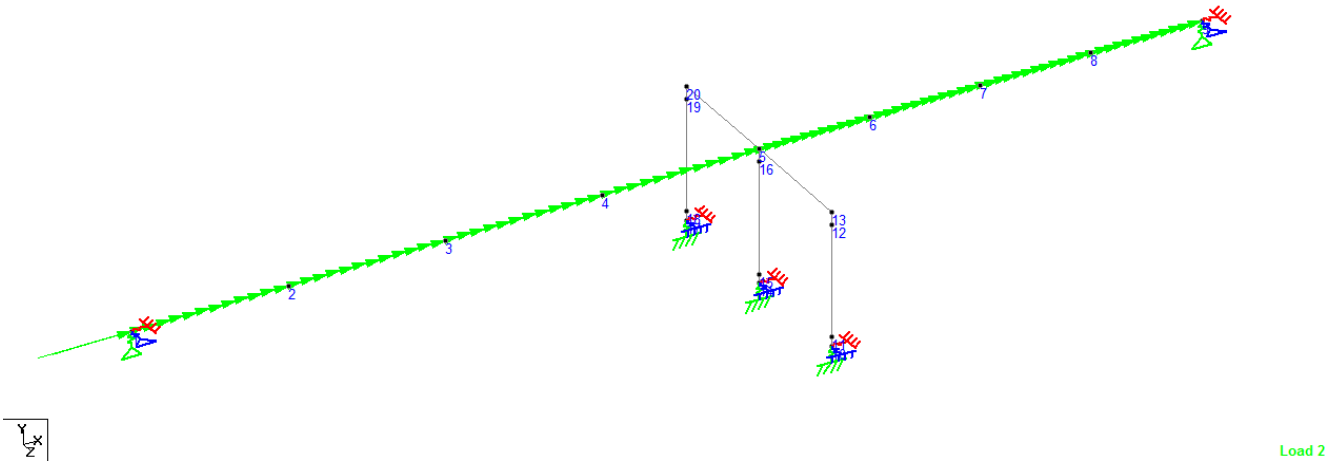

Figure C11. Bridge Model under Longitudinal Load of 100 kip/ft

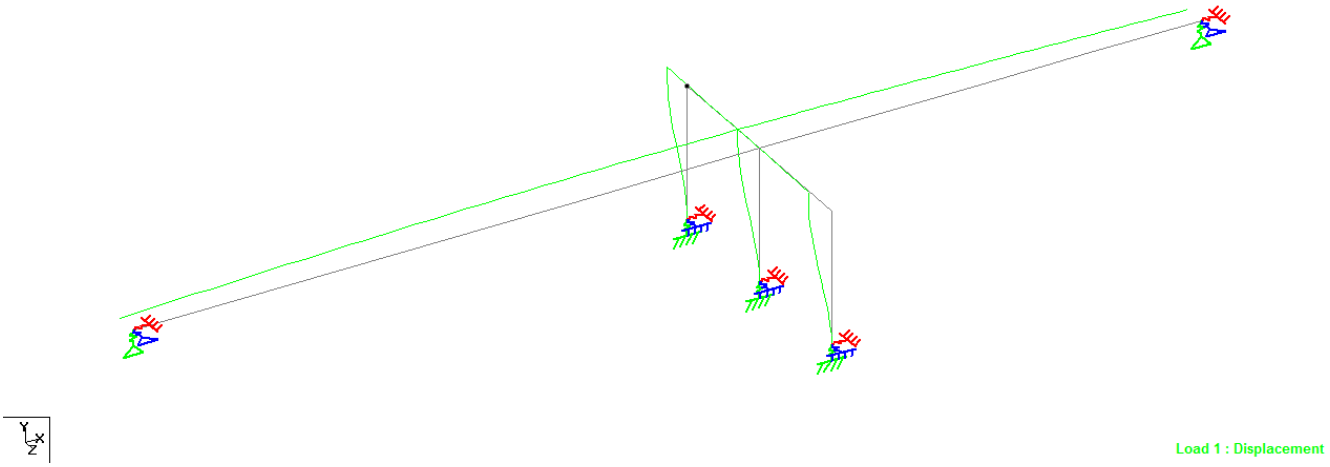

Figure C12. Displaced Shape under Transverse Load of 100 kip/ft

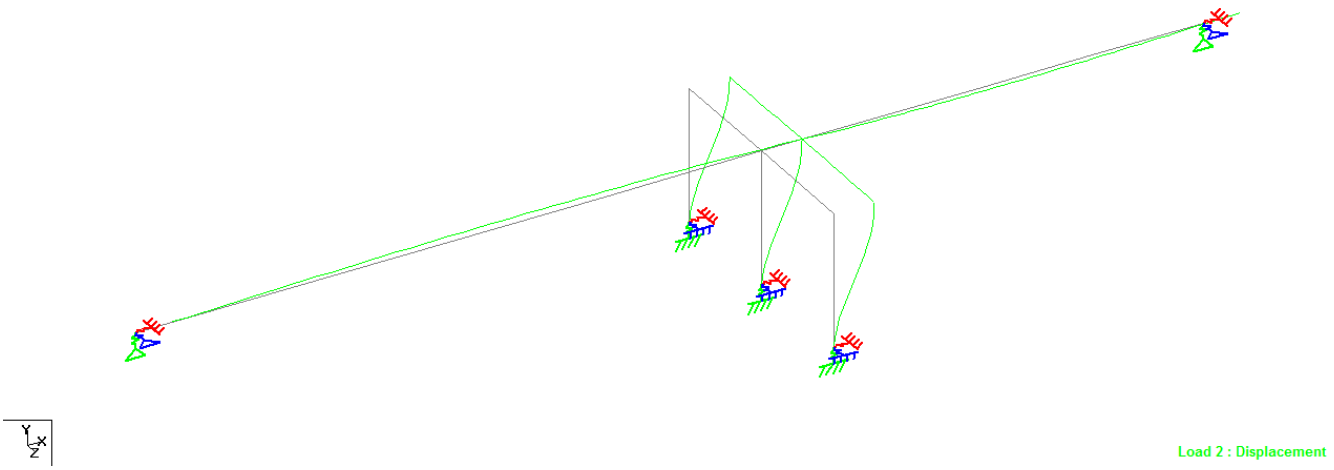

Figure C13. Displaced Shape under Longitudinal Load of 100 kip/ft

Portion of the STAAD output file is shown in Table C3. Only the superstructure nodal displacements are shown. Dimensions are in inch and Radian. Load 1 is transverse load and Load 2 is longitudinal load.

Table C3. Portion of the STAAD Output File

JOINT DISPLACEMENT (INCH RADIANS) STRUCTURE TYPE = SPACE

JOINT	LOAD	X-TRANS	Y-TRANS	Z-TRANS	X-ROTAN	Y-ROTAN	Z-ROTAN
1	1	0.00000	0.00000	-2.60926	0.00000	0.00197	0.00000
	2	1.69719	0.00000	0.00000	0.00000	0.00000	0.00040
2	1	0.00000	0.00000	-3.41182	-0.00002	0.00173	0.00000
	2	1.76542	0.15965	0.00000	0.00000	0.00000	0.00032
3	1	0.00000	0.00000	-4.02684	-0.00004	0.00111	0.00000
	2	1.80935	0.25550	0.00000	0.00000	0.00000	0.00010
4	1	0.00000	0.00000	-4.33284	-0.00006	0.00030	0.00000
	2	1.82896	0.22375	0.00000	0.00000	0.00000	-0.00027
5	1	0.00000	0.00000	-4.28043	-0.00008	-0.00054	0.00000
	2	1.82426	0.00060	0.00000	0.00000	0.00000	-0.00080
6	1	0.00000	0.00000	-4.03535	-0.00006	-0.00109	0.00000
	2	1.80993	-0.15663	0.00000	0.00000	0.00000	-0.00027
7	1	0.00000	0.00000	-3.63766	-0.00004	-0.00155	0.00000
	2	1.78355	-0.17923	0.00000	0.00000	0.00000	0.00010
8	1	0.00000	0.00000	-3.12099	-0.00002	-0.00187	0.00000
	2	1.74511	-0.11205	0.00000	0.00000	0.00000	0.00032
9	1	0.00000	0.00000	-2.53670	0.00000	-0.00199	0.00000
	2	1.69461	0.00000	0.00000	0.00000	0.00000	0.00040

OpenSees Model and Results

The geometric transformation of the elements are the same as those in Figure C7. The same node and element numbers are used as before. However, more nodes are added to define the zero-length elements used for springs. These nodes are: 100, 900, 1000, 1400, and 1700. See Figure C14.

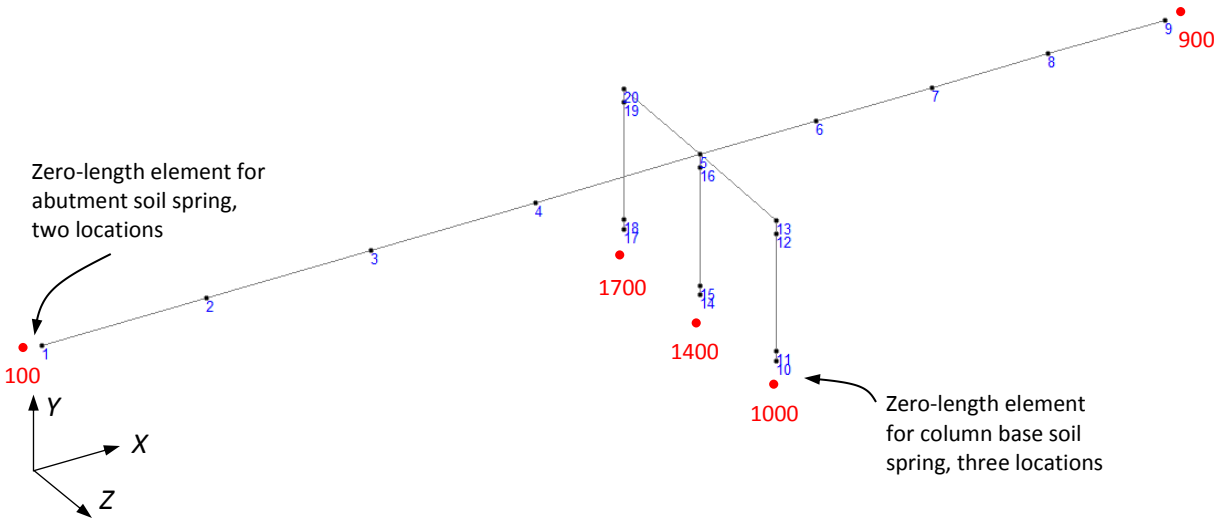

Figure C14. Nodes Needed in OpenSees for the Zero-length Spring Elements

The OpenSees input file for the linear-elastic Spring Support Condition model is shown below.

```
#Clear cached data existing in the program
wipe
#Create Model with 3 dimensions and 6 degrees of freedom
model BasicBuilder -ndm 3 -ndf 6

#Create 6 DOF nodes
#      tag    X       Y        Z
node   1    0.00   30.17     0.000
node   2   35.50   30.17     0.000
node   3   71.00   30.17     0.000
node   4  106.50   30.17     0.000
node   5  142.00   30.17     0.000
node   6  167.00   30.17     0.000
node   7  192.00   30.17     0.000
node   8  217.00   30.17     0.000
node   9  242.00   30.17     0.000
node  10  142.00    0.00    28.375
node  11  142.00    2.00    28.375
node  12  142.00   27.34    28.375
node  13  142.00   30.17    28.375
node  14  142.00    0.00     0.000
node  15  142.00    2.00     0.000
node  16  142.00   27.34     0.000
node  17  142.00    0.00   -28.375
node  18  142.00    2.00   -28.375
node    19  142.00   27.34   -28.375
node    20  142.00   30.17   -28.375
```

```
node   100    0.00   30.17     0.000
node   900  242.00   30.17     0.000
node  1000  142.00    0.00    28.375
node  1400  142.00    0.00     0.000
node  1700  142.00    0.00   -28.375

# Constraints
fix 100   1  1  1  1  1  1
fix 900   1  1  1  1  1  1
fix 1000  1  1  1  1  1  1
fix 1400  1  1  1  1  1  1
fix 1700  1  1  1  1  1  1

# Superstructure main beam elements
geomTransf Linear 1  0 0 1
# element elasticBeamColumn $eleTag $iNode $jNode $A $E $G $J $Iy $Iz $transfTag <-mass
$massDens> <-cMass>
element elasticBeamColumn 1  1  2  120  518400  222000  1e10  51000  575  1
element elasticBeamColumn 2  2  3  120  518400  222000  1e10  51000  575  1
element elasticBeamColumn 3  3  4  120  518400  222000  1e10  51000  575  1
element elasticBeamColumn 4  4  5  120  518400  222000  1e10  51000  575  1
element elasticBeamColumn 5  5  6  120  518400  222000  1e10  51000  575  1
element elasticBeamColumn 6  6  7  120  518400  222000  1e10  51000  575  1
element elasticBeamColumn 7  7  8  120  518400  222000  1e10  51000  575  1
element elasticBeamColumn 8  8  9  120  518400  222000  1e10  51000  575  1

# Substructure column elements
# geomTransf Linear 2  0 0 1
geomTransf PDelta 2  0 0 1; # PDelta may be needed when nonlinear material under gravity load
is used.

element elasticBeamColumn  9  10  11  12.6  518400  222000  25  6.3  6.3  2
element elasticBeamColumn 10  11  12  12.6  518400  222000  25  6.3  6.3  2
element elasticBeamColumn 11  12  13  1e10  518400  222000  1e10  1e10  1e10  2
element elasticBeamColumn 12  14  15  12.6  518400  222000  25  6.3  6.3  2
element elasticBeamColumn 13  15  16  12.6  518400  222000  25  6.3  6.3  2
element elasticBeamColumn 14  16   5   1e10 518400  222000  1e10  1e10  1e10  2
element elasticBeamColumn 15  17  18  12.6  518400  222000  25  6.3  6.3  2
element elasticBeamColumn 16  18  19  12.6  518400  222000  25  6.3  6.3  2
element elasticBeamColumn 17  19  20  1e10  518400  222000  1e10  1e10  1e10  2

# Superstructure cap beam elements
geomTransf Linear 3  -1 0 0
element elasticBeamColumn 18  20  5  25  518400  222000  1e10  1e10  1e10  3
element elasticBeamColumn 19   5  13  25  518400  222000  1e10  1e10  1e10  3

# Spring elastic material stiffness values for abutment soil support
uniaxialMaterial Elastic 1 83000;    # translational stiffness along local x axis kip/ft
uniaxialMaterial Elastic 2 1e12;     # translational stiffness along local y axis kip/ft
uniaxialMaterial Elastic 3 52000;    # translational stiffness along local z axis kip/ft
uniaxialMaterial Elastic 4 1e12;     # Rotational stiffness along local x axis kip.ft/radian
uniaxialMaterial Elastic 5 0;        # Rotational stiffness along local y axis kip.ft/radian
uniaxialMaterial Elastic 6 0;        # Rotational stiffness along local z axis kip.ft/radian

# Spring elements for abutment soil support
# element zeroLength $eleTag $iNode $jNode -mat $matTag1 $matTag2 ... -dir $dir1 $dir2 ...
element zeroLength 20 100 1 -mat 1 2 3 4 5 6 -dir 1 2 3 4 5 6
element zeroLength 21 9 900 -mat 1 2 3 4 5 6 -dir 1 2 3 4 5 6

# Spring elastic material stiffness values for column base soil support
uniaxialMaterial Elastic 10 1e12;     # translational stiffness along local x axis kip/ft
```

```
uniaxialMaterial Elastic 20 1e12;     # translational stiffness along local y axis kip/ft
uniaxialMaterial Elastic 30 1e12;     # translational stiffness along local z axis kip/ft
uniaxialMaterial Elastic 40 4.8e6;    # Rotational stiffness along local x axis kip.ft/radian
uniaxialMaterial Elastic 50 1e12;     # Rotational stiffness along local y axis kip.ft/radian
uniaxialMaterial Elastic 60 4.8e6;    # Rotational stiffness along local z axis kip.ft/radian

# Spring elements for abutment soil support
# element zeroLength $eleTag $iNode $jNode -mat $matTag1 $matTag2 ... -dir $dir1 $dir2 ...
element zeroLength 22 1000 10 -mat 10 20 30 40 50 60 -dir 1 2 3 4 5 6
element zeroLength 23 1400 14 -mat 10 20 30 40 50 60 -dir 1 2 3 4 5 6
element zeroLength 24 1700 17 -mat 10 20 30 40 50 60 -dir 1 2 3 4 5 6

#Create recorder files for displacements
recorder Node -file SpringSupportNodes1-9DisplTrans.out -time -nodeRange 1 9 -dof 3 disp
recorder Node -file SpringSupportNodes1-9DisplLong.out -time -nodeRange 1 9 -dof 1 disp

# 100 lb/ft transverse load
# Create a Plain load pattern with a linear TimeSeries:
# command pattern Plain $tag $timeSeriesTag { $loads }
pattern Plain 1 Linear {
# eleLoad -ele $eleTag1 <$eleTag2 ....> -type -beamUniform $Wy $Wz <$Wx>
  eleLoad -ele 1 2 3 4 5 6 7 8 -type beamUniform 0 100 0
}

# 100 lb/ft longitudinal load
pattern Plain 2 Linear {
# eleLoad -ele $eleTag1 <$eleTag2 ....> -type -beamUniform $Wy $Wz <$Wx>
  eleLoad -ele 1 2 3 4 5 6 7 8 -type beamUniform 0 0 100
}

# Create the system of equations
system BandSPD
# Create the DOF numberer, the reverse Cuthill-McKee algorithm
numberer RCM
# Create the constraint handler, a Plain handler is used as homo constraints
constraints Plain
# Create the integration scheme, the LoadControl scheme using steps of 1.0
integrator LoadControl 1.0
# Create the solution algorithm, a Linear algorithm is created
algorithm Linear
# create the analysis object
analysis Static
analyze 1
```

Comparison of Results

The displacements obtained from STAAD, OpenSees and those given in the FHWA Design Example 1 for the superstructure node 5 (directly above the cap beam) are given in Table C4.

Table C4. Node 5 Displacements under 100 kip/ft for Spring Support Condition

Displacement	FHWA Example 1	STAAD	OpenSees
Transverse, ft	0.357	0.357	0.357
Longitudinal, ft	0.152	0.152	0.152

Appendix D
Procedures for Estimating Integral Abutment Stiffness Values

The procedures for estimating bridge transverse and longitudinal abutment stiffness values are presented in this appendix. For simplicity, in the procedures outlined below, it is assumed that both abutments have: (a) the same pile lateral force-displacement behavior, (b) identical wingwalls (if present), and (c) identical abutment wall area. In the bridge under consideration, some of these assumptions may not apply and procedure may have to be slightly revised. For example, in one of the Idaho bridges considered, the abutments of the bridge had different pile force-displacement behavior. Also, the procedures below assume that the strong direction of H-piles is oriented longitudinally, while weak direction is oriented in transverse direction.

Longitudinal Stiffness

This procedure assumes the same value of longitudinal abutment stiffness for both abutments. This longitudinal stiffness is half of the sum of the longitudinal stiffness values from the two sets of abutment piles and the stiffness of one abutment backfill. As shown in Figure D1, a linear relation is assumed between the abutment backfill reaction and the corresponding displacement from zero displacement to $0.02H_{aw}$ where, H_{aw} = height of abutment wall. The corresponding maximum force to mobilize the full passive backfill resistance of $7.7\ k/ft^2$ is $\left(7.7\frac{k}{ft^2}\right)A_{aw}$. Where, A_{aw} is the area of the abutment wall = $H_{aw}\ L_{aw}$ with L_{aw} being the length of the abutment wall. It is further assumed that the full maximum force remains constant beyond the displacement of $0.02H_{aw}$.

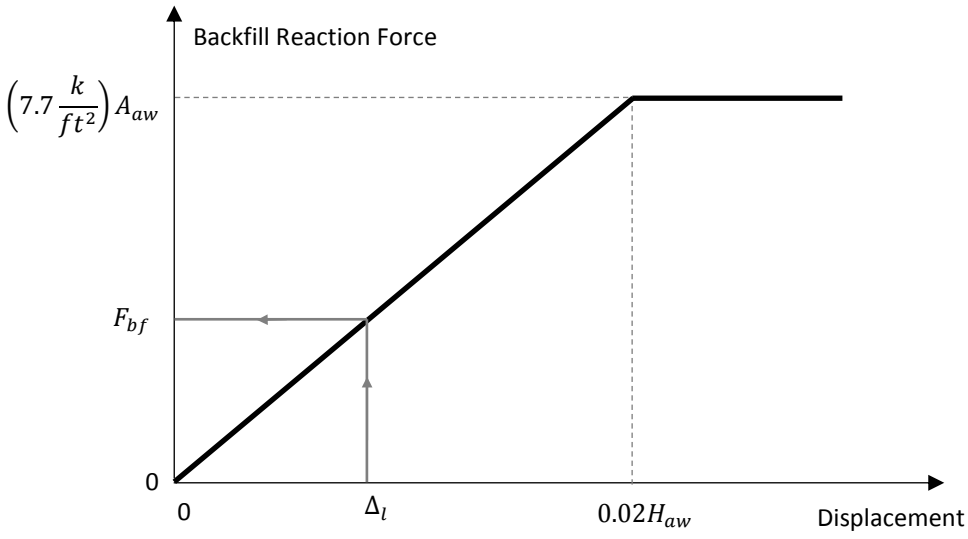

Figure D1. Abutment Backfill Reaction Force versus Displacement

Figure D2 shows a typical top of the pile lateral force versus displacement while the pile is bending about the strong axis. In the bridge model, the initial longitudinal pile stiffness is assumed based on $\Delta_o = 1\ in.$ Here, subscript "*o*" indicates initial estimates. From the pile force versus displacement in the strong direction, the initial force in the strong direction corresponding to displacement of 1 in. is estimated as F_{so}. The initial pile stiffness in the strong direction is $k_{so} = \frac{F_{so}}{\Delta_o}$.

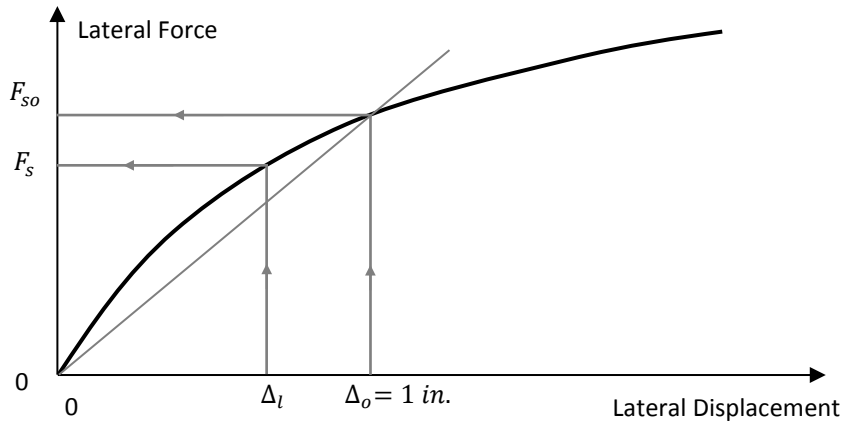

Figure D2. Top of the Pile Lateral Force versus Displacement, Bending about the Strong Axis

The initial abutment longitudinal stiffness K_{lo}, to be used for both abutments, is estimated as:

$$K_{lo} = \frac{(n_1 + n_2)k_{so} + \left(\frac{7.7A_{aw}}{d}\right)}{2}$$

Figure D3. Equation for Initial Abutment Longitudinal Stiffness

Where, n_1 = the number of piles in Abutment 1, n_2 = the number of piles in Abutment 2, k_{so} = the initial pile stiffness in the strong direction, A_{aw} = the area of the abutment wall = $H_{aw}\ L_{aw}$, H_{aw} = height of abutment wall, L_{aw}= length of abutment wall, and d = $0.02\ H_{aw}$ = deflection needed to mobilize the full passive resistance of $7.7\ k/ft^2$.

After loading the bridge linear-elastic model in the longitudinal direction, the average of the bridge longitudinal abutment displacement, Δ_l, is obtained. The average value of longitudinal displacements is used since in this direction the abutment displacements are very close to one another. In addition, determine the longitudinal seismic forces R_{l1} and R_{l2} for Abutments 1 and 2. Let's assume that Δ_l is less than 1 in. As shown in Figures D1 and D2, with the new Δ_l value, an abutment backfill reaction force F_{bf} and a revised pile lateral reaction force, F_s is obtained. Check to see if the equilibrium is reached between the sum of longitudinal seismic forces and abutment backfill resistance, and the lateral pile resistance forces as shown by equation in Figure D4:

$$R_{l1} + R_{l2} \stackrel{?}{\cong} (n_1 + n_2)F_s + F_{bf}$$

Figure D4. Equation for Longitudinal Force Equilibrium

The symbol $\stackrel{?}{\cong}$ is used to indicate whether the two sides are approximately equal to each other. If equation in Figure D4 is not satisfied, change the value of longitudinal abutment stiffness and find the revised average value of longitudinal displacements and abutment seismic forces. With the revised average displacement, find the longitudinal abutment backfill resistance force and the lateral pile resistance forces and see if equation in Figure D4 is satisfied. This process is repeated a few times until the two sides of equation in Figure D4 are within 10%. When evaluating a pier it is recommended to keep the abutment stiffness on the lower side. This would generally result in higher forces and displacements at the pier(s).

Example

Let's assume the initial springs based on 1" displacement result in ¾" displacement and the corresponding force of 600kips at each abutment (1200kips total longitudinal force to be resisted by abutments). Let's also assume we have 10 piles at each abutment and they resist 30kips each at ¾" displacement, so the total pile resistance from both abutments would be 2*10*30=600kips, leaving 1200-600=600kips to be resisted by one abutment backfill. Now we need to check how much backfill resistance we get from ¾" displacement, assuming linear relation from 0" (0kips) to d=0.02H" ($7.7A_{aw}$). (Any displacement higher than 0.02H" will result in a constant backfill resistance of $7.7A_{aw}$). If ¾" displacement results in backfill resistance considerably higher than 600kips, we might increase abutment stiffness, which would give us higher acting seismic force, but smaller displacements. On the other hand, if ¾" results in backfill resistance quite lower than 600kips, we may need to soften the abutment springs in order to reduce the acting force, but increase the displacement and associated resistance from piles and backfill. We repeat the process until we get good correlation (within 10%) between abutment acting seismic forces and resulting resistance from piles and backfill based on acting displacement.

Transverse Stiffness

In this procedure abutment forces and displacements are evaluated individually. The wing shear capacity can only be considered effective if it is larger than the difference between acting seismic forces and the piles reaction under given displacement. If otherwise, it is assumed that the wingwall has failed and it does not contribute to the transverse stiffness or resistance. The shear force V_c is calculated using equation in Figure D5:

$$V_c = 0.0316\beta\sqrt{f_c'}b_v d_v$$

Figure D5. Equation for Shear Force Capacity

Where, β = 2, f_c'= compressive strength of the concrete, ksi, b_v = the height of the wingwall at the interface of wing and abutment, $d_v = \max\left[d_e - \frac{a}{2}, 0.9d_e, 0.72h\right]$, d_e = the effective depth = distance to the center of the back reinforcement from the face of the wingwall = $h - cover - bar\ diameter/2$, $a = \frac{A_s f_y}{0.85 f_c' b_v}$ = depth of the equivalent compression block; A_s = area of the flexural reinforcement on the backfill side; $f_y = 60\ ksi$ = yield strength of the flexural reinforcement, and h = the depth of the wingwall (typically 12 in.).

Figure D6 shows a typical top of pile lateral force versus displacement while the pile is bending about the weak axis. Note that here the force values are shown smaller compared to Figure D2 (i.e., less force required for a given displacement in the weak direction compared to the strong direction).

In the bridge model, the initial transverse pile stiffness is assumed based on $\Delta_o = 1\ in.$ Here, again the subscript "*o*" indicates initial estimates. From the pile force versus displacement in the weak direction (Figure D6), the initial force in the weak direction corresponding to displacement of 1 in. is estimated as F_{wo}. The initial pile stiffness in the weak direction is $k_{wo} = \frac{F_{wo}}{\Delta_o}$.

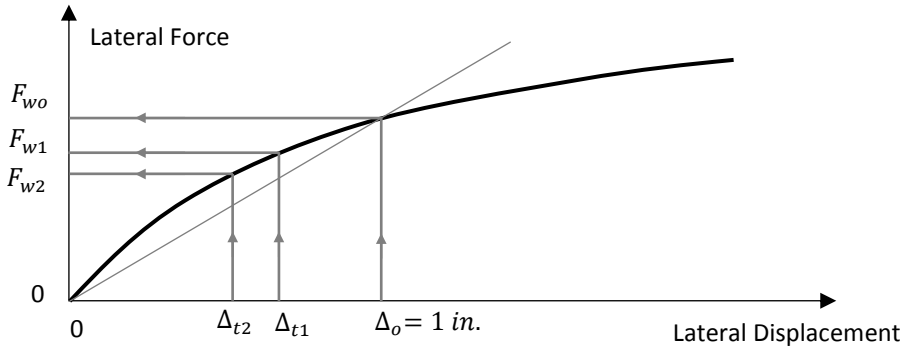

Figure D6. Top of the Pile Lateral Force versus Displacement, Bending about the Weak Axis

For one of the two abutments, let's say Abutment 1, the initial value for the transverse stiffness is estimated using equation in Figure D7. Here, initially the contribution of the wing is not included.

$$K_{t1,o} = n_1 k_{wo}$$

Figure D7. Equation for Initial Transverse Stiffness for Abutment 1

Where, n_1 = the number of piles in Abutment 1, and k_{wo} = the initial pile stiffness in the weak direction.

Repeat the same process for Abutment 2 to obtain initial value for its transverse stiffness, $K_{t2,o}$:

$$K_{t2,o} = n_2 k_{wo}$$

Figure D8. Equation for Initial Transverse Stiffness for Abutment 2

Where, n_2 = the number of piles in Abutment 2.

With the above initial estimates for the abutment transverse stiffness values, load the bridge linear-elastic model in the transverse direction. Determine the transverse displacements and the corresponding seismic forces for Abutments 1 and 2. Note, here unlike the longitudinal direction, the abutment displacements may be significantly different and the use of average value may not be suitable. Let's call the transverse displacements Δ_{t1} and Δ_{t2} and call the transverse forces R_{t1} and R_{t2}. Let's also assume that the displacements are both less than 1 in. with the corresponding top of the pile reactions in the weak direction as F_{w1} and F_{w2} as shown in Figure D3. Now, examine to see if the force equilibrium is maintained as shown by equations in Figures D9 and D10.

$$R_{t1} \stackrel{?}{\cong} n_1 F_{w1} + F_{wing}$$

Figure D9. Equation for Transverse Equilibrium of Abutment 1

$$R_{t2} \stackrel{?}{\cong} n_2 F_{w2} + F_{wing}$$

Figure D10. Equation for Transverse Equilibrium of Abutment 2

Where, F_{wing} is the shear force demand on a single wing with a value $F_{wing} \leq V_c$.

If the left hand sides of equations in Figures D9 and D10 are larger than the right hand side, reduce the transverse spring stiffness values K_{t1} and K_{t2}. This will result in larger transverse displacements and thus lead to larger values for F_{w1} and F_{w2} (see Figure D6). This process is repeated a few times until the two sides of equations in Figures D9 and D10 are within 10%. Again, it is recommended to keep the abutment stiffness values on the lower side. This would generally result in higher forces and displacements at the pier(s). The numerical example below assumes a symmetrical bridge with the same number of piles in each abutment (i.e., $n_1 = n_2$).

Example

Let's assume that initial abutment springs based on 1" displacement result in ½" movement with 400kips of acting seismic force at each abutment. Assuming that ½" top of pile movement results in 20kips resistance, we would get 10*20=200kips of pile resistance at each abutment, leaving 400-200=200kips to be resisted by one wing. If one wing can resist only 100kips, we might try to reduce abutment springs as to reduce the acting seismic force, but increase displacement, which in turn will increase pile reactions and reduce demand on the wing. Assume that softer springs would result in the movement of ¾" and the acting force of 350kips per abutment. Now the resistance from piles may be

increased to let's say 10*30kips/pile=300kips leaving 350-300=50kips to be resisted by a wing, which is ok, since the wing resistance is 100kips. If on other hand we conclude that acting seismic force is higher than combined resistance of piles and one wing (despite the softening of abutment springs) we may assume the wing will be sheared off and we may have to adjust the abutment springs based on piles alone, until we get good convergence again between acting force and pile resistance under given displacement.

Appendix E
Bridge Computer Models and Output Data

Introduction

In this appendix, the details of computer modeling and seismic analyses of the three selected Idaho bridges are presented. For brevity, the OpenSees input files are only presented for the Parma bridge.

Bridge over US95 at Parma, Idaho

Background

The bridge at Parma is a two-span bridge with a three column bent. The skew in the bridge was removed for ease of modeling. The overall dimensions of the bridge were maintained and the bent and abutment lengths were shortened to match the deck width. The superstructure is made up of an 8 in. thick deck that rests on 5 prestressed WF66G girders. The substructure is made up of a pier cap, three columns, and their footings all of which are cast-in-place.

Spring Support Condition

Support stiffness:	Springs at abutments, fixed column bases
Abutment type:	Integral
Restraint of superstructure:	Abutments with springs in longitudinal and transverse directions, unrestrained rotation about the C.L. abutment.

Soil Spring Stiffness

Each abutment wall has eight 14X89 H-piles. Each H-pile is oriented with its strong axis parallel to the abutment wall length and its weak axis perpendicular to the abutment wall length. The dimensions of one wall are:

H_{aw} = 10.67’	Height of abutment wall
L_{aw} = 42’	Length of abutment wall

The soil spring stiffness for the H-piles were derived from the Phase IV Foundation Investigation Report. Figures E1 and E2 show force and deflection up to 48 ft of depth for one H-pile. Since spring stiffness equals force divided by deflection ($K = F/d$) the spring stiffness can be estimated by determining the force at 1 in of deflection. About the strong axis the force at 1 in of deflection is 95 kip, and about the weak axis the force at 1 in of deflection is 57.5 kip.

k_s = 95 kip/in = 1,140 kip/ft.
k_w = 57.5 kip/in = 690 kip/ft.

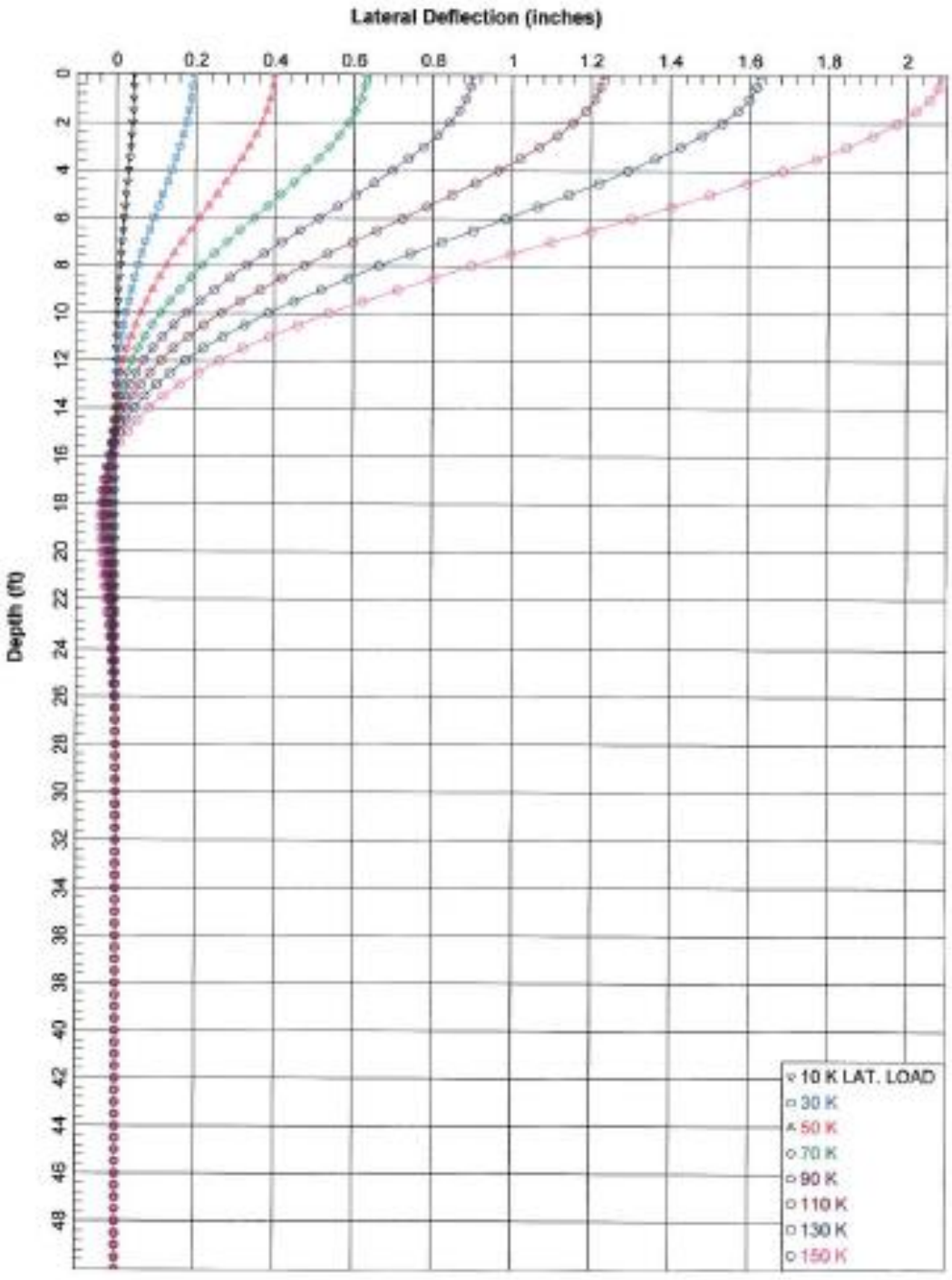

Figure E1. Parma Bridge Lateral Deflection vs. Depth of an H-Pile about the Strong Axis

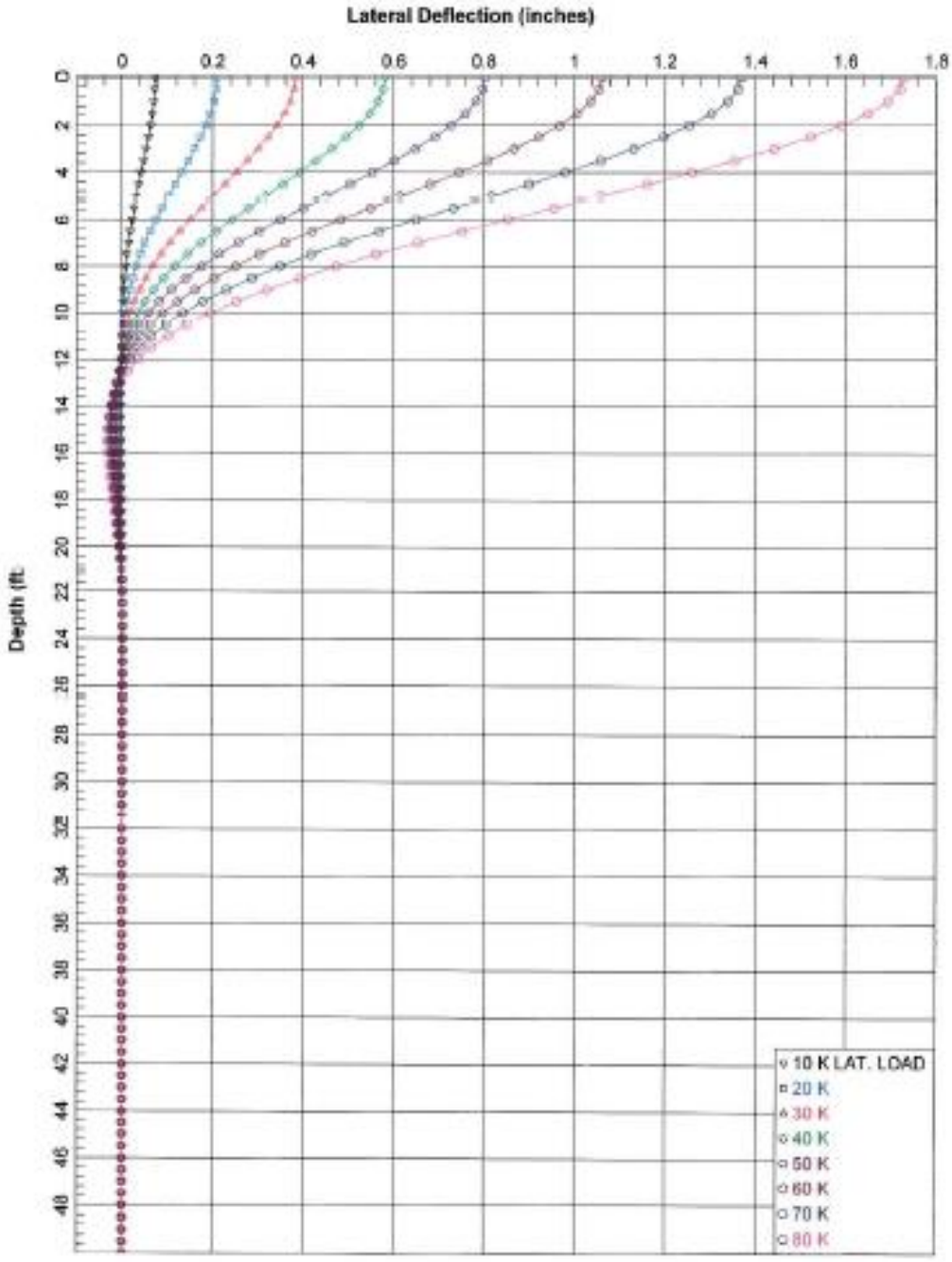

Figure E2. Parma Bridge Lateral Deflection vs. Depth of an H-Pile about the Weak Axis

The initial value due to abutments spring stiffness in the longitudinal direction is calculated by

$$K_l = \frac{2nk_s + (7.7A_{aw}/d)}{2}$$

Where:

K_l = The abutments spring stiffness in the longitudinal direction

n = The number of H-piles in one abutment wall = 8
k_s = The spring stiffness for one H-pile about the strong axis = 1,140 kip/ft
A_{aw} = The area of the abutment wall = $H_{aw}\,L_{aw}$ = 448 ft^2
d = deflection needed to mobilize full passive resistance = 0.02H_{aw} = 0.2134 ft.

Initial value for the soil spring stiffness in the transverse direction is calculated by

$$K_t = nk_w$$

Where:

K_t = The spring stiffness in the transverse direction
k_w = The spring stiffness for one H-pile about the weak axis = 690 kip/ft
K_l = 17,202 kip/ft Spring stiffness at abutments in the longitudinal direction
K_t = 5,520 kip/ft Spring stiffness at abutments in the transverse direction

A large spring stiffness (1e12 kip/ft) was used for all other degrees of freedom (DOF's) except the rotation about the centerline (C. L.) of the abutments, which were assigned a value of zero.

Superstructure

Properties of the superstructure and its elements are as follows

L = 282'-2⅜" Overall length of bridge
A_{Sup} = 58.40 ft^2 Cross-sectional area of superstructure without parapets
A_{gSup} = 62.50 ft^2 Gross cross-sectional area of superstructure including parapets for weight calculations
f'_{cCIP} = 4.0 ksi Compressive strength of cast-in-place concrete
$f'_{cPrestressed}$ = 8.0 ksi Compressive strength of prestressed concrete
$E_{CIP} = 33000*0.145^{1.5}\sqrt{f'_{cCIP}}$ = 33000(0.145$^{1.5}$)√4.0 = 3,644 ksi
Modulus of elasticity of cast-in-place concrete

$E_{Prestressed} = 33000(0.14+0.001f'_{cPrestressed})^{1.5}\sqrt{f'_c}$ = 33000(0.14+(0.001*8.0))$^{1.5}$ √8.0 = 5314.37 ksi
Modulus of elasticity of prestressed concrete

$n = E_{Prestressed}/E_{CIP}$ = 5314/3644 = 1.458 Modular ratio of elasticity

The moments of inertia of the superstructure were determined by calculating the moments of inertia of the prestressed girders and the transformed moment of inertia of the deck and using the parallel axis theorem,

$$I_s = \sum I_o + Ad^2$$

Where:

I_s = the moment of inertia of the superstructure

I_o = the moment of inertia of a section (girder or deck) of the superstructure
A = the area of a section of the superstructure
d = the distance from the centroid of the section to the centroid of the superstructure

A_{Girder} = 6.08 ft^2 Cross-sectional area of one girder
$I_{yGirder}$ = 3.48 ft^4 Moment of inertia of one girder about the y axis
$I_{zGirder}$ = 27.14 ft^4 Moment of inertia of one girder about the z axis

The transformed moment of inertia and area for the deck was calculated by dividing the value of I_{zDeck}, I_{yDeck} and A_{Deck} by the modular ratio, *n.* The parapets on the outside edge of the deck were not included in these calculations.

A_{tDeck} = 19.2 ft^2 Transformed area of deck
I_{yDeck} = 2823 ft^4 Transformed moment of inertia of the deck about the y axis
I_{zDeck} = 0.7113 ft^4 Transformed moment of inertia of the deck about the z axis
$d_{zGirder}$ = 1.20 ft Distance from the centroid of the girder to centroid of superstructure along the y-axis

d_{zDeck} = 1.90 ft Distance from the centroid of the deck to the centroid of superstructure along the y-axis

$d_{yGirder1,5}$ = 17.5 ft Distance from the centroid of the first and fifth girders to the centroid of the superstructure along the z-axis

$d_{yGirder2,4}$ = 8.75 ft Distance from the centroid of the second and fourth girders to the centroid of the superstructure along the z-axis

$d_{yGirder3}$ = 0 ft Distance from the centroid of the third girder to the centroid of the superstructure along the z-axis

d_{yDeck} = 0 ft Distance from the centroid of the deck to the centroid of superstructure along the z-axis

$$I_{ySup} = 2823ft^4 + 5(3.48ft^4) + 6.08ft^2[2(17.2ft)^2 + 2(8.75ft)^2] = 7495.5ft^4$$
Transformed moment of inertia of the superstructure about the y axis

$$I_{zSup} = 0.7113ft^4 + 19.20ft^2(1.90ft)^2 + 5[27.14ft^4 + 6.08ft^2(1.20ft)^2] = 249.3ft^4$$
Transformed moment of inertia of the superstructure about the z axis

$$A_{tSup} = A_{tDeck} + \sum A_{Girder} = 19.2ft^2 + 5(6.08ft^2) = 49.6ft^2$$
Transformed area of the superstructure

The modulus of rigidity, *G*, for the cast-in-place and prestressed concrete are calculated by

$$G = \frac{E}{2(1+\nu)}$$

Where:

ν = Poisson's ratio, typically from 0.15 - 0.2.

$G_{prestressed}$ = 5314.37/2(1+0.2) = 2,214.3 ksi =318,862.2 ksf

G_{CIP} = 3644/2(1+0.2) = 1,518.3 ksi = 218,640 ksf

Substructure

Properties of the substructure and its elements are as follows

L_p = 42'-0"	Length of pier cap
A_{pyz} = 25.23 ft^2	Cross-sectional area of pier cap in the x-y plane
I_{pz} = 60.9 ft^4	Moment of inertia about the z axis
L_c = 25'-7.75"	Column height
D_c = 3'-6"	Column diameter
A_{cg} = 9.62 ft^2	Cross-sectional area of one column
I_{cg} = πd^4/64 = 7.366 ft^4	Gross moment of inertia of one column

Column Reinforcement

The columns are reinforced with 16 #10 two-bar bundles and a #5 spiral with a 3 in pitch. There is 1.5 in of cover concrete as shown in Figure E3.

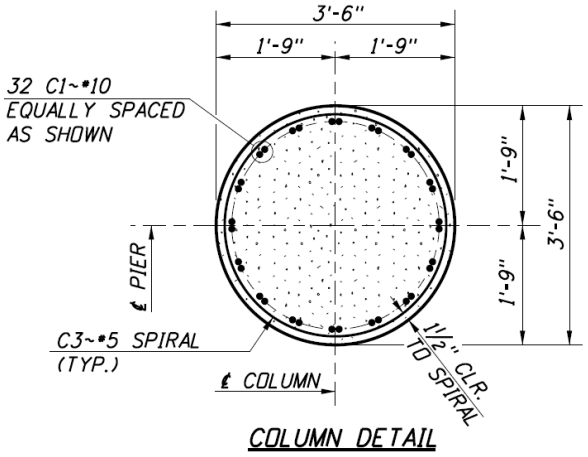

Figure E3. Parma Bridge Reinforced Column Detail

To accommodate the grouted couplers 16 single reinforcing bars need to be used instead of the two-bar bundles. A #14 bar has the closest cross-sectional area to that of the two #10 bars.

A_{r10} = 1.270 in^2	Cross-sectional area of a #10 bar

A_{r14} = 2.25 in^2 = 0.015625 ft^2	Cross-sectional area of a #14 bar
d_{r14} = 1.693 in = 0.141083 ft	Diameter of a #14 reinforcing bar
d_s = 0.625”	Diameter of spiral reinforcing
A_{st14} = 16A_{r14} = 0.25 ft^2	Total longitudinal steel in one column with #14 bars
R_{14} = 1.502 ft	Distance from the center of the column to the center of the #14 bars

Effective Moment of Inertia and Torsional Moment of Inertia of the Columns

For the effective moment of inertia the gross moment of inertia is multiplied by the Elastic Stiffness Ratio (I_{eff}/I_{cg}). This is obtained from Figure E4 with the Axial Load Ratio and the ratio of reinforcing steel to concrete.

Axial Load Ratio = P/f'_cA_{cg}

Where:

P = the axial load to the column from the self-weight of the bridge = 627.07 kips

The axial load on one column is from half the weight of each span divided by three plus the weight on the node in the pier cap above the column plus half the weight of one column. The dead load to each node is given in Table E1.

P/f'_cA_{cg} = 0.113
A_{st}/A_{cg} =0.25 ft^2/9.62 ft^2 = 0.029
I_{eff}/I_{cg} = 0.57

I_{ceff} = 0.57 * I_{cg} = 4.199 ft^4	Effective moment of inertia of one column
$J_{gross} = \frac{\pi D^4}{32}$ =π(3.5^4)/32 = 14.7 ft^4	Gross torsional moment of inertia
J_{eff} = 0.2J_{gross} = 2.95 ft^4	Effective torsional moment of inertia

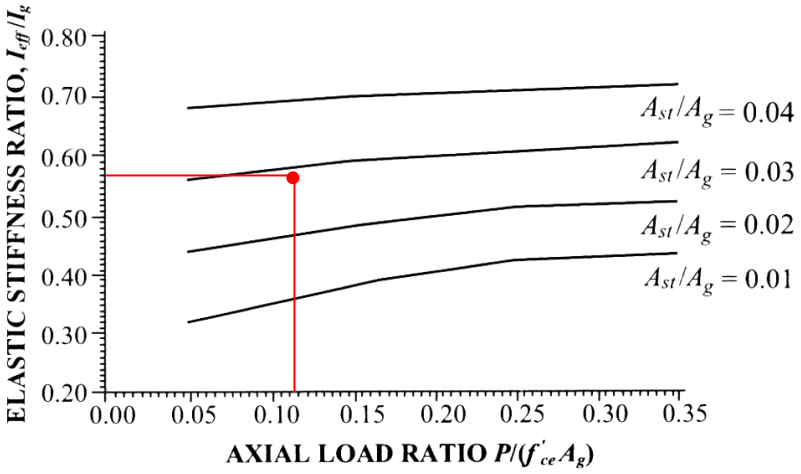

Figure E4. Parma Bridge Column Elastic Stiffness Ratio[21]

Table E1. Parma Bridge Weight of Structure to Nodes from Deck, Pier Cap, and Top Half of Columns

Section	X-sec. Area (ft^2)	Length (ft)	Weight of concrete ($kips/ft^3$)	Weight of diaphragms (kips)	Weight of deck forms and future wearing surface (klf)	Weight to node (kips)
Deck						
node 1	62.5	17.629	0.15	0	1.89	198.585
node 2	62.5	35.275	0.15	20.754	1.89	418.127
node 3	62.5	35.275	0.15	20.754	1.89	418.127
node 4	62.5	35.275	0.15	20.754	1.89	418.127
node 5	62.5	35.275	0.15	0	1.89	397.373
node 6	62.5	35.275	0.15	20.754	1.89	418.127
node 7	62.5	35.275	0.15	20.754	1.89	418.127
node 8	62.5	35.275	0.15	20.754	1.89	418.127
node 9	62.5	17.629	0.15	0	1.89	198.585
Pier cap						
node 13	25.23	13.339	0.15	N/A	N/A	50.481
node 17	25.23	15.322	0.15	N/A	N/A	57.986
node 21	25.23	13.339	0.15	N/A	N/A	50.481
Top half of columns						
node 12	9.62	12.823	0.15	N/A	N/A	18.504
node 16	9.62	12.823	0.15	N/A	N/A	18.504
node 20	9.62	12.823	0.15	N/A	N/A	18.504
				Total		3517.766
				w(x) kip/ft		12.466

Linear Elastic Model of the Structure

Each span of the superstructure is modeled as four elements (35.275' each) attached end to end from south to north. A rigid element with a large moment of inertia attaches the superstructure to the pier bent at the midpoint of both. This element starts at the center of gravity of the pier bent and ends at the center of gravity of the superstructure (6.154'). At the top of each column there is another rigid element that starts at the top of the column and ends at the center of gravity of the pier bent (2.701'). The footings of the columns are modeled as an element at the bottom of the columns with the same properties as the columns, except that they are rigid, and are half the depth of the footings in length (2.0'). To model the spring support condition an extra node and *zeroLength* element is assigned to the abutment ends of the superstructure.

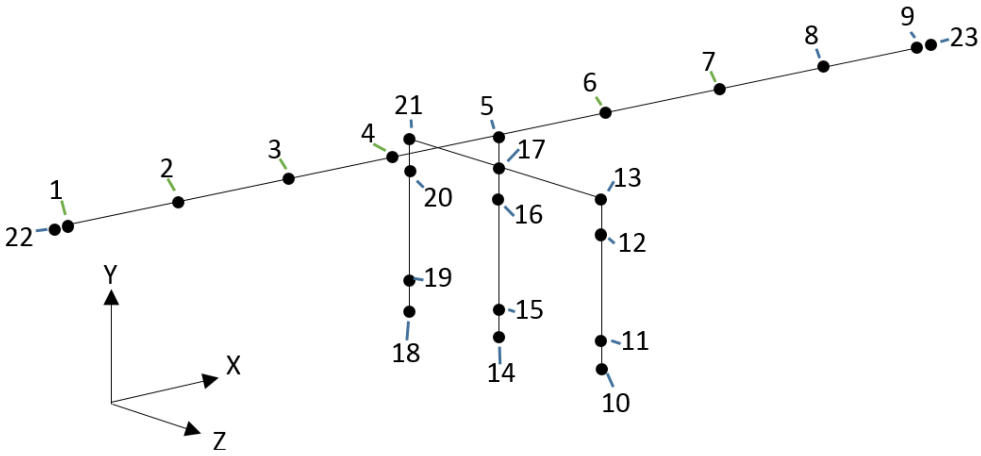

Figure E5. Parma Bridge Linear Elastic Model with Node Numbers.

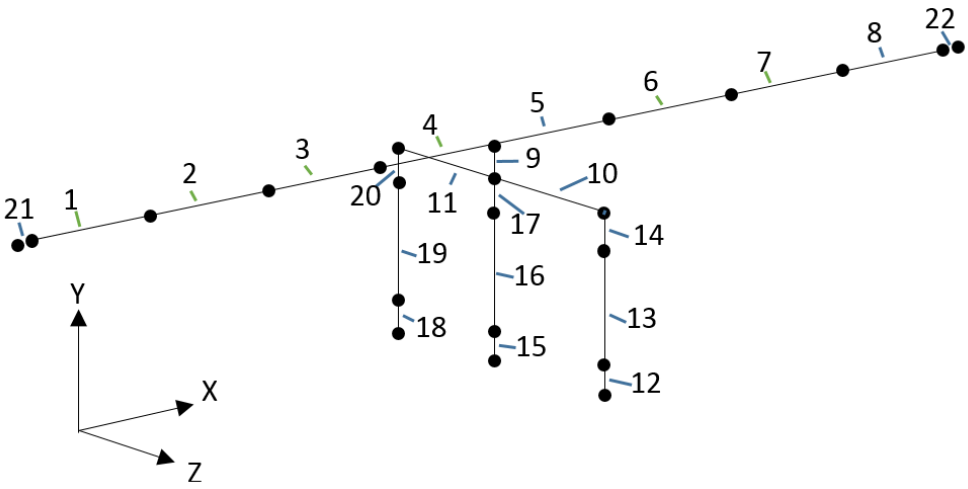

Figure E6. Parma Bridge Linear Elastic Model with Element Numbers.

Calculation of Seismic Loads

The bridge will be subject to more seismically active conditions than that found near Parma, ID. Montpelier, ID is the most seismically active city in Idaho where there might be a bridge. Figure E7 shows the Design Maps Summary Report for Montpelier, ID.

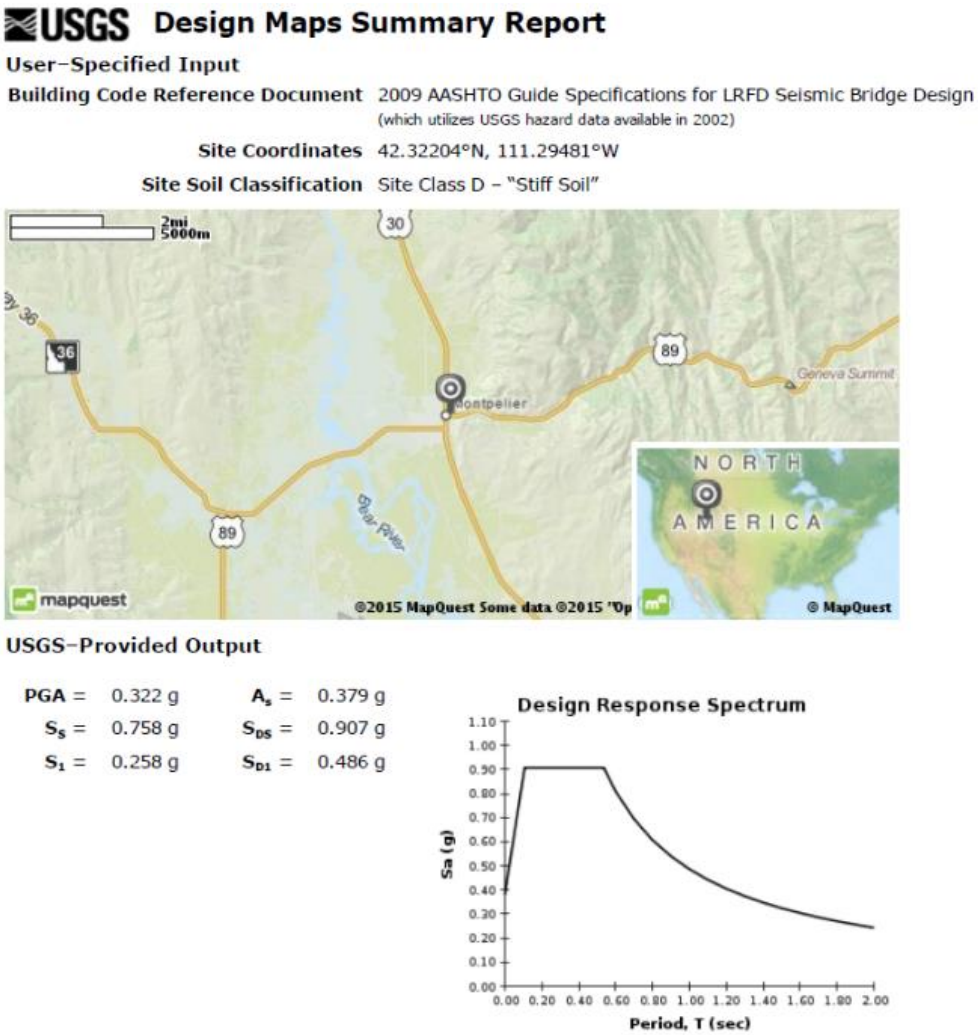

Figure E7. USGS Design Maps Summary Report

To calculate the seismic loads on the deck of the bridge the displacements at the deck nodes from a uniformly distributed load of 10 kip/ft in the longitudinal and transverse direction are determined and used to calculate the factors α, β, and γ. The factors are used to calculate the loads (*pe (x)*) at the nodes on the deck. The distributed seismic loads on each element is the average of the loads on the nodes. These loads are shown in column 9 of Tables E2 and E3.

$$\alpha = \int_0^L v_s(x)\, dx$$

$$\beta = \int_0^L w(x) v_s(x) dx$$
$$\gamma = \int_0^L w(x) v_s(x)^2 dx$$

Where

$v_x(x)$ = Displacement due to a uniformly distributed load of 10 kip/ft.
$w(x)$ = Weight of the bridge per unit length = 12.466 kip/ft
dx = Tributary length
L = Total length of bridge

$$p_e(x) = \beta C_{sm} w(x) * v_s(x)/\gamma$$

Where

$C_{sm} = S_{DS}$ = 0.907 for $T_o < T_m < T_s$ and
$C_{sm} = S_{D1}/T_m$ for $T_m > T_s$

Where

$T_m = 2\pi\sqrt{\gamma/P_0 g\alpha}$ = 0.344s for longitudinal loads
$T_m = 2\pi\sqrt{\gamma/P_o g\alpha}$ = 0.548s for transverse loads
$T_s = S_{D1}/S_{DS}$ = 0.5358
$T_o = 0.2T_s$ = 0.1072
g = 32.2 ft/s^2
P_o = 10 kip/ft

Table E2. Parma Bridge Calculation of Seismic Loads in the Transverse Direction

Nodes	x (ft)	dx (ft)	v_s(x) (ft)	α(x) (ft^2)	β(x) (k-ft)	γ(x) (k-ft^2)	p_e(x) (k/ft)	ave. (k/ft)
1	0	0	-0.188	0.000	0.000	0.000	10.611	
2	35.27	35.27	-0.192	-6.703	-83.563	15.880	10.789	10.700
3	70.55	35.27	-0.197	-6.856	-85.464	16.611	11.098	10.943
4	105.82	35.27	-0.201	-7.022	-87.534	17.425	11.319	11.208
5	141.01	35.27	-0.202	-7.111	-88.646	17.871	11.383	11.351
6	176.37	35.27	-0.201	-7.111	-88.652	17.873	11.320	11.352
7	211.65	35.27	-0.197	-7.023	-87.549	17.431	11.100	11.210
8	246.91	35.27	-0.192	-6.857	-85.484	16.618	10.792	10.946
9	282.18	35.27	-0.189	-6.705	-83.586	15.889	10.614	10.703
Totals		282.19		-55.389	-690.478	135.597		

Table E3. Parma Bridge Calculation of Seismic Loads in the Longitudinal Direction

Nodes	x (ft)	dx (ft)	v_s(x) (ft)	α(x) (ft^2)	β(x) (k-ft)	γ(x) (k-ft^2)	p_e(x) (k/ft)	ave. (k/ft)
1	0.00	0.00	0.0753	0.000	0.000	0.000	11.084	
2	35.27	35.27	0.0764	2.676	33.360	2.531	11.237	11.161
3	70.55	35.27	0.0771	2.707	33.746	2.590	11.342	11.290
4	105.82	35.27	0.0775	2.726	33.987	2.627	11.399	11.370
5	141.01	35.27	0.0775	2.734	34.084	2.642	11.407	11.403
6	176.37	35.27	0.0775	2.734	34.084	2.642	11.399	11.403
7	211.65	35.27	0.0771	2.726	33.987	2.627	11.342	11.370
8	246.91	35.27	0.0764	2.707	33.746	2.590	11.237	11.290
9	282.18	35.27	0.0753	2.676	33.360	2.531	11.084	11.161
Totals		282.19		21.687	270.354	20.779		

Linear Elastic OpenSees Input File for Seismic Load in Transverse Direction

```
#Two-span Bridge on US95 at Parma, Idaho
wipe
#Create model with 3 dimensions and 6 DOF
model BasicBuilder -ndm 3 -ndf 6
#Units are kips and feet
#Create 6 DOF nodes
#Superstructure nodes
#       tag         x             y            z

node     1         0.0         36.459         0.0
node     2        35.275       36.459         0.0
node     3        70.549       36.459         0.0
node     4       105.824       36.459         0.0
node     5       141.009       36.459         0.0
node     6       176.374       36.459         0.0
node     7       211.648       36.459         0.0
node     8       246.914       36.459         0.0
node     9       282.179       36.459         0.0

#Substructure nodes

node    10       141.009        0.0          15.322
node    11       141.009        2.0          15.322
node    12       141.009       27.646        15.322
node    13       141.009       30.347        15.322
node    14       141.009        0.0           0.0
node    15       141.009        2.0           0.0
node    16       141.009       27.646         0.0
node    17       141.009       30.347         0.0
node    18       141.009        0.0         -15.322
node    19       141.009        2.0         -15.322
node    20       141.009       27.646       -15.322
node    21       141.009       30.347       -15.322

#Spring support nodes
```

```
node    22         0.0         36.459         0.0
node    23       282.179       36.459         0.0

#Specify geometric transformation

geomTransf Linear 1  0  0  1
geomTransf Linear 2 -1  0  0
geomTransf PDelta 3  0  0  1

# Fix column bases and abutments in all DOF's

fix 22 1 1 1 1 1 1
fix 23 1 1 1 1 1 1
fix 10 1 1 1 1 1 1
fix 14 1 1 1 1 1 1
fix 18 1 1 1 1 1 1


# Create deck elements

# element elasticBeamColumn $eleTag $iNode $jNode $A $E $G $J $Iy $Iz $transfTag

element elasticBeamColumn 1  1  2  49.60  765269.3  318862.2  1e10  7495.5  244.3  1
element elasticBeamColumn 2  2  3  49.60  765269.3  318862.2  1e10  7495.5  244.3  1
element elasticBeamColumn 3  3  4  49.60  765269.3  318862.2  1e10  7495.5  244.3  1
element elasticBeamColumn 4  4  5  49.60  765269.3  318862.2  1e10  7495.5  244.3  1
element elasticBeamColumn 5  5  6  49.60  765269.3  318862.2  1e10  7495.5  244.3  1
element elasticBeamColumn 6  6  7  49.60  765269.3  318862.2  1e10  7495.5  244.3  1
element elasticBeamColumn 7  7  8  49.60  765269.3  318862.2  1e10  7495.5  244.3  1
element elasticBeamColumn 8  8  9  49.60  765269.3  318862.2  1e10  7495.5  244.3  1

# Create pier bent elements

element elasticBeamColumn  9  5 17  196.00   524736  218640 1e10  1e10  1e10  3
element elasticBeamColumn 10 13 17   25.23   524736  218640 1e10  1e10  1e10  2
element elasticBeamColumn 11 17 21   25.23   524736  218640 1e10  1e10  1e10  2

# Create column elements

element elasticBeamColumn 12 10 11  9.62  524736  218640 1e10  4.199  4.199 3
element elasticBeamColumn 13 11 12 9.62  524736  218640 2.95  4.199  4.199 3
element elasticBeamColumn 14 12 13  1e10  524736  218640 1e10  1e10  1e10  3
element elasticBeamColumn 15 14 15 9.62  524736  218640 1e10  4.199  4.199 3
element elasticBeamColumn 16 15 16 9.62  524736  218640 2.95  4.199  4.199 3
element elasticBeamColumn 17 16 17  1e10  524736  218640 1e10  1e10  1e10  3
element elasticBeamColumn 18 18 19 9.62  524736  218640 1e10  4.199  4.199 3
element elasticBeamColumn 19 19 20 9.62  524736  218640 2.95  4.199  4.199 3
element elasticBeamColumn 20 20 21  1e10  524736  218640 1e10  1e10  1e10  3

# Create spring elements

# Initial abutment stiffnesses to be used with the uniform loads to determine the seismic
loads

#uniaxialMaterial Elastic 1 17.202e3;   # Translational stiffness of the abutments along x
axis, kip/ft
#uniaxialMaterial Elastic 3 5.52e3;   # Translational stiffness of the abutments along z axis,
kip/ft

# Final abutment stiffnesses
```

```
uniaxialMaterial Elastic 1 17.042e3;   # Translational stiffness  of the abutments along x
axis, kip/ft
uniaxialMaterial Elastic 2 1e12;       # Translational stiffness of the abutments along y
axis, kip/ft
uniaxialMaterial Elastic 3 3.2e3;      # Translational stiffness of the abutments along z
axis, kip/ft
uniaxialMaterial Elastic 4 1e12;       # Rotational stiffness of the abutments about x axes,
kip.ft/radian
uniaxialMaterial Elastic 5 1e12;       # Rotational stiffness of the abutments about y axes,
kip.ft/radian
uniaxialMaterial Elastic 6 0;          # Rotational stiffness of the abutments about z axes,
kip.ft/radian


# Spring elements using above stiffness values
# element zeroLength $eleTag $iNode $jNode -mat $matTag1 $matTag2 ... -dir $dir1 $dir2 ...

element zeroLength 21 22  1 -mat 1 2 3 4 5 6 -dir 1 2 3 4 5 6
element zeroLength 22  9 23 -mat 1 2 3 4 5 6 -dir 1 2 3 4 5 6

# Create recorder files

recorder Node -file Nodes1-9DisplLong_Parma_elastic.out -time -nodeRange 1 9 -dof 1 disp
recorder Node -file Nodes1-9DispTrans_Parma_elastic.out -time -nodeRange 1 9 -dof 3 disp
recorder Node -file Node22_Reaction_Parma_eleastic_long.out -time -node 22 -dof 1 reaction
recorder Node -file Node23_Reaction_Parma_eleastic_long.out -time -node 23 -dof 1 reaction

# Assign gravity loads

pattern Plain 1 Constant {
#    tag    FX       FY      FZ   MX   MY   MZ
load  1     0.0    -198.585  0.0  0.0  0.0  0.0
load  2     0.0    -418.127  0.0  0.0  0.0  0.0
load  3     0.0    -418.127  0.0  0.0  0.0  0.0
load  4     0.0    -418.127  0.0  0.0  0.0  0.0
load  5     0.0    -397.373  0.0  0.0  0.0  0.0
load  6     0.0    -418.127  0.0  0.0  0.0  0.0
load  7     0.0    -418.127  0.0  0.0  0.0  0.0
load  8     0.0    -418.127  0.0  0.0  0.0  0.0
load  9     0.0    -198.585  0.0  0.0  0.0  0.0
load 13     0.0     -68.98   0.0  0.0  0.0  0.0
load 17     0.0     -76.49   0.0  0.0  0.0  0.0
load 21     0.0     -68.98   0.0  0.0  0.0  0.0
}
constraints Plain

numberer Plain
system BandGeneral
test NormDispIncr 1.0e-8  6
algorithm Newton
integrator LoadControl 1
analysis Static
analyze 1
#Reset time to perform pushover analysis
loadConst -time 0.0


# Create load pattern for horizontal loading
#The 10 kip/ft load should be activated when placing a uniform load of 10 kip/ft in the
longitudinal or transverse direction
#These loads should be used with the initial abutment stiffnesses
```

```
#pattern Plain 2 Linear {
# eleLoad -ele $eleTag1 <$eleTag2 ....> -type -beamUniform $Wy $Wz <$Wx>
# eleLoad -ele 1 2 3 4 5 6 7 8 -type beamUniform 0 0 10
#}

#pattern Plain 3 Linear {
# eleLoad -ele $eleTag1 <$eleTag2 ....> -type -beamUniform $Wy $Wz <$Wx>
# eleLoad -ele 1 2 3 4 5 6 7 8 -type beamUniform 0 -10 0
#}

#Transverse seismic loads

pattern Plain 4 Linear {
eleLoad -ele 1 -type beamUniform 0 10.7 0
}

pattern Plain 5 Linear {
eleLoad -ele 1 -type beamUniform 0 10.943 0
}

pattern Plain 6 Linear {
eleLoad -ele 2 -type beamUniform 0 11.208 0
}

pattern Plain 7 Linear {
eleLoad -ele 2 -type beamUniform 0 11.351 0
}

pattern Plain 8 Linear {
eleLoad -ele 3 -type beamUniform 0 11.352 0
}

pattern Plain 9 Linear {
eleLoad -ele 3 -type beamUniform 0 11.21 0
}

pattern Plain 10 Linear {
eleLoad -ele 4 -type beamUniform 0 10.946 0
}

pattern Plain 11 Linear {
eleLoad -ele 4 -type beamUniform 0 10.703 0
}

constraints Plain
numberer Plain
system BandGeneral
test NormDispIncr  1.0e-8  6
algorithm Newton
integrator LoadControl 1
analysis Static
analyze 1
```

Determination of Final Soil Spring Stiffness

The final estimations of the bridge transverse and longitudinal abutment stiffness values are accomplished with an iterative process outlined in Appendix D. The final estimation for the abutment stiffness values are

K_l = 17,042 kips/ft — Longitudinal abutment stiffness
K_t = 3,200 kips/ft — Transverse abutment stiffness

As a check, the final abutment stiffness values were used in the OpenSees program with the uniformly distributed load used for calculating the seismic loads to see how the new stiffness values would affect the calculation of the seismic loads. The difference in the transverse values was less than 2% and the difference in the longitudinal values was less than 0.01%.

Linear-elastic Analysis Results

Tables E4 and E5 show the displacements and column base reactions for the longitudinal and transverse directions, respectively.

Table E4. Parma Bridge Linear Elastic Displacements and Column Base Reactions for Seismic Loads in the Longitudinal Direction

Nodes	Displacement (ft.)
Deck	
1	0.08589
2	0.08707
3	0.08788
4	0.08832
5	0.08838
6	0.08832
7	0.08788
8	0.08707
9	0.08589
Top of the Columns	
12	0.08195
16	0.08195
20	0.08195

Columns	Shear (k)	Axial (k)	Moment (k-ft)
1	-87.578	752.152	1297.780
2	-87.578	752.152	1297.780
3	-87.578	752.152	1297.780

Table E5. Parma Bridge Linear Elastic Displacements and Column Base Reactions for Seismic Loads in the Transverse Direction

Nodes	Displacement (ft.)
Deck	
1	0.30660
2	0.30909
3	0.31297
4	0.31512
5	0.31539
6	0.31518
7	0.31307
8	0.30921
9	0.30674
Top of the Columns	
12	0.31494
16	0.31539
20	0.31494

Columns	Shear (k)	Axial (k)	Moment (k-ft)
1	-385.104	752.175	-5434.940
2	-385.650	752.136	-5442.630
3	-385.105	752.097	-5434.940

The drift in the longitudinal and transverse directions for top of the columns are shown in Table E6.

Table E6. Parma Bridge Linear Elastic Calculated Drift for Top of the Columns

Node	12	16	20
Long. drift (%)	0.3195	0.3195	0.3195
Trans. drift (%)	1.2280	1.2298	1.2280

Nonlinear CIP Model of the Structure

The non-linear model of the bridge superstructure and the column bent is the same as that of the linear elastic model. The columns are modeled with a *nonlinearBeamColumn* and a fiber section which describes the dimensions and properties of the reinforcing steel in the column. Additionally a *zeroLength* element is placed at the top and bottom of the columns to model bond-slip at the column-footing and column-bent interfaces and the footing is removed from the model.

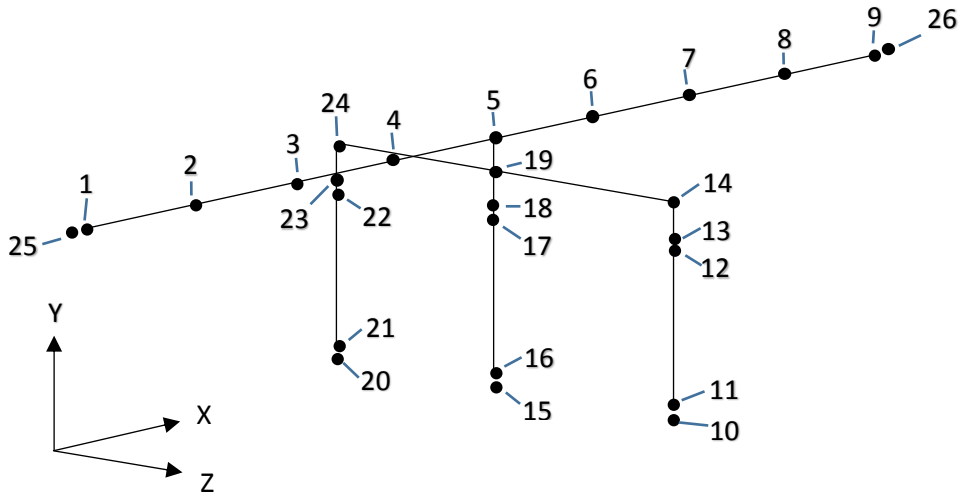

Figure E8. Parma Bridge Nonlinear Cast-in-place Model with Node Numbers

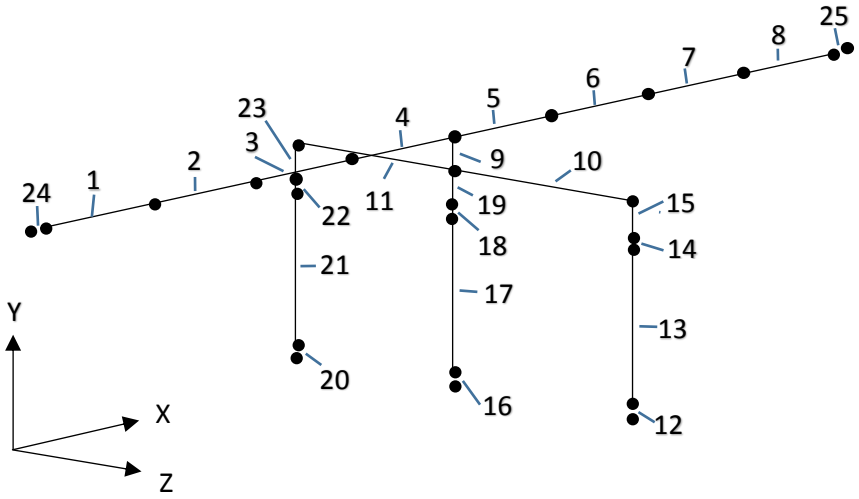

Figure E9. Parma Bridge Nonlinear Cast-in-place Model with Element Numbers

The following dimensions are required for modeling the fiber section.

d_{r14} = 1.693 in = 0.141083 ft	Diameter of a #14 reinforcing bar
d_s = 0.625”	Diameter of spiral reinforcing
R_{14} = 1.502 ft	Distance from the center of the column to the center of the #14 bars

An illustration of the OpenSees model of the nonlinear fiber section can be seen in the Figure E10.

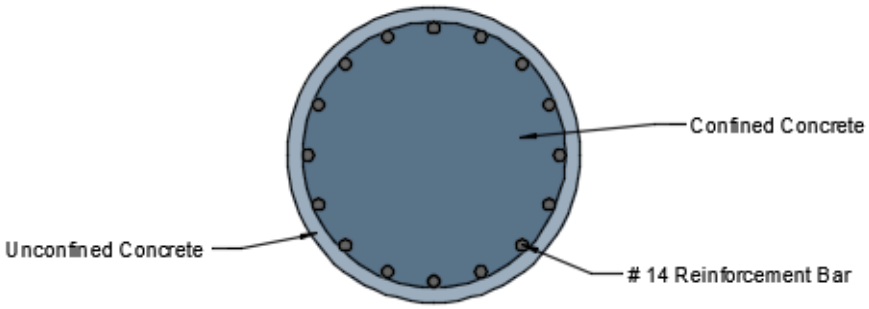

Figure E10. Parma Bridge Nonlinear CIP Fiber Section

Material Properties

Unconfined Concrete

As previously determined the modulus of elasticity, *E*, and the modulus of rigidity, *G*, for cast-in-place concrete are:

E_{CIP} = 3,644 ksi = 524,736 ksf — Modulus of elasticity of cast-in-place concrete
G_{CIP} = 218,640 ksf — Modulus of rigidity of cast-in-place concrete

Peak strain for 4000 psi concrete is 0.002 and ultimate strain is 0.005.

Reinforcing Steel

The grade of the steel is specified in the plans. For the Parma Bridge the steel is Grade 60. The following properties are found in Table 8.4.2-1 in the AASHTO Guide Specifications for LRFD Seismic Bridge Design, 2011, Sec. 8-4.
f_y = 68 ksi = 9,792 ksf
f_u = 95 ksi = 13,680 ksf
The strain for a #14 bar at strain hardening is
e_{sh} = 0.0075
The ultimate strain is
e_u = 0.09
The modulus of elasticity for steel is
E = 29,000 ksi = 4,176,000 ksf
The slope of the line at strain hardening is
E_{sh} = 1247 ksi = 179,568 ksf

Confined Concrete Strength Using Theoretical Stress-Strain Model Developed by Mander et al.

AASHTO Guide Specifications for LRFD Seismic Bridge Design, Sec. 8.4.4, Concrete Modeling, specifies that confined concrete should be modeled based on Mander's stress-strain model. Following the procedure outlined by Mander et al., we obtained the following properties for the confined concrete [18]

f'_{cc} = 6.08 ksi = 875.6 ksf	Confined concrete compressive strength
ε_{cc} = 0.0072	Confined concrete strain at maximum strength
ε_{cu} = 0.019	Confined concrete ultimate strain

Modeling Bond-slip

To model the bond-slip of the reinforcing steel at the interfaces between the footing and column and the bent cap and the column a *zeroLength* element with hysteretic material properties is used. The *uniaxialMaterial Hysteretic* command in OpenSees requires values from a moment-curvature analysis of the cross-section of the column. We followed the same process as that outlined in Appendix A, section "Procedure for Determining Bond-Slip Model Parameters." Table E7 shows the moment and rotation values corresponding to the points labeled $\left(M_1^+,\ \theta_1^+\right)$ and $\left(M_2^+,\ \theta_2^+\right)$ in Figure 18 of Chapter 3. Because of the symmetry of the column the moments and rotations in the negative direction are the same as those in the positive direction.

Table E7. Ends of the Column Bond-slip Moment-rotation Values for Parma Bridge

	Moment (kip-ft)	Rotation (rad)
Point 1	3,583	0.0035
Point 2	4,239	0.0300

Nonlinear Cast-in-place OpenSees Input File for Seismic Load in Transverse Direction

```
#Two-span Bridge on US95 at Parma, Idaho
wipe
#Create model with 3 dimensions and 6 DOF
model BasicBuilder -ndm 3 -ndf 6
#Units are kips and feet
#Create 6 DOF nodes

#Superstructure nodes
#       tag         x            y           z
node     1         0.0         34.459        0.0
node     2        35.275       34.459        0.0
node     3        70.549       34.459        0.0
node     4       105.824       34.459        0.0
node     5       141.009       34.459        0.0
node     6       176.374       34.459        0.0
node     7       211.648       34.459        0.0
node     8       246.914       34.459        0.0
node     9       282.179       34.459        0.0

#Substructure nodes

node    10       141.009        0.0          15.322
node    11       141.009        0.0          15.322
node    12       141.009       25.646        15.322
node    13       141.009       25.646        15.322
node    14       141.009       28.347        15.322
node    15       141.009        0.0           0.0
node    16       141.009        0.0           0.0
node    17       141.009       25.646         0.0
```

```
node    18       141.009       25.646         0.0
node    19       141.009       28.347         0.0
node    20       141.009        0.0         -15.322
node    21       141.009        0.0         -15.322
node    22       141.009       25.646       -15.322
node    23       141.009       25.646       -15.322
node    24       141.009       28.347       -15.322

#Spring support nodes

node    25         0.0         34.459         0.0
node    26       282.179       34.459         0.0

#Specify geometric transformation

geomTransf Linear 1  0  0  1
geomTransf Linear 2 -1  0  0
geomTransf PDelta 3  0  0  1

# Fix column bases and abutments in all DOF's

fix 25 1 1 1 1 1 1
fix 26 1 1 1 1 1 1
fix 10 1 1 1 1 1 1
fix 15 1 1 1 1 1 1
fix 20 1 1 1 1 1 1

#Create uniaxial materials for concrete and steel
# uniaxialMaterial Concrete01 $matTag $fpc $epsc0 $fpcu $epsU
uniaxialMaterial Concrete01  1  -576.0  -0.002  0  -0.005
# uniaxialMaterial Concrete04 $matTag $fc $ec $ecu $Ec <$ft $et> <$beta>
uniaxialMaterial Concrete04 2  -875.6  -0.0072  -0.019  524736

# uinaxialMaterial ReinforcingSteel $matTag $fy $fu $Es $Esh $esh $eult
uniaxialMaterial ReinforcingSteel  3  9792  13680  4176000  179568  0.0075  0.09

#Create hysteretic uniaxial material to model bond-slip
# uniaxialMaterial Hysteretic $matTag $s1p $e1p $s2p $e2p $s1n $e1n $s2n $e2n $pinchX $pinchY
$damage1 $damage2 <$beta>
uniaxialMaterial Hysteretic 4  3583  .0035  4239  .03  -3583  -0.0035   -4239.0  -.03    1  1
0  0  0.35
uniaxialMaterial Elastic 5  1e12

#Create fiber section with Defined Concrete and Rebar

section Fiber  1  {
#patch circ $matTag $numSubdivCirc $numSubdivRad $yCenter $zCenter $intRad $extRad <$startAng
endAng>
patch circ 2  44  10  0  0  0  1.573  0  360
patch circ 1 44 2  0  0  1.573 1.75 0  360
#layer circ $matTag $numBar $areaBar $yCenter $zCenter $radius <$startAng $endAng>
layer circ 3  16  0.015625  0  0  1.502 0 360
}

# Define shear stiffness (GJ) elastic material

set Gc 218640
set Jc  2.95
set GJ [expr $Gc*$Jc]
uniaxialMaterial Elastic 6  $GJ
```

```
section Aggregator 2  6 T -section  1

# Create deck elements

# element elasticBeamColumn $eleTag $iNode $jNode $A $E $G $J $Iy $Iz $transfTag

element elasticBeamColumn 1  1  2  49.60  765269.3  318862.2  1e10  7493.7  242.06  1
element elasticBeamColumn 2  2  3  49.60  765269.3  318862.2  1e10  7493.7  242.06  1
element elasticBeamColumn 3  3  4  49.60  765269.3  318862.2  1e10  7493.7  242.06  1
element elasticBeamColumn 4  4  5  49.60  765269.3  318862.2  1e10  7493.7  242.06  1
element elasticBeamColumn 5  5  6  49.60  765269.3  318862.2  1e10  7493.7  242.06  1
element elasticBeamColumn 6  6  7  49.60  765269.3  318862.2  1e10  7493.7  242.06  1
element elasticBeamColumn 7  7  8  49.60  765269.3  318862.2  1e10  7493.7  242.06  1
element elasticBeamColumn 8  8  9  49.60  765269.3  318862.2  1e10  7493.7  242.06  1

# Create pier bent elements

element elasticBeamColumn  9  5 19  196.00   524736  218640  1e10  1e10  1e10  3
element elasticBeamColumn 10 14 19   25.23   524736  218640  1e10  1e10  60.9  2
element elasticBeamColumn 11 19 24   25.23   524736  218640  1e10  1e10  60.9  2

# Create column elements

# element nonlinearBeamColumn $eleTag $iNode $jNode $numintgrPts $secTag $transfTag
# element zeroLength $eleTag $iNode $jNode -mat $matTag1 $matTag2 ... -dir $dir1 $dir2 ...

element zeroLength 12 10  11 -mat 5 5 5 4 4 4 -dir 1 2 3 4 5 6
element nonlinearBeamColumn 13 11 12 9 2 3
element zeroLength 14  12  13 -mat 5 5 5 4 4 4 -dir 1 2 3 4 5 6
element elasticBeamColumn 15  13  14  1e10  524736  218640  1e10  1e10  1e10  3
element zeroLength 16  15  16 -mat 5 5 5 4 4 4 -dir 1 2 3 4 5 6
element nonlinearBeamColumn 17  16  17 9 2 3
element zeroLength 18  17  18 -mat 5 5 5 4 4 4 -dir 1 2 3 4 5 6
element elasticBeamColumn 19  18  19  1e10  524736  218640  1e10  1e10  1e10  3
element zeroLength 20  20  21 -mat 5 5 5 4 4 4 -dir 1 2 3 4 5 6
element nonlinearBeamColumn 21  21  22 9 2 3
element zeroLength 22  22  23 -mat 5 5 5 4 4 4 -dir 1 2 3 4 5 6
element elasticBeamColumn 23  23  24  1e10  524736  218640  1e10  1e10  1e10  3

# Create spring elements

uniaxialMaterial Elastic 7 17.202e3;   # Translational stiffness along X axis of the
abutments, kip/ft
uniaxialMaterial Elastic 8 1e12;   # Translational stiffness along Y axis of the abutments,
kip/ft
uniaxialMaterial Elastic 9 3.2e3;   # Translational stiffness along Z axis of the abutments,
kip/ft
uniaxialMaterial Elastic 10 1e12;   # Rotational stiffness about X axes o10f the abutments,
kip.ft/radian
uniaxialMaterial Elastic 11 1e12;      # Rotational stiffness about Y axis of the abutments,
kip.ft/radian
uniaxialMaterial Elastic 12 0;      # Rotational stiffness about the Z axis of the abutment,
kip.ft/radian

# Spring elements using above stiffness values
# element zeroLength $eleTag $iNode $jNode -mat $matTag1 $matTag2 ... -dir $dir1 $dir2 ...

element zeroLength 24 25  1 -mat 7 8 9 10 11 12 -dir 1 2 3 4 5 6
element zeroLength 25  9 26 -mat 7 8 9 10 11 12 -dir 1 2 3 4 5 6

# Create recorder files
```

```
recorder Node -file Nodes1-9_NonLin_Disp_Long_Parma.out -time -nodeRange 1 9 -dof 1 disp
recorder Node -file Nodes1-9_NonLin_Disp_Trans_Parma.out -time -nodeRange 1 9 -dof 3 disp
recorder Node -file Column_1_Reaction_Parma.out -time -node 10 -dof 1 2 3 4 5 6 reaction
recorder Node -file Column_2_Reaction_Parma.out -time -node 15 -dof 1 2 3 4 5 6 reaction
recorder Node -file Column_3_Reaction_Parma.out -time -node 20 -dof 1 2 3 4 5 6 reaction

# Assign gravity loads

pattern Plain 1 Constant {
#    tag    FX       FY      FZ   MX   MY   MZ
load  1     0.0    -198.585  0.0  0.0  0.0  0.0
load  2     0.0    -418.127  0.0  0.0  0.0  0.0
load  3     0.0    -418.127  0.0  0.0  0.0  0.0
load  4     0.0    -418.127  0.0  0.0  0.0  0.0
load  5     0.0    -397.373  0.0  0.0  0.0  0.0
load  6     0.0    -418.127  0.0  0.0  0.0  0.0
load  7     0.0    -418.127  0.0  0.0  0.0  0.0
load  8     0.0    -418.127  0.0  0.0  0.0  0.0
load  9     0.0    -198.585  0.0  0.0  0.0  0.0
load 14     0.0     -68.98   0.0  0.0  0.0  0.0
load 19     0.0     -76.49   0.0  0.0  0.0  0.0
load 24     0.0     -68.98   0.0  0.0  0.0  0.0
}

constraints Plain
numberer Plain
system BandGeneral
test NormDispIncr 1.0e-8  6
algorithm Newton
integrator LoadControl 1
analysis Static
analyze 1

#Reset time to perform pushover analysis
loadConst -time 0.0

# Create horizontal load patterns
# Transverse seismic loads

pattern Plain 4 Linear {
# eleLoad -ele $eleTag1 <$eleTag2 ....> -type -beamUniform $Wy $Wz <$Wx>
eleLoad -ele 1 -type beamUniform 0 10.7 0
}

pattern Plain 5 Linear {
# eleLoad -ele $eleTag1 <$eleTag2 ....> -type -beamUniform $Wy $Wz <$Wx>
eleLoad -ele 2 -type beamUniform 0 10.943 0
}

pattern Plain 6 Linear {
# eleLoad -ele $eleTag1 <$eleTag2 ....> -type -beamUniform $Wy $Wz <$Wx>
eleLoad -ele 3 -type beamUniform 0 11.208 0
}

pattern Plain 7 Linear {
# eleLoad -ele $eleTag1 <$eleTag2 ....> -type -beamUniform $Wy $Wz <$Wx>
eleLoad -ele 4 -type beamUniform 0 11.351 0
}

pattern Plain 8 Linear {
```

```
# eleLoad -ele $eleTag1 <$eleTag2 ....> -type -beamUniform $Wy $Wz <$Wx>
eleLoad -ele 5 -type beamUniform 0 11.352 0
}

pattern Plain 9 Linear {
# eleLoad -ele $eleTag1 <$eleTag2 ....> -type -beamUniform $Wy $Wz <$Wx>
eleLoad -ele 6 -type beamUniform 0 11.21 0
}

pattern Plain 10 Linear {
# eleLoad -ele $eleTag1 <$eleTag2 ....> -type -beamUniform $Wy $Wz <$Wx>
eleLoad -ele 7 -type beamUniform 0 10.946 0
}

pattern Plain 11 Linear {
# eleLoad -ele $eleTag1 <$eleTag2 ....> -type -beamUniform $Wy $Wz <$Wx>
eleLoad -ele 8 -type beamUniform 0 10.703 0
}

constraints Plain
numberer RCM
system BandSPD
algorithm Linear
integrator LoadControl 0.01
analysis Static
analyze 100
```

Nonlinear CIP Model Analysis Results

Tables E8 and E9 show the displacements and column base reactions for the longitudinal and transverse directions, respectively.

Table E8. Parma Bridge Nonlinear CIP Displacements and Column Base Reactions for Seismic Loads in the Longitudinal Direction

Nodes	Displacement (ft.)
Deck	
1	0.08509
2	0.08626
3	0.08705
4	0.08748
5	0.08753
6	0.08748
7	0.08706
8	0.08626
9	0.08509
Top of the Columns	
12	0.08061
17	0.08061
22	0.08061

Columns	Shear (k)	Axial (k)	Moment (k-ft)
1	-96.663	752.384	1347.070
2	-96.663	752.384	1347.070
3	-96.663	752.384	1347.070

Table E9. Parma Bridge Nonlinear CIP Displacements and Column Base Reactions for Seismic Loads in the Transverse Direction

Nodes	Displacement (ft.)
Deck	
1	0.35992
2	0.36349
3	0.36976
4	0.37430
5	0.37565
6	0.37435
7	0.36984
8	0.36358
9	0.36002
Top of the Columns	
12	0.37534
17	0.37565
22	0.37534

Columns	Shear (k)	Axial (k)	Moment (k-ft)
1	-271.576	753.687	-3623.890
2	-271.585	753.865	-3624.150
3	-271.577	753.672	-3623.890

The drift in the longitudinal and transverse directions for top of the columns are as shown in Table E10.

Table E10. Parma Bridge Nonlinear CIP Calculated Drift for Top of the Columns

Node	12	17	22
Long. drift (%)	0.3143	0.3143	0.3143
Trans. drift (%)	1.4635	1.4647	1.4635

Nonlinear Model of Structure with Grouted Couplers

The grouted couplers are modeled as separate elements within the columns. They are located at the top and bottom of each column. In addition to the zeroLength elements that model bond slip a small monitoring element with the same section as the part of the column without couplers was placed between the zeroLength elements and the grouted couplers to observe the behavior of the materials immediately beyond the coupler region. The node and element placement can be seen in Figures E11 and E12.

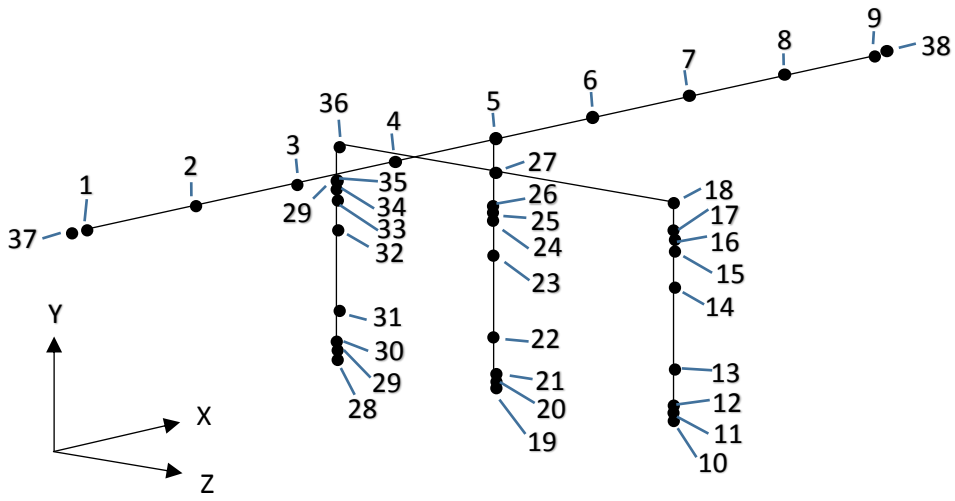

Figure E11. Parma Nonlinear Bridge Model with Grouted Couplers with Node Numbers

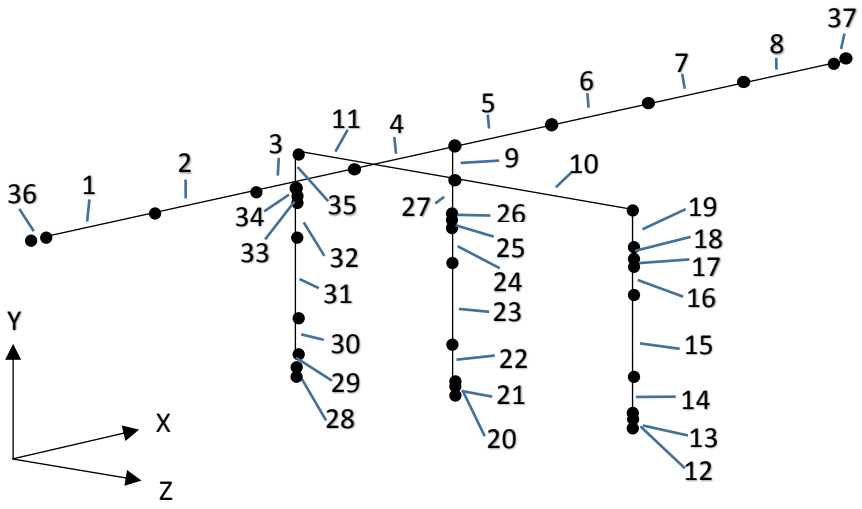

Figure E12. Parma Nonlinear Bridge Model with Grouted Couplers with Element Numbers

Material Properties of Grouted Couplers

The material properties of the grouted couplers were obtained from the manufacturer, Splice Sleeve North America (SSNA). The following values apply to the SSNA No. 14 U-X Grouted Coupler which is used for a #14 reinforcing bar.

$A_{coupler}$ = 9.449 in^2	cross-sectional area of coupler
$L_{coupler}$ = 2.034 ft	length of coupler
f_y = 9312.5 ksf	yield stress of the coupler
f_u = 13186.1 ksf	ultimate stress at fracture
E_s = 5707497.6 ksf	modulus of elasticity of coupler
E_{sh} = 378000 ksf	slope of the stress-strain curve at strain hardening
e_{sh} = 0.0019	strain at strain hardening
e_{ult} = 0.0185	ultimate strain

Coupler Section

To model the behavior of the couplers within the columns an area equal to the cross-sectional area of the coupler was left empty where each coupler was located. The couplers were modeled with the same cross-sectional area as the #14 bars but having the material properties listed above. This prevented the material properties of the concrete from affecting the behavior of the couplers. The column cross-section is modeled in OpenSees as seen in Figure E13.

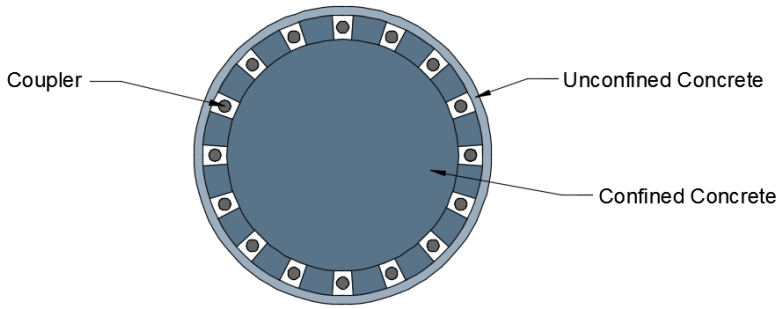

Figure E13. Parma Bridge OpenSees Model of Column Cross-section with Grouted Couplers

Nonlinear Grouted Coupler OpenSees Input File for Seismic Loads in Transverse Direction

```
#Two-span Bridge on US95 at Parma, Idaho, with grouted couplers at the top and bottom of each
column
wipe

#Create model with 3 dimensions and 6 DOF
model BasicBuilder -ndm 3 -ndf 6

#Units are kips and feet
#Create 6 DOF nodes

#Superstructure nodes
#       tag         x             y            z

node     1         0.0         34.459         0.0
node     2        35.275       34.459         0.0
node     3        70.549       34.459         0.0
node     4       105.824       34.459         0.0
node     5       141.009       34.459         0.0
node     6       176.374       34.459         0.0
node     7       211.648       34.459         0.0
node     8       246.914       34.459         0.0
node     9       282.179       34.459         0.0

#Substructure nodes
#       tag         x             y            z

node    10       141.009        0.0          15.322
node    11       141.009        0.0          15.322
node    12       141.009        0.001        15.322    #small monitoring element
node    13       141.009        2.034        15.322
node    14       141.009       23.612        15.322
node    15       141.009       25.646        15.322
node    16       141.009       25.647        15.322    #small monitoring element
node    17       141.009       25.647        15.322
node    18       141.009       28.347        15.322
node    19       141.009        0.0           0.0
node    20       141.009        0.0           0.0
node    21       141.009        0.001         0.0      #small monitoring element
node    22       141.009        2.034         0.0
node    23       141.009       23.612         0.0
node    24       141.009       25.646         0.0
node    25       141.009       25.647         0.0      #small monitoring element
```

```
node    26       141.009       25.647         0.0
node    27       141.009       28.347         0.0
node    28       141.009        0.0         -15.322
node    29       141.009        0.0         -15.322
node    30       141.009        0.001       -15.322    #small monitoring element
node    31       141.009        2.034       -15.322
node    32       141.009       23.612       -15.322
node    33       141.009       25.646       -15.322
node    34       141.009       25.647       -15.322    #small monitoring element
node    35       141.009       25.647       -15.322
node    36       141.009       28.347       -15.322

#Spring support nodes at the abutments

node    37         0.0         34.459         0.0
node    38       282.179       34.459         0.0

#Specify geometric transformation

geomTransf Linear 1  0  0  1
geomTransf Linear 2 -1  0  0
geomTransf PDelta 3  0  0  1

#Fix column bases and abutments in all DOF's

fix 37 1 1 1 1 1 1
fix 38 1 1 1 1 1 1
fix 10 1 1 1 1 1 1
fix 19 1 1 1 1 1 1
fix 28 1 1 1 1 1 1

#Create uniaxial materials for concrete and steel and zeroLength elements in the columns

#uniaxialMaterial Concrete01 $matTag $fpc $epsc0 $fpcu $epsU
uniaxialMaterial Concrete01  1  -576.0  -0.002  0  -0.005

#uniaxialMaterial Concrete04 $matTag $fc $ec $ecu $Ec <$ft $et> <$beta>
uniaxialMaterial Concrete04 2  -875.6  -0.0072  -0.019  524736

#uinaxialMaterial ReinforcingSteel $matTag $fy $fu $Es $Esh $esh $eult
uniaxialMaterial ReinforcingSteel  3  9792  13680  4176000  179568  0.0075  0.09
uniaxialMaterial ReinforcingSteel  4  9312.5  13186.1  5707497.6  378000  0.0023  0.0185

#uniaxialMaterial Hysteretic $matTag $s1p $e1p $s2p $e2p $s1n $e1n $s2n $pinchX $pinchY
$damage1 $damage2 <beta>

uniaxialMaterial Hysteretic 5 3583 .0035  4239.0  .03  -3583  -0.0035   -4239.0  -.03    1  1
0  0  0.35
uniaxialMaterial Elastic 6  1e12

#Create fiber sections with Defined Concrete and Rebar
#for CIP column section

section Fiber  1  {
#patch circ $matTag $numSubdivCirc $numSubdivRad $yCenter $zCenter $intRad $extRad <$startAng
endAng>
patch circ 2  44  10  0  0  0  1.573  0  360
patch circ 1  44  2  0  0  1.573 1.75 0  360
#layer circ $matTag $numBar $areaBar $yCenter $zCenter $radius <$startAng $endAng>
layer circ 3  16  0.015625  0  0  1.502 0 360
}
```

```
#for grouted coupler section

section Fiber  2  {
#patch circ $matTag $numSubdivCirc $numSubdivRad $yCenter $zCenter $intRad $extRad <$startAng
endAng>
patch circ 2  44  10  0  0  0  1.360  0  360
patch circ 1  44  2  0  0  1.647  1.75 0  360
patch circ 2  44  1  0  0  1.360  1.647 4.353 18.148
patch circ 2  44  1  0  0  1.360  1.647 26.853 40.648
patch circ 2  44  1  0  0  1.360  1.647 49.353 63.148
patch circ 2  44  1  0  0  1.360  1.647 71.853 85.648
patch circ 2  44  1  0  0  1.360  1.647 94.353 108.148
patch circ 2  44  1  0  0  1.360  1.647 116.853 130.648
patch circ 2  44  1  0  0  1.360  1.647 139.353 153.148
patch circ 2  44  1  0  0  1.360  1.647 161.853 175.648
patch circ 2  44  1  0  0  1.360  1.647 184.353 198.148
patch circ 2  44  1  0  0  1.360  1.647 206.853 220.648
patch circ 2  44  1  0  0  1.360  1.647 229.353 243.148
patch circ 2  44  1  0  0  1.360  1.647 251.853 265.648
patch circ 2  44  1  0  0  1.360  1.647 274.353 288.148
patch circ 2  44  1  0  0  1.360  1.647 296.853 310.648
patch circ 2  44  1  0  0  1.360  1.647 319.353 333.148
patch circ 2  44  1  0  0  1.360  1.647 341.853 355.648
#layer circ $matTag $numBar $areaBar $yCenter $zCenter $radius <$startAng $endAng>
layer circ 4  16  0.015625  0  0  1.502 0 360
}

#Define shear stiffness (GJ) elastic material

set Gc 218640
set Jc  2.95
set GJ [expr $Gc*$Jc]
uniaxialMaterial Elastic 7  $GJ

section Aggregator 3  7 T -section  1
section Aggregator 4  7 T -section  2

#Create deck elements
#element elasticBeamColumn $eleTag $iNode $jNode $A $E $G $J $Iy $Iz $transfTag

element elasticBeamColumn 1  1  2  49.60  765269.3  318862.2  1e10  7493.7  242.06  1
element elasticBeamColumn 2  2  3  49.60  765269.3  318862.2  1e10  7493.7  242.06  1
element elasticBeamColumn 3  3  4  49.60  765269.3  318862.2  1e10  7493.7  242.06  1
element elasticBeamColumn 4  4  5  49.60  765269.3  318862.2  1e10  7493.7  242.06  1
element elasticBeamColumn 5  5  6  49.60  765269.3  318862.2  1e10  7493.7  242.06  1
element elasticBeamColumn 6  6  7  49.60  765269.3  318862.2  1e10  7493.7  242.06  1
element elasticBeamColumn 7  7  8  49.60  765269.3  318862.2  1e10  7493.7  242.06  1
element elasticBeamColumn 8  8  9  49.60  765269.3  318862.2  1e10  7493.7  242.06  1

#Create pier bent elements
#element elasticBeamColumn $eleTag $iNode $jNode $A $E $G $J $Iy $Iz $transfTag

element elasticBeamColumn  9  5 27  196.00   524736  218640  1e10  1e10  1e10  3
element elasticBeamColumn 10 18 27   25.23   524736  218640  1e10  1e10  1e10  2
element elasticBeamColumn 11 27 36   25.23   524736  218640  1e10  1e10  1e10  2

#Create column elements

#element elasticBeamColumn $eleTag $iNode $jNode $A $E $G $J $Iy $Iz $transfTag
#element nonlinearBeamColumn $eleTag $iNode $jNode $numintgrPts $secTag $transfTag
```

```
#element zeroLength $eleTag $iNode $jNode -mat $matTag1 $matTag2 ... -dir $dir1 $dir2 ...
#element zeroLengthSection $eleTag $iNode $jNode $secTag <-orient $x1 $x2 $x3 $yp1 $yp2 $yp3>

element zeroLength 12 10 11 -mat 6 6 6 5 5 5 -dir 1 2 3 4 5 6   #bondslip
element nonlinearBeamColumn 13 11 12 9 3 3                                  #small
monitoring element
element nonlinearBeamColumn 14 12 13 9 4 3                                  #grouted
coupler
element nonlinearBeamColumn 15 13 14 9 3 3                                  #CIP
element nonlinearBeamColumn 16 14 15 9 4 3                                  #grouted
coupler
element nonlinearBeamColumn 17 15 16 9 3 3                                  #small
monitoring element
element zeroLength 18 16 17 -mat 6 6 6 5 5 5 -dir 1 2 3 4 5 6   #bondslip
element elasticBeamColumn 19 17 18  1e10  524736  218640  1e10  1e10  1e10  3

element zeroLength 20 19 20 -mat 6 6 6 5 5 5 -dir 1 2 3 4 5 6   #bondslip
element nonlinearBeamColumn 21 20 21 9 3 3                                  #small
monitoring element
element nonlinearBeamColumn 22 21 22 9 4 3                                  #grouted
coupler
element nonlinearBeamColumn 23 22 23 9 3 3                                  #CIP
element nonlinearBeamColumn 24 23 24 9 4 3                                  #grouted
coupler
element nonlinearBeamColumn 25 24 25 9 3 3                                  #small
monitoring element
element zeroLength 26 25 26 -mat 6 6 6 5 5 5 -dir 1 2 3 4 5 6   #bondslip
element elasticBeamColumn 27 26 27 1e10  5524736  218640  1e10  1e10  1e10  3

element zeroLength 28 28 29 -mat 6 6 6 5 5 5 -dir 1 2 3 4 5 6   #bondslip
element nonlinearBeamColumn 29 29 30 9 3 3                                  #small
monitoring element
element nonlinearBeamColumn 30 30 31 9 4 3                                  #grouted
coupler
element nonlinearBeamColumn 31 31 32 9 3 3                                  #CIP
element nonlinearBeamColumn 32 32 33 9 4 3                                  #grouted
coupler
element nonlinearBeamColumn 33 33 34 9 3 3                                  #small
monitoring element
element zeroLength 34 34 35 -mat 6 6 6 5 5 5 -dir 1 2 3 4 5 6   #bondslip
element elasticBeamColumn 35 35 36  1e10  524736  218640  1e10  1e10  1e10  3

#Create uniaxialMaterial for abutment springs

uniaxialMaterial Elastic 8 17.042e3;   # Translational stiffness along X axis of the
abutments, kip/ft
uniaxialMaterial Elastic 9 1e12;   # Translational stiffness along Y axis of the abutments,
kip/ft
uniaxialMaterial Elastic 10 3.2e3;   # Translational stiffness along Z axis of the abutments,
kip/ft
uniaxialMaterial Elastic 11 1e12;   # Rotational stiffness about X axes o10f the abutments,
kip.ft/radian
uniaxialMaterial Elastic 12 1e12;      # Rotational stiffness about Y axis of the abutments,
kip.ft/radian
uniaxialMaterial Elastic 13 0;      # Rotational stiffness about the Z axis of the abutment,
kip.ft/radian

#Create spring elements using above stiffness values

#element zeroLength $eleTag $iNode $jNode -mat $matTag1 $matTag2 ... -dir $dir1 $dir2 ...
```

```
element zeroLength 36 37  1 -mat 8 9 10 11 12 13 -dir 1 2 3 4 5 6
element zeroLength 37  9 38 -mat 8 9 10 11 12 13 -dir 1 2 3 4 5 6

#Create recorder files
#recorder Node -file Nodes1-9_GCNP_Disp_Long_Parma.out -time -nodeRange 1 9 -dof 1 disp
recorder Node -file Nodes1-9_GCNP_Disp_Trans_Parma.out -time -nodeRange 1 9 -dof 3 disp
recorder Node -file Column_Reactions_Trans.out -time -node 10 19 28 -dof 3 2 4 reaction
recorder Node -file Column_Displacement_Trans.out -time -node 15 24 33 -dof 3 disp
recorder Element -file Stress-Strain_Steel_Tension_Trans.out -time -ele 21 section 1 fiber 0 -
1.502 3 stressStrain
recorder Element -file Stress-Strain_Steel_Compression_Trans.out -time -ele 21 section 1 fiber
0 1.502 3 stressStrain
recorder Element -file StressStrain_Coupler_Trans_Tension.out -ele 22 section 1 fiber  0 -
1.502 4 stressStrain
recorder Element -file StressStrain_Coupler_Trans_Compression.out -ele 22 section 1 fiber  0
1.502 4 stressStrain
recorder Element -file Stress-Strain_Concrete_Compression_Trans.out -time -ele 22 section 1
fiber 0 1.502 2 stressStrain

#Create vertical load pattern
pattern Plain 1 Constant {
#    tag    FX       FY      FZ   MX   MY   MZ
load  1     0.0    -198.585  0.0  0.0  0.0  0.0
load  2     0.0    -418.127  0.0  0.0  0.0  0.0
load  3     0.0    -418.127  0.0  0.0  0.0  0.0
load  4     0.0    -418.127  0.0  0.0  0.0  0.0
load  5     0.0    -397.373  0.0  0.0  0.0  0.0
load  6     0.0    -418.127  0.0  0.0  0.0  0.0
load  7     0.0    -418.127  0.0  0.0  0.0  0.0
load  8     0.0    -418.127  0.0  0.0  0.0  0.0
load  9     0.0    -198.585  0.0  0.0  0.0  0.0
load 18     0.0     -68.98   0.0  0.0  0.0  0.0
load 27     0.0     -76.49   0.0  0.0  0.0  0.0
load 36     0.0     -68.98   0.0  0.0  0.0  0.0
}

constraints Plain
numberer RCM
system BandSPD
algorithm Linear
integrator LoadControl 0.1
analysis Static
analyze 10
puts "this so far"
#Reset time to perform pushover analysis
loadConst -time 0.0

#Create horizontal load patterns
#Transverse seismic loads

pattern Plain 4 Linear {
eleLoad -ele 1 -type beamUniform 0 10.7 0
}

pattern Plain 5 Linear {
eleLoad -ele 2 -type beamUniform 0 10.943 0
}

pattern Plain 6 Linear {
eleLoad -ele 3 -type beamUniform 0 11.208 0
}
```

```
pattern Plain 7 Linear {
eleLoad -ele 4 -type beamUniform 0 11.351 0
}

pattern Plain 8 Linear {
eleLoad -ele 5 -type beamUniform 0 11.352 0
}

pattern Plain 9 Linear {
eleLoad -ele 6 -type beamUniform 0 11.21 0
}

pattern Plain 10 Linear {
eleLoad -ele 7 -type beamUniform 0 10.946 0
}

pattern Plain 11 Linear {
eleLoad -ele 8 -type beamUniform 0 10.703 0
}

constraints Plain
numberer RCM
system BandSPD
algorithm Linear
integrator LoadControl 0.01
analysis Static
analyze 100
```

Results of Nonlinear Model with Grouted Couplers

Tables E11 and E12 show the displacements and column base reactions for the longitudinal and transverse directions, respectively.

Table E11. Parma Bridge Nonlinear Model with Grouted Couplers Displacements and Column Base Reactions for Seismic Loads in the Longitudinal Direction

Nodes	Displacement (ft.)
Deck	
1	0.08498
2	0.08614
3	0.08693
4	0.08736
5	0.08741
6	0.08736
7	0.08693
8	0.08614
9	0.08498
Top of the Columns	
15	0.08039
24	0.08039
33	0.08039

Columns	Shear (k)	Axial (k)	Moment (k-ft)
1	-97.992	752.371	1365.820
2	-97.992	752.371	1365.820
3	-97.992	752.365	1365.830

Table E12. Parma Bridge Nonlinear Model with Grouted Couplers Displacements and Column Base Reactions for Seismic Loads in the Transverse Direction

Nodes	Displacement (ft.)
Deck	
1	0.35954
2	0.36310
3	0.36936
4	0.37388
5	0.37522
6	0.37392
7	0.36943
8	0.36319
9	0.35964
Top of the Columns	
15	0.37490
24	0.37521
33	0.37490

Columns	Shear (k)	Axial (k)	Moment (k-ft)
1	-272.388	753.540	-3634.250
2	-272.397	753.703	-3634.510
3	-272.388	753.522	-3634.250

The drift in the longitudinal and transverse directions for top of the columns are shown in Table E13.

Table E13. Parma Bridge Nonlinear Model with Grouted Couplers Calculated Drift for Top of the Columns

Node	15	24	33
Long. drift (%)	0.3135	0.3135	0.3135
Trans. drift (%)	1.4644	1.4657	1.4644

Bridge on SH-22 over I-15 at Dubois

Background

The Superstructure is broken down into eight elements, 29 ft each, attached end to end from south to north. At midpoint a rigid element, with large moment of inertia, connects the superstructure to the pier bent. This element starts at the center of gravity of the pier bent, and ends at the center of gravity of the superstructure. The upper portion of each column contains a rigid element that starts at the top of the column and ends at the center of gravity of the pier bent (2.355 ft). Finally, the footings are included in the model as rigid elements that are located at the bottom of the columns. They are modeled using the same properties as the columns, but they are half the depth of the footings in length (2 ft). To model the spring support conditions, extra nodes and *ZeroLength* elements are assigned to the abutment ends of the superstructure.

Superstructure

- $Overall\ Length$

$L_d = 230\ ft$

- $Compressive\ Strength\ of\ Cast\ in\ Place\ Concrete - Deck\ Slab\ and\ Parapet$

$f^{'}_c = 4.0\ ksi$

- $Modulus\ of\ Elasticity\ of\ Cast\ in\ Place\ Concrete$

$E_c = 3{,}300 \times 0.145^{1.5}\sqrt{f^{'}_c} = 3{,}644\ ksi$

- $Modulus\ of\ Elasticity\ of\ Steel$

$E_s = 29{,}000\ ksi$

- $Modular\ Ratio\ \ of\ Elasticity$

$n = \dfrac{E_s}{E_c} = \dfrac{29{,}000\ ksi}{3{,}644\ ksi} = 7.96$

- $Cross\ Sectional\ Area\ of\ Small\ Girder$

$A_g = \left(2 \times (1.25\ in\ \times 18\ in) + (0.625\ in \times 40\ in)\right) =\ 70\ in^2 = 0.48\ ft^2$

- $Cross\ Sectional\ Area\ of\ Big\ Girder$

$A_g = \left(2 \times (1.375\ in\ \times 18\ in) + (0.625\ in \times 58\ in)\right) =\ 85.75\ in^2 = 0.60\ ft^2$

- $Cross\ Sectional\ Area\ of\ Deck$

$A_d = \left(\dfrac{672\ in}{7.96}\ \times 8\ in\right) = 675.38\ in^2 = 4.69\ ft^2$

- $Centroid\ Deck +\ Small\ Girders$

$\overline{y_1} = \dfrac{\left(8 \times A_{g_1} \times \overline{y_{g_1}}\right) + (A_d \bar{y}_d)}{8A_{g_1} + A_d} = 35.08\ in$

- $Centroid\ Deck +\ Big\ Girders$

$\overline{y_2} = \dfrac{\left(8 \times A_{g_2} \times \overline{y_{g_2}}\right) + (A_d \bar{y}_d)}{8A_{g_2} + A_d} = 47.43\ in$

- $Average\ Centroid$

$\bar{y}_{avg} = \dfrac{35.08\ in + 47.43\ in}{2} = 41.26\ in$

- $Moment\ of\ Inertia\ About\ Strong\ Axis\ (Deck +\ Small\ Girders)$

$$\bar{I}_{z_1} = (\sum \bar{I}_{g_1})_{strong} + \bar{I}_d + 2\left(A_{Flange_1} {d_{Flange_1}}^2\right) + \left(\sum A_{g_1} {d_{1_1}}^2\right) + \left(A_d {d_2}^2\right) = 18.260\ ft^4$$

- *Moment of Inertia About Strong Axis (Deck + Big Girdes)*

$$\bar{I}_{z_2} = (\sum \bar{I}_{g_2})_{strong} + \bar{I}_d + 2\left(A_{Flange_2} {d_{Flange_2}}^2\right)\left(\sum A_{g_2} {d_{1_2}}^2\right) + \left(A_d {d_2}^2\right) = 40.322\ ft^4$$

- *Average Moment of Inertia About Strong Axis*

$$\bar{I}_z = \frac{\bar{I}_{z_1} + \bar{I}_{z_2}}{2} = 29.291\ ft^4$$

- *Moment of Inertia About Weak Axis (Deck + Small Girders)*

$$\bar{I}_{y_1} = (\sum \bar{I}_{g_1})_{weak} + \frac{\left(\frac{t}{n}\right) b^3}{12} + \left(\sum A_{g_{y1}} {d_{1y_1}}^2\right) + x\left(A_d {d_2}^2\right) = 2{,}226.57\ ft^4$$

- *Moment of Inertia About Weak Axis (Deck + Big Girders)*

$$\bar{I}_{y_2} = (\sum \bar{I}_{g_2})_{weak} + \frac{\left(\frac{t}{n}\right) b^3}{12} + \left(\sum A_{g_{y2}} {d_{1y_2}}^2\right) + x\left(A_d {d_2}^2\right) = 2{,}451.71\ ft^4$$

- *Average Moment of Inertia About Weak Axis*

$$\bar{I}_y = \frac{\bar{I}_{y_1} + \bar{I}_{y_2}}{2} = 2{,}339.14\ ft^4$$

- *Steel Shear Modulus of Elasticity*

$$G = \frac{E_s}{2(1+\nu)} = \frac{(29{,}000\ ksi\ \times (144\frac{in^2}{ft^2})}{2\ (1+0.3)} = 1{,}606{,}153.85\ kip/ft^2$$

- *Polar Moment of Inertia*

$$J = 1 \times 10^{10}$$

Substructure

- *Pier Cap Length*

$$L_{pc} = 56\ ft$$

- *Pier Cap Height*

$$H_{pc} = 4.71\ ft$$

- *Pier Cap Cross − Sectional Area in x − y Plane*

$$A_{pc_{xy}} = (4.71\ ft\ \times 4\ ft) = 18.84\ ft^2$$

- *Column Height*

$$H_c = 14.05\ ft$$

- *Column Diameter*

$$D_c = 3.5\ ft$$

- *Column and Footing Cross − Sectional Area*

$$A_c = \frac{\pi d^2}{4} = \frac{\pi(3.5ft)^2}{4} = 9.62\ ft^2$$

- *Gross Moment of Inertia of One Column*

$$I_{cg} = \frac{\pi d^4}{64} = 7.366\ ft^4$$

- *Polar moment of Inertia of One Column*

$$J_g = \frac{\pi d^4}{32} = 14.732\ ft^4$$

Effective Polar Moment of Inertia of One Column

$$J_{eff} = 0.2J_g = 0.2(14.732\ ft^4) = 2.946\ ft^4$$

Column Reinforcement

The columns are reinforced with 13 No. 11 bars, and a No. 4 spiral with a 3 inch cover as shown in Figure

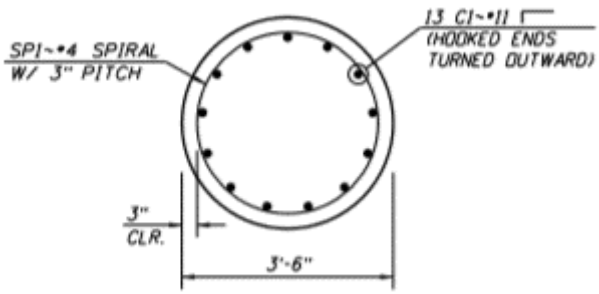

E14.

Figure E14. Dubois Bridge Column Detail

- $Cross - Sectional\ Area\ of\ No. 11\ bar$

$A_r = 1.56\ in^2 = 0.0108\ ft^2$

- $Total\ Longitudinal\ Steel\ in\ one\ Column\ Cross - Section$

$A_{st} = 13 \times A_r = 20.28\ in^2 = 0.141\ ft^2$

- $Diameter\ of\ No. 11\ Rebar$

$D_r = 1.41\ in$

- $Diameter\ of\ Spiral\ Reinforcing$

$D_s = 0.5\ in$

Linear Elastic Bridge Model

The linear-elastic models of the Dubois bridge with node and element placement are shown in Figures E15 and E16, respectively.

Spring Support Conditions

1. Support stiffness: Springs at abutments, fixed column bases
2. Abutment type: Seat type
3. Restraint of superstructure: Abutments with springs in longitudinal and transverse directions, unrestrained rotation about the z axis, and infinite restraint in all other DOF's

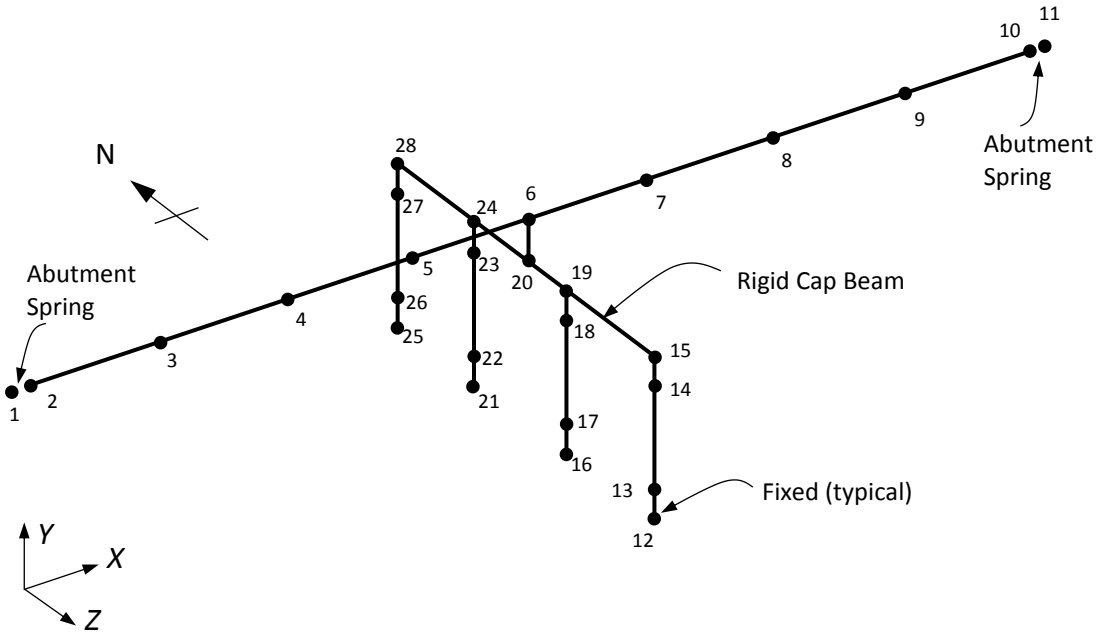

Figure E15. Dubois Bridge Linear Elastic Model with Node Numbers

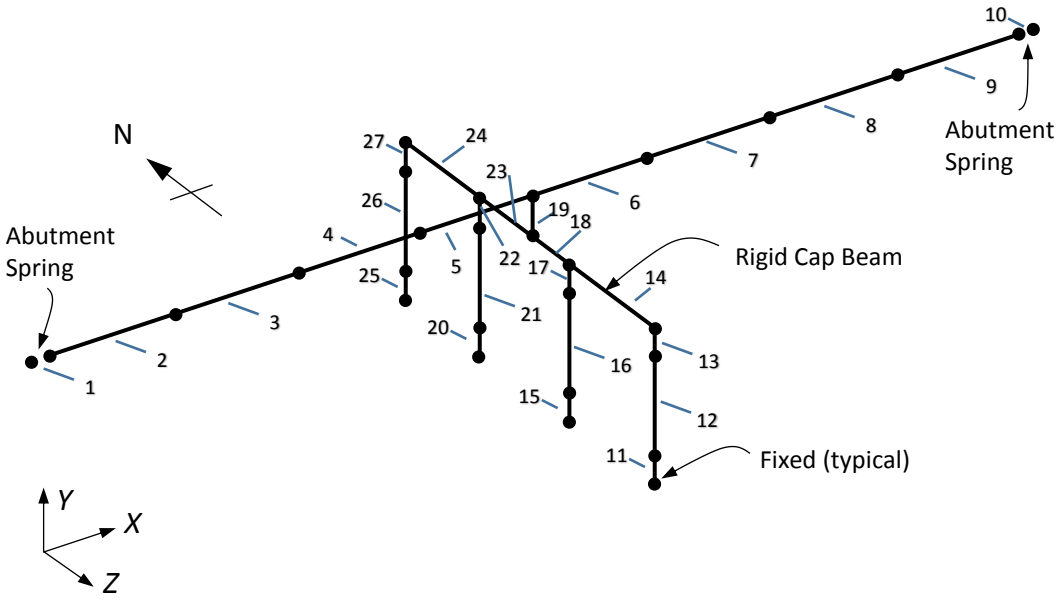

Figure E16. Dubois Bridge Linear Elastic Model with Element Numbers

Soil Spring Stiffness

Each abutment wall has eight 14X117 H-piles. Each H-pile is oriented with its strong axis parallel to the abutment wall length and its weak axis perpendicular to the abutment wall length. The dimensions of the abutment walls are:

$H_{aw_E} = 8.39\ ft$ $\quad Height\ of\ East\ Abutment\ Wall$
$H_{aw_W} = 8.38\ ft$ $\quad Height\ of\ West\ Abutment\ Wall$
$L_{aw} = 56\ ft$ $\quad Length\ of\ East\ and\ West\ Abutment\ Walls$

The soil spring stiffness for the H-piles were derived from the Phase IV Foundation Investigation Report. Figures E17-E20 show force versus deflection graphs up to 11 and 22 ft of depth for one H-pile in the East and West Abutments for the strong and weak axis. The initial spring stiffness can be estimated by determining the force at 1 in of deflection. About the strong axis the force at 1 in of deflection is:

$$k_{s_E} = 91\frac{kip}{in}$$
$$= 1{,}092\frac{kip}{ft} \quad Force\ about\ strong\ axis\ (longitudinal)\ at\ 1\ in.defl. - East\ abutment$$
$$k_{s_W} = 116\frac{kip}{in}$$
$$= 1{,}392\frac{kip}{ft} \quad Force\ about\ strong\ axis\ (longitudinal)\ at\ 1\ in.defl. - West\ abutment$$

And about the weak axis the force at 1 in of deflection is:

$$k_{w_E} = 57\frac{kip}{in} = 684\frac{kip}{ft} \quad Force\ about\ weak\ axis\ (transverse)\ at\ 1\ in.defl. - East\ abutment$$
$$k_{w_W} = 72\frac{kip}{in} = 864\frac{kip}{ft} \quad Force\ about\ weak\ axis\ (transverse)\ at\ 1\ in.defl. - West\ abutment$$

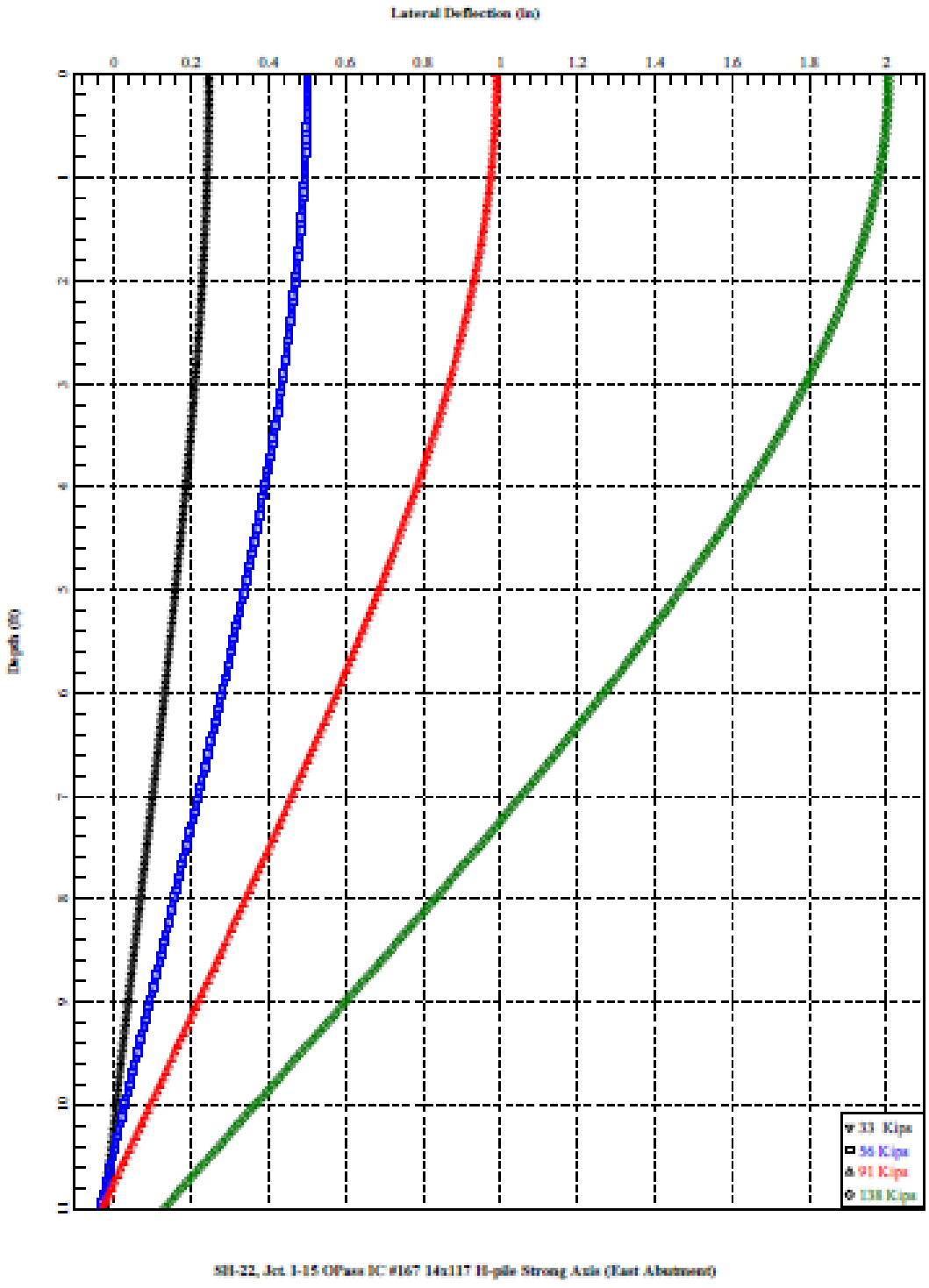

Figure E17. Dubois Bridge East Abutment Lateral Deflection vs. Depth of an H-Pile about Strong Axis

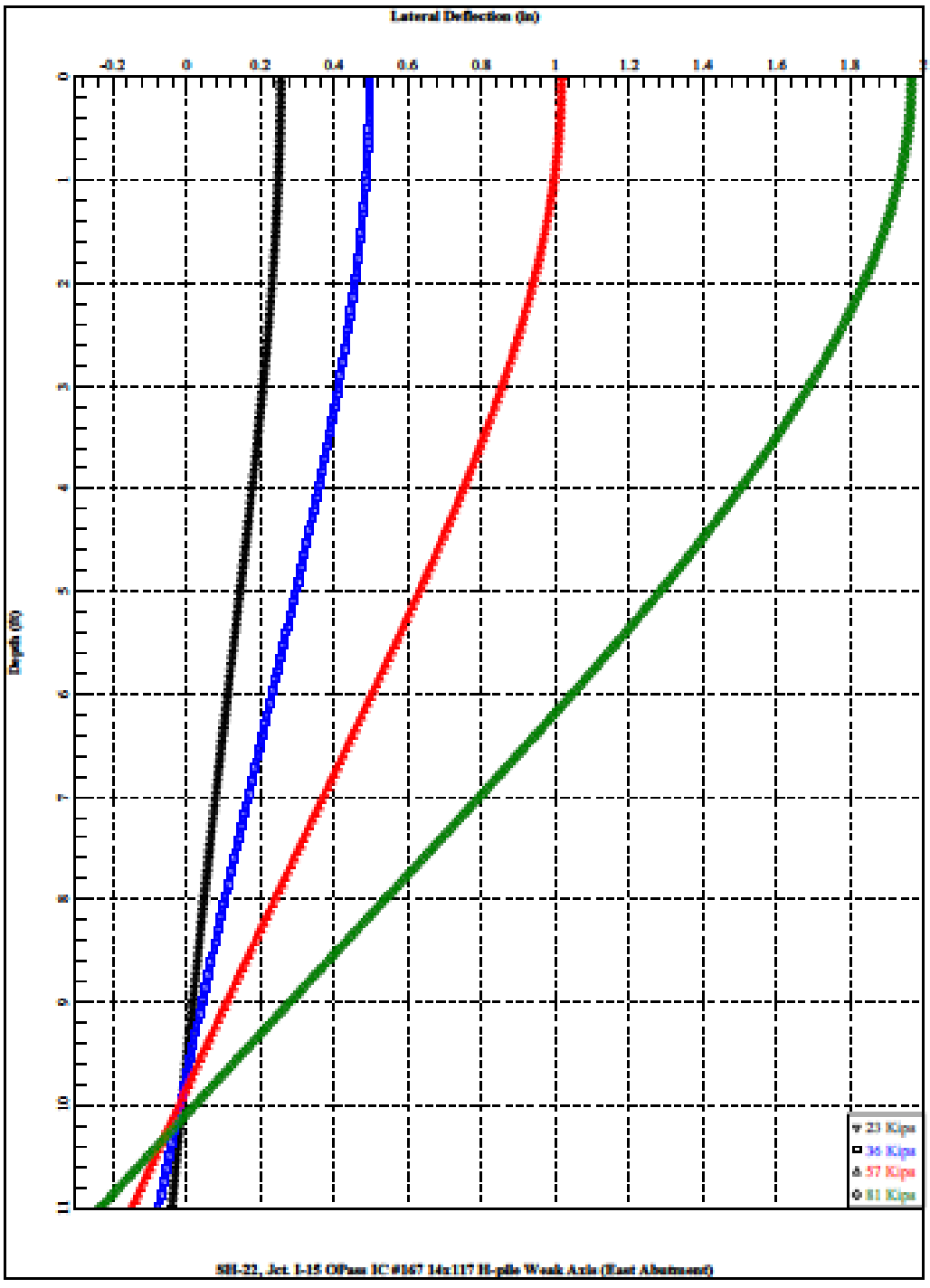

Figure E18. Dubois Bridge East Abutment Lateral Deflection vs. Depth of an H-Pile about Weak Axis

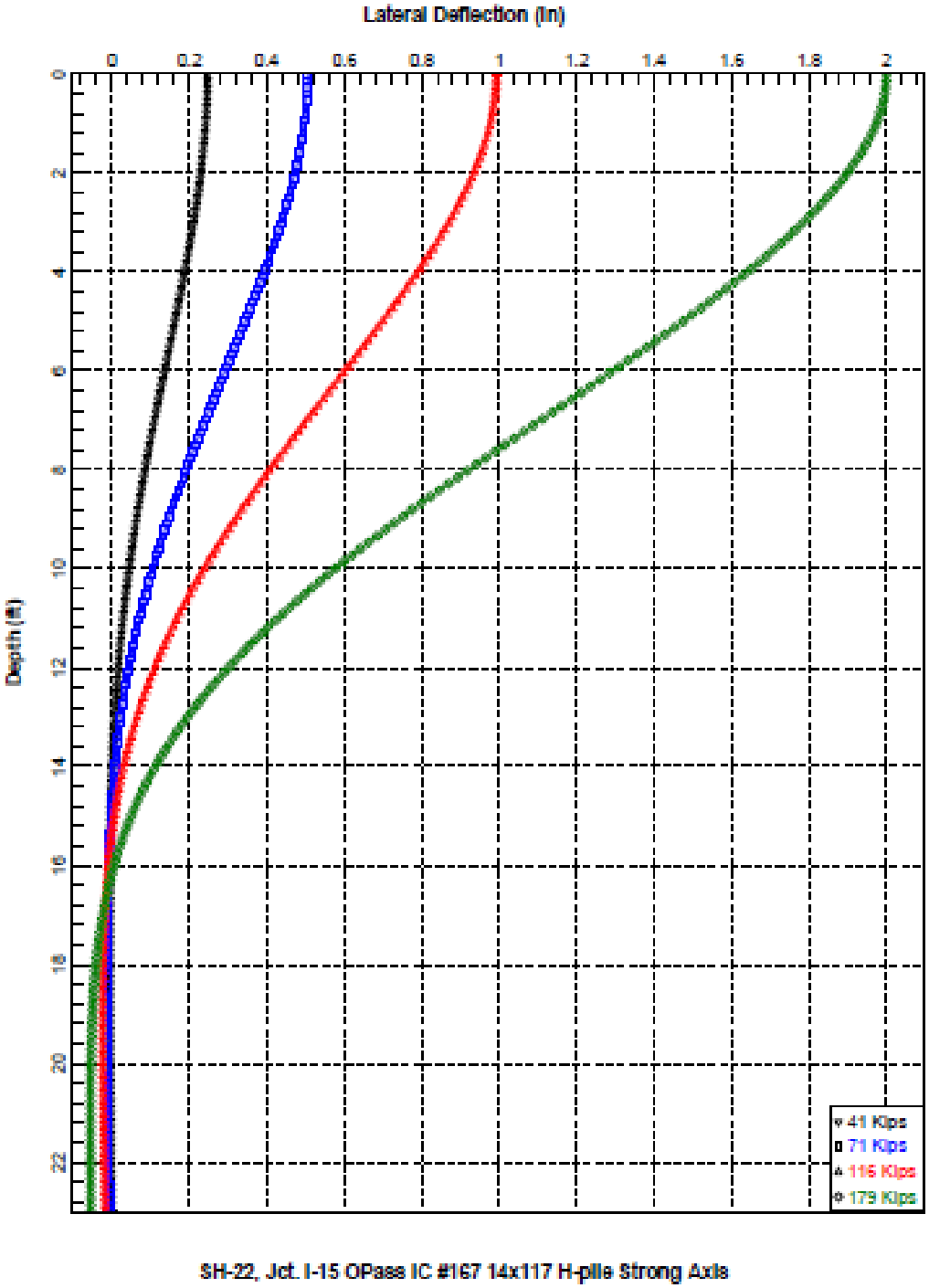

Figure E19. Dubois Bridge West Abutment Lateral Deflection vs. Depth of an H-Pile about Strong Axis

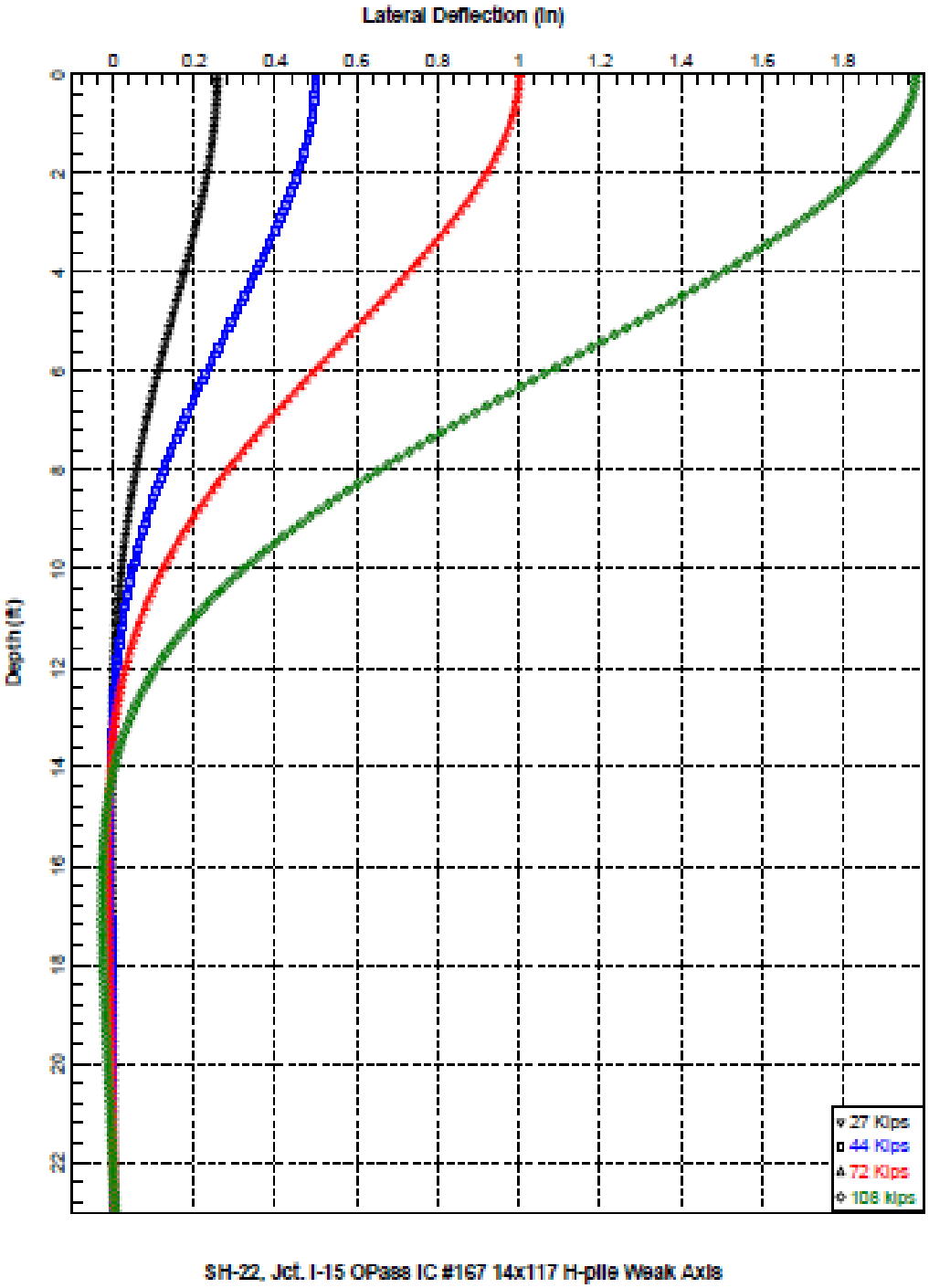

Figure E20. Dubois Bridge West Abutment Lateral Deflection vs. Depth of an H-Pile about Weak Axis

The initial value for the soil spring stiffness in the x direction (longitudinal) is calculated by

$$K_{longitudinal} = \frac{nk_{s_E} + nk_{s_W} + \left(\frac{7.7A}{d}\right)}{2}$$

Where,

$K_{longitudinal} = soil\ spring\ stiffness\ in\ x-direction$
$n = number\ of\ H\ piles\ in\ one\ abutment\ wall = 8$
$k_s = East\ or\ West\ soil\ spring\ stiffness\ for\ one\ H-pile\ in\ longitudinal\ direction$
$A_{aw_E} = East\ abutment\ wall\ area = H_{aw_E} \times L_{aw} = 469.84\ ft^2$
$A_{aw_W} = West\ abutment\ wall\ area = H_{aw_W} \times L_{aw} = 469.28\ ft^2$
$d_E = deflection\ needed\ to\ mobilize\ full\ passive\ resistanc - East = 0.02H_{aw_E} = 0.1678\ ft$
$d_W = deflection\ needed\ to\ mobilize\ full\ passive\ resistanc - West = 0.02H_{aw_W} = 0.1676\ ft$

- For the East Abutment, the soil spring stiffness in the strong direction (longitudinal) is:

$$K_{longitudinal_E} = 20{,}716\frac{kip}{ft}$$

- For the West Abutment, the soil spring stiffness in the strong direction (longitudinal) is:

$$K_{longitudinal_W} = 20{,}716\frac{kip}{ft}$$

The initial value for the soil spring stiffness in the z direction (transverse) is calculated by

$$K_{transverse} = nk_w$$

Where,
$K_{transverse} = soil\ spring\ stiffness\ in\ z-direction$
$n = number\ of\ H\ piles\ in\ one\ abutment\ wall = 8$
$k_w = East\ or\ West\ soil\ spring\ stiffness\ for\ one\ H-pile\ in\ transverse\ direction$

If the reactions at the ends of the bridge are greater than the force needed to displace the H-piles times the number of H-piles in a wingwall the excess seismic load will be resisted by the shear capacity of one wingwall, V_c. If the excess seismic force is greater than V_c it can be assumed that the wingwall has broken off and only the H-pile capacity resists the seismic force.

$$V_c = shear\ capacity\ of\ one\ wingwall = 0.0316\beta(\sqrt{f'_c})b_v d_v$$

Where,
$\beta = 2.0$
$b_{v_E} = height\ of\ East\ wingwall = 99.72\ in$
$b_{v_W} = height\ of\ West\ wingwall = 99.48\ in$
$d_v = thickness\ of\ wingwall\ minus\ distance\ from\ backfill\ face\ to\ main\ flexural\ reinf.$
$= 9.625\ in$

$V_{c_E} = 121.32\ kip$
$V_{c_W} = 121.03\ kip$

- For the East Abutment, the soil spring stiffness in the weak direction is:

$$K_{transverse_E} = 8\left(684\frac{kip}{ft}\right) = 5{,}472\frac{kip}{ft}$$

- For the West Abutment, the soil spring stiffness in the weak direction is:

$$K_{transverse_W} = 8\left(864\frac{kip}{ft}\right) = 6{,}912\frac{kip}{ft}$$

A large spring stiffness (1e12 kip/ft) was used for all other DOF's except the rotation about the z axes of the abutments, which were assigned a value of zero.

Weight of Structure

The values for the weight of the structure are given in Tables E14-E16.

Table E14. Dubois Bridge Weight of Structure to Nodes from Deck, Pier Cap, and Top Half of Columns

SECTION	CROSS-SECTIONAL AREA (ft^2)	LENGTH (ft)	WEIGTH OF MATERIAL ($kips/ft^3$)	OVERALL WEIGHT (kips)	WEIGTH PER FOOT (kips/ft)
Wearing Surface					1.568
Deck	37.333	230	0.150	1288.00	5.600
Girders	3.889	230	0.490	438.28	1.906
Parapets	2.389	230	0.150	82.41	0.358
Metal Deck Forms					0.952
Future Utilities					0.050
Intermediate Diaphragms	0.118	49	0.490	28.34	0.123
Exterior Diaphragms	0.181	49	0.490	4.33	0.019
Columns	9.621	14.05	0.150	81.10	11.545
Pier Cap	18.840	56	0.150	158.26	3.230

Table E15. Dubois Bridge Weight Assigned to Nodes at Superstructure

SUPERSTRUCTURE	LENGTH (ft)	MATERIALS INVOLVED	WEIGTH TO NODE (kips)
Node 2	14.375	Concrete, steel, wearing surface	152.03
Node 3	28.750	Concrete, steel, wearing surface	304.06
Node 4	28.750	Concrete, steel, wearing surface	304.06
Node 5	28.750	Concrete, steel, wearing surface	304.06
Node 6	28.750	Concrete, steel, wearing surface	304.06
Node 7	28.750	Concrete, steel, wearing surface	304.06
Node 8	28.750	Concrete, steel, wearing surface	304.06
Node 9	28.750	Concrete, steel, wearing surface	304.06
Node 10	14.375	Concrete, steel, wearing surface	152.03

Table E16. Dubois Bridge Weight Assigned to Nodes at Substructure

SUBSTRUCTURE	LENGTH (ft)	MATERIALS INVOLVED	WEIGTH TO NODE (kips)
Node 15	11.667	Concrete	47.818
Node 19	16.33	Concrete	62.890
Node 24	16.33	Concrete	62.890
Node 28	11.667	Concrete	47.818

From the above tables, the total weigh of the structure is 2,654 kips giving a distributed load of w(x) = 11.54 kip/ft. The axial force to one interior column is 366.95 kips.

Effective Moment of Inertia of Columns

For the effective moment of inertia, the gross moment of inertia is multiplied by the Elastic Stiffness Ratio ($\frac{I_{eff}}{I_{cg}}$). This is obtained from Figure E21 with the Axial Load Ratio and the ratio of reinforcing steel to concrete.

$$Axial\ Load\ Ratio = \frac{P}{f'_c \times A_c}$$

Where,

$P = Axial\ load\ to\ column\ from\ self - weight\ of\ bridge = 361.879\ kips$

The axial load on one column is from half the weight of each span divided by four (four columns in total) plus the weight on the node in the pier cap above the column plus half the weight of one column.

$$\frac{P}{f'_c \times A_c} = \frac{(366.948\ kips)}{(4\ ksi\ \times 144\ in^2/ft^2 \times 9.62\ ft^2)} = 0.0662$$

$$\frac{A_{st}}{A_{cg}} = \frac{0.141\ ft^2}{9.62\ ft^2} = 0.0146$$

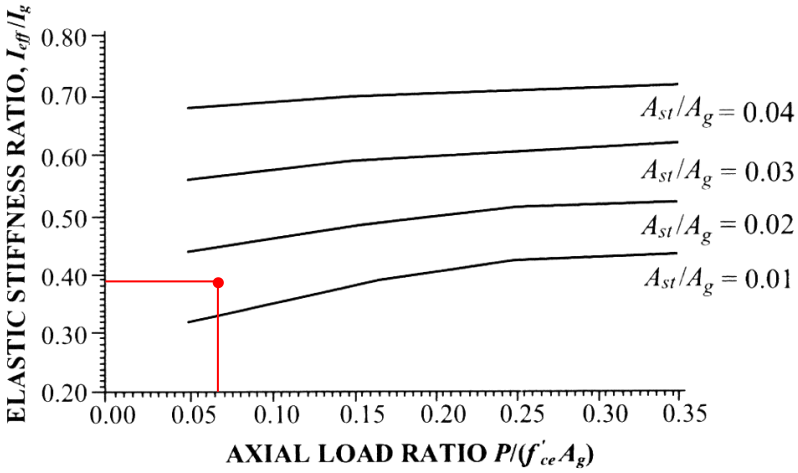

Figure E21. Dubois Bridge Elastic Stiffness Ratio[21]

$\frac{I_{eff}}{I_{cg}} = 0.39$

- $Effective\ Moment\ of\ Inertia\ of\ One\ Column$

$I_{eff} = 0.39 \times I_{cg} = 0.39 \times 7.366\ ft^4 = 2.873\ ft^4$

Seismic Loads

The same USGS seismic design summary report data as given in Figure E7 is also used for the Dubois bridge. To calculate the seismic loads on the deck of the bridge the displacements at the deck nodes from a uniformly distributed load of 10 kip/ft in the longitudinal and transverse direction are determined and used to calculate the factors α, β, and γ. The factors are used to calculate the loads (p_e *(x)*) at the nodes on the deck. The distributed seismic loads on each element is the average of the loads on the nodes. These loads are shown in column 9 of Tables E17 and E18.

$\alpha = \int_0^L v_s(x)\,dx$
$\beta = \int_0^L w(x)v_s(x)dx$
$\gamma = \int_0^L w(x)v_s\,(x)^2 dx$

Where,

$v_s(x) = Displacement\ due\ to\ uniformly\ distributed\ load\ of\ 10\frac{kip}{ft}$
$w(x) = Weight\ of\ bridge\ per\ unit\ length = 11.539\ kip/ft$
$dx = Tributary\ length$
$L = Total\ bridge\ length$

$$p_e(x) = \beta C_{sm} w(x) v_s(x)/\gamma$$

Where,

$$C_{sm} = A_s + (S_{DS} - A_s)\left(\frac{T_m}{T_o}\right) \quad for \;\; T_m < T_o$$
$$C_{sm} = S_{DS} = 0.907 \quad for \;\; T_o < T_m < T_s$$
$$C_{sm} = \frac{S_{D1}}{T_m} \quad for \;\; T_m > T_s$$

Where,

$$T_m = 2\pi\sqrt{\frac{\gamma}{P_0 g\alpha}} = 2\pi\sqrt{\frac{5.7}{(\frac{10kip}{ft})(\frac{32.2ft}{s^2})(10.658ft^2)}} = 0.256s \quad for\ longitudinal\ loads$$

$$T_m = 2\pi\sqrt{\frac{\gamma}{P_0 g\alpha}} = 2\pi\sqrt{\frac{14.702}{(\frac{10kip}{ft})(\frac{32.2ft}{s^2})(17.119ft^2)}} = 0.324s \quad for\ transverse\ loads$$

$T_s = \frac{S_{D1}}{S_{DS}} = 0.5358$

$T_0 = 0.2T_s = 0.1072$

$g = 32.2\frac{ft}{s^2}$

$P_0 = 10\frac{kip}{ft}$

Table E17. Dubois Bridge Seismic Load Calculations in Longitudinal Direction

Nodes	x (ft)	dx (ft)	vs(x) (ft)	α(x) (ft^2)	β(x) (k-ft)	γ(x) (k-ft^2)	pe(x) (k/ft)	avg. pe (k/ft)
2	0	0	0.0455	0.000	0.000	0.000	10.267	
3	28.75	28.75	0.0461	1.325	15.295	0.705	10.412	10.339
4	57.5	28.75	0.0465	1.337	15.431	0.718	10.504	10.458
5	86.25	28.75	0.0467	1.342	15.490	0.723	10.545	10.524
6	115	28.75	0.0466	1.341	15.474	0.722	10.533	10.539
7	143.75	28.75	0.0467	1.342	15.490	0.723	10.545	10.539
8	172.5	28.75	0.0465	1.337	15.431	0.718	10.504	10.524
9	201.25	28.75	0.0461	1.325	15.295	0.705	10.412	10.458
10	230	28.75	0.0455	1.307	15.082	0.686	10.267	10.339
	Total	230		10.658	122.988	5.700		
						Average	10.443	

Table E18. Dubois Bridge Seismic Load Calculations in Transverse Direction

Nodes	x (ft)	dx (ft)	vs(x) (ft)	α(x) (ft^2)	β(x) (k-ft)	γ(x) (k-ft^2)	pe(x) (k/ft)	avg. pe (k/ft)
2	0	0	0.0746	0.000	0.000	0.000	10.484	
3	28.75	28.75	0.0747	2.148	24.784	1.852	10.505	10.494
4	57.5	28.75	0.0747	2.146	24.766	1.849	10.497	10.501
5	86.25	28.75	0.0742	2.133	24.609	1.825	10.430	10.464
6	115	28.75	0.0738	2.122	24.480	1.806	10.376	10.403
7	143.75	28.75	0.0742	2.133	24.609	1.825	10.430	10.403
8	172.5	28.75	0.0747	2.146	24.766	1.849	10.497	10.464
9	201.25	28.75	0.0747	2.148	24.784	1.852	10.505	10.501
10	230	28.75	0.0746	2.143	24.734	1.844	10.484	10.494
	Total	230		17.119	197.532	14.702		
						Average	10.468	

Determination of Final Soil Spring Stiffness

Longitudinal Direction:

The reactions at the abutments, Node 1 and 11 = $R_1 = R_2 = 985.595$ k
The deflections at the abutments, Node 2 and 10 = 0.0475765 ft.
From Figures E17 and E19:
$F_W = 71$ k and $F_E = 55$ k
The demand is: $R_1 + R_2 = 985.595$ k + 985.595 k = 1971.19 k
From Figure D1 of Appendix D, $F_{bf} = 1017.86$ k
The capacity is: $n_1 F_E + n_2 F_w + F_{bf} = 8(55\text{ k}) + 8(71\text{ k}) + 1017.86\text{ k} = 2025.86$ k

Comparing the demand and capacity,
1971.19 k ≅ 2025.86 k → (2025.86 – 1971.19)/ (2025.86) *100 = 2.7% difference.
Therefore, $K_{Longitudinal\ East} = K_{Longitudinal\ West} = 20{,}716\frac{kip}{ft}$

Transverse Direction:

The reactions (the demand) at the west abutment is: $R_{t1} = 551.823$ k
Displacement at the west abutment = 0.0798355 ft.
From Figure E20:
$F_W = 69.2$ k
The capacity at the west abutment is: $n_1 F_W = 8(69.2\text{ k}) = 553.6$ k
Comparing demand and capacity,
551.823 k ≅ 553.6 k → (553.6-551.823)/ (553.6) *100 = 0.32% difference,
Therefore, no force in the wing wall is needed.
$K_{Transverse\ West} = 6912$ k/ft. OK

The reactions (the demand) at the east abutment is: $R_{t1} = 462.724$ k

Displacement at the west abutment = 0.0845621 ft.
From Figure E18:
F_W = 57 k
The capacity at the east abutment is: $n_1 F_W$ = 8(57 k) = 456 k
Comparing demand and capacity,
462.724 k ≅ 456 k → (462.724 -456)/ (462.724) *100 = 1.45% difference,
Therefore, no force in the wing wall is needed.
$K_{Transverse\ East}$ = 5472 k/ft. OK

Therefore, we get good correlation (within 10%) between abutment acting seismic forces and resulting resistance in both longitudinal and transverse directions. The abutment spring stiffness values remain the same.

$$K_{Longitudinal\ East} = 20{,}716\frac{kip}{ft}$$
$$K_{Longitudinal\ West} = 20{,}716\frac{kip}{ft}$$
$$K_{Transverse\ East} = 5{,}472\frac{kip}{ft}$$
$$K_{Transverse\ West} = 6{,}912\frac{kip}{ft}$$

Linear-elastic Analysis Results

Tables E19 and E20 show the displacements and column base reactions for the longitudinal and transverse directions, respectively. The drift in the longitudinal and transverse directions for top of the columns are shown in Table E21.

Table E19. Dubois Bridge Linear-elastic Displacements and Column Base Reactions for Seismic Loads in the Longitudinal Direction

Nodes	Displacement (ft.)
Deck	
2	0.04758
3	0.04825
4	0.04868
5	0.04887
6	0.04882
7	0.04887
8	0.04868
9	0.04825
10	0.04758
Top of the Columns	
14	0.03621
18	0.03621
23	0.03621
27	0.03621

Columns	Shear (k)	Axial (k)	Moment (k-ft)
1	-108.94	436.733	1011.02
2	-108.94	436.733	1011.02
3	-108.94	436.733	1011.02
4	-108.94	436.733	1011.02

Table E20. Dubois Bridge Linear-elastic Displacements and Column Base Reactions for Seismic Loads in the Transverse Direction

Nodes	Displacement (ft.)
Deck	
2	0.07928
3	0.07958
4	0.07991
5	0.08003
6	0.08043
7	0.08177
8	0.08318
9	0.08392
10	0.08404
Columns	
14	0.07929
18	0.07986
23	0.07986
27	0.07929

Columns	Shear (k)	Axial (k)	Moment (k-ft)
1	344.634	436.825	-2781.58
2	347.108	436.764	-2801.56
3	347.109	436.702	-2801.56
4	344.635	436.64	-2781.59

Table E21. Dubois Bridge Linear-elastic Calculated Drift for Top of the Columns

Node	14	18	23	27
Long. drift (%)	0.2577	0.2577	0.2577	0.2577
Trans. drift (%)	0.5643	0.5684	0.5684	0.5643

Nonlinear CIP Bridge Model

The nonlinear models of the Dubois bridge with node and element placement are shown in Figures E22 and E23, respectively.

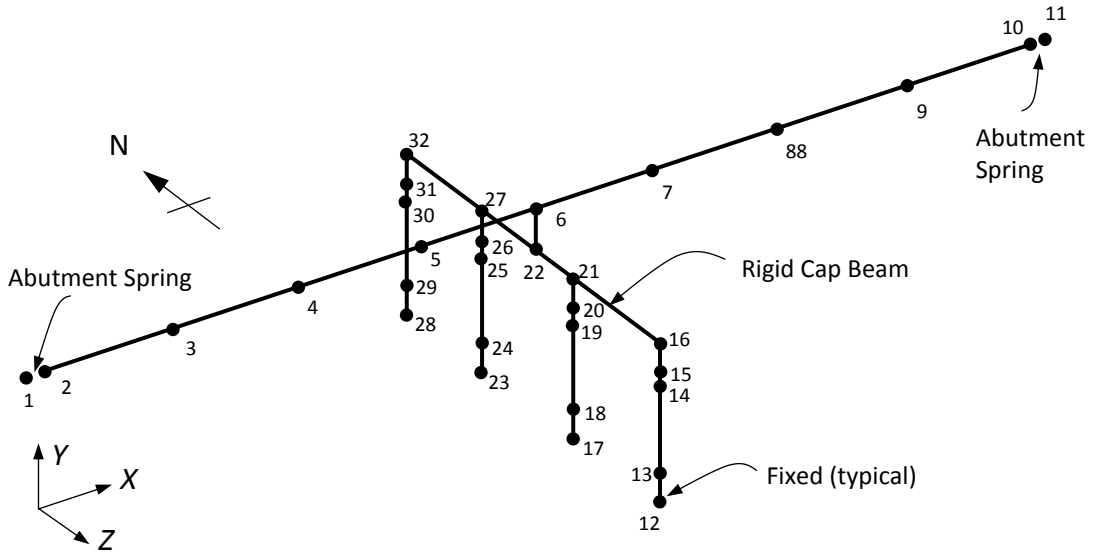

Figure E22. Dubois Bridge Nonlinear CIP Model of the Bridge with Node Numbers

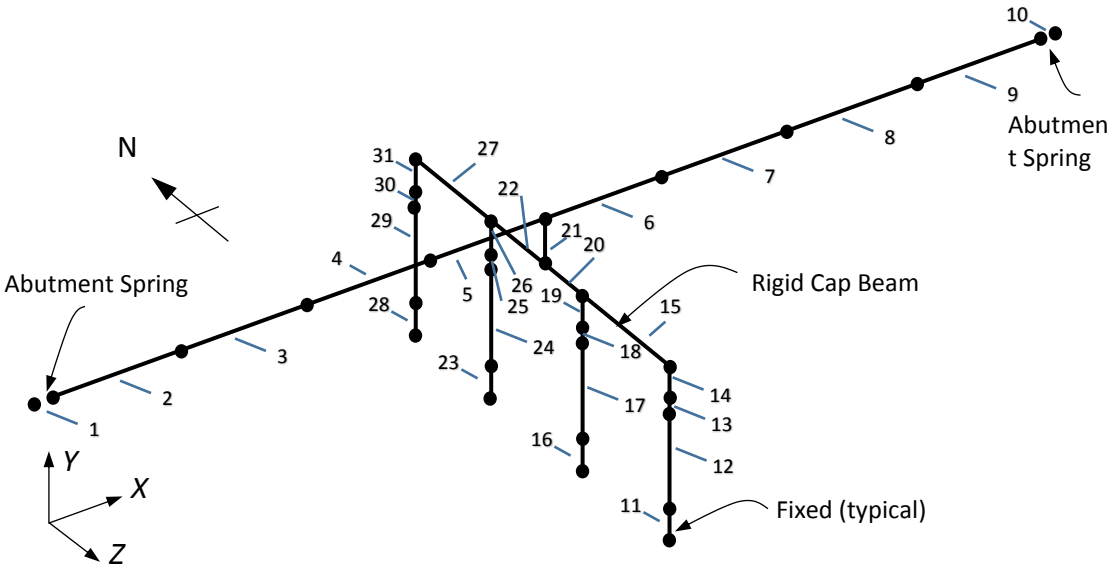

Figure E23. Dubois Bridge Nonlinear CIP Model of the Bridge with Element Numbers

Bond-slip Rotation Parameters

The rotation caused by the bond-slip at the base of the column is modeled using a rotational spring with a *Hysteretic* material behavior. The calculation process for obtaining the moment-rotation (M-θ) curve and the moment-curvature input file are presented in Appendix A. Using the approach outlined in Appendix A, Table E22 shows the moment and rotation values corresponding to the points labeled $\left(M_1^+,\ \theta_1^+\right)$ and $\left(M_2^+,\ \theta_2^+\right)$ in Figure 18 of Chapter 3. The same values were used in both the "push" and "pull" directions.

Table E22. Ends of the Column Bond-slip Moment-rotation Values for Dubois Bridge

	Moment (kip-ft)	**Rotation (rad)**
Point 1	1,700	0.0020
Point 2	1,947	0.0197

Nonlinear CIP Analysis Results

Tables E23 and E24 show the displacements and column base reactions for the longitudinal and transverse directions, respectively. The drift in the longitudinal and transverse directions for top of the columns are shown in Table E25.

Table E23. Dubois Bridge Nonlinear CIP Model Displacements and Column Base Reactions for Seismic Loads in the Longitudinal Direction

Nodes	Displacement (ft.)
Deck	
2	0.04668
3	0.04734
4	0.04776
5	0.04793
6	0.04787
7	0.04793
8	0.04776
9	0.04734
10	0.04668
Columns	
14	0.03514
19	0.03514
25	0.03514
30	0.03514

Columns	Shear (k)	Axial (k)	Moment (k-ft)
1	-118.191	436.834	991.367
2	-118.191	436.834	991.367
3	-118.191	436.834	991.367
4	-118.191	436.834	991.367

Table E24. Dubois Bridge Nonlinear CIP Model Displacements and Column Base Reactions for Seismic Loads in the Transverse Direction

Nodes	Displacement (ft.)
Deck	
2	0.11219
3	0.11300
4	0.11450
5	0.11585
6	0.11702
7	0.11828
8	0.11906
9	0.11908
10	0.11885
Columns	
14	0.11620
19	0.11661
25	0.11661
30	0.11620

Columns	Shear (k)	Axial (k)	Moment (k-ft)
1	-245.304	437.091	-1748.62
2	-245.346	437.237	-1749.04
3	-245.346	437.228	-1749.06
4	-245.303	437.087	-1748.69

Table E25. Dubois Bridge Nonlinear CIP Model Calculated Drift for Top of the Columns

Node	14	19	25	30
Long. drift (%)	0.2501	0.2501	0.2501	0.2501
Trans. drift (%)	0.8270	0.8300	0.8300	0.8270

Nonlinear Model with Grouted Couplers

The nonlinear models of the Dubois bridge with grouted couplers are shown in Figures E24 and E25, respectively.

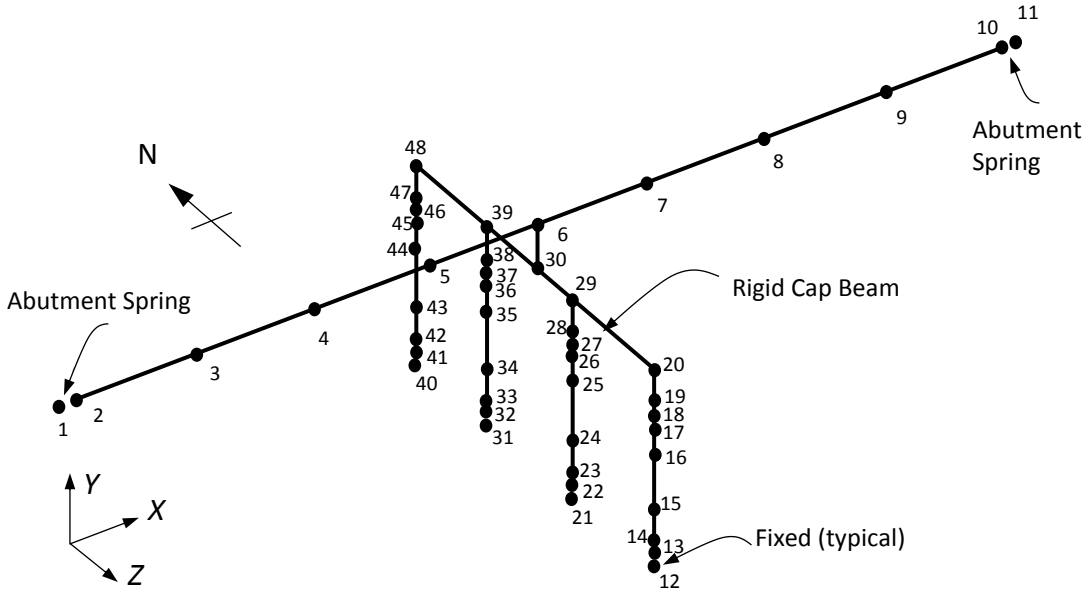

Figure E24. Dubois Bridge Nonlinear Model with Grouted Couplers Showing Node Numbers

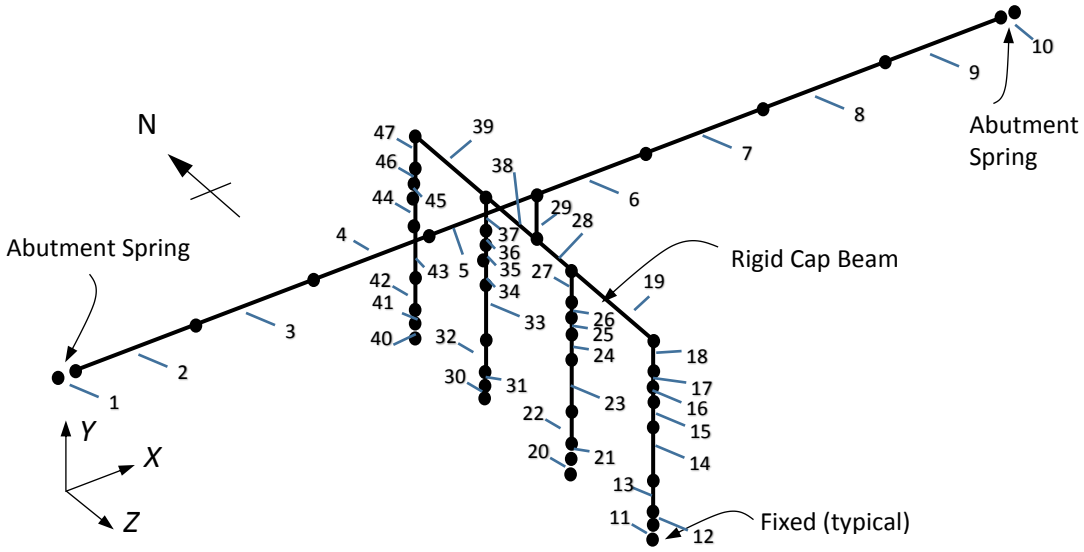

Figure E25. Dubois Bridge Nonlinear Model with Grouted Couplers Showing Element Numbers

Results for Nonlinear Model with Grouted Couplers

Tables E26 and E27 show the displacements and column base reactions for the longitudinal and transverse directions, respectively. The drift in the longitudinal and transverse directions for top of the columns are shown in Table E28.

Table E26. Dubois Bridge Nonlinear Model with Grouted Couplers Displacements and Column Base Reactions for Seismic Loads in the Longitudinal Direction

Nodes	Displacement (ft.)
Deck	
2	0.04678
3	0.04744
4	0.04786
5	0.04803
6	0.04797
7	0.04803
8	0.04786
9	0.04744
10	0.04678
Columns	
17	0.03534
26	0.03534
36	0.03534
45	0.03534

Columns	Shear (k)	Axial (k)	Moment (k-ft)
1	-117.191	436.833	981.169
2	-117.191	436.833	981.168
3	-117.191	436.832	981.168
4	-117.191	436.832	981.168

Table E27. Dubois Bridge Nonlinear Model with Grouted Couplers Displacements and Column Base Reactions for Seismic Loads in the Transverse Direction

Nodes	Displacement (ft.)
Deck	
2	0.11227
3	0.11309
4	0.11459
5	0.11595
6	0.11711
7	0.11838
8	0.11916
9	0.11918
10	0.11894
Columns	
17	0.12287
26	0.12328
36	0.12328
45	0.12287

Columns	Shear (k)	Axial (k)	Moment (k-ft)
1	-245.03	437.101	-1746.84
2	-245.073	437.235	-1747.27
3	-245.073	437.235	-1747.29
4	-245.03	437.091	-1746.92

Table E28. Dubois Bridge Nonlinear Model with Grouted Couplers Calculated Drift for Top of the Columns

Node	17	26	36	45
Long. Drift (%)	0.2515	0.2515	0.2515	0.2515
Trans. Drift (%)	0.8745	0.8774	0.8774	0.8745

Bridge on SH-75 over Salmon River East of Clayton

Background

The bridge over the Salmon River east of Clayton is a 260 foot three-span bridge with two piers located 90 ft and 210 ft from the south end of the bridge. The skew in the bridge was removed to make it easier to model. The overall dimensions of the bridge were maintained and the pier cap and abutment lengths were shortened to match the deck width of 43.54 ft. The superstructure is made up of 8-½" precast deck panels and five 72" prestressed bulb-tee girders. The substructure has a pier cap and a single oval column which rests on a cast-in-place footing in each pier. The pier caps and columns are made of precast concrete.

Spring Support Condition

Support stiffness:	Fixed column bases
Abutment type:	Integral
Restraint of superstructure:	Abutments with springs in longitudinal and transverse directions, unrestrained rotation about the C. L. abutment.

Soil Spring Stiffness

The south abutment wall has ten 14X117 H-piles. The north abutment wall has eight 14X117 H-piles. Each H-pile is oriented with its strong axis parallel to the abutment wall length and its weak axis perpendicular to the abutment wall length. Both walls have the same dimensions which are:

H_{aw} = 11.375'	Height of abutment wall
L_{aw} = 43.542'	Length of abutment wall

The soil spring stiffness for the H-piles were derived from the Phase IV Foundation Investigation Report for the Salmon River Bridge. Figures E26 and E27 show force and deflection up to 50 ft of depth for one H-pile. Since spring stiffness equals force divided by deflection ($K = F/d$) the spring stiffness can be estimated by determining the force at 1 in of deflection. About the strong axis the force at 1 in of deflection is 116 kip, and about the weak axis the force at 1 in of deflection is 72 kip.

k_s = 116 kip/in = 1,392 kip/ft.
k_w = 72 kip/in = 864 kip/ft.

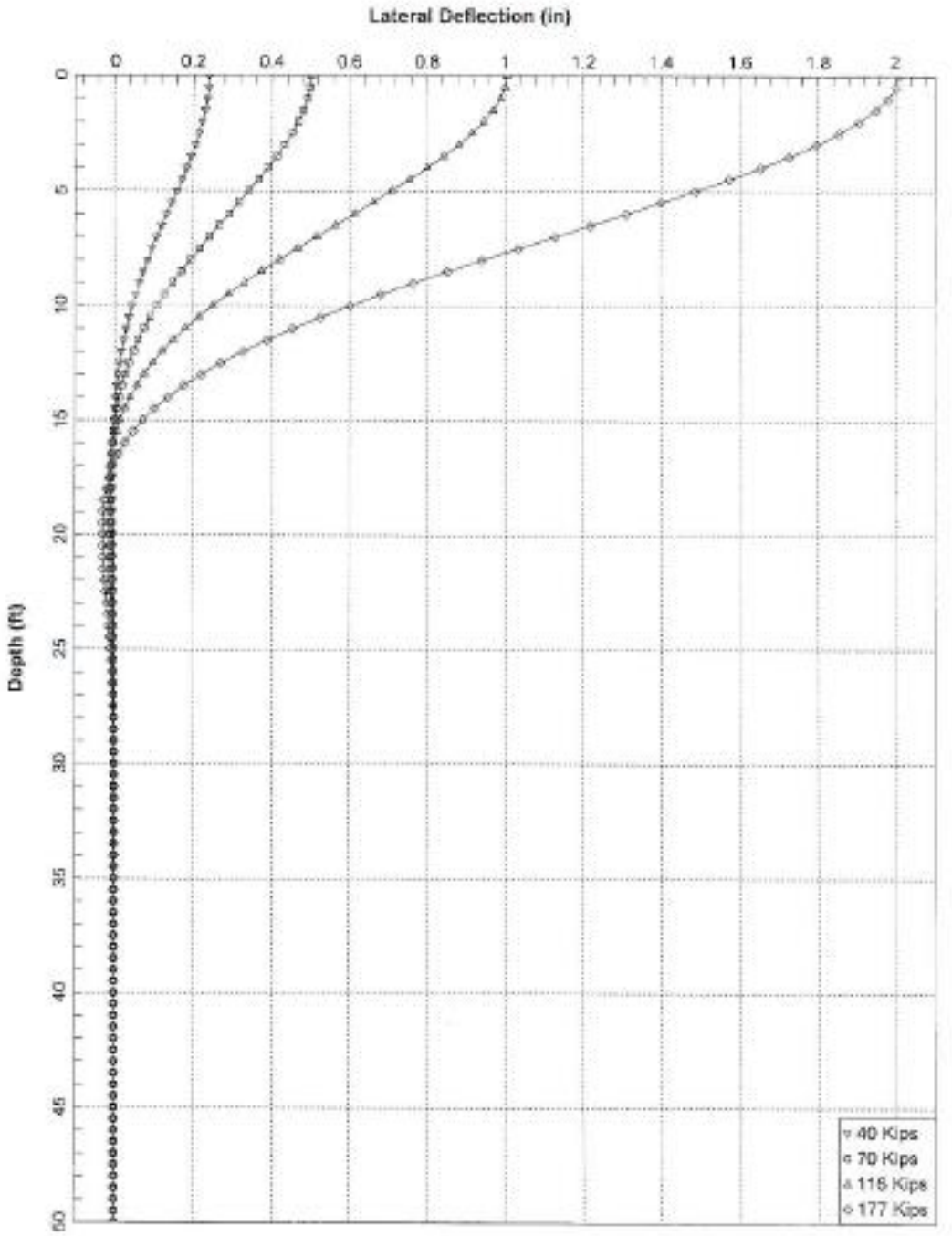

Figure E26. Salmon River Bridge Lateral Deflection vs. Depth of an H-Pile in the Abutment about the Strong Axis

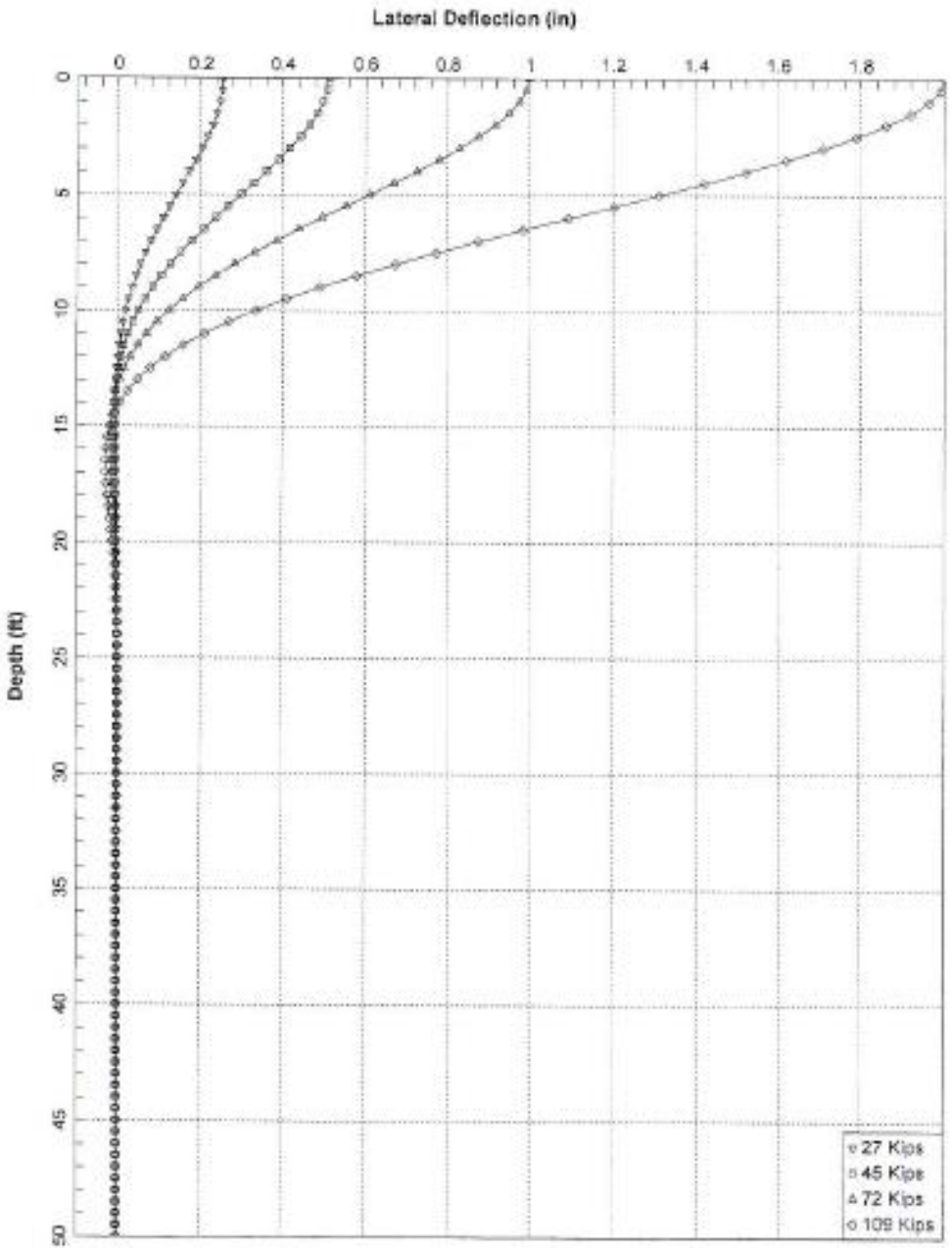

Figure E27. Salmon River Bridge Lateral Deflection vs. Depth of an H-Pile in the Abutment about the Weak Axis

The initial value due to abutments spring stiffness in the longitudinal direction is calculated by

$K_l = \frac{n_s k_s + n_n k_s + (7.7 A_{aw}/d)}{2}$

Where:

K_l = the abutments spring stiffness in the longitudinal direction

n_s = the number of H-piles south abutment wall =10

n_n = the number of H-piles north abutment wall = 8

k_s = the initial spring stiffness for one H-pile about the strong axis = 1,392 kip/ft
A_{aw} = the area of the abutment wall = H_{aw} L_{aw} = 495.29 ft^2
d = deflection needed to mobilize full passive resistance = 0.02H_{aw} = 0.23 ft.

Initial value for the soil spring stiffness in the transverse direction at the south abutment is calculated by

$K_{ts} = n_s k_w$

Where:
K_{ts} = the initial spring stiffness in the transverse direction at the south abutment

k_w = the initial spring stiffness of one H-pile about the weak axis = 72 kip/in

The shear strength of the wingwall (V_c) can be used to resist the transverse seismic forces if those forces do not exceed the shear strength.

$V_c = 0.0316\beta\sqrt{f_c'}\, b_v d_v$

Where:
β = 2
f'_c = compressive strength of concrete of the closure pour = 4.0 ksi
b_v = the height of the wingwall = 128 in
d_v = greater of 0.9d_e or 0.72h = 8.6625 in
h = the depth of the wingwall = 12 in
d_e = the distance to the center of the back reinforcement from the face of the wingwall = 9.625 in

V_c = 140.15 kips

Initial value for the soil spring stiffness in the transverse direction at the north abutment is calculated by

$K_{tn} = n_n k_w$

Where:
K_{tn} = the initial spring stiffness in the transverse direction at the north abutment

K_l = 20,818.7 kip/ft	spring stiffness at abutments in the longitudinal direction
K_{ts} = 8,640 kip/ft	spring stiffness at south abutment in transverse direction
K_{tn} = 6,912 kip/ft	spring stiffness at north abutment in transverse direction

A large spring stiffness (1e12 kip/ft) was used for all other DOF's except the rotation about the C. L. abutments, which were assigned a value of zero.

Superstructure

Properties of the superstructure and its elements are as follows

L_d = 260'-0" Overall length of bridge

A_{sup} = 56.9 ft^2 Gross cross-sectional area of superstructure with curb, to be used for weight calculations

f'_{cCIP} = 4.0 ksi Compressive strength of cast-in-place concrete

$f'_{cPrecast}$ = 5.0 ksi Compressive strength of precast concrete

$f'_{cPrestressed}$ = 7.0 ksi Compressive strength of prestressed concrete

$E_{CIP} = 33000*0.145^{1.5}\sqrt{f'_c}$ = 33000(0.145$^{1.5}$)√4.0 = 3,644 ksi
Modulus of elasticity of cast-in-place concrete

$E_{Precast} = 33000*0.145^{1.5}\sqrt{f'_c}$ = 33000(0.145$^{1.5}$)√5.0 = 4,074 ksi
Modulus of elasticity of precast concrete

$E_{Prestressed} = 33000(0.14+0.001f'_c)^{1.5}\sqrt{f'_c}$ = 33000(0.14+(0.001*7.0))$^{1.5}$ √7.0 = 4,921 ksi
Modulus of elasticity of prestressed concrete

To create a transformed moment of inertia for the superstructure the value of I_z and I_y of the deck is divided by the modular ratio *n* before the moment of inertia of the composite section is calculated. The section properties of the curbs are ignored in these calculations.

$n = E_{Prestressed}/E_{Precast}$ = 4921/4074 = 1.208
Modular ratio of elasticity

I_{yd} = 4034 ft^4 Transformed moment of inertia of the deck about the y axis

I_{zd} = 1.068 ft^4 Transformed moment of inertia of the deck about the z axis

The distance from the bottom of the superstructure to the centroid of the girder is 34.34 in. The distance from the bottom of the superstructure to the centroid of the deck is 76.25 in. The centroid of the superstructure was calculated to be 55.17 in from the bottom of the superstructure.
The moments of inertia of each section (the girders and the deck) of the superstructure were added to the area of the section which was multiplied by the distance between the centroid of the section and the centroid of the superstructure. These values were totaled to give the transformed moment of inertia for the superstructure. The transformed area of the superstructure was obtained by dividing the gross area of the deck, without the curbs, by the modular ratio, n, and adding it to the areas of the girders.

I_{ysup} = 8383.7 ft^4 Transformed moment of inertia of the superstructure about the y axis

I_{zsup} = 273.3 ft^4 Transformed moment of inertia of the superstructure about the z axis

A_T = 51.38 ft^2 Transformed area of the superstructure

The torsional moment of inertia is calculated by

$$J = \frac{A^4}{40I_p}$$ (AASHTO LRFD Specifications eq. C 4.6.2.2.1-2)

Where:

J = Torsional moment of inertia
I_p = Polar moment of inertia = $I_x + I_y$ = 8383.7 ft^4 + 273.3 ft^4 = 8657.0 ft^4
J_{sup} = (51.38 ft^2)^4/40(8657.0 ft^4) = 20.13 ft^4

Where:

ν = Poisson's ratio, typically from 0.15 - 0.2.

$G_{Precast}$ = 4074/2(1+0.2) = 1,697.5 ksi = 244,440 ksf
$G_{prestressed}$ = 4921/2(1+0.2) = 2050.4 ksi =295,260 ksf

Substructure

Properties of the substructure and its elements are as follows:

L_p = 43.542 ft	Length of pier cap
A_{pxz} = 174.17 ft^2	Cross-sectional area of pier cap in the x-z plane
L_1 = 15.469 ft	Southwest column height
L_2 = 15.969 ft	Northeast column height
W_c = 3.50 ft	Column width
L_c = 9.50 ft	Column length
A_{cg} = 30.62 ft^2	Cross-sectional area of one column
I_{cy} = 199.8 ft^4	Gross moment of inertia of one column about the y axis
I_{cz} = 28.80 ft^4	Gross moment of inertia of one column about the z axis

Column Reinforcement

The columns are reinforced with 34 #11 bars within 4 #5 spirals in the main part of the column. The spiral reinforcing has a 4" pitch. At the base of the column there are 34 splice sleeves within 5 sets of 4 #5 hoops as shown in Figure E28.

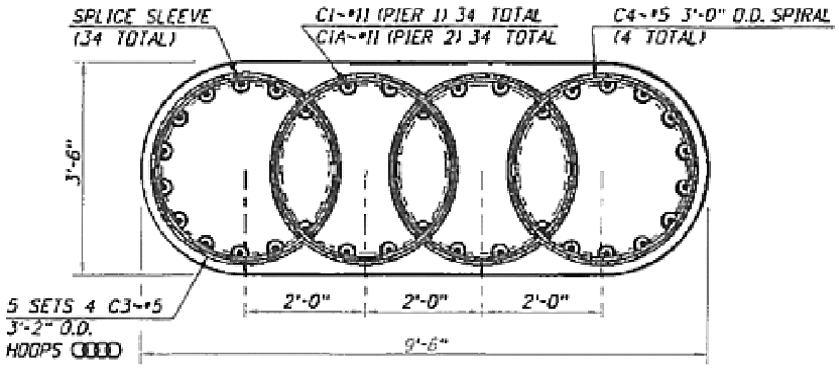

Figure E28. Salmon River Bridge Reinforced Column Detail

A_{r11} = 1.56 in^2 = 0.01083 ft^2 Cross-sectional area of a #11 bar

d_{r11} = 1.410 in = 0.1175 ft — Diameter of a #11 reinforcing bar
d_s = 0.625" — Diameter of #5 spiral reinforcing
$A_{st11} = 34A_{r11}$ = 0.3683 ft^2 — Total longitudinal steel in one column

Effective Moment of Inertia and Torsional Moment of Inertia of the Columns

For the effective moment of inertia the gross moment of inertia is multiplied by the Elastic Stiffness Ratio (I_{eff}/I_{cg}). This is obtained from Figure 4 with the Axial Load Ratio and the ratio of reinforcing steel to concrete.

Axial Load Ratio = P/f'_cA_{cg}

Where:

P = the axial load to the column from the self-weight of the bridge

The axial load on one column is from half the weight of each span that the column supports plus the weight on the node in the pier cap above the column plus half the weight of one column. The dead load to each node is given in Table E29.

Table E29. Salmon River Bridge Weight of Structure to Nodes from Deck, Pier Cap, and Top Half of Columns

Section	X-sec. Area (ft^2)	Length (ft)	Weight of Concrete (kips/ft^3)	Wearing Surface and Utilities/Future Utilities (klf)	Braces (kips)	Weight to Node (kips)
Deck						
Node 101	56.9	15	0.15	2.607	1.4	168.53
Node 102	56.9	30	0.15	2.607	1.4	335.66
Node 103	56.9	30	0.15	2.607	1.4	335.66
Node 104	56.9	30	0.15	2.607	1.4	335.66
Node 105	56.9	30	0.15	2.607	1.4	335.66
Node 106	56.9	30	0.15	2.607	1.4	335.66
Node 107	56.9	30	0.15	2.607	1.4	335.66
Node 108	56.9	27.5	0.15	2.607	1.4	307.81
Node 109	56.9	25	0.15	2.607	1.4	279.95
Node 110	56.9	12.5	0.15	2.607	1.4	140.68
Pier Cap 1						
Node 203	141.03	8	0.15	N/A	N/A	169.24
Pier Cap 2						
Node 303	141.03	8	0.15	N/A	N/A	169.24
Top Half of Columns						
Node 203	30.62	7.73	0.15	N/A	N/A	35.50
Node 303	30.62	7.98	0.15	N/A	N/A	36.65
				Total Weight of Bridge		3321.55
				w(x) (kip/ft)		12.78

Effective moment of inertia for southwest column is obtained as follows:

P = 1,379.55 kips
f'_c = 720 ksf
A_{cg} = 30.62 ft^2
P/f'_cA_{cg} = 1,379.55 kips/720 ksf * 30.62 ft^2 = 0.063
A_{st}/A_{cg} =0.3683 ft^2/30.62 ft^2 = 0.012
I_{eff}/I_{cg} = 0.36
I_{ceffy} = 0.36 * I_{cy} = 71.93 ft^4 Effective moment of inertia about the y axis
I_{ceffz} = 0.36 * I_{cz} = 10.37 ft^4 Effective moment of inertia about the z axis

Effective moment of inertia for northeast column is obtained as follows:

P = 1,157.16 kips
P/f'_cA_{cg} = 1,157.16 kips/720 ksf * 30.62 ft^2 = 0.052
I_{eff}/I_{cg} = 0.35
I_{ceffy} = 0.35 * I_{cy} = 69.93 ft^4 Effective moment of inertia about the y axis
I_{ceffz} = 0.35 * I_{cz} = 10.08 ft^4 Effective moment of inertia about the z axis

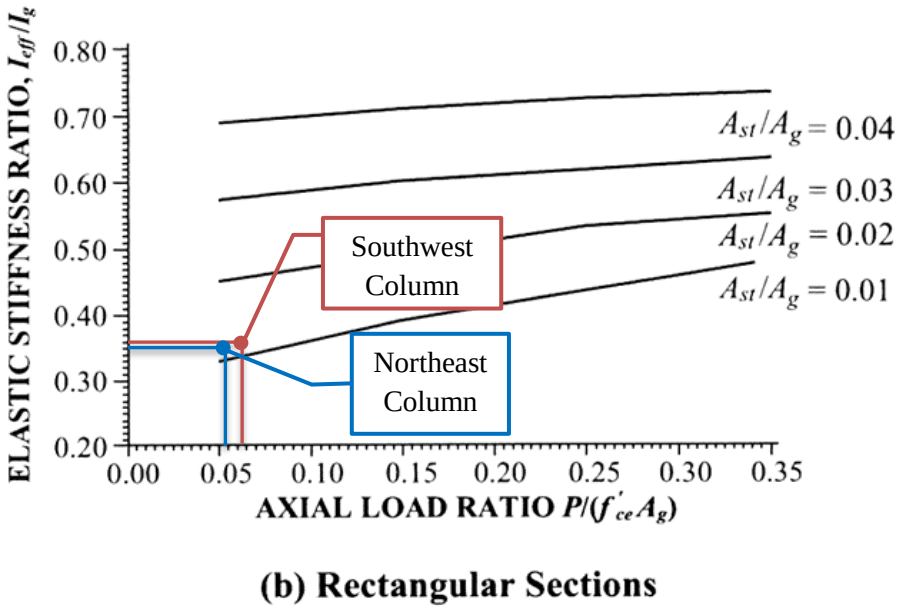

(b) Rectangular Sections

Figure E29. Salmon River Bridge Elastic Stiffness Ratio

$J_{gross} = \beta ab^3$
Where:
β = 0.249
a = 8.75 ft
b = 3.5 ft
J_{gross} = 93.4 ft^2 Gross torsional moment of inertia
J_{eff} = 0.2J_{gross} = 18.68 ft^4 Effective torsional moment of inertia

Linear Elastic Model of the Structure

The bridge has three spans of different lengths. The first span, beginning at the centerline of the southwest abutment and ending at the centerline of the southwest pier, is 90 ft and is divided into three elements that are 30 ft long. The second span, beginning at the centerline of the southwest pier and ending at the centerline of the northeast pier, is 120 ft and has four elements that are 30 ft long. The third span, beginning at the centerline of the northeast pier and ending at the centerline of the northeast abutment, is 50 ft and has two elements that are 25 ft long.

The piers consist of a single column that is precast with a column cap at the top and a cast-in-place footing that is 5 ft deep. There is a rigid element that joins the superstructure with the column caps that starts at the centroid of the superstructure and ends at the top of the column cap (4.60 ft). There is one element that is representative of the column cap which begins at the top of the column cap and ends at the top of the column (8.042 ft). The length of the southwest column is 15.47 ft and the length of the northeast column is 15.97 ft. The element at the base of the column is representative of the footing and begins at the base of the column and ends at the midpoint of the footing (2.5 ft). The footing element is modeled with the same properties as the column. To model the spring support condition an extra node and zeroLength element is assigned to the abutment ends of the superstructure.

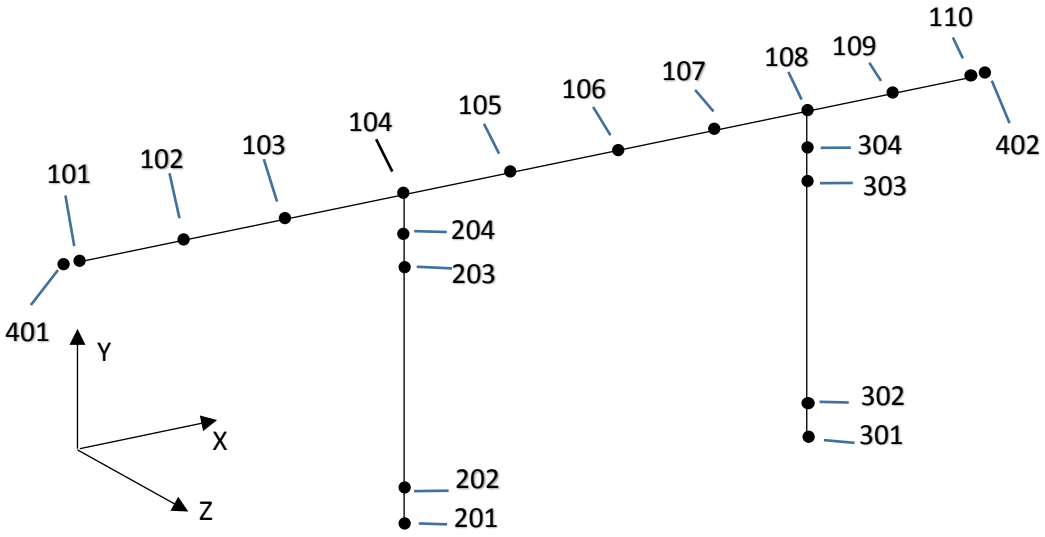

Figure E30. Salmon River Bridge Linear Elastic Model with Node Numbers

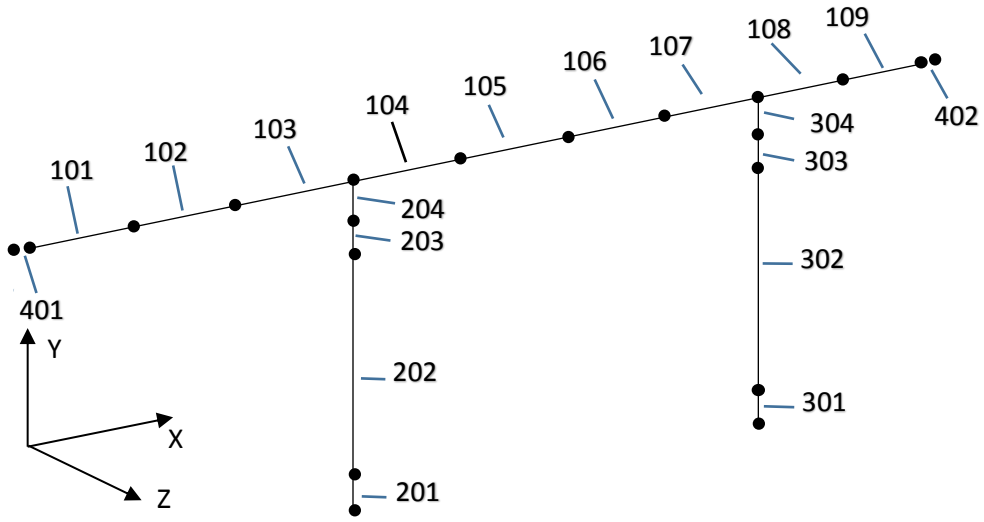

Figure E31. Salmon River Bridge Linear Elastic Model with Element Numbers

Calculation of Seismic Loads

The same USGS seismic design summary report data as given in Figure E7 is also used for the Salmon River bridge. To calculate the seismic loads on the deck of the bridge the displacements at the deck nodes from a uniformly distributed load of 10 kip/ft in the longitudinal and transverse direction are determined and used to calculate the factors α, β, and γ. The factors are used to calculate the loads (*pe (x)*) at the nodes on the deck. The distributed seismic loads on each element is the average of the loads on the nodes. These loads are shown in column 9 of Tables E30 and E31.

$\alpha = \int_0^L v_s(x)\, dx$

$\beta = \int_0^L w(x) v_s(x) dx$

$\gamma = \int_0^L w(x) v_s\,(x)^2 dx$

Where:

$v_x\,(x)$ = Displacement due to a uniformly distributed load of 10 kip/ft.

$w(x)$ = Weight of the bridge per unit length = 12.70 kip/ft

dx = Tributary length

L = Total length of bridge

$p_e(x) = \beta C_{sm} w(x) * v_s(x)/\gamma$

Where:

$C_{sm} = S_{DS}$ = 0.907 for $T_o < T_m < T_s$ *and*

$C_{sm} = S_{D1}/T_m$ for $T_m > T_s$

Where:

$T_m = 2\pi\sqrt{\gamma/P_0 g\alpha}$ = 0.260s for longitudinal loads

$T_m = 2\pi\sqrt{\gamma/P_o g\alpha}$ = 0.411s for transverse loads

$T_s = S_{D1}/S_{DS}$ = 0.5358

$T_o = 0.2T_s$ = 0.1072

g = 32.2 ft/s^2

P_o = 10 kip/ft

Table E30. Salmon River Bridge Calculation of Seismic Loads in the Longitudinal Direction

Nodes	x (ft)	dx (ft)	vs(x) (ft)	α(x) (ft^2)	β(x) (k-ft)	γ(x) (k-ft^2)	pe(x) (k/ft)	ave. (k/ft)
101	0.00	0.00	0.0426	0.000	0.000	0.000	11.420	
102	30.00	30.00	0.0432	1.288	16.359	0.702	11.582	11.501
103	60.00	30.00	0.0436	1.303	16.544	0.718	11.679	11.631
104	90.00	30.00	0.0437	1.310	16.634	0.726	11.709	11.694
105	120.00	30.00	0.0439	1.314	16.683	0.730	11.748	11.729
106	150.00	30.00	0.0438	1.314	16.690	0.731	11.720	11.734
107	180.00	30.00	0.0434	1.307	16.604	0.724	11.626	11.673
108	210.00	30.00	0.0428	1.293	16.423	0.708	11.466	11.546
109	235.00	25.00	0.0425	1.066	13.537	0.577	11.374	11.420
110	260.00	25.00	0.0420	1.055	13.401	0.566	11.237	11.305
	Totals	260.00		11.250	142.874	6.183		

Table E31. Salmon River Bridge Calculation of Seismic Loads in the Transverse Direction

Nodes	x (ft)	dx (ft)	vs(x) (ft)	α(x) (ft^2)	β(x) (k-ft)	γ(x) (k-ft^2)	pe(x) (k/ft)	ave. (k/ft)
101	0	0	-0.101	0.000	0.000	0.000	10.824	
102	30.00	30.00	-0.103	-3.063	-38.898	3.971	11.026	10.925
103	60.00	30.00	-0.107	-3.146	-39.958	4.191	11.420	11.223
104	90.00	30.00	-0.110	-3.255	-41.334	4.484	11.799	11.609
105	120.00	30.00	-0.113	-3.345	-42.478	4.736	12.062	11.931
106	150.00	30.00	-0.113	-3.384	-42.974	4.847	12.078	12.070
107	180.00	30.00	-0.110	-3.350	-42.543	4.750	11.820	11.949
108	210.00	30.00	-0.107	-3.256	-41.348	4.487	11.407	11.613
109	235.00	25.00	-0.104	-2.630	-33.399	3.513	11.107	11.257
110	260.00	25.00	-0.103	-2.579	-32.759	3.380	10.975	11.041
	Totals	260.00		-25.428	-322.933	34.981		

Determination of Final Soil Spring Stiffness

The final estimations of the bridge transverse and longitudinal abutment stiffness values are accomplished with an iterative process outlined in Appendix D. The final estimation for the abutment stiffness values are:

K_l = 23,672 kips/ft	Longitudinal abutment stiffness
K_{ts} = 7,200 kips/ft	Transverse stiffness of south abutment
K_{tn}= 5,760 kips/ft	Transverse stiffness of north abutment

As a check, the final abutment stiffness values were used in the OpenSees program with the uniformly distributed load used for calculating the seismic loads to see how the new stiffness values would affect the calculation of the seismic loads. The difference in the transverse values was no more than 1.7% and the difference in the longitudinal values was no more than 0.27%.

Linear-elastic Results

Column drift is defined as the displacement at the top of a column under a lateral load divided by the column height. The resulting longitudinal and transverse displacements at all of the superstructure nodes and at the top of the columns with the revised abutment stiffness values are shown in Tables E32 and E33.

Table E32. Salmon River Bridge Linear Elastic Model Longitudinal Displacement of Column and Superstructure Nodes

Node	101	102	103	104	105	106	107	108	109	110	203	303
Displ. (ft)	0.045	0.046	0.046	0.047	0.047	0.047	0.046	0.046	0.045	0.044	0.036	0.046

Table E33. Salmon River Bridge Linear Elastic Model Transverse Displacement of Column and Superstructure Nodes

Node	101	102	103	104	105	106	107	108	109	110	203	303
Displ. (ft)	0.131	0.133	0.137	0.141	0.143	0.143	0.140	0.136	0.133	0.131	0.063	0.062

The column height of the southwest column is 15.469 ft and the column height of the northeast column is 15.969 ft. The distance from the top of the column to the centroid of the superstructure is 12.642 ft. This added to the column height gives the height of the bridge at that column. The height of the bridge at the southwest column, node 104, is 28.11 ft and at the northeast column, node 108, 28.61 ft. The drift in the longitudinal and transvers directions at nodes 104, 108, 203, and 303 are shown in Table E34. Tables E35 and E36 show the reactions at the column bases.

Table E34. Salmon River Bridge Linear Elastic Model Calculated Drift for Selected Nodes

Node	104	108	203	303
Long. drift (%)	0.1657	0.1592	0.235	0.2909
Trans. drift (%)	0.5004	0.4748	0.4074	0.388

Table E35. Salmon River Bridge Linear Elastic Model Reactions for the Base of the Columns for Longitudinal Loading

Column	Shear (k)	Axial (k)	Moment (k-ft)
SW	-362.50	1488.59	3555.73
NE	-527.31	1280.06	4873.76

Table E36. Salmon River Bridge Linear Elastic Model Reactions for the Base of the Columns for Transverse Loading

Column	Shear (k)	Axial (k)	Moment (k-ft)
SW	-678.55	1526.14	-20560.3
NE	-618.41	1291.87	-18729.6

Nonlinear Cast-in-place (CIP) Model of the Structure

The nonlinear model of the bridge superstructure is the same as that of the linear elastic model. The columns are modeled with a *nonlinearBeamColumn* and a fiber section which describes the dimensions and properties of the reinforcing steel in the column. Additionally a *zeroLength* element is placed at the top and bottom of the columns to model bond-slip at the column-footing and column-bent interfaces and the footing is removed from the model. Figures E32 and E33 show the nodes and elements of the model with nonlinear CIP columns.

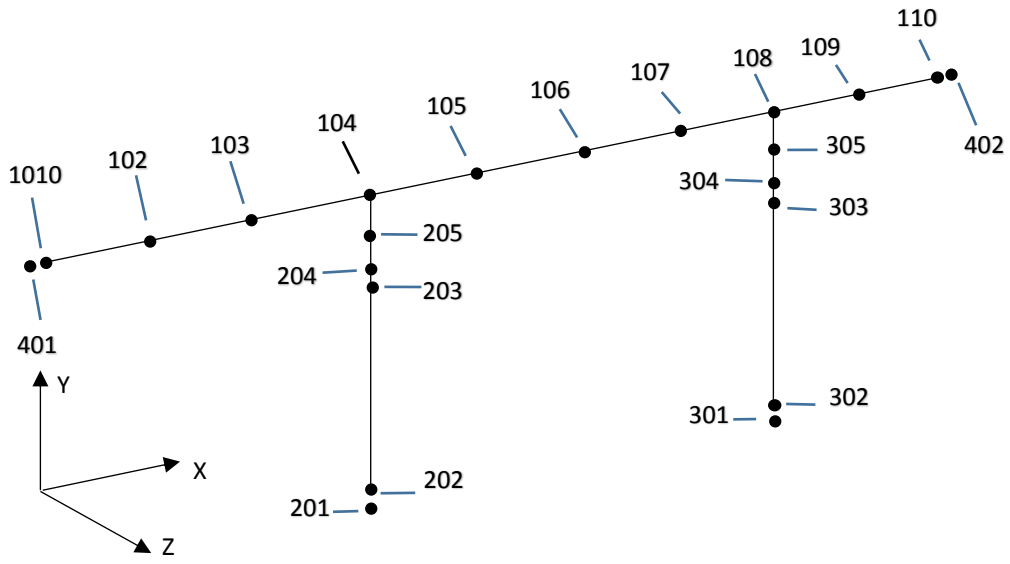

Figure E32. Salmon River Bridge Nonlinear Cast-in-place Model with Node Numbers

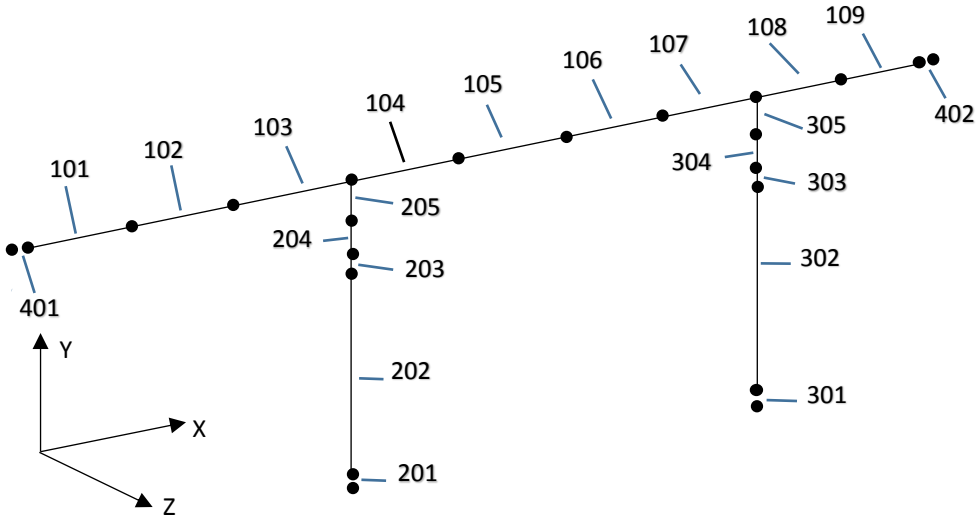

Figure E33. Salmon River Bridge Nonlinear Cast-in-place Model with Element Numbers

Material Properties

Unconfined Concrete

As previously determined the modulus of elasticity, *E*, and the modulus of rigidity, *G*, for precast concrete are:

$E_{Precast}$ = 4,074 ksi = 586,656 ksf Modulus of elasticity of precast concrete
$G_{Precast}$ = 1,697.5 ksi = 244,440 ksf Modulus of rigidity of precast concrete

Peak strain for the 5000 psi concrete is 0.002 and ultimate strain is 0.005.

Reinforcing Steel

The grade of the steel is specified in the plans. For the Salmon River Bridge the steel is Grade 60. The following properties are found in Table 8.4.2-1 in the AASHTO Guide Specifications for LRFD Seismic Bridge Design, 2011, Sec. 8-4.

f_y = 68 ksi = 9,792 ksf
f_u = 95 ksi = 13,680 ksf

The strain for a #11 bar at strain hardening is
e_{sh} = 0.0115

The ultimate strain is
e_u = 0.09

The modulus of elasticity for steel is
E = 29,000 ksi = 4,176,000 ksf

The slope of the line at strain hardening is
E_{sh} = 1247 ksi = 179,568 ksf

Confined Concrete Strength Using Theoretical Stress-Strain Model Developed by Mander et al.

AASHTO Guide Specifications for LRFD Seismic Bridge Design, Sec. 8.4.4, Concrete Modeling, specifies that confined concrete should be modeled based on Mander's stress-stain model. Following the procedure outlined by Mander et al., we obtained the following properties for the confined concrete [18]

f'_{cc} = 6.71 ksi = 966.1 ksf	Confined concrete compressive strength
ε_{cc} = 0.00542	Confined concrete strain at maximum strength
ε_{cu} = 0.015	Confined concrete ultimate strain

Modeling Column Reinforcement

The nonlinear model of the Salmon River Bridge requires a section be included in the model of the *nonLinearBeamColumn*. The section consists of patch commands for the outer unconfined concrete, two circular and two rectangular, and the inner confined concrete, two circular and one rectangular, with fiber commands for each of the 34 steel reinforcement bars. An illustration of the section for the OpenSees file can be seen in Figure E34.

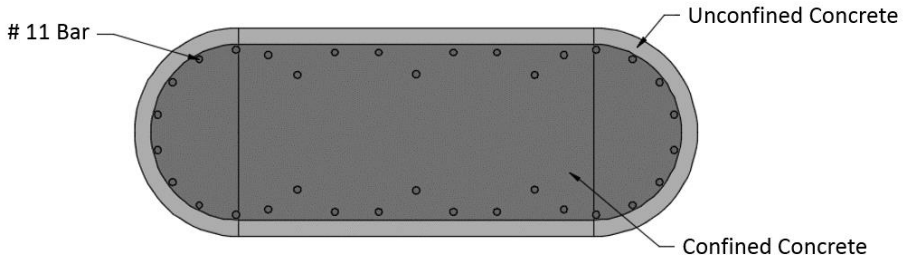

Figure E34. Salmon River Bridge Cross-section of a CIP Column with Reinforcing

Column Deflection Check with Longitudinal Reinforcing

To check the validity of the section for the OpenSees model separate files for a column (fixed-free) of confined concrete, a column of all steel, and a column of the reinforcing bars only was created. The displacements were calculated using a 1 kip horizontal force at the free end. Table E37 show the comparison of the OpenSees and hand calculated results.

Table E37. Comparison of Hand Calculated with OpenSees Displacements

Material	Hand Calculated Displacement, x10^{-6} ft		OpenSees Displacement, x10^{-6} ft	
	Bending about strong axis	Bending about weak axis	Bending about strong axis	Bending about weak axis
All Confined Concrete (with axial compression)	2.84	19.7	2.85	19.8
Rebars Only	25.8	167	25.8	169
All Steel	0.40	2.77	0.40	2.78

Modeling Bond-slip

To model the bond-slip of the reinforcing steel at the interfaces between the footing and column and the bent cap and the column a zeroLength element with hysteretic material properties is used. The uniaxialMaterial Hysteretic command in OpenSees requires values from a moment-curvature analysis of the cross-section of the column. We followed the same process as that outlined in Appendix A, section "Procedure for Determining Bond-Slip Model Parameters." Because of the symmetry of the column the moments and rotations in the negative direction are the same as those in the positive direction. The oblong shape of the column cross-section resulted in two different sets of bond-slip moment and rotation values. One set of values are for bridge loading in the transverse direction (or strong axis bending of the column) and one for loading in the longitudinal direction (or weak axis bending of the column). Table E38 shows the moment and rotation values corresponding to the points labeled $(M_1^+,\ \theta_1^+)$ and $(M_2^+,\ \theta_2^+)$ in Figure 18 of Chapter 3.

Table E38. Ends of the Column Bond-slip Moment-rotation Values for Salmon River Bridge

	Bridge under Transverse Load		Bridge under Longitudinal Load	
	Moment (kip-ft)	**Rotation (rad)**	**Moment (kip-ft)**	**Rotation (rad)**
Point 1	14,879	0.00084	5,278	0.00182
Point 2	18,100	0.01018	6,025	0.01276

Nonlinear Model with CIP Column Results

The resulting longitudinal and transverse displacements at all of the superstructure nodes and at the top of the columns are shown in Tables E39 and E40.

Table E39. Salmon River Nonlinear Model with CIP Columns Longitudinal Displacement of Column and Superstructure Nodes

Node	101	102	103	104	105	106	107	108	109	110	203	303
Displ. (ft)	0.0431	0.0438	0.0442	0.0444	0.0445	0.0445	0.0441	0.0434	0.0430	0.0424	0.0335	0.0440

Table E40. Salmon River Nonlinear Model with CIP Columns Transverse Displacement of Column and Superstructure Nodes

Node	101	102	103	104	105	106	107	108	109	110	203	303
Displ. (ft)	0.1454	0.1478	0.1525	0.1571	0.1601	0.1602	0.1571	0.1522	0.1487	0.1471	0.0721	0.0698

From previous sections the column height of the southwest column is 15.469 ft and the column height of the northeast column is 15.969 ft. The height of the bridge at the southwest column, node 104, is 28.11 ft and at the northeast column, node 108, 28.61 ft. The drift in the longitudinal and transverse directions at nodes 104, 108, 203, and 303 are shown in Table E41. Tables E42 and E43 show the reactions at the base of the columns for longitudinal and transverse loading, respectively.

Table E41. Salmon River Nonlinear Model with CIP Columns Calculated Drift for Selected Nodes

Node	104	108	203	303
Long. drift (%)	0.1580	0.1517	0.2166	0.2755
Trans. drift (%)	0.5589	0.5320	0.4661	0.4371

Table E42. Salmon River Nonlinear Model with CIP Columns Reactions at the Base of the Columns for Longitudinal Loading

Column	Shear (k)	Axial (k)	Moment (k-ft.)
SW	-432.7	1,485.3	3,691
NE	-556.2	1,298.2	4,455

Table E43. Salmon River Nonlinear Model with CIP Columns Reactions at the Base of the Columns for Transverse Loading

Column	Shear (k)	Axial (k)	Moment (k-ft.)
SW	-552.9	1,522.0	-1,5312
NE	-549.6	1,310.5	-1,5144

Nonlinear Model of Structure with Grouted Couplers

The grouted couplers are modeled as separate elements within the columns. They are located at the top and bottom of each column. In addition to the *zeroLength* elements that model bond slip small (0.001 ft in length) *nonlinearBeamColumn* elements with the same cross-section as the part of the column without couplers was added to the top and bottom of each column to observe the behavior of the materials immediately beyond the coupler region. The node and element placement can be seen in Figures E35 and E36.

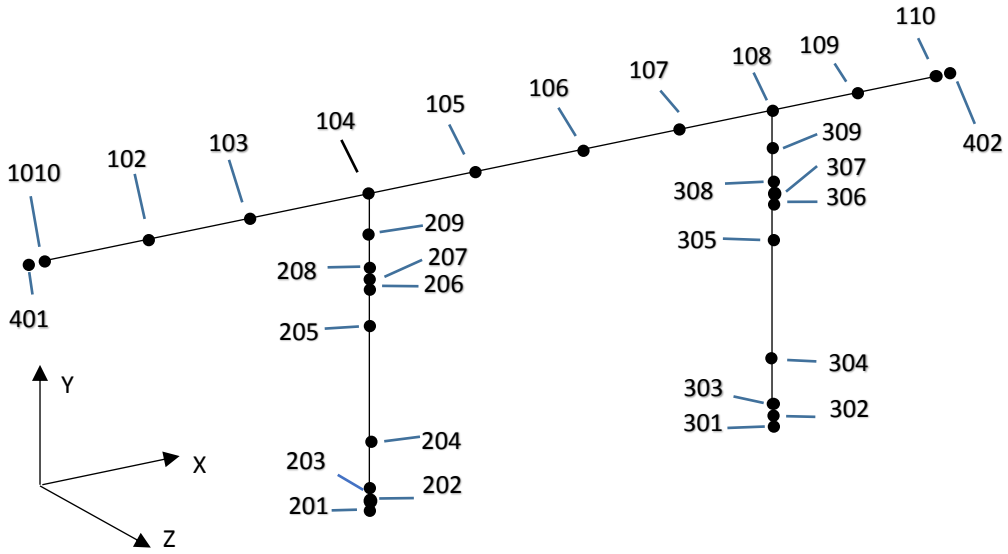

Figure E35. Salmon River Nonlinear Bridge Model with Grouted Couplers with Node Numbers

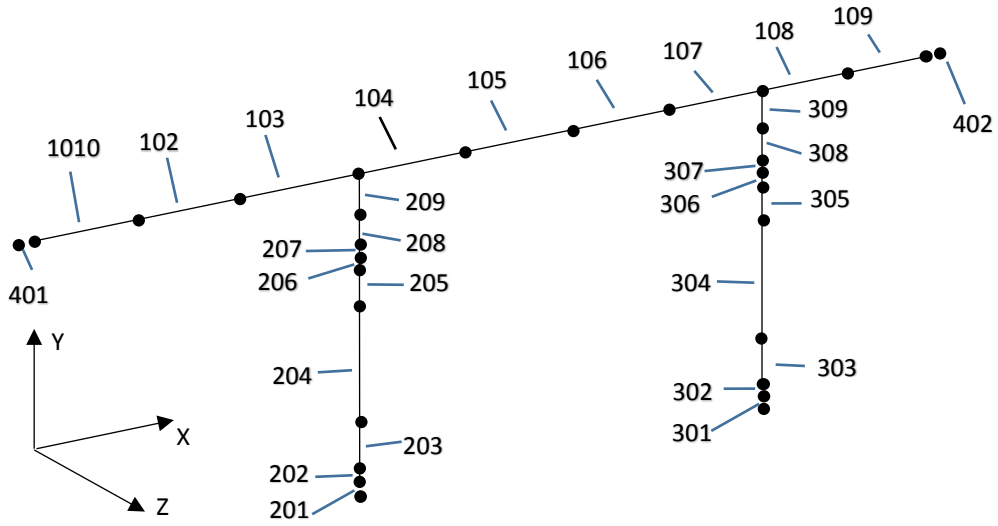

Figure E36. Salmon River Nonlinear Bridge Model with Grouted Couplers with Element Numbers

Material Properties of Grouted Couplers

The material properties of the grouted couplers were obtained from the manufacturer, Splice Sleeve North America (SSNA). The following values apply to the SSNA No. SNX11 Grouted Coupler which is used for a #11 reinforcing bar.

$A_{coupler}$ = 7.3118 in^2	cross-sectional area of coupler
$L_{coupler}$ = 1.624 ft	length of coupler
f_y = 9685 ksf	yield stress of the coupler

f_u = 13188 ksf — ultimate stress at fracture
E_s = 3992874 ksf — modulus of elasticity of coupler
E_{sh} = 317216 ksf — slope of the stress-strain curve at strain hardening
e_{sh} = 0.00307 — strain at strain hardening
e_{ult} = 0.0165 — ultimate strain

Coupler Section

To model the behavior of the couplers within the columns an area equal to the cross-sectional area of the coupler was left empty where each coupler was located. This prevented the material properties of the concrete from affecting the behavior of the couplers. The locations of the circular and rectangular patches are shown in Figure E37.

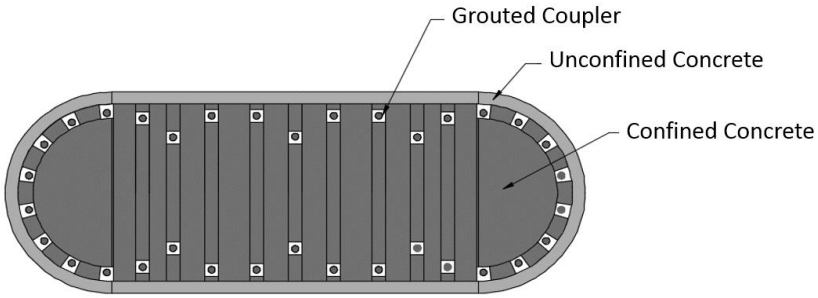

Figure E37. Salmon River OpenSees Model of Column Cross-section with Couplers

Nonlinear Model with Column Grouted Coupler Results

The resulting longitudinal and transverse displacements at all of the superstructure nodes and at the top of the columns are shown in Tables E44 and E45.

Table E44. Salmon River Nonlinear Model with Column Grouted Couplers Longitudinal Displacement of Column and Superstructure Nodes

Node	101	102	103	104	105	106	107	108	109	110	206	306
Displ. (ft)	0.0437	0.0444	0.0448	0.0449	0.0451	0.0450	0.0446	0.0440	0.0436	0.0430	0.0343	0.0447

Table E45. Salmon River Nonlinear Model with Column Grouted Couplers Transverse Displacement of Column and Superstructure Nodes

Node	101	102	103	104	105	106	107	108	109	110	206	306
Displ. (ft)	0.1457	0.1481	0.1528	0.1574	0.1604	0.1605	0.1574	0.1525	0.1490	0.1474	0.0714	0.0690

From previous sections the column height of the southwest column is 15.469 ft and the column height of the northeast column is 15.969 ft. The height of the bridge at the southwest column, node 104, is 28.11 ft and at the northeast column, node 108, 28.61 ft. The drift in the longitudinal and transverse

directions at nodes 104, 108, 205, and 305 are shown in Table E46. Tables E47 and E48 show the reactions at the base of the columns for longitudinal and transverse loading, respectively.

Table E46. Salmon River Nonlinear Model with Column Grouted Couplers Calculated Drift for Selected Nodes

Node	104	108	206	306
Long. drift (%)	0.1597	0.1538	0.2217	0.2799
Trans. drift (%)	0.5600	0.5330	0.4616	0.4321

Table E47. Salmon River Nonlinear Model with Column Grouted Couplers Reactions at the Base of the Columns for Longitudinal Loading

Column	Shear (k)	Axial (k)	Moment (k-ft.)
SW	-423.5	1,486.5	3,617
NE	-539.8	1,301.2	4,339

Table E48. Salmon River Nonlinear Model with Column Grouted Couplers Reactions at the Base of the Columns for Transverse Loading

Column	Shear (k)	Axial (k)	Moment (k-ft.)
SW	-551.1	1,522.4	-15,241
NE	-547.8	1,315.4	-15,068

Appendix F
Grouted Coupler Detailed Information

Introduction

This appendix provides background information for the use of grouted couplers. It also provides figures and tables giving grouted coupler dimensions and mechanical properties.

Key Items Found in the Literature or by Contacting the Manufacturers

- The total length of mechanical bar splice shall not exceed $15d_b$, where d_b is the longitudinal bar diameter. This requirement is to minimize the adverse effect of coupler length on the rotational capacity of a ductile member (Tazarv and Saiidi, 2015).[9]
- A spliced bar shall fracture outside coupler region regardless of the loading type. Coupler region is defined as the length of coupler plus $1.0d_b$ from each face of the coupler (Tazarv and Saiidi, 2015).[9]
- Strain capacity of the spliced bar outside coupler region should exceed 12% for No. 10 and smaller bars, and should exceed 9% for No. 11 bars and larger (AASHTO Guide Specifications for LRFD Seismic Bridge Design, 2015).[17]
- Mechanical couplers in areas away from plastic hinge zones must develop 125% of the specified yield strength of the connected reinforcing. Mechanical couplers in areas adjacent to or in plastic hinge zones must develop 150% of the specified yield strength of the connected reinforcing (UDOT Manual, 2015).[10]
- Clear cover:
  - Generally, the clear cover is more than the cast-in-place sections (Tazarv and Saiidi, 2015).[9]
  - Adjust the cover to the reinforcing and spiral or ties to accommodate the larger grouted splice coupler section (UDOT Manual, 2015).[10]
  - Question posed to SSNA, Inc.: "*What suggestions do you have regarding minimum cover for the couplers?*" Answer: "*I believe just same as the minimum concrete cover for the reinforcements based upon ACI 318*."
  - Precast concrete (manufactured under plant control conditions), concrete exposed to earth or weather, members other than wall panels, No. 14 and No. 18 bars, prestressing tendons larger than 1-1/2 in. diameter, use 2 in. cover. No. 6 through No. 11 bars, prestressing tendons larger than 5/8 in. diameter through 1-1/2 in. diameter, use 1.5" cover. (ACI 318, Section 7.7.3).[24]
  - Cover for pretensioned prestressing strand, anchorage hardware, and mechanical connections for reinforcing bars or post-tensioned prestressing strands shall be the same as for reinforcing steel. According to AASTHO LRFD Bridge Specs. Table 5.12.3-1, for unprotected main reinforcing steel for exterior other than direct exposure to salt water, cast against earth, coastal, exposure to deicing salts, deck surfaces subjected to

tire studs or chain wear, use 2.0 in. cover (AASHTO LRFD Bridge Design Specification, 2014, Section 5.12.3).[20]

- Coating:
  - Question posed to SSNA, Inc.: "*What suggestions do you have regarding coating requirements for the couplers, the longitudinal reinforcing bars being connected, and the hoops/ties?*" Answer: "*Since the sleeves are encased in concrete, just black sleeves are good for most occasions, but for DOT projects, quite often epoxy coated and galvanized sleeves are used for corrosion protection*."
- Minimum gap between the couplers:
  - Minimum and maximum clear distances between mechanical couplers are recommended to be the same as those specified for reinforcing bars (Tazarv and Saiidi, 2015).[9]
  - Detail the minimum gap between the grouted couplers to be the greatest of (1) 1 in., (2) 1.33 times the maximum aggregate size of the coarse aggregate, and (3) nominal diameter of the connected reinforcing (UDOT Manual, 2015).[10]
  - Minimum spacing of reinforcing bars: For precast concrete manufactured under plant control conditions, the clear distance between parallel bars in a layer shall not be less than: (1) the nominal diameter of the bars, (2) 1.33 times the maximum size of the coarse aggregate, or (3) 1.0 in. (AASHTO LRFD Bridge Design Specification, 2014, Section 5.10.3.1.2).[20]
  - In spirally reinforced or tied reinforced compression members, clear distance between longitudinal bars shall be not less than $1.5d_b$ nor less than 1-1/2 in. See also Sec. 3.3.2. (ACI 318, Section 7.6.3). Nominal maximum size of coarse aggregate shall be not larger than: (a) 1/5 the narrowest dimension between sides of forms, nor (b) 1/3 the depth of slabs, nor (c) 3/4 the minimum clear spacing between individual reinforcing bars or wires, bundles of bars, individual tendons, bundled tendons, or ducts. (ACI 318, Section 3.3.2).[24]
- Grout:
  - Only use the manufacturer's grout (SS Mortar, in the case of NMB grouted couplers; ICC-ES Report ESR-3433, 2016).[25]
  - For grouted couplers, grout shall be provided by the manufacturer (Tazarv and Saiidi, 2015).[9]

Grouted Coupler Dimensions

Figure F1 shows the connector configuration for the NMB Type U-X and A11W splice-sleeves. Figure F2 shows connector configuration for the NMB SNX11 splice-sleeve. Tables F1 and F2 show the dimensions and the required rebar embedment lengths corresponding to Figures F1 and F2, respectively.

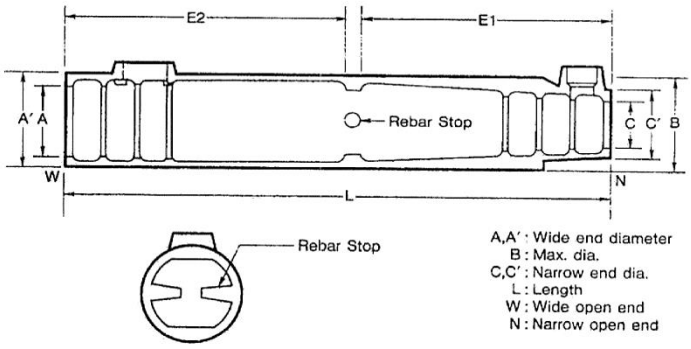

Figure F1. NMB Type U-X and A11W Splice Sleeves[25]

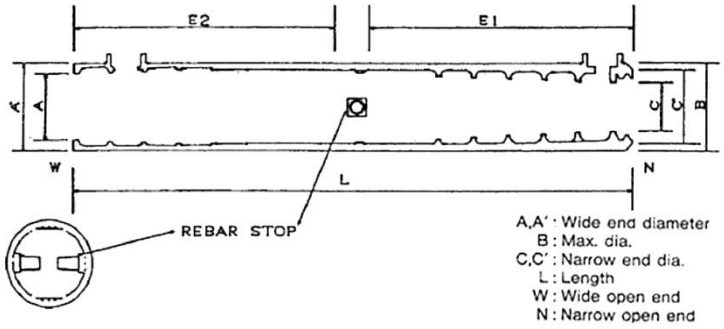

Figure F2. NMB SNX11 Splice Sleeve[25]

Table F1. Dimensions of NMB Type U-X and A11W Splice-Sleeves[25]

DIMENSIONS OF NMB U-X SLEEVES											REQUIRED REBAR EMBEDMENT LENGTH			
Sleeve No.	Bar Diameter (in.) [mm]	Bar Size		Sleeve Length (in.) [mm]	Narrow End Diameter (in.) [mm]		Maximum Diameter (B) (in.) [mm]	Wide End Diameter (in.) [mm]			Dowel (E1) (in.) [mm]		Dowel (E2) (in.) [mm]	
		ASTM	JIS		I.D. (C)	O.D. (C')		I.D. (A)	Total Tolerance [1]	O.D (A')	Min.	Max.	Min.	Max.
5U-X	0.625 [16]	#5	D16	9.65 [245]	0.87 [22]	1.50 [38]	1.89 [48.0]	1.26 [32.0]	0.63 [16.0]	1.89 [48.0]	4.13 [105]	4.33 [110]	4.13 [105]	4.92 [125]
6U-X	0.750 [19]	#6	D19	11.22 [285]	1.02 [26]	1.65 [42]	2.05 [52.0]	1.42 [36.0]	0.67 [17.0]	2.05 [52.0]	4.92 [125]	5.12 [130]	4.92 [125]	5.71 [145]
7U-X	0.875 [22]	#7	D22	12.80 [325]	1.14 [29]	1.77 [45]	2.36 [60.0]	1.73 [44.0]	0.86 [21.8]	2.36 [60.0]	5.71 [145]	5.91 [150]	5.71 [145]	6.50 [165]
8U-X	1.000 [25]	#8	D25	14.57 [370]	1.30 [33]	1.93 [49]	2.52 [64.0]	1.89 [48.0]	0.89 [22.6]	2.52 [64.0]	6.50 [165]	6.69 [170]	6.50 [165]	7.48 [190]
9U-X	1.128 [29]	#9	D29	16.34 [415]	1.42 [36]	2.06 [52.4]	2.67 [67.9]	2.01 [51.0]	0.89 [22.6]	2.67 [67.9]	7.40 [188]	7.56 [192]	7.40 [188]	8.35 [212]
10U-X	1.270 [32]	#10	D32	17.91 [455]	1.57 [40]	2.28 [58]	2.87 [73.0]	2.17 [55.0]	0.89 [22.6]	2.87 [73.0]	8.19 [208]	8.35 [212]	8.19 [208]	9.13 [232]
11U-X	1.410 [36]	#11	D36	19.49 [495]	1.73 [44]	2.40 [61]	3.03 [77.0]	2.32 [59.0]	0.91 [23.1]	3.03 [77.0]	8.98 [228]	9.13 [232]	8.98 [228]	9.92 [252]
14U-X	1.693 [43]	#14	D43	24.41 [620]	2.01 [51]	2.80 [71]	3.46 [88.0]	2.60 [66.0]	0.91 [23.1]	3.46 [88.0]	11.42 [290]	11.61 [295]	11.42 [290]	12.40 [315]
A11W	1.410 [36]	#11	D36	19.49 [495]	1.73 [44]	3.31 [84]	3.31 [84.0]	2.60 [66.0]	1.19 [30.2]	3.31 [84.0]	8.86 [225]	9.69 [246]	8.27 [210]	9.50 [241]

[1]Total tolerance is determined by subtracting bar diameter from the wide end inside diameter (A).

Table F2. Dimensions of NMB SNX11 Splice-Sleeve[25]

DIMENSIONS OF NMB SNX SLEEVE											REQUIRED REBAR EMBEDMENT LENGTH			
Sleeve No.	Bar Diameter (in.) [mm]	Bar Size		Sleeve Length (in.) [mm]	Narrow End Diameter (in.) [mm]		Maximum Diameter (B) (in.) [mm]	Wide End Diameter (in.) [mm]			Dowel (E1) (in.) [mm]		Dowel (E2) (in.) [mm]	
		ASTM	JIS		I.D. (C)	O.D. (C')		I.D. (A)	Total Tolerance[1]	O.D (A')	Min.	Max.	Min.	Max.
SNX11	1.410 [36]	#11	D36	19.09 [485]	1.69 [43]	3.03 [77]	3.03 [77.0]	2.32 [59]	0.91 [23.1]	3.03 [77]	8.86 [225]	9.25 [235]	8.27 [210]	9.45 [240]

[1]Total tolerance is determined by subtracting bar diameter from the wide end inside diameter (A).

Figure F3 shows the connector configuration for Erico's Lenton Interlok couplers and Table F3 shows the dimensions and cut length for reinforcing steel.

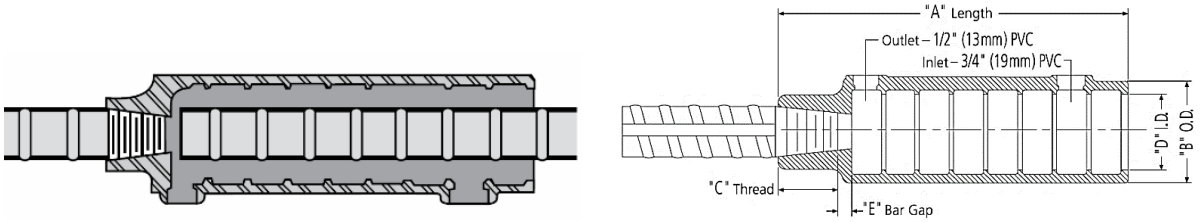

Figure F3. Erico's Lenton Interlok Rebar Splicing System[26]

Table F3. Coupler Dimensions and Bar Cut Lengths for Lenton Interlok System[26]

Rebar Size in-lb	Rebar Size Canadian	Coupler Part No.	"A"	"B"	"C"	"D"	"E" Reference	"X" Max.	"X" Min. Type 1*	"X" Min. Type 2**
#5	15M	LK5	7-13/16"	2-9/16"	7/8"	1-7/8"	13/16"	6-1/8"	5-1/4"	5-1/2"
#6	20M	LK6	7-13/16"	2-9/16"	1-1/8"	1-7/8"	9/16"	6-1/8"	5-1/4"	5-3/8"
#7	---	LK7	7-13/16"	2-9/16"	1-1/4"	1-7/8"	7/16"	6-1/8"	5-1/4"	
#8	25M	LK8	8-5/8"	2-11/16"	1-3/8"	2"	1/4"	7"	6"	
#9	30M	LK9	9-3/4"	2-13/16"	1-1/2"	2-1/8"	1/4"	8"	6-7/8"	
#10	---	LK10	10-13/16"	3"	1-9/16"	2-5/16"	1/4"	9"	7-3/4"	
#11	35M	LK11	11-15/16"	3-1/8"	1-11/16"	2-7/16"	3/8"	9-7/8"	8-1/2"	
#14	45M	LKT14	15-3/16"	3-11/16"	2-1/8"	2-3/4"	5/16"	12-3/4"	11"	
#18	55M	LKT18	20-5/16"	4-1/2"	2-3/4"	3-1/4"	9/16"	17"	14-3/4"	

* "X" Min. Type 1 will develop 125% of the specified yield strength of the rebar in tension and compression (125% f_y).
** "X" Min. Type 2 meets Type 1 and will develop the specified tensile strength of the rebar in tension (f_u).

Table F4 summarizes the data from Tables F1 to F3 and also includes the recommendations by the latest University of Nevada, Reno report.[9]

Table F4. Ratio of Sleeve Length to Reinforcing Bar Diameter[25, 26, 9]

Bar Size	Bar Diam., in.	Ratio of Sleeve Length to Reinforcing Bar Diameter		
		Splice Sleeve North America, Inc.	Erico's Lenton Interlok	Recommended by UNR Report (Tazarv & Saiidi, 2015)
#4	0.500	--	--	≤ 15
#5	0.625	15.44	12.50	≤ 15
#6	0.750	14.96	10.42	≤ 15
#7	0.875	14.63	8.93	≤ 15
#8	1.000	14.57	8.63	≤ 15
#9	1.128	14.49	8.64	≤ 15
#10	1.270	14.10	8.51	≤ 15
#11	1.410	13.82, 13.82, 13.54 [a]	8.47	≤ 15
#14	1.693	14.42	8.97	≤ 15
#18	2.257	--	9.00	≤ 15

[a] For Sleeve Nos. 11U-X, A11W, and SNX11, respectively.

Using ratio of 15 seems reasonable. As shown in Table F5, most SSNA couplers meet this requirement. All Erico's Lenton Interlok couplers meet this requirement.

U.S. Code Requirements on Mechanical Bar Couplers

- ACI 318 Type 1 and Type 2 bar couplers:
  - Type 1 couplers are capable of developing 125% of the specified yield of the bar in tension (i.e., $1.25\ f_y$). Type 1 bar couplers are not to be used in the plastic hinge of ductile members of special moment frames neither in longitudinal nor in transverse bars (ACI 318-2014 Section 18.2.7).[24]
  - Type 2 couplers meet Type 1 requirement and are capable of developing the specified tensile strength of the bar in tension (i.e., $1.0\ f_u$). Type 2 bar couplers are not to be used within one-half of the beam depth in special moment frames but are allowed in any other members at any location (ACI 318-2014 Section 18.2.7 & 25.5.7).[24]
- Caltrans Seismic Design Criteria (2013), Chapter 8: For ductile members, no splicing is allowed in the plastic hinge region. "Ultimate" splices are permitted outside of the plastic hinge zones of ductile members. "Service" splices are allowed in capacity protected members (i.e., members that are not likely to experience seismic damage).[27]
  - Service splices must be able to accommodate a minimum strain of 2% in the spliced bar.
  - Ultimate splices must be able to accommodate a minimum strain of 6% in No. 11 and larger bars and 9% in No. 10 and smaller bars.
- AASHTO Full Mechanical Connection (FMC) Requirements (AASHTO LRFD Bridge Design Specifications, Section 5.11.5.2.2): FMC couplers must not be used in the plastic hinge zones of

columns in SDC C and D (*AASHTO Guide Specifications for LRFD Seismic Bridge Design*, Section 8.8.3).[20, 17]

- The FMC couplers must be able to achieve 1.25 times the specified yield stress (i.e., $1.25\ f_y$) of the coupled bar.
- The FMC couplers must have a maximum slip of 0.01 in. for No. 3-14 bars and 0.03 in. for No. 18 bar. Slip within the coupler is measured by loading the spliced bar from 3 ksi in tension to 30 ksi in tension and then unloading to 3 ksi in tension. Displacement is measured over the coupler region for the initial and final 3 ksi loading. The difference between these two measurements is the slip.

Tensile Capacities of Splice Sleeve and Lenton Interlok Grouted Couplers

- NMB Splice Sleeve: Splice Sleeve North America, Inc. NMB Splice Sleeve grouted couplers for Grade 60 bar with sizes of No. 6, 8, 11 and 14 met at least 150% of specified bar tensile yield strength. See Table 10 of Laboratory Test Report ER-5645 (Wiss, Jenney, Elstner Associates, Inc., 2013). This table is repeated here as Table F5 with appropriate values in a red box. Note that the last five rows of Table F5 are for Grade 100 bar and should not be considered. Assuming a specified 90 ksi ultimate strength for Grade 60 bars, these couplers meet the ACI Type 2 and AASHTO FMC coupler strength requirements (i.e., $1.0\ f_u$ and $1.25\ f_y$, respectively).
- Erico Lenton Interlok: All Lenton Interlok grouted couplers listed in Table F4 of this document meet ACI Type 1 requirement in tension and compression and the ACI Type 2 requirement in tension. They also meet the AASHTO FMC strength requirement.

Table F5. Tensile Strength Data for NMB Splice Sleeve Couplers[13]

Test I.D. No.	Bar Size	Bar Lot	Bar Area (in^2)	Alignment	Deformation Pattern	Grout Batch	Average Grout Strength	Cyclic Load Levels (Stages 1, 2, 3)				Cycles Applied			Tensile Strength (Stage 4)					Final Result
								P_{min} (kips)	P_{max1} (kips)	P_{max2} (kips)	P_{max3} (kips)	n_1	n_2	n_3	(kips)	(ksi)	($\%f_{y=60}$)	($\%f_{ya}$)	($\%f_{u=90}$)	
4388	6	A	0.44	Misaligned	Diagonal	PII-7	13,023	-13.2	25.1	29.0	33.7	20	4	4	46.1	104.8	175%	166%	116%	Bar break
4389	6	A	0.44	Misaligned	Diagonal	PII-7	13,023	-13.2	25.1	29.0	33.7	20	4	4	46.1	104.8	175%	166%	116%	Bar break
4390	6	A	0.44	Misaligned	Diagonal	PII-7	13,023	-13.2	25.1	29.0	33.7	20	4	4	46.0	104.5	174%	165%	116%	Bar break
4391	6	A	0.44	Misaligned	Diagonal	PII-7	13,023	-13.2	25.1	29.0	33.7	20	4	4	46.0	104.5	174%	165%	116%	Bar break
4392	6	A	0.44	Misaligned	Diagonal	PII-7	13,023	-13.2	25.1	29.0	33.7	20	4	4	46.1	104.8	175%	166%	116%	Bar break
4382	8	C	0.79	Misaligned	Diagonal	PII-7	13,023	-23.7	45.0	59.5	67.0	20	4	4	87.5	110.8	185%	159%	123%	Bar break
4383	8	C	0.79	Misaligned	Diagonal	PII-7	13,023	-23.7	45.0	59.5	67.0	20	4	4	87.7	111.0	185%	159%	123%	Bar break
4384	8	C	0.79	Misaligned	Diagonal	PII-7	13,023	-23.7	45.0	59.5	67.0	20	4	4	87.6	110.9	185%	159%	123%	Bar break
4384	8	C	0.79	Misaligned	Diagonal	PII-7	13,023	-23.7	45.0	59.5	67.0	20	4	4	87.6	110.9	185%	159%	123%	Bar break
4386	8	C	0.79	Misaligned	Diagonal	PII-7	13,023	-23.7	45.0	59.5	67.0	20	4	4	87.6	110.9	185%	159%	123%	Bar break
4396	14	G	2.25	Misaligned	Diamond	PII-10	12,208	-67.5	128.3	143.0	158.0	20	4	4	208.3	92.6	154%	145%	103%	Bar break
4397	14	G	2.25	Misaligned	Diamond	PII-10	12,208	-67.5	128.3	143.0	158.0	20	4	4	208.5	92.7	154%	145%	103%	Bar break
4398	14	G	2.25	Misaligned	Diamond	PII-10	12,208	-67.5	128.3	143.0	158.0	20	4	4	209.3	93.0	155%	146%	103%	Pullout - wide end
4399	14	G	2.25	Misaligned	Diamond	PII-10	12,208	-67.5	128.3	143.0	158.0	20	4	4	207.9	92.4	154%	145%	103%	Pullout - wide end
4400	14	G	2.25	Misaligned	Diamond	PII-10	12,208	-67.5	128.3	143.0	158.0	20	4	4	208.4	92.6	154%	145%	103%	Bar break
4402	SNX11	A	1.56	Misaligned	Bamboo	PII-11	12,213	-46.8	88.9	101.0	109.0	20	4	4	154.4	99.0	165%	152%	110%	Bar break
4403	SNX11	A	1.56	Misaligned	Bamboo	PII-11	12,213	-46.8	88.9	101.0	109.0	20	4	4	154.3	98.9	165%	152%	110%	Bar break
4404	SNX11	A	1.56	Misaligned	Bamboo	PII-11	12,213	-46.8	88.9	101.0	109.0	20	4	4	154.6	99.1	165%	152%	110%	Bar break
4405	SNX11	A	1.56	Misaligned	Bamboo	PII-11	12,213	-46.8	88.9	101.0	109.0	20	4	4	153.8	98.6	164%	152%	110%	Bar break
4406	SNX11	A	1.56	Misaligned	Bamboo	PII-11	12,213	-46.8	88.9	101.0	109.0	20	4	4	154.2	98.8	165%	152%	110%	Bar break
4662	10	D	1.27	Misaligned	Diagonal	PII-21	12,627	-38.1	72.4	80.3	87.9	20	4	4	135.0	106.3	177%	N/A	118%	Coupler
4663	10	D	1.27	Misaligned	Diagonal	PII-21	12,627	-38.1	72.4	80.3	87.9	20	4	4	165.1	130.0	217%	N/A	144%	Pullout - wide end
4664	10	D	1.27	Misaligned	Diagonal	PII-21	12,627	-38.1	72.4	80.3	87.9	20	4	4	118.5	93.3	156%	N/A	104%	Coupler
4665	10	D	1.27	Misaligned	Diagonal	PII-21	12,627	-38.1	72.4	80.3	87.9	20	4	4	170.9	134.6	224%	N/A	150%	Pullout - wide end
4666	10	D	1.27	Misaligned	Diagonal	PII-21	12,627	-38.1	72.4	80.3	87.9	20	4	4	139.7	110.0	183%	N/A	122%	Coupler

Slip Behavior of Splice Sleeve and Lenton Interlok Grouted Couplers

In a study by Jansson (2008), NMB Splice Sleeve and Lenton Interlok couplers for No. 6 and 11 bars passed the AASHTO slip requirements for FMC couplers (see Tables 4.1 and 5.1 of the report by Jansson, 2008).[11] In addition, the NMB Splice Sleeve couplers for No. 8 bar passed the laboratory slip tests conducted by Haber, et al. (2013).[1] Table F6 summarizes the slip test results of these two studies. Three tests were performed for each type of coupler considered. As noted in Section 4 of this document, the maximum slip in AASHTO's FMC couplers for No. 3 to No. 14 bars is limited to 0.01 in.

Table F6. Grouted coupler slip test results[11, 1]

Coupler for Bar Size	Slip, in.	
	NMB Splice Sleeve	Lenton Interlok
#6	0.008, 0.007, 0.006	0.004, 0.003, 0.005
#8	0.001, 0.000, 0.002	--
#11	0.010, 0.009, 0.009	0.006, 0.006, 0.003

Cyclic Behavior of Grouted Couplers

The fatigue of grouted couplers has been studied in low amplitude fatigue tests by Jansson (2008) as well as Haber, et al. (2013).[11, 1] In both cases, the grouted couplers performed well in the standard fatigue tests. However, no information was found on grouted couplers tested individually in large amplitude fatigue tests. In experimental work on columns with grouted couplers with both ends grouted, no fracture of the grouted couplers were reported by Haber et al. (2013) and Pantelides, et al. (2014).[1, 6] However, failures due to bond-slip in grouted-threaded couplers (i.e., by Erico) were observed at higher column drifts according to the University of Utah's report (Pantelides, et al., 2014). Therefore, one can observe that grouted-grouted couplers perform better in the columns than the grouted-threaded couplers. Furthermore, couplers with both ends grouted force the rebar to fracture away from the couplers which is the desired mode of failure.